Micro-pocket fission detectors: development of advanced, real-time, in-core, neutron-flux sensors

by

MICHAEL ANTHONY REICHENBERGER

B.S., Kansas State University, 2012

AN ABSTRACT OF A DISSERTATION

submitted in partial fulfillment of the requirements for the degree

DOCTOR OF PHILOSOPHY

Department of Mechanical and Nuclear Engineering
College of Engineering

KANSAS STATE UNIVERSITY
Manhattan, Kansas

2017

Abstract

Advancements in nuclear reactor core modeling and computational capability have encouraged further development of in-core neutron sensors. Measurement of the neutron-flux distribution within the reactor core provides a more complete understanding of the operating conditions in the reactor than typical ex-core sensors. Micro-Pocket Fission Detectors (MPFDs) have been developed and tested previously but have been limited to single-node operation and have utilized highly specialized designs. The development of a widely deployable, multi-node MPFD assembly will enhance nuclear research capabilities. In-core neutron flux measurements include many challenges because of the harsh environment within the reactor core. Common methods of in-core neutron measurement are also limited by geometry and other physical constraints. MPFDs are designed to be small and robust while offering a real-time, spatial measurement of neutron flux. Improvements to the MPFD design were developed based on shortcomings of prior research in which many of the theoretical considerations for MPFDs were examined. Fabrication techniques were developed for the preparation of MPFD components and electrodeposition of fissile material. Numerous arrays of MPFDs were constructed for test deployments at the Kansas State University TRIGA Mk. II research nuclear reactor, University of Wisconsin Nuclear Reactor, Transient REActor Test facility at the Idaho National Laboratory (INL), and Advanced Test Reactor at INL. Preliminary testing of a single MPFD sensor at KSU yielded a linear response to reactor power between 10 kWth and 750 kWth and followed both positive and negative reactivity insertions in real-time. A $1.50 reactor pulse was monitored from the Intra-Reflector Irradiation System, located in reflector region of the KSU TRIGA Mk. II core with 1-ms time resolution. Improved multi-node MPFD arrays were then designed, fabricated, and deployed in flux ports between fuel rods and within an iron-wire flux port which was inserted into the central thimble of the KSU TRIGA Mk. II research nuclear reactor. Work continues to develop MPFDs for deployment at research reactors at INL and elsewhere. Results from the MPFD measurements will be useful for future validation of computational modeling and as part of advanced nuclear fuel development efforts.

Micro-pocket fission detectors: development of advanced, real-time, in-core, neutron-flux sensors

by

MICHAEL ANTHONY REICHENBERGER

B.S., Kansas State University, 2012

A DISSERTATION

submitted in partial fulfillment of the requirements for the degree

DOCTOR OF PHILOSOPHY

Department of Mechanical and Nuclear Engineering
College of Engineering

KANSAS STATE UNIVERSITY
Manhattan, Kansas

2017

Approved by:

Major Professor
Douglas S. McGregor

Copyright

Abstract

Advancements in nuclear reactor core modeling and computational capability have encouraged further development of in-core neutron sensors. Measurement of the neutron-flux distribution within the reactor core provides a more complete understanding of the operating conditions in the reactor than typical ex-core sensors. Micro-Pocket Fission Detectors (MPFDs) have been developed and tested previously but have been limited to single-node operation and have utilized highly specialized designs. The development of a widely deployable, multi-node MPFD assembly will enhance nuclear research capabilities. In-core neutron flux measurements include many challenges because of the harsh environment within the reactor core. Common methods of in-core neutron measurement are also limited by geometry and other physical constraints. MPFDs are designed to be small and robust while offering a real-time, spatial measurement of neutron flux. Improvements to the MPFD design were developed based on shortcomings of prior research in which many of the theoretical considerations for MPFDs were examined. Fabrication techniques were developed for the preparation of MPFD components and electrodeposition of fissile material. Numerous arrays of MPFDs were constructed for test deployments at the Kansas State University TRIGA Mk. II research nuclear reactor, University of Wisconsin Nuclear Reactor, Transient REActor Test facility at the Idaho National Laboratory (INL), and Advanced Test Reactor at INL. Preliminary testing of a single MPFD sensor at KSU yielded a linear response to reactor power between 10 kWth and 750 kWth and followed both positive and negative reactivity insertions in real-time. A $1.50 reactor pulse was monitored from the Intra-Reflector Irradiation System, located in reflector region of the KSU TRIGA Mk. II core with 1-ms time resolution. Improved multi-node MPFD arrays were then designed, fabricated, and deployed in flux ports between fuel rods and within an iron-wire flux port which was inserted into the central thimble of the KSU TRIGA Mk. II research nuclear reactor. Work continues to develop MPFDs for deployment at research reactors at INL and elsewhere. Results from the MPFD measurements will be useful for future validation of computational modeling and as part of advanced nuclear fuel development efforts.

Table of Contents

List of Figures

List of Tables

Acknowledgements

There are so many people who have played a role in this research and in my continued education. Dr. McGregor eagerly accepted me as his student in 2012. I still remember when I was taking NE612 and the turning-point conversation where he strongly encouraged me to work up to my full potential. The whole S.M.A.R.T. Laboratory (current and former members) has been instrumental in my research. In particular, I am incredibly fortunate to have shared an office with Ryan Fronk. I have learned so much from Ryan, extending well beyond academic affairs. Dr. Shultis, Dr. Dunn, Dr. Geuther, and Dr. Roberts have also played active roles in my continued education and research and I must acknowledge their contributions to my development as a scientist and to the academic works that have been produced by our research. Dr. Geuther was also instrumental in the acquisition of a research project which drove the most fast-pace MPFD development. This would not have been possible without his vision and dedication to make this research a reality. Similarly, Troy Unruh has been an undying advocate for MPFDs at Idaho National Laboratory, securing research funding which initiated my career. Dr. Ito of the Kansas State University chemistry department contributed a great deal of work developing the electrodeposition process early in this project, a process which was critical to the subsequent endeavors.

I have had the distinct pleasure to work with amazing people in industry throughout this project. Heather Brassell, Gary Vaillancourt, and Jeremy Dobish at NFT truly turned a page in MPFD fabrication when we began working together to supply alumina components. How serendipitous that Heather and I would meet in Brussels during my second year of graduate school. Andreas Ruben at Wiener has been incredibly helpful in the development of advanced electronics systems for MPFDs, especially helping me to learn in the process. Tim Sobering, Dave

Huddleston, and Russell Taylor at EDL contributed in numerous ways from the fabrication of test systems to useful discussion regarding noise and electronic design that greatly accelerated MPFD development.

Most importantly, I have had the wonderful opportunity to mentor an amazing team of undergraduate and graduate students who have been indispensable. Tyrel George began working with me in 2014 and made great contributions as part of his Master's Thesis. Sarah Stevenson was the first undergraduate whom I hired. Sarah has grown into an amazing scientist, was instrumental in developing and enhancing the electrodeposition process, and will certainly go on to accomplish many great things. Dan Nichols was the second student I hired to work on the MPFD project, and he has recently begun the pursuit of his Ph.D., continuing to enhance MPFDs. Hai Vo-Le began working for Tyrel and then transitioned to work with me when Tyrel graduated. How fortunate I am that Hai was willing to put in whatever hours were necessary to meet the demands of our projects. Hai is a master wire threader if there ever was one. Tanner Swope and Caden Hilger joined our team in 2016 and have already contributed to the continued enhancements of the MPFD fabrication process. Finally, I was lucky to work with Kevin Tsai during a summer internship at the Idaho National Laboratory. Kevin was a pleasure to work with in Idaho and continues to develop a calibration process to confirm the MPFD mass measurements conducted at KSU as he completes his Master's research at Idaho State University.

This work has been funded by US Department of Energy Office of Nuclear Energy contracts DE-AC07-05ID14517, DE-NE0008305, DE-NE0008408.

Dedication

"Nothing tends so much to the advancement of knowledge as the application of a new instrument" – Sir Humphry Davy – Elements of Chemical Philosophy, 1812

I never feel more alive than when I've gained a new understanding. This quote by Sir Humphry Davy perfectly exemplifies why I was so drawn to nuclear instrumentation. I am so fortunate to have been surrounded by inquisitive and insightful friends through the course of my B.S. to encourage my own curiosity and continue my education. My intention was not originally to pursue a PhD, I thought this was only for some elite class of man, which I certainly am not! It was only by the continued support of my closest friends and family that I have been able to achieve any of this.

"A good companion shortens the longest road" – Turkish Proverb

My wife, Rachel, is the most important reason that I have completed this work. There is no doubt that there were many difficult days and nights in the past 5 years. Just when times were bleakest, God brought Rachel into my life. I am so blessed to have had such an intelligent, caring, and supportive companion for this journey, and for the rest of my life to come.

"In every conceivable manner, the family is link to our past, bridge to our future" – Alex Haley

My Family: My parents, Barbara and Kevin, and my sisters, Emily, Rachel, Amanda, Cecilia, Laura, and Kaylie have all been instrumental in getting me to this place in my life. My parents are shining examples of perseverance through difficulty. Emily, Rachel, and Amanda were there through the early years and continue to be an important part of my life. Cecilia, Laura, and Kaylie remind me just how quickly this life passes us by and that we must cherish every moment.

Thank you.

Chapter 1 Introduction

The following is a brief summary of the motivation for the present work which has led to this dissertation, the resulting scientific contributions, and the organization of the remaining chapters. The need for advanced neutron sensors for research nuclear reactors is the primary motivation for this work. Many of the contributions to the science originate from the need to develop fabrication methods and enhanced signal processing capabilities for the specialized neutron sensors presented.

1.1 Motivation for the Thesis

Nuclear reactor research and development has been of interest worldwide for over half a century [1]. During this period, the field of nuclear energy has experienced multiple changes of support and decent; however, nuclear power remains a prominent technology for the world's energy supply now and into the future. The evolution of nuclear power from its beginning to its present form was driven by brilliant theorists and experimentalists alike. Investigation of novel nuclear reactor designs and materials necessitates enhanced instrumentation. Advances in computational power over the past several decades have tilted the scales of research towards simulation and theoretical calculations. The days of 'trial-and-error' reactor experimentation are long gone and the future development of reactor technologies rests upon extensive reactor modeling and simulation, followed necessarily by validation. Although these improvements have certainly benefited the field, experimental validation of novel nuclear reactor designs and materials have not kept pace. There are several reasons for this shortcoming in experimental research, not the least of which is nuclear reactor instrumentation.

In the past, theoretical reactor physics models required extensive simplification from the real-world environment [1]. In making these assumptions, it was challenging to solve problems involving temperature and time independence. Most experimental validation, therefore, revolved around similarly simplified problems. Reactor materials were tested on a trial-and-error basis (after theoretical consideration of course), and neutron fluence for a given experiment was sufficient given that time-dependent neutron flux solutions were not commonly available for models of that time. High-power computing and advances in computational modeling have now made time- and

temperature-dependent solutions commonplace however, in-core nuclear instrumentation still relies primarily on fluence-based measurements.

Research nuclear reactors commonly utilize neutron-sensitive radiation detectors located external to the reactor core to monitor reactor power [1, 2]. Advancements in nuclear reactor core modeling and computational capability have encouraged further development of in-core neutron sensors. Measurement of the neutron-flux distribution within the reactor core provides a more complete understanding of the operating conditions in the reactor than ex-core sensors. Solutions presently exist to monitor the neutron fluence experienced during reactor experiments; however, time-dependent information regarding minute variations in flux due to local fuel burnup, control-rod motion, and experimental effects are not captured. Testing and qualification of new reactor materials would greatly benefit from a well-defined experimental environment.

Small, accurate, and robust neutron-flux sensors are an important development for the enhancement of advanced nuclear fuel testing [3]. The environment within a nuclear reactor core is not ideal for the operation of many types of radiation detectors. The high-radiation fields of neutrons, gamma-rays, and beta-particles quickly overwhelm most conventional radiation detectors. Even specially developed neutron detectors (such as Self-Powered Neutron Detectors (SPNDs) and sub-miniature neutron detectors) must make corrections to the measured data to compensate for the significant burnup induced by neutron-fluxes that are often on the order of 10^{14} cm^{-2} s^{-1} [2, 4, 5]. Conventional in-core sensors often utilize neutron-sensitive coatings with large neutron-absorption cross-sections, whose presence can drastically perturb neutron-flux near the sensor, skewing the measured results from the actual flux. The availability of small, robust neutron sensors capable of real-time neutron flux measurements in the harsh environment of the nuclear reactor can close the widening gap between experimental and theoretical nuclear engineering [3].

Micro-Pocket Fission Detectors (MPFDs) are poised as the instrument that takes nuclear reactor testing to the next level. Constructed from radiation-hard materials, and specifically designed to minimize flux perturbations while maintaining exceptionally low gamma-ray sensitivity, MPFDs can be deployed into the confined spaces and high-radiation environments found within a nuclear reactor core. MPFDs can be used to validate reactor core simulations and experimental reactor materials [6]. The real-time measurements that MPFDs provide can be used to observe different neutron flux profiles in a reactor core during transient testing and high-fluence

experiments without significantly perturbing the local neutron flux; therefore, enhancing the experimental capabilities of nuclear research facilities [7].

Previous MPFD development was challenged by poor neutron-sensitive coating methods and inadequate signal processing. The present work addresses these concerns by developing a reliable and reproducible method by which to deposit small amounts of uranium- and thorium-based compounds onto MPFD substrates [8]. Superior materials were selected to reduce signal attenuation between the MPFD sensors and signal processing electronics. Additional efforts were made to select proper signal processing components to maximize the MPFD neutron-induced signal while minimizing noise from other sources. Finally, MPFDs were tested at the KSU TRIGA Mk. II research nuclear reactor, showing linear detector response with reactor power and tracking both positive and negative reactivity insertions [9]. MPFDs were also developed for testing at numerous research facilities around the United States.

1.2 Contributions to the Science

Previous studies of MPFDs have fallen short of the full potential of this technology. Although significant progress has been made beyond previous MPFD development efforts, there remains room for improvement. The sensor substrate material has always been of concern. In the past, rough alumina samples caused the evaporated metallic electrode to peel. Also, the parallel plate design of previous MPFDs required a wire-bond or other adhesive measure to secure electrical contact to the MPFD metallic substrate. New higher purity alumina was sourced for the present work, producing less activation after testing. Polishing the alumina substrate, coupled with changes to the evaporated metallic coating thickness, yielded metallic substrates with better adhesion. The transition to a multi-wire design also eliminated the need to secure an electrical lead wire to the metallic substrate, enhancing sensor durability and making the fissile material electrodeposition more consistent. The multi-wire design also enhanced the electric field within the sensor. Furthermore, the electrodeposition process was also improved. Previous studies relied on a proprietary electrolysis method which was designed to yield high deposition efficiency. In contrast, the present work modified well-established electrodeposition methods used for electro-chemical analysis of other materials. The new electrodeposition method was also characterized to determine how best to deposit a specific amount of uranium or thorium onto an MPFD electrode

surface. These improvements all compounded to enable the development and testing of the smallest fission chambers ever built.

The smallest MPFDs thus far produced have a 330-μm diameter surface of neutron-reactive material. The electrodeposition method was used to deposit < 0.5 μg of uranium onto these surfaces, yielding a neutron sensitivity < 10^{-9} cm^2 [8]. These MPFDs were deployed into iron-wire flux ports and successfully used to measure neutron fluxes in excess of 10^{15} cm^{-2} s^{-1}. Larger MPFDs were also developed for deployment at several other nuclear reactor test facilities.

The larger MPFD design utilized a 2-mm diameter surface with typically ≈ 1 μg of neutron-reactive material [7]. MPFDs were designed for the ATF-2 sensor qualification, ATF-3 multi-SERTTA, and AGR-5/6/7 experiments at the Idaho National Laboratory (INL). These tests included multiple MPFD deployments at both the advanced test reactor (ATR) and transient research reactor (TREAT) facilities. Results of the experiments at the INL are pending.

A 6-ft long modular MPFD sensor array was also developed for testing at the Kansas State University (KSU) TRIGA Mk. II research nuclear reactor and at the University of Wisconsin Nuclear Reactor (UWNR) facilities. The modular design allowed for support electronics and cabling to be deployed at both facilities and for the arrays to be tested at KSU before being shipped to UWNR. The shorter design of the modular MPFD sensor array also decreased complications that came with the long flux ports used for other experiments. The standard design utilized by the modular MPFD sensory array was necessary to meet the demand of deploying at least 25 MPFD nodes at the UWNR facility, achieved by deploying 7 arrays composed of 4 MPFD nodes each. Standardization of signal processing equipment was also necessary for all of the aforementioned projects.

Two approaches to signal processing for MPFDs have been attempted in the past. Preliminary MPFD research relied on highly custom electronics, built entirely in-house. While this system worked, it was neither practical nor desirable to reproduce that system for the present work because of differences in the MPFD design. Most of the present work utilized off-the-shelf (OTS) NIM-compatible components. Although bulky, these OTS components were flexible when attempting to determine optimal operating conditions for the MPFDs. All of the experience developed by testing MPFDs was compiled to work with a commercial nuclear electronics supplier (Mesytec Detector Readout Systems) to develop an integrated electronics package. The MPFD integrated electronics package includes high-voltage supply, pre-amplification, shaping, and discrimination.

All of the previously discussed contributions will be described in greater detail in subsequent chapters. The contribution of a standardized design for the MPFD sensor array and support electronics will greatly aid in future efforts to make MPFDs commercially available.

1.3 Organization of the Dissertation

Prior research publications have described many of the theoretical considerations for MPFDs, which will be summarized. Fabrication and testing of these neutron sensors is the primary focus of the present work. Important background information is presented in Chapter 2, including the harsh environment of the nuclear reactor core, challenges of in-core neutron flux measurement, and common experimental methods of determining in-core neutron flux. Chapter 3 describes important design features of the MPFD sensor, summarizing previous research and supplementing where necessary. The fabrication of MPFD sensors and arrays is presented in Chapter 4. Many of the contributions of the present work is also presented in greater detail in Chapter 4, including substrate preparation, electrodeposition, alternative material considerations, high-temperature effects, and MPFD electrode design. Examined in chapter 5 are the MPFD support systems, including facility test ports, MPFD deployment methods, and signal processing. In-core test results for various MPFD sensors and arrays will be presented in Chapter 6. Finally, Chapter 7 includes a discussion of the conclusions which can be drawn from this research, contributions to the science, ongoing, and future applications of the MPFD technology.

Chapter 2 Background

Nuclear reactor theory is the topic of numerous texts spanning the history of the field of nuclear science and engineering [1]. The following is a brief discussion of the critical aspects of neutron production in a nuclear reactor and current in-core neutron detection methods.

2.1 The Environment of a Nuclear Reactor Core

Nuclear reactors utilize the energy released from the fission of atoms in the nuclear fuel to generate power. The atoms of the nuclear fuel (particularly ^{235}U) fission after absorbing a neutron, yielding fission products which include fission fragment atoms, neutrons, gamma rays, and other sub-atomic particles. Fission products contain a large amount of kinetic energy [1]. As the fission products interact in the fuel and other materials in the core, they deposit energy in the form of heat which can be used to produce electricity [1]. The neutrons, however, go on to induce additional fissions, sustaining a nuclear chain reaction. It is therefore critical to understand the neutron population at a given region of a nuclear reactor, within a specified period of time when designing a nuclear reactor or nuclear experiment. The neutron flux, φ, is defined as the neutron density at a particular point in space and time multiplied by the speed of the neutrons at that point and has units of $cm^{-2}\ s^{-1}$ [1]. Quantifying φ in a nuclear reactor is complicated by the fact that neutrons are born through nuclear fission with a distribution of energies, and lose energy through material interactions in the reactor [1]. During this process, some neutrons are absorbed without causing fission, others escape the reactor, and only a portion induce fission. The study of the 'neutron economy' in a nuclear reactor has been of great interest since the conception of the first nuclear chain reactions and is the primary motivating factor for the present work.

Analytical methods can be used to estimate the neutron flux distribution within the core of simplified nuclear reactor designs [1]. As the reactor geometry gains complexity, it is typical that computational modeling and simulation is required, but often an analytical solution can still be found [1]. The challenge lies in experimentally confirming these computer aided analytical method solutions. Detecting the presence of neutrons is difficult because of their non-ionizing nature [10]. Secondary reactions between a 'converter material' and the neutron is typically necessary to detect neutrons [10]. Determining the energy of the incident neutron is even more difficult. For this

reason, the neutron flux within a reactor is commonly separated into fast and slow energy groups for measurement purposes [1]. The division between fast and slow neutrons is commonly determined by the cut-off energy for neutron absorption in ^{113}Cd of 0.5 eV [2]. The 'cadmium cutoff' energy is a convenient transition point from slow to fast energies because of the sharp decrease in the neutron absorption cross section for ^{113}Cd at 0.5 eV, as shown in Fig. 2.1. Further simplifications can be made by referring to the "fast-to-thermal" ratio defined as the ratio of the integrated flux in the fast region divided by the integrated flux in the slow region. The magnitude of these two neutron flux values is of great interest for nuclear reactor testing.

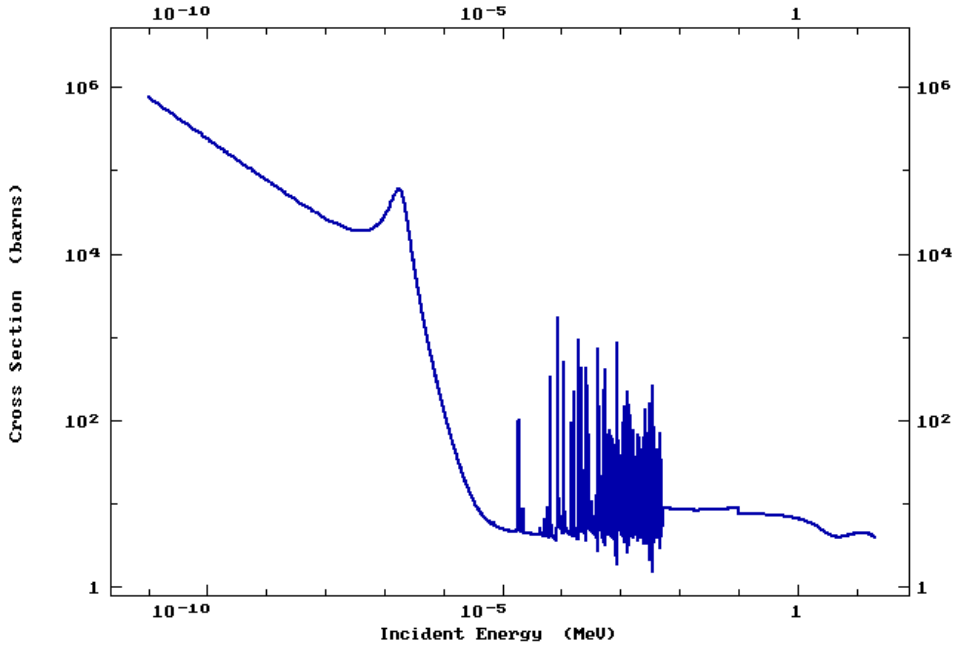

Fig. 2.1 The total neutron interaction cross section for ^{113}Cd drops off rapidly above 0.5 eV [11].

Measurement of the neutron flux near an experiment and throughout the reactor core is necessary to properly characterize the effects of radiation on a material as well as the effects of an experimental material on the criticality of a nuclear reactor. Computer simulations and models have come a long way in predicting these results, but the validation of such codes is a separate area of research interest. Neutron detectors of various designs have been developed which can measure or infer the neutron flux during steady-state operations [2]. There are, however, numerous challenges faced when measuring the neutron flux within a nuclear reactor core, particularly at nuclear research facilities.

2.2 Challenges of In-Core Neutron Flux Measurements

The environment within a nuclear reactor is not conducive to the operation of electronic devices. High radiation fields, fluid flow, temperatures, and radio-frequency (RF) interference are only a few of the obstacles that must be overcome to measure the in-core neutron flux in a nuclear reactor. Additional challenges arise when designing measurement devices for experimental facilities. The desired neutron flux measurement is within an experimental capsule, near test sample locations, but must be conducted without significantly affecting the neutron flux in the experiment. The substantial shielding and remote access at advanced reactor test facilities also complicates the electronic support systems required for in-core neutron detection.

2.2.1 High Radiation Field

The radiation field within the core of a nuclear reactor is diverse and intense. Prompt and delayed gamma rays, alpha particles, neutrons, and beta particles from nuclear fission and fission fragment decay are present in a nuclear reactor core [1]. The intensity of each of these groups of particles varies based on the fuel and moderator composition, but is always a significant factor when attempting to design radiation detectors to measure neutron flux. The effects of alpha particles are simplest to negate. With penetration depths on the order of micrometers in most solids, even energetic alpha particles emitted by fission product decay are stopped by the casings encapsulating most radiation detectors. Beta particles are the next particle to consider. With relatively small specific energy deposition (the amount of energy deposited by the particle per unit distance that it travels), beta particles typically deposit little energy in the small detection volumes of in-core neutron detectors. Gamma rays are the most challenging particle to discriminate against in the reactor core. Unlike alpha particles and beta particles which are primarily born from radioactive decay of fission products, gamma rays are produced by both prompt (fission) and delayed (radioactive decay) sources. Gamma rays born in the reactor core also have relatively long ranges and can travel from almost any location within the core to interact in the detection medium.

Two approaches are common when designing in-core and near-core neutron detection systems. The first, and most common method is to compensate for the presence of gamma rays by constructing two detectors, one with and one without neutron-sensitive material. A conversion material is typically necessary for neutron detectors. The detector signal contribution from

neutrons can be determined by subtracting the signal developed by the non-sensitive detector from the detector which is sensitive to both gamma rays and neutrons [2]. This method requires additional support systems which complicate the design and extends signal processing time. Alternatively, the sensor can be designed to be insensitive to gamma rays. This method proves challenging for in-core and near-core neutron detectors due to their size and common dependency on current-mode operation (described later). However, this present mode of operation is preferred, particularly for test reactors where a fast response to changes in the neutron flux are desired and space for sensors is limited.

2.2.2 Physical Constraints

With regards to the present work, research and test reactors come in essentially three varieties: accessible open-pool reactors, high-flux research reactors, and flux-wire port reactors. The starting point for in-core testing of MPFDs is at open-pool reactors, both for ease of access and, in one case, for proximity to the sensor fabrication facilities. Two such reactors are test-beds for MPFDs, the Kansas State University (KSU) TRIGA Mk. II research reactor, and the University of Wisconsin Nuclear Reactor (UWNR). Each of these facilities possess specific benefits for the development of MPFDs. The KSU TRIGA Mk. II research reactor has been utilized for MPFD testing since the first prototypes were developed [6]. Access to the reactor facility is simplified by the proximity of the facility to the Semiconductor Materials and Radiological Technologies (S.M.A.R.T.) Laboratory where MPFDs are fabricated. The KSU facility also has three unique irradiation ports that are useful for testing MPFDs under different conditions. First, the central thimble at the KSU reactor facility provides access through a water-filled 1.33-in diameter straight tube to the center of the reactor core. Thermal neutron flux in the central thimble exceeds 10^{13} cm^{-2} s^{-1} [12]. The IRIS test port, located inside the reflector of the KSU TRIGA core is a dry flux port with highly thermalized neutron flux exceeding 10^{11} cm^{-2} s^{-1} [12]. Finally, specially drilled access holes in the top grid-plate of the KSU facility allow for the insertion of small (< 8 mm) closed probes in-between fuel elements, as depicted in Fig. 2.2 [13].

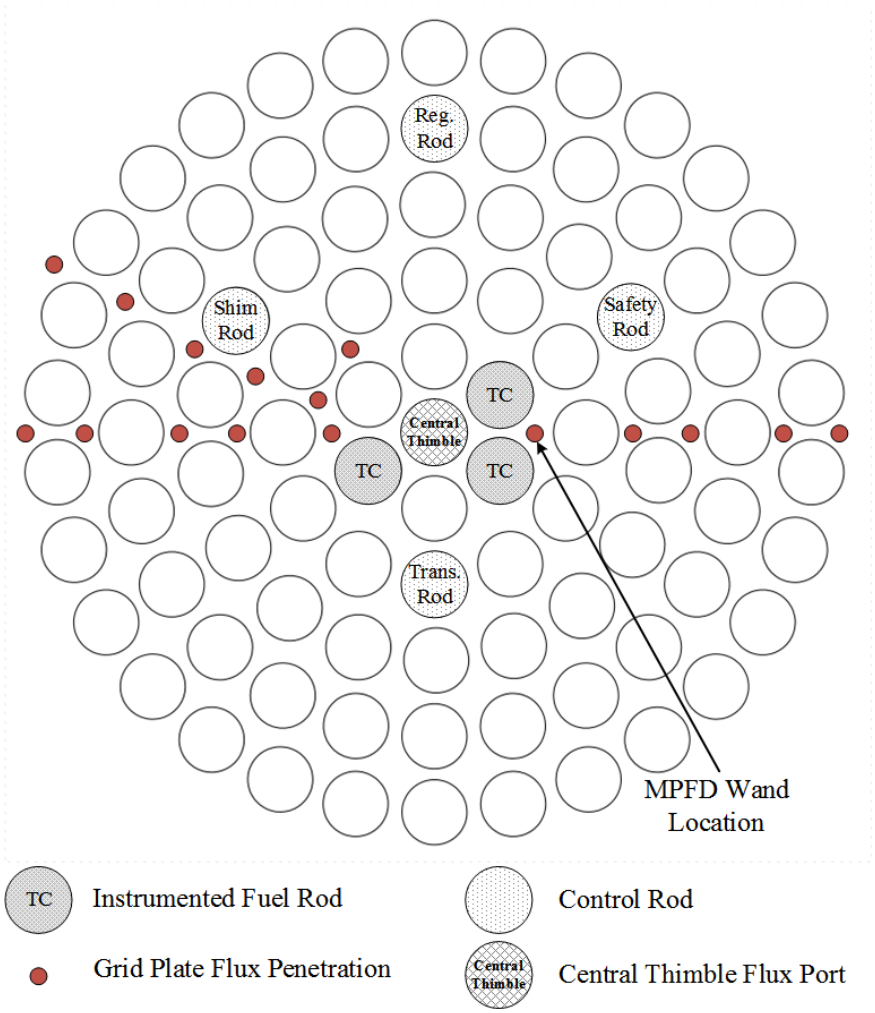

Fig. 2.2 Sixteen flux irradiation ports with 8-mm diameters are located between fuel pins in the KSU TRIGA Mk. II reactor top grid plate [13].

The UWNR facility is attractive for MPFD testing for two reasons. First, the UWNR core has recently been converted with fresh low-enriched fuel. This makes simulation validation simpler than at a facility with significant fuel burn-up. Also, the fuel bundles at the UWNR have ¾-in diameter holes between each bundle, allowing for easy access with encapsulated detector arrays as illustrated in [14]. The UWNR facility, with core configuration shown in Fig. 2.3, also shares the open-pool design that simplifies experimental access.

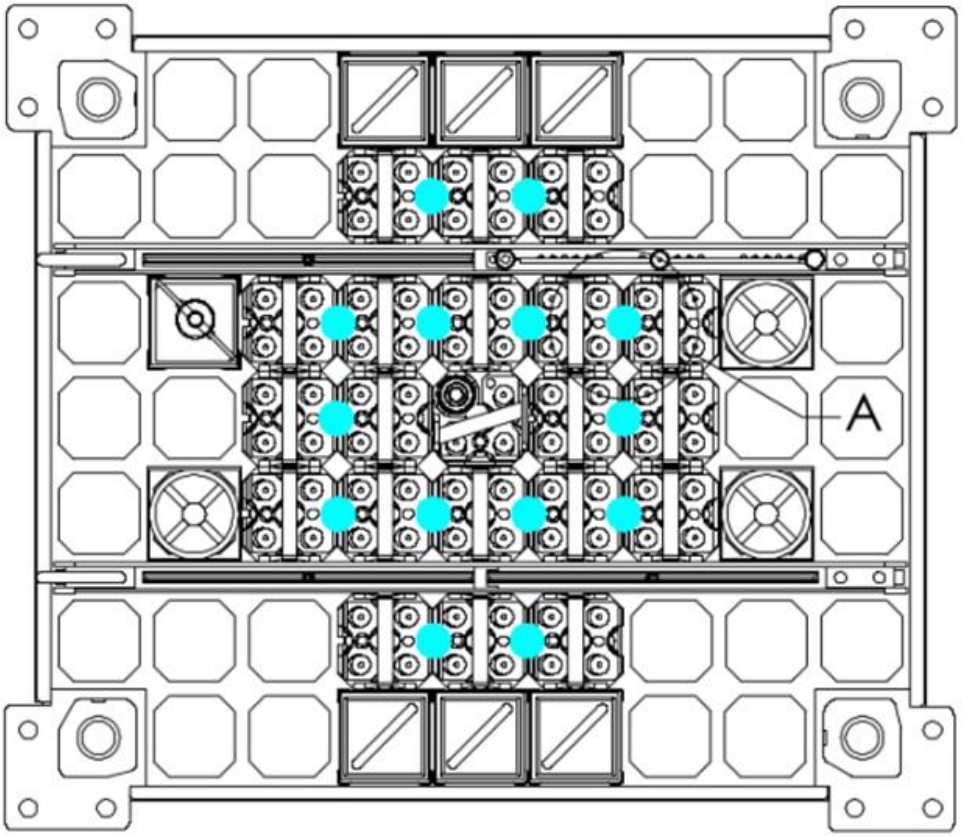

Fig. 2.3 The UWNR reactor core has access locations located between each fuel pin, indicated on the figure with blue markers.

The first two reactor facilities described are located at universities, and are relatively accessible year-round for testing. Two more test reactor facilities, located at Idaho National Laboratory (INL) present additional challenges. First operated in 1959, the Transient REActor Test Facility (TREAT) at Idaho National Laboratory (INL) is capable of executing reactor pulses up to 20 GWth [4, 15]. The TREAT reactor has an air-cooled reactor core composed of 329 regular fuel assemblies with 1.2 m fueled regions containing a dilute graphite/uranium-oxide fuel mixture, depicted in Fig. 2.4 [4].

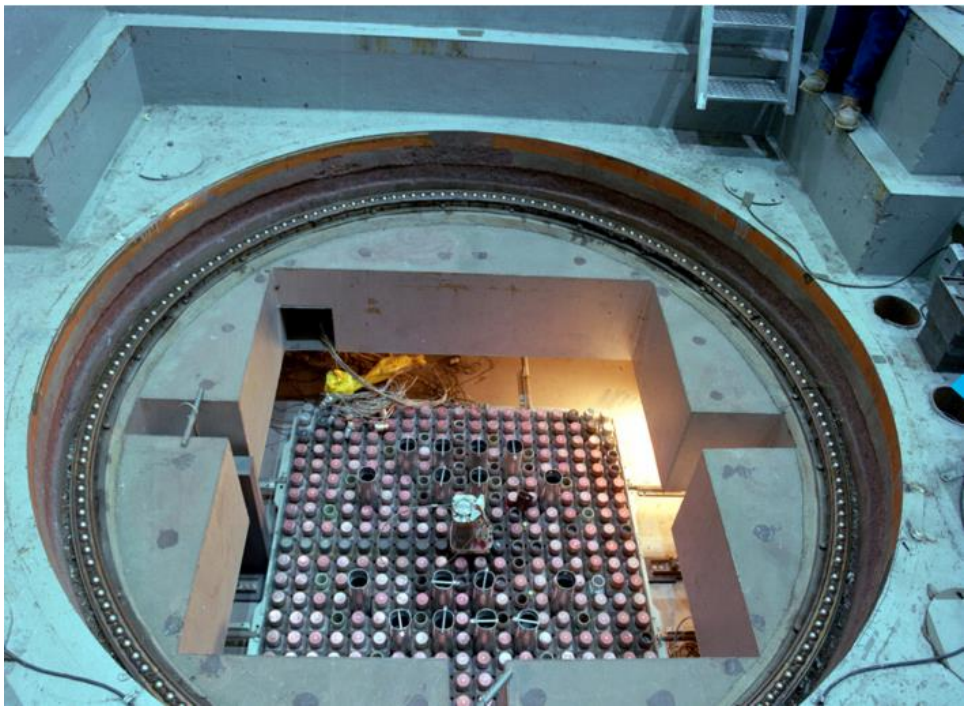

Fig. 2.4 The top view of the TREAT reactor illustrates the unique air-cooled design which is one of many features which differentiates TREAT from other nuclear reactors in the world [15].

Test ports within the core can be used to subject experimental test assemblies to a wide range of conditions, most significantly to extreme transient conditions similar to those experienced during an accidental positive reactivity excursion at a nuclear power facility [15]. The renewed effort to develop accident tolerant fuel has increased interest in restarting the TREAT facility which ceased operations in 1994. Experiments are already being designed to utilize the TREAT facility following the restart, specifically calling for the qualification of MPFDs for active neutron flux monitoring. A determination of the neutron flux during transient experiments is necessary to properly characterize nuclear fuel and materials for advanced reactor designs. The high thermal neutron flux (up to 10^{17} cm^{-2} s^{-1}) during transient experiments at TREAT makes active neutron monitoring exceptionally difficult [4]. The TREAT reactor has the distinct advantage of being air-cooled, greatly simplifying sensor housing design because water is of no concern. However, like other national laboratory reactors, the planning to deploy a test requires years of preparation. Although this preparation helps identify problems with the support systems, it certainly does decrease the frequency with which experiments can be performed by an individual research group.

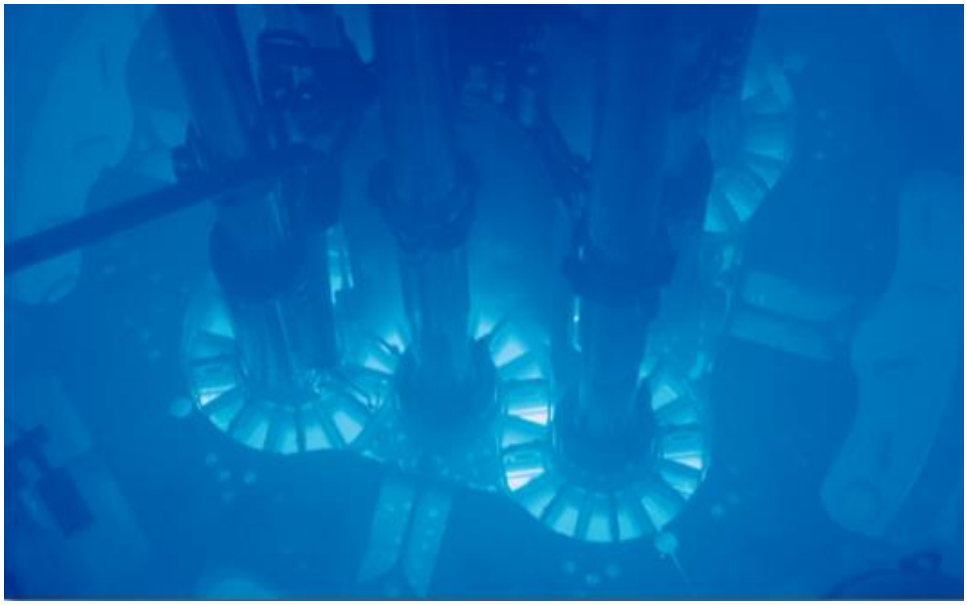

Fig. 2.5 The ATR is used for reactor material irradiation research and is the "only research reactor capable of large-volume, high-flux neutron irradiation experiments" [16].

The Advanced Test Reactor (ATR) is another unique facility where plans for sensor qualification tests are underway. The ATR has 77 highly customizable (with regards to physical conditions of the coolant) irradiation test ports and is capable of producing sustained neutron fluxes with fast/thermal ratios ranging from 0.1 to 1.0 [16]. The unique fuel arrangement depicted in Fig. 2.5 can be used to independently control the neutron flux profile in different regions of the core [16]. The nature of the ATR facility, like many test nuclear reactors, makes access difficult and location of support electronics especially challenging. Originally, ATR facility engineers requested that the MPFD support electronics be located over 60 m from the pressure boundary penetration at the top of the reactor containment. Placing the preamplifier this far from the sensor is not practicable (as will be described later) and fortunately a location within 6 m of the pressure boundary was located during an inspection of the facility.

Most other research reactor facilities do not have the capability of inserting specially designed experimental systems into the reactor core. Iron-wire ports, common to most reactor, can be used to deploy specially designed MPFD arrays [12]. The preliminary development and testing of these specialized MPFDs was the focus of previous work [12], but also contributed significantly to the present work, and will therefore be reviewed in detail. The flux-wire ports of interest present even more challenges than the aforementioned reactors due to their small size, and the necessity to thread the MPFD array far (> 6 m) into a blind metal tube. Similar to the ATR, these facilities have

restricted access. Common to all reactor facilities is the challenge of designing and locating the MPFD support electronics to reduce problems with various sources of electronic noise while providing appropriate radiation shielding.

2.2.3 Measurement Device Coupling and Support System

The support electronics are an integral part of any radiation detection system. Like other pulse-mode fission chambers, MPFDs require a high voltage power supply (HVPS), preamplifier, shaping amplifier, discriminator, and a means by which to count the pulses [2]. The HVPS, shaping amplifier, discriminator, and scalar/counter systems will be described in detail in Ch. 5.3 however the preamplifier (which will also be discussed further) is of particular interest.

MPFDs measure charge created by ionization within the detector [2]. The charge deposited in the gas chamber of an MPFD is small, however, and intermediate amplification is necessary. A charge-sensitive preamplifier is used for MPFDs, which provides limited pulse shaping to the output and is mainly used to couple to other pulse-processing electronics. The fast rise-time of the preamplifier output depends predominantly on the charge collection time of the sensor, while a long (50 to 100 μs) decay time allows for full charge collection [2]. The amplitude of the electronic noise, a strong function of input capacitance, is one important characteristic of a preamplifier [2]. Increasing input capacitance increases the inherent noise in the preamplifier, which can distort the signal. The MPFD chamber, being a small gas chamber separating two wires, has low capacitance. However, the signal cable which connects the MPFD sensor to the preamplifier adds capacitance linearly with distance.

Consequently, a convention is to place the preamplifier as close as possible to the neutron sensor to minimize noise induced by line capacitance in the signal cable. There are two reasons that MPFD preamplifiers cannot usually be placed closer than ≈ 6 m from the sensor. First, most preamplifiers are not water-proof, thereby making the water moderator surrounding an open-pool nuclear reactor problematic. However even for reactors that do not use water as a moderator, the high radiation fields near the reactor core would destroy the preamplifier. Therefore, the minimum distance between the MPFD sensor and the preamplifier in most cases is nearly 6 m. Specifying electrical signal cabling that is both well-shielded and low-capacitance has proven to be an important step in maximizing the MPFD signal and increasing the signal-to-noise ratio for MPFD systems. Often times however, an experimenter does not have the freedom to choose every

component of the support system. At the ATR facility, engineers design and specify cabling and pressure boundary penetrations for all of the instrumentation systems. In this case, it is important to communicate with the design engineer the importance of isolating the MPFD signal cable to prevent cross-talk to/from other systems, to use low-capacitance cabling, and to locate the preamplifier as close to the pressure boundary as possible. Signal wire isolation and shielding is important at nuclear reactor facilities to reduce noise. Background electronic noise at reactor facilities is notoriously bad. Cooling systems with large mechanical pumps, electronic valves, ground loops, and RF interference are all sources of significant noise. The age of nuclear reactor facilities also means that numerous changes have been made to the original configuration of the electrical system for the facility, which was also not engineered to modern standards. Finally, most experimental facilities request that control electronics be placed hundreds of feet from the experiment in order to reduce the likelihood that any accidents occur, and to eliminate the need to work in a radiation environment to operate the detector system. Fortunately, the electronics support system can be designed in such a way to accommodate most of the requests of the reactor facility and still yield a strong signal for remote operation of the MPFD system.

With limited space available near the experiment location for most MPFD tests, the design of custom electronic hardware enables sensor support without interfering with the requests of facility managers. First, multiple components can be combined into an integrated solution, reducing the overall size of the support system. Typical experimental electronics configurations utilize large, single-channel units with adjustable settings. These units are useful during the development phase where sensor parameters change frequently. However, once the electronics are properly configured, these components can be built in such a way that takes up significantly less space. Additionally, multi-channel support can be incorporated, once again reducing the physical dimensions of the system. Finally, some signal processing can take place remotely. The selection of components which can be controlled remotely meets the facility needs while still allowing the experimenter to adjust the electronics unit as necessary. Pulse counting and experiment monitoring can also be performed remotely if the output signal from the electronics unit is tailored to travel such distances. All of these methods were used to design an MPFD integrated electronic support system (described in Ch. 5.3) that can be located close to the experiment, but that can also be controlled and monitored remotely.

2.3 Common Methods of Determining In-Core Flux

The need to measure neutrons within the core of a nuclear reactor is a mature problem. Information about the spatial variation of the neutron flux in a reactor core is often needed to properly understand the power distribution within the reactor [2]. Typical geometric constraints and operating conditions however limit the applicability of most ex-core detectors [2].

2.3.1 Common In/Near-Core Neutron Detectors

Fission chambers are common ex-core neutron detectors for nuclear reactor applications. Constructed by coating a thin layer of fissile material on the inner wall of an ion-chamber, fission chambers utilize the high energy deposition of fission fragments to measure neutron flux [2]. However, the high specific energy deposition, and relatively small neutron fission cross-section of the fissile material (compared to He^3 or B^{10}), limit the efficiency of common fission chambers to < 1% [2]. Many fission chambers are several centimeters in diameter and in length and are filled with pressurized ionization gas to maximize fission-fragment energy deposition. The fissile material utilized for common fission chambers (enriched uranium) suffers from signal degradation due to burnup and causes significant detector dead-time at moderate neutron flux levels. The large physical size of common fission chambers limits their deployment to ex-core locations. Therefore, interior flux estimates can only be made by applying empirical or calculated correction factors to the measurements made from external detectors. In order to overcome dead-time observed in pulse-mode operation, fission chambers can be operated in current mode. Current-mode operation does expand the operational range of fission chambers, but they still are not able to provide the spatial resolution desired for in-core measurements. They also perturb the local neutron flux due to the large neutron-absorption cross section of the fissile coating.

Prompt Self-Powered Neutron Detectors (SPNDs) were possibly the most promising existing technology in regard to real-time, in-core neutron flux measurement. One landmark study examined the performance of hafnium and gadolinium SPNDs in the Transient Test Reactor (TREAT) reactor at the Idaho National Laboratory (INL, previously known as Argonne National Laboratory-West, ANL-W) [4]. The (n, γ) reactions from neutron absorption in Hf and Gd are utilized as emitters in prompt SPNDs, depicted in Fig. 2.6. The prompt gamma rays subsequently interact in the emitter material, primarily by internal conversion, Compton scattering, and

photoelectric absorption, producing free electrons [4]. By connecting a pico-ammeter to the SPND extension cable, this small amount of current can be measured and equated to a particular neutron flux after sensor calibration.

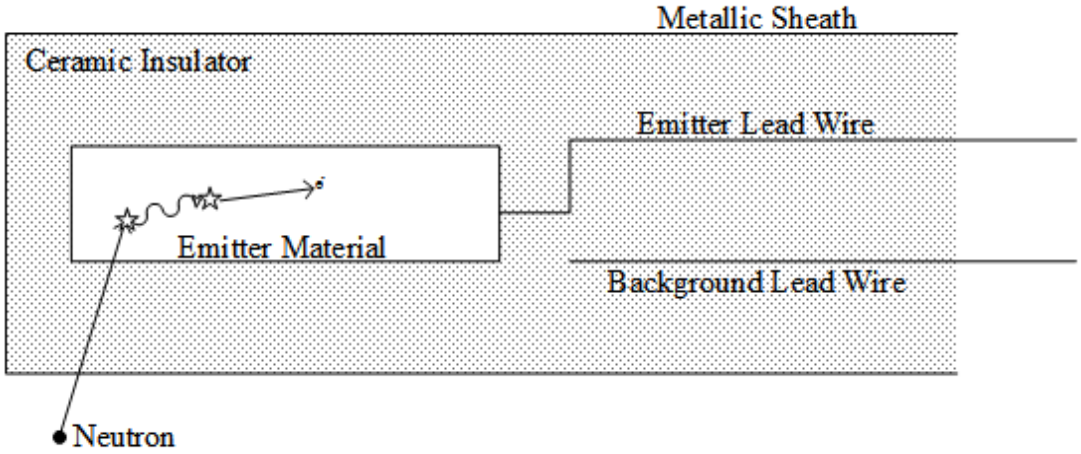

Fig. 2.6 SPNDs are constructed of robust materials, utilizing elements with large neutron-absorption cross sections [4].

Prompt SPNDs were successfully calibrated and tested at the TREAT facility, measuring the FWHM of reactor pulses as 113 ms, compared to external monitors which yielded pulse FWHM of 137 ms, as shown in Fig. 2.7 [4]. The study concluded signal contribution from delayed gamma rays in the external gamma-ray monitors broaden the peak signal in those sensors, and that the pulse FWHM measured using SPNDs was a more accurate representation of the in-core neutron flux [4]. Although SPNDs have many advantages, robust materials, simple construction, wide operational range to name a few, there exists one important flaw. Like most neutron detectors, SPNDs do not directly measure neutrons, moreover, SPNDs do no not directly measure the immediate product of a neutron interaction (the prompt gamma ray in this case). Instead, SPNDs measure the tertiary particle (the free electrons) produced by interactions from the secondary reaction products. The number of prompt gamma rays present in the reactor core during operation is much greater than that number produced by interactions in the emitter material. These gamma rays from alternate sources interact in the lead wire, sheath, emitter, and background lead wire indiscriminately. Truly the background lead wire can be used to subtract those interactions which occur in the lead wire, however previous studies have determined that the signal contribution from external sources (i.e. not from the emitter) can be as high as 50% of the total current for hafnium SPNDs [17]. These prompt gamma rays are also proportional to the neutron flux [18]. However,

prompt gamma rays can originate from throughout the reactor core and still contribute to the signal in an SPND, making these sensors ineffective for the spatially dependent measurement of neutron flux and near reflector regions of the reactor. Small fission chambers have been constructed however which do measure the reactions products from fission in the nuclear reactor core. One such detector, the back-to-back fission chamber, was utilized to calibrate SPNDs [4].

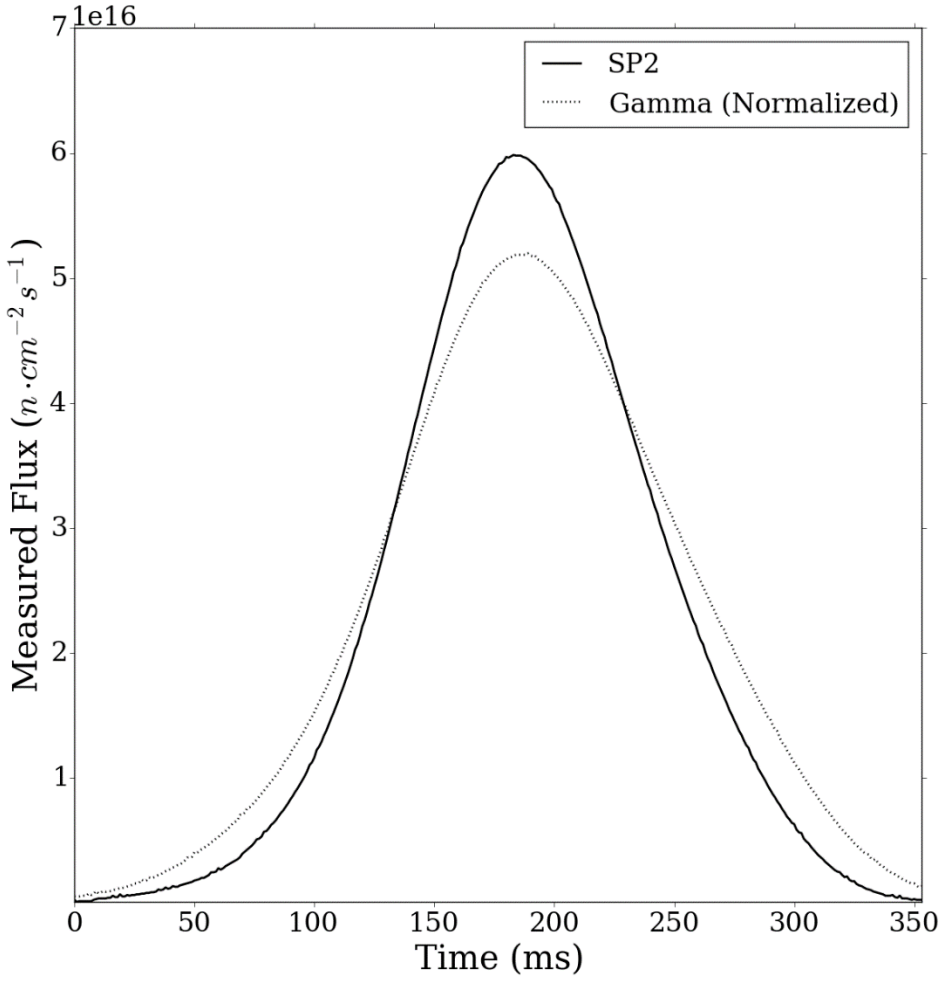

Fig. 2.7 SPNDs yielded more accurate neutron flux measurements than external gamma-ray detectors (figure reproduced with permission) [4].

Back-to-back fission chambers can be used to measure the absolute neutron flux in research nuclear reactors at low powers. Bisecting an aluminum sphere and inserting two enriched uranium-electroplated steel discs creates two hemi-spherical chambers. The two conducting planes are isolated and P-10 gas (a mixture of 90% argon and 10% methane), a common ionization gas, is supplied into the chambers. Ionization of the P-10 gas from fission fragments can be measured by

applying an electric potential between the two aluminum hemispheres and the steel disks [4]. Back-to-back fission chambers are commonly operated in current-mode for nuclear reactor testing, even at low power. Therefore, back-to-back fission chambers suffer from signal contribution from gamma-ray interactions, and consequently their signals must be compensated.

Similarly, sub-miniature fission chambers (SMFCs) have also been developed for in-core neutron flux measurements [5]. The coaxial design of SMFCs enables charge multiplication, enhancing the signal produced by fission-fragments, emitted by the fissile material coating (typically enriched uranium) on the anode or cathode wall, in the ionization gas as depicted in Fig. 2.8 [5]. Even with this enhancement however, SMFCs must compensate for the radiation-induced signal in the metal components of the sensor as well as the gamma-ray contribution in the sensitive region of the sensor [5]. Operated in current mode, SMFCs can be utilized for in-core neutron measurements for thermal-neutron fluxes as high as 4×10^{14} cm^{-2} s^{-1} [5].

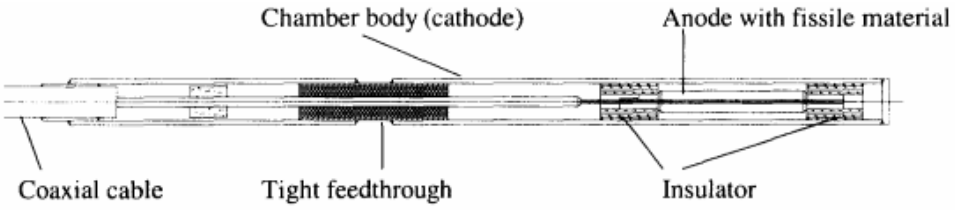

Fig. 2.8 SMFCs utilize a coaxial design to enhance the neutron-induced signal [5].

One significant disadvantage of SPNDs, back-to-back fission chambers, and SMFCs alike is the utilization of materials with large neutron absorption cross sections. In the case of reactor flux mapping, each of these earlier technologies could be used to measure the local neutron flux without significantly affecting the reactivity of the reactor, however large arrays of these devices would have a more meaningful effect. For material experiments, the neutron flux close to the sample is of greatest interest. Use of a sensor with a large neutron-absorption cross section reduces the neutron flux in the experiment by absorbing neutrons in the immediate vicinity of the experiment (flux depression). Compounding these disadvantages with the experimental uncertainty of current-mode operation has reduced the application of such detectors a small sub-set of reactor experiments.

2.3.2 Neutron Fluence Measurement Methods

The most common alternative mode to determine thermal neutron flux for nuclear reactor experiments is to use a neutron-fluence measurement to calculate the average flux. Materials used to measure neutron fluence by the radioactivity induced in the material by a neutron flux are commonly referred to as activation foils. The mass of such activation foils is commonly small because of the large neutron-absorption cross sections of the materials, thereby reducing the flux perturbation near the experiment and reducing the effects of self-absorption. The saturation activity of a sample can be described as A_∞ in Eq. 1 and Eq. 2. The neutron flux, φ(E), can be calculated by combining Eq. 1 and Eq. 2. into Eq. 3. Commonly approximations of $\sigma(E)_a$ are made such that a single value, $\bar{\sigma}_a$, can be applied broadly to a wider range of neutron energies. Therefore, in order to determine the average neutron flux, $\bar{\varphi}$, the average neutron-absorption cross section, $\bar{\sigma}_a$, number of sample atoms, N_d, decay constant, λ, irradiation time, t_1, transit time, t_2, and measurement time, t_3, detector efficiency, ϵ, and branching ratio of the measured decay, f, must all be known. Then, a measurement of gross counts from the activated sample (C) and background (B) can be used to calculate φ using Eq. 3 [2].

$$\boldsymbol{A_\infty = N_d \bar{\varphi}_t \bar{\sigma}_a}, \tag{1}$$

$$\boldsymbol{A_\infty = \frac{\lambda(C-B)}{f\epsilon\left(e^{\lambda t_1}-1\right)\left(e^{-\lambda t_2}-e^{-\lambda t_3}\right)}}, \tag{2}$$

$$\boldsymbol{\bar{\varphi}_t = \frac{\lambda(C-B)}{f\epsilon\left(e^{\lambda t_1}-1\right)\left(e^{-\lambda t_2}-e^{-\lambda t_3}\right)\bar{\sigma}_a N_d}}. \tag{3}$$

The measured activity of a hypothetical activated sample is depicted in Fig. 2.9. Activation foils are commonly used to characterize reactor core neutron fluxes in a steady-state condition, for instance measuring the axial thermal-neutron-flux distribution in the central thimble of the KSU TRIGA Mk. II nuclear reactor [12] or for sensor calibration at nuclear reactor facilities [4]. Although this method does provide a measurement of the total neutron fluence experienced by a sample, only the time averaged neutron flux can be determined. Additional correction factors must be considered for non-1/v absorption, the use of cadmium filters, flux perturbation, and self-shielding [19]. For many advanced test nuclear reactor experiments, the time-dependent neutron flux is desired.

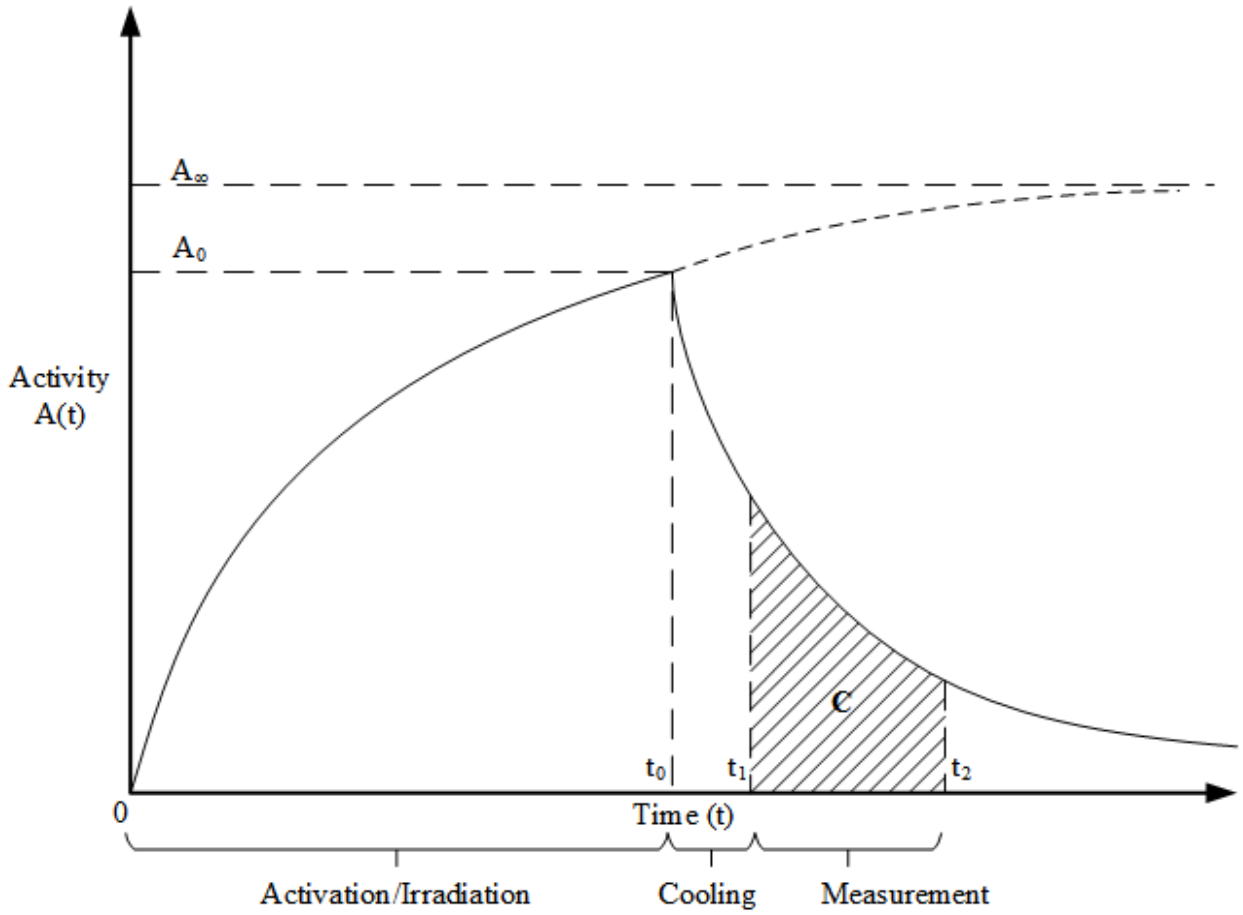

Fig. 2.9 The activity of a sample between times t_1 and t_2 can be used to calculate the average thermal neutron flux to which the activation foil was exposed.

2.3.3 Typical Experimental Calibration Procedures

The extreme neutron flux in experimental nuclear reactors (in excess of 10^{17} thermal $cm^{-2}s^{-1}$ at TREAT) makes most traditional methods of neutron monitoring impossible [4]. Extensive efforts have been made to relate measurements from ex-core instruments (commonly BF_3 or ^3He detectors [2]) to the in-core fission rate. The inferred value from these correlations is referred to as the 'power coupling factor' [4]. Most of the experimental time at the TREAT facility is spent conducting pre-experiments to determine power coupling factors in the following manner [20]:

1. Ex-core ion chambers are calibrated by operating the reactor at steady state with a mockup of the experiment in the reactor.
2. The experimental test pin is irradiated under steady state reactor conditions in the mockup and chemical analysis is used to determine the fission rate and average power coupling factor for the test pin.

3. A fluence monitoring wire is then irradiated in the same conditions as the test pin and the subsequent fission rate is found chemically to determine the power coupling factor between the fluence wire and test pin.
4. A final fluence monitoring wire is irradiated with the mockup under transient conditions equal to those planned for the experiment. The 'transient correction factor' is applied to adjust for the effects of high neutron flux and heat over short transients in comparison to lower neutron flux over longer steady-state operation in previous steps. All of the previous factors: power coupling, relative power coupling, & transient correction are combined to determine the final power coupling factor for the experiment.

Using this calibration method, in-core dosimetry deployed alongside the experiment, and ex-core active flux monitors, the total fluence and average flux for a transient can be estimated [20]. However, the aforementioned methods necessarily neglect the time-dependent effects of the high-flux transients that are the unique feature of these test nuclear reactors [4]. In addition to the expected ramp-up and -down of neutron flux by pulsing, effects of control-rod motion and temperature are also neglected. With advances of nuclear reactor modeling and simulation, along with the restart of the TREAT facility, great interest exists for the development of real-time neutron flux sensors that can capture this data. Such a device would provide superior data for researchers and decrease the amount of time required for each nuclear reactor experiment.

Chapter 3 Micro-Pocket Fission Detector (MPFD) Device Design

The original conception of the micro-pocket fission detector was a proof-of-concept for the deviation from traditional fission chambers [6, 21]. However, the fabrication methods used for early permutations of MPFDs proved challenging to implement and standardize [13]. The improvements discussed herein benefit from advances in material science, improved electronic capabilities, and innovative new approaches to solve fabrication and deployment problems encountered in the past. However, the fundamental physics that make MPFDs possible remain unchanged from previous studies. Like previous designs, the prominent design feature of MPFDs is their small size. This feature has been taken to a new extreme with the smallest fission-chamber detectors discussed herein [9]. Radiation-hard materials are still used for the detector substrate, and a thin coating of neutron-reactive material is used to convert neutrons into fission-fragments which are detected by an electric field applied between two electrodes separated by a small gas chamber. While previous studies of MPFDs have resulted in complex solutions to the difficult problem of manufacturing and deploying these exceptionally small radiation detectors, the present work made great effort to refine the design to produce a simple sensor that could be easily constructed. The following sections will describe the basic design features of MPFDs, significant improvements to the design, and various aspects of the sensor response in the presence of neutrons.

3.1 Basic Operating Principles of MPFDs

Like traditional fission chambers, MPFDs rely on the conversion of neutrons in a fissile coating. The fission fragments, which are emitted by the neutron-sensitive coating upon fission, ionize gas situated between two electrodes, a bias applied between the electrodes causes the electrons and ions in the gas to move, inducing a current in the anode and cathode which can be measured [2]. Sharing ≈200 MeV, the fission fragments (only one of which enters into the ionization chamber) deposit energy into the fission-chamber gas, causing most traditional fission chambers to be relatively insensitive to non-neutron radiation in low flux environments. However, when fission chambers are used in high-flux environments (specifically near-core and in-core) compensation for the gamma-ray-induced signal is required [2]. For this reason, it is common to use fission chambers as a power-monitoring device for near-core neutron flux measurements, but

in-core solutions are less common. The large specific energy deposition of fission fragments is precisely what makes the small size of MPFDs possible [6]. While traditional fission chambers attempt to capture all of the energy of the fission fragments by using large gas chambers, or high ionization gas pressure to discriminate background gamma-ray interactions, MPFDs minimize the size of the ionization chamber to reduce gamma-ray signal contribution. The highly energetic fission fragments deposit large amounts of energy into small chambers while gamma-ray and other particle interactions deposit relatively little energy [6]. MPFDs are also constructed of radiation hard, temperature resistant materials enabling deployment at nuclear test reactors which operate well beyond the typical parameters of power reactors [6].

3.2 Modern MPFD Design Enhancements

The specific design of MPFDs has changed over the years and an in-depth discussion of previous research can be found elsewhere [22]. Previous research culminated in the design of the "MPFD^3-T" design, depicted in Fig. 3.1. The MPFD^3-T sensors were constructed of a 96% alumina substrate material which had holes machined into it to allow for the passage of wires, 3 MPFD chambers, and two gas reservoirs. These sensors were eventually constructed and tested at the KSU TRIGA Mk. II research nuclear reactor, yielding linear power tracking up to 200 kWth where significant dead-time was observed.

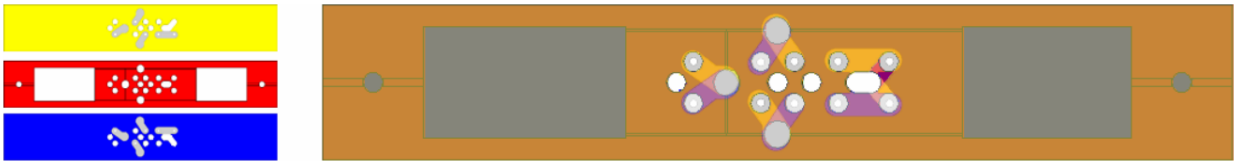

Fig. 3.1 Previous designs utilized a complex system of overlays and gas channels to deploy three-chambers in a single device [22].

Two designs exist for the modern MPFD, both of which utilize advances in the design which make them more robust and simpler to construct than previous designs. The first is a sensor which was specifically designed to fit into small flux-wire ports at research reactors [12]. The development of these detectors, the smallest fission chambers ever constructed, is ongoing and will be the topic of further discussion. In addition to the size difference depicted in Fig. 3.2, two other distinctions can be made between the modern MPFD and previous iterations. First, modern

MPFDs utilized a loose-assembly which allows ionization gas to flow into and out of the active chamber and removes the need for ceramic bonding, a significant improvement from past designs. Secondly, a multi-wire design has been developed which allows the neutron-reactive material to be coated on various different faces within the MPFD, and which removes the need to over-coat the fissile layer with a conductive electrode as was suggested in the past [22]. The multi-wire design also enhances the electric field near the electrodes, improving the electrical response of the sensor.

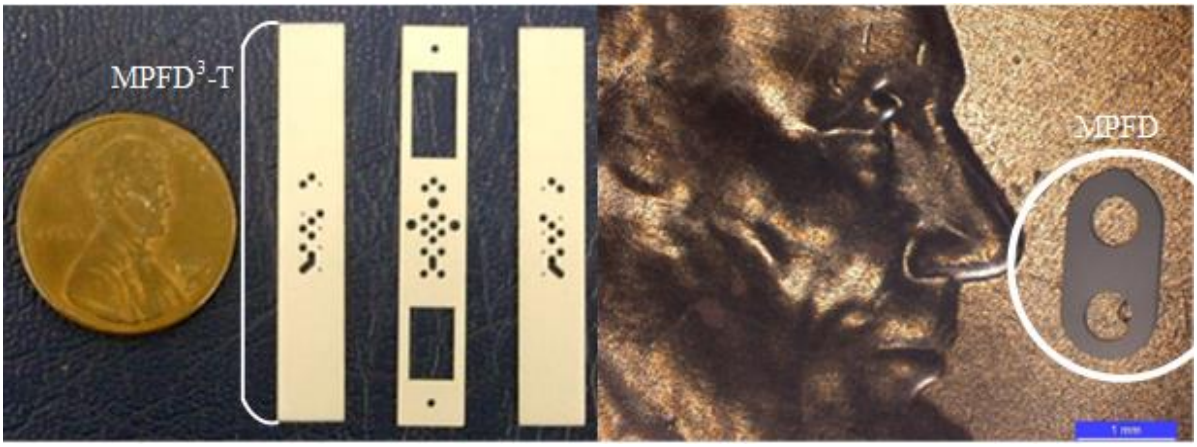

Fig. 3.2 The MPFD^3-T design (left) was large in comparison to the smallest MPFDs produced to date (right) [22].

The smallest version of MPFDs are constructed from three pieces of alumina which are threaded onto electrode wires as illustrated in Fig. 3.3. Like other MPFD designs, neutron-sensitive material is deposited between the anode and cathode to convert neutrons into fission fragments. The gas chamber in the smallest of the MPFDs constructed are as small as 0.5 mm tall with a fissile coating only 1/3 mm^2. The methods developed to deposit uranium and thorium onto these small metal electrodes is discussed in greater detail in Ch. 4.4. The anode and cathode wires extend to the top of the reactor test port and connect to readout electronics. The first deployment of such small MPFDs was reported in 2015 [9]. Furthermore, a common cathode design can be utilized to construct these small MPFD sensors into arrays which can also fit into limited space, particularly flux wire ports at nuclear reactor facilities. Arrays of such devices can be used to measure the neutron flux at different axial locations within the reactor core simultaneously. Preliminary construction of such multi-nodal MPFD arrays is the topic of continued research, and has been refined as discussed in Ch. 6.3.

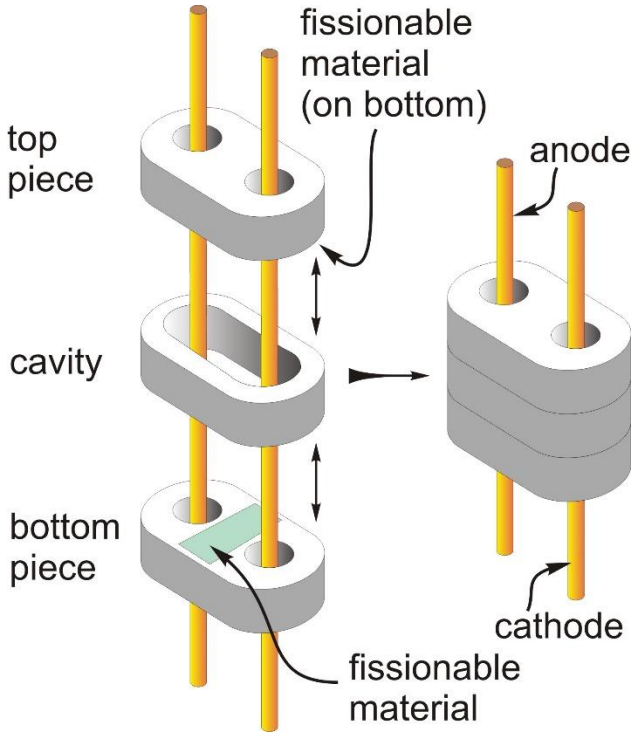

Fig. 3.3 Advances in the MPFD design allow the sensors to be constructed smaller than previously possible without the use of any adhesives.

There are many particularly difficult challenges to overcome with the fabrication of such small fission chambers. A larger MPFD, depicted in Fig. 3.4, is also being designed to fill the need of research reactors. The larger design shares many of the advantages of the small design (loose assembly, multi-wire, relatively small size, and radiation hard materials) and is being deployed as part of several irradiation experiments at nuclear test facilities where the magnitude of the neutron flux near a test sample is to be measured. The design is also being adapted to support a modular MPFD wand to be deployed in transient testing at the UWNR and TREAT facilities as depicted in Fig. 3.4. The modular MPFD array consists of 4 sensor regions, or nodes. Each node is separated by SiO_2 insulated alumel wire. Additional insulated wire extends the full length of the array, out of the high gamma/neutron flux operating environment. The configuration is inserted into a 5/16 x 0.020-in diameter stainless steel tube with a welded cap. A vacuum/gas fill system installed near the top of the module allows ionization gas to be added to the array. Finally, the array is sealed with a water-tight plug which couples the module to an extension cable and subsequently to the electronics system.

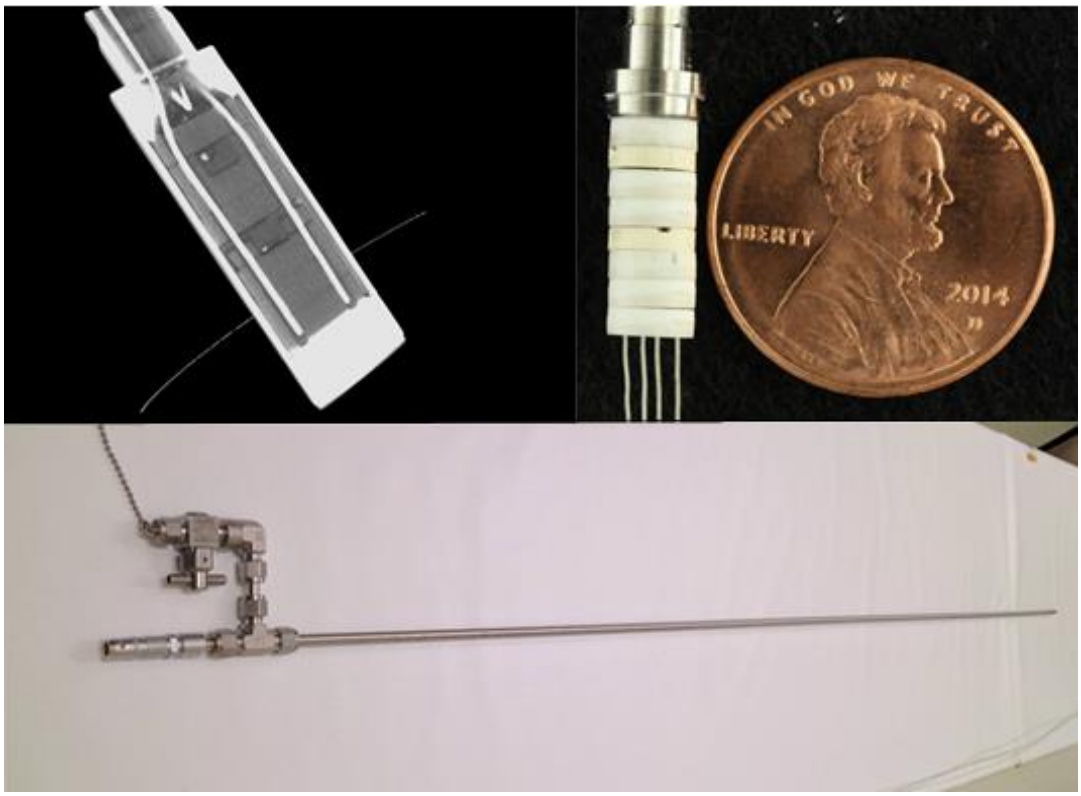

Fig. 3.4 The larger MPFD design is being developed for experiments which will deploy arrays of MPFDs to measure neutron flux near an experimental sample (top) and for larger modular wands (bottom) to be deployed throughout research reactor cores.

Although the various MPFD designs are planned for deployment at different reactor facilities, and in different test ports, they all must capitalize on the intrinsic gamma-ray insensitivity that is characteristic of MPFDs.

3.3 Simulated Gamma-Ray and Beta-Particle Sensitivity

Radiation fields within the core of a nuclear reactor can reach high levels [1]. Previous studies have shown the superior gamma-ray discrimination ability of MPFDs in the presence of high radiation fields [6]. Although the neutron flux is the desired quantity to measure with MPFDs, the large presence of heavy charged particle, gamma-ray, and beta-particle radiation commonly interfere with in-core neutron measurements [20]. Heavy charged particles are easily shielded from the MPFD sensor by the sheathing material, however energetic gamma rays and beta particles can penetrate the instrument and contaminate the MPFD signal. Discrimination of gamma-ray and beta-particle induced signal is common practice for SPNDs and miniature fission chambers

however the small sensor region of MPFDs greatly reduces the signal contribution from these sources [4-6]. Monte Carlo simulation was previously used to determine the maximum and average energy deposited into MPFD chambers of various thicknesses ranging from 0.25 mm to 25 cm and filled by 1 atm of argon gas. Present designs of MPFDs include ionization chambers ranging from 0.5-mm to 2-mm across, and from 0.5-mm to 1-mm tall. These studies were conducted for gamma rays and beta particles ranging from 5 keV to 10 MeV in energy [22]. The results of the gamma-ray and beta-particle sensitivity study are summarized in Fig. 3.5, where the energy deposition of these particles is compared to the energy deposition of two common fission fragments for MPFD chambers of various thicknesses [22].

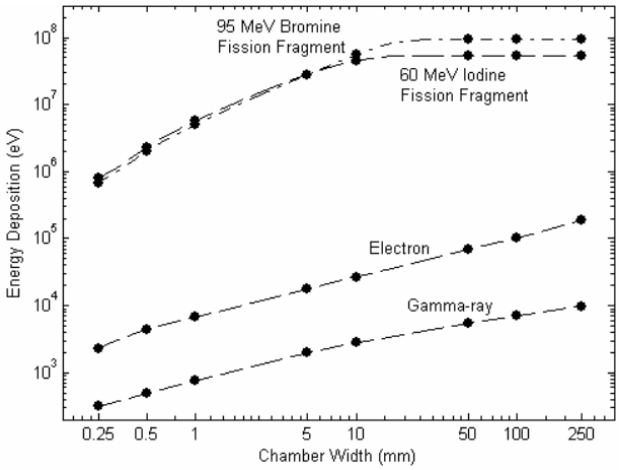

Fig. 3.5 The energy deposited by gamma rays and beta particles is nearly 1000 times less than for a typical fission fragment in MPFD chambers less than 1 cm in thickness [22].

Although each individual interaction contributes little energy, the likelihood of interaction for gamma rays and beta particles is greater in the MPFD chamber than that of the neutrons. The summation of many small events does not produce a pulse but does create a steady current of ionization, resulting in increased electronic noise and baseline signal voltage. This can be discriminated by a differential-mode preamplifier as discussed in Ch. 5.3.2, but must be compensated for when operated in current mode [2].

3.4 Calculated Neutron Response

One of the important qualification tests for MPFDs is scheduled to take place at the TREAT facility as part of the Multi-Static Environment Rodlet Transient Test Apparatus (Multi-SERTTA)

experiment [23]. Simulations were conducted to determine the neutron flux energy profile expected in the Multi-SERTTA experiment module, and subsequent sensitivity of the MPFDs located within [23]. The Multi-SERTTA test assembly will be located in a test train which is inserted into the center of the TREAT as illustrated in Fig. 3.6.

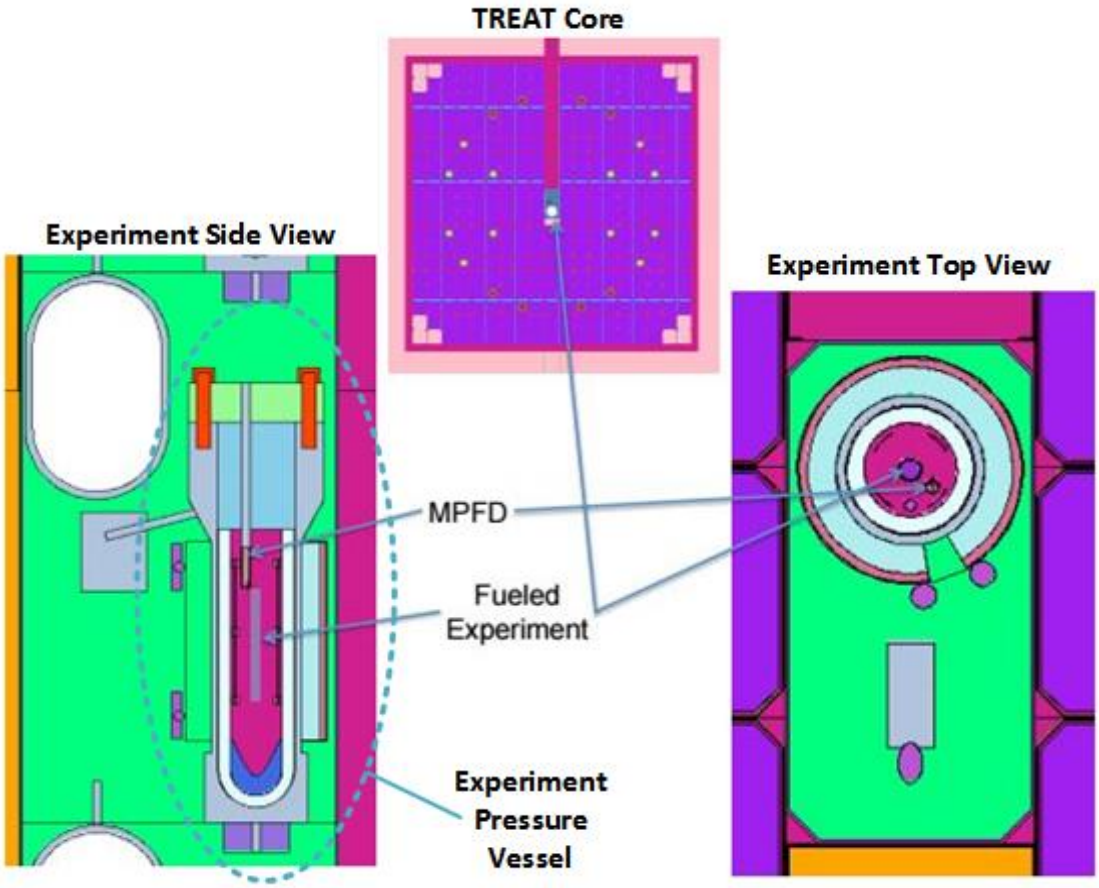

Fig. 3.6 The Multi-SERTTA and included MPFD assembly will be deployed in the central test channel at TREAT [23].

The neutron sensitivity of an MPFD to a particular neutron flux can be found by determining the fission rate in the sensor using Eq. 4. The neutron sensitivity, with units of cm^2, represents the interaction rate of neutrons in the fissile layer of material within an MPFD per unit flux such that the multiple of the detector sensitivity and flux amplitude, with units of $cm^{-2}\ s^{-1}$, yields the expected interaction rate for the detector, with units of s^{-1}. Other factors which affect the eventual count rate of the detector system such as the lower level discriminator setting were not considered when determining detector sensitivity. The detector sensitivity ϵ is represented by dividing the fission rate, e.g., the product of the total fission cross section $\sum_{f,E}$ and energy dependent neutron flux,

$\varphi(E)$, integrated over all energies and fissile layer volume V by the total flux, e.g., energy-integrated neutron flux as follows,

$$\epsilon = \frac{\int \int_{E,V} \Sigma_f \varphi dE dV}{\int_E \varphi dE}, \tag{4}$$

MCNP6 was used to determine these values at 300 K. The neutron sensitivity of MPFDs coated with 300 Å of different fissile material is summarized in Table 3.1 [23]. A KCODE and NPS simulation were both used to determine the neutron flux energy profile for the Multi-SERTTA region within TREAT. As illustrated in Fig. 3.7, the neutron energy profile is highly thermalized in TREAT, increasing the sensitivity of the MPFDs in comparison to other reactors which commonly have a fast to thermal ratio closer to 1.

Table 3.1 MPFD sensitivities in the TREAT core for 300 Å of fissile material [23]

Fissile Material	Simulated Sensitivity (cm^2)
^{242}Pu	7.69E-10 ± 2.31E-11
^{232}Th	1.68E-11 ± 6.93E-13
Natural Uranium	2.85E-09 ± 4.49E-11
93% Enriched ^{235}U	4.05E-07 ± 5.42E-09

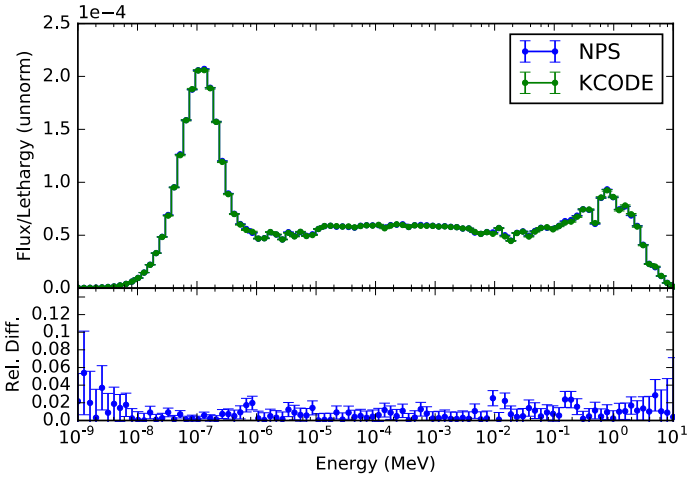

Fig. 3.7 The flux profiles calculated using KCODE and NPS simulation agree well, showing a highly thermalized neutron flux [23].

The resulting sensitivities can be easily used to calculate the interaction rate of the MPFD at different power levels by multiplying the sensitivity reported in Table 3.1 by the magnitude of the total neutron flux expected for a particular power level (or power excursion). For example, at steady-state operation of 50W, a total neutron flux of $\approx 10^8$ cm^{-2} s^{-1} can be expected, resulting in an expected fission rate of ≈ 7 fissions/sec (7×10^{-8} cm^2 * 10^8 cm^{-2} s^{-1}). Likewise, a fission rate of $\approx 7 \times 10^9$ fissions/sec (7×10^{-8} cm^2 * 10^{17} cm^{-2} s^{-1}) can be expected at the peak of a 19 GW pulse at TREAT. These high fission rates do indeed paralyze a pulse-mode operated MPFD [12], however current mode operation is still possible for these high-power transients. The effects of burnup were not considered for the neutron sensitivity of MPFDs in TREAT. However, it is possible to design MPFDs with mixed, or specially enriched coatings which reduce the fluxuation in signal due to fissile material burnup in high-fluence applications [7].

3.5 Simulated Reaction Product Energy Deposition Spectrum

The energy deposition of the fission fragments into the MPFD ionization chamber is also of great interest to confirm the results of previous studies [6]. The MPFDs utilized in the Multi-SERTTA experiments are of the larger variety and therefore have different dimensions from those previously considered. A simulation of the MPFD sensor region for the Multi-SERTTA experiment is illustrated in Fig. 3.8. The anode and cathode wires are separated by 0.20 cm of argon gas at 1 atm. The ionization chamber is 0.20 cm tall, surrounded by alumina on all sides with the exception of a 1-mm thick and 1-mm wide trench which allows for charge extraction via the electrodes. The total ionization by fission fragments within this gas chamber was considered to determine the relative magnitude of the signal pulses (or current at high powers).

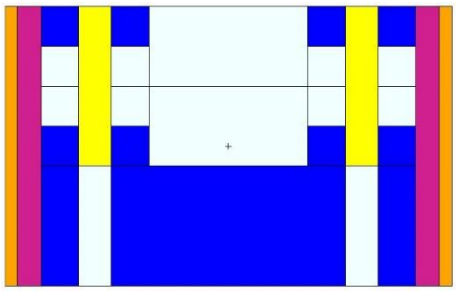

Fig. 3.8 The MPFD model used for the TREAT simulation in MCNP6 is larger than those previously considered [23].

Although former studies showed results for similar simulations in a small (1 mm × 0.5 mm) chamber and a large (30 mm × 30 mm) MPFD chamber, no results were presented for a chamber similar to those to be used in the Multi-SERTTA experiment. For small fission chambers, ≈ 3 MeV average energy deposition is expected [6]. For larger fission chambers the energy deposition can exceed 50 MeV [13]. The average energy deposited by fission fragments for this design fell between the values previously reported at ≈ 13 MeV as shown in Fig. 3.9.

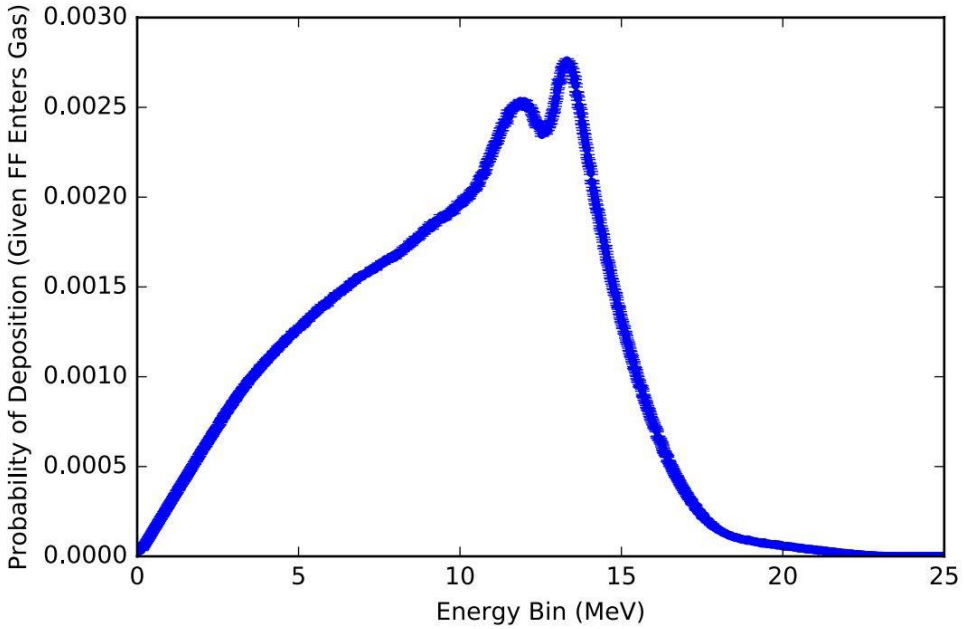

Fig. 3.9 Energy deposition spectrum by fission fragments which enter into the ionization chamber of the Multi-SERTTA MPFD geometry, typical of the larger MPFD, with 300 Å of fissile material [23].

The effect of the fissile coating thickness was also of interest. Even thin coatings of material may attenuate the fission fragments before they are able to escape into the ionization gas because fission fragments have high specific ionization.

3.6 Neutron-Sensitive Coating Optimization

Previous studies have considered the effects of fissile material coating thickness, and even the effect of over-coatings [13]. However, the trend for the Multi-SERTTA MPFDs was desired in order to better understand the response of the MPFDs in the TREAT reactor. Two competing phenomena exist when adding neutron reactive material to the MPFD. As more material is added,

the fission rate increases linearly with mass. However, as the material gets thicker, more fission fragments are attenuated before escaping into the ionization gas. Therefore, an active layer thickness thin enough to minimize the effects of fission fragment attenuation is desired within the reasonable thicknesses that can be deposited. The comparison of ion production rate and fission fragment crossing rate (into the ionization chamber) is illustrated in Fig. 3.10. Although the increase in fission fragment production is linear with material thickness, the crossing rate decreases logarithmically (eventually reaching an asymptotic value not shown [24]). Fissile material coatings < 2500 Å show almost no decrease in crossing rate, while the effect is small even up to 5000 Å (0.5 µm).

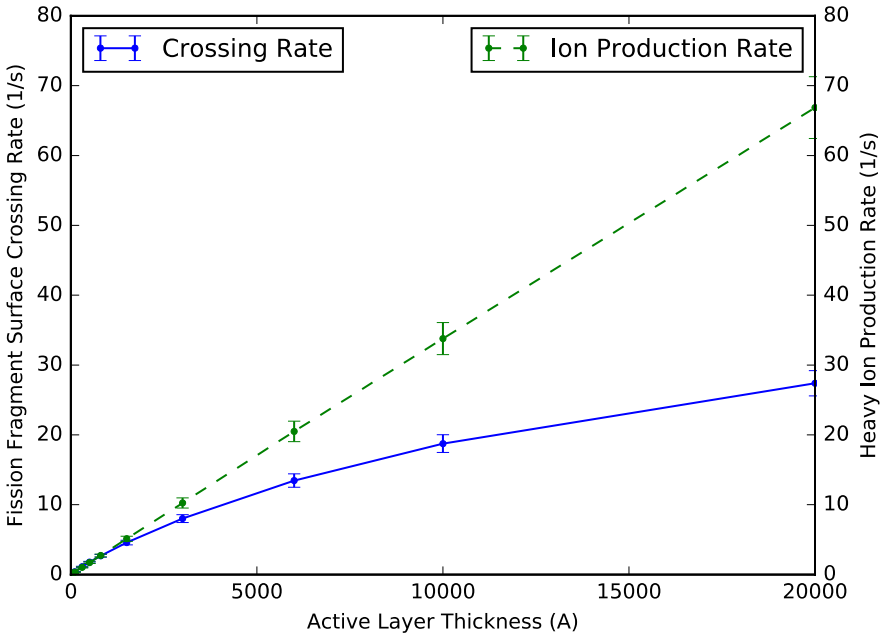

Fig. 3.10 Active material thickness has little effect on the overall MPFD sensitivity for thicknesses < 2500 Å (0.25 µm) [23]

Commonly when such thin layers of material are desired, evaporation or sputtering techniques are used. However due to the radioactive nature of the materials used for the fissile coating of MPFDs, no such system is available. Therefore, electrolysis is a common method of depositing uranium and transuranic elements onto metallic surfaces. Previous research investigated method of electrolysis [22], and still other groups have successfully deposited thick layers of such materials onto metallic substrates [25]. The methods previously used for MPFD manufacture were difficult

to reproduce, and required a complex electrolysis system [22]. A new method of electrodeposition which could accommodate the small electrodes for the most modern MPFDs, and which was highly characterizable was developed [8].

MPFDs typically require fissile coatings with a thickness < 350 µg cm^{-2} onto substrates which can be < 1.0 mm^2 in total area. A specialized electrodeposition cell was developed which allows a conductive probe to be carefully maneuvered to make contact with the small sample working electrode on the MPFD sample, illustrated in Fig. 3.11 [8]. Uranyl nitrate hexahydrate (99.9%) and thorium nitrate hydrate (99.8%) were each used for electrolytic solution sources for electrodeposition. A 0.02 M solution was prepared and cyclic voltammetry was used to deposit precise amounts of neutron reactive material onto the small platinum electrodes [8]. The deposition was confirmed by visual inspection, SEM, and XRF analysis. Then alpha particle spectrometry was used to determine the final coating mass. The electrodeposition process is described in further detail in Ch. 4.4, however an example substrate with uranium electrodeposition is depicted in Fig. 3.12 [7].

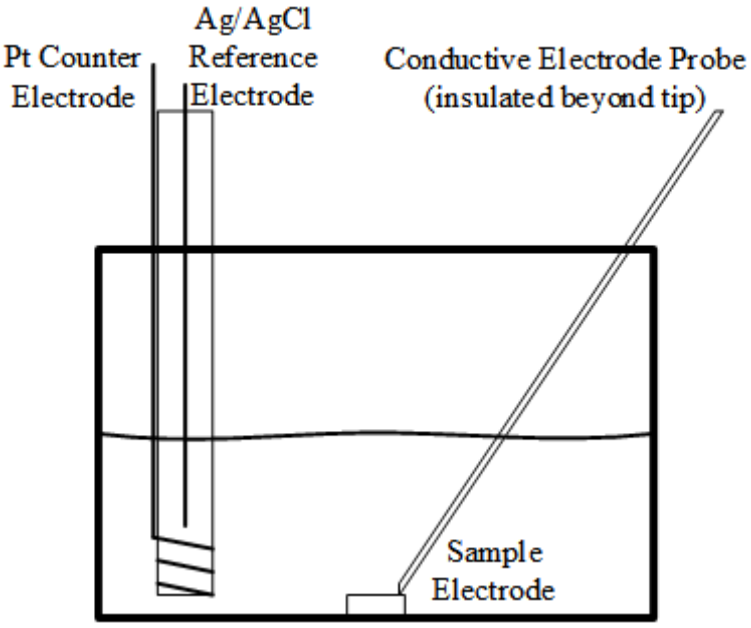

Fig. 3.11 The reference electrode and counter electrode were held stationary while the conductive probe was positioned to make contact with the working electrode.

Fission chambers are typically equipped with fissile coatings of highly enriched ^{235}U [2]. The large neutron absorption cross section of ^{235}U provides high interaction rates, but also quickly depletes in a high neutron flux [26]. Most fission chambers become 10% less sensitive to neutrons

after a fluence of only 1.5×10^{20} cm^{-2} in a typical light water reactor [26]. The stable lifetime of a fission chamber can be extended by reducing the enrichment of uranium and adding a breeding material. Previous studies have shown by a first order approximation that a mixture of natural uranium and thorium can be used to extend stable device lifetime [22, 27]. The lifetime calculation was performed by solving the series of linear differential equations generated by the decay, fission, and transmutation of 17 fertile and fissile isotopes and concluded that an optimal mixture of 23.6% ^{232}Th and 76.4% natural uranium should be used to maximize stable device lifetime in a TRIGA reactor [27]. However, the first order approximation greatly underestimated the effects of epithermal neutron absorption and subsequent transmutation of ^{238}U and ^{232}Th. Therefore, a more accurate calculation was needed.

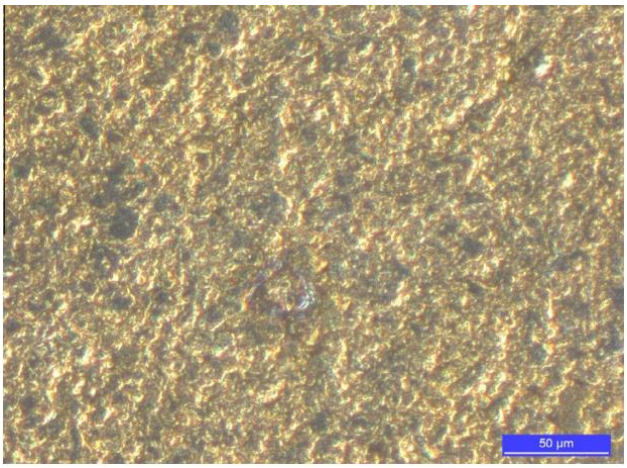

Fig. 3.12 The uranium electrodeposition can be distinguished by the yellow color by using optical microscopy.

First, the neutron energy spectra for both a PWR and TRIGA reactor were generated with ORIGEN-S [28]. The difference in the neutron energy spectra is visible in Fig. 3.13, where the TRIGA flux has a larger Maxwellian thermal energy peak compared to the PWR spectrum [7]. The small dimensions of the MPFD allow for the fissile coating to be treated as infinitely dilute, negating any effects of spatial or energy self-shielding. Therefore, the time-dependent signal of the MPFD can be determined specific to a particular neutron energy spectrum [7]. ORIGIN-S was used to compute the fission rate as a function of time for both PWR and TRIGA reactor flux profiles with a combination of ^{232}Th, ^{233}U, ^{235}U, and ^{239}U. A constant neutron flux of 3×10^{13} and 3×10^{14} cm^{-2} s^{-1} were assumed for the TRIGA and PWR fluxes over a five year period. The optimal compositions and maximum deviation from the maximum signal are summarized for each reactor

type in Table 3.2 [7]. Although an optimal composition for the PWR spectrum was determined using ^{233}U, another comparable composition was found which did not require the use of this hard-to-acquire isotope. The strong dependence of signal deviation on flux profile and fissile coating composition was expected. Additionally, the 5-year period was not ideal for either the TRIGA nor PWR case. A typical TRIGA reactor does not operate near 100% uptime (commonly only a few hours per week). In contrast, 5 years represents approximately 3 fuel cycles for a PWR. Interest exists to determine the optimal composition with the consideration of outages which would allow for the decay of transmuted isotopes in the fissile coating.

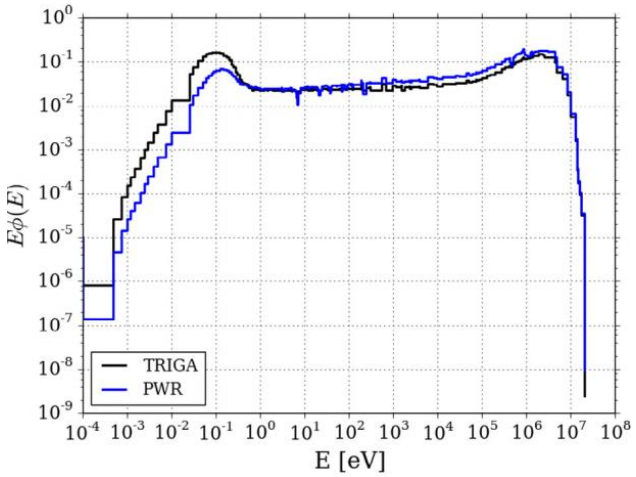

Fig. 3.13 A highly thermalized neutron-energy spectrum is typical for a TRIGA reactor compared to the harder spectrum of a typical PWR.

Table 3.2 Optimal fissile coating mass compositions for TRIGA and PWR spectra were determined for constant full-power operation over 5 years [7]

Spectrum	^{232}Th	^{233}U	^{235}U	^{238}U	Max % Deviation
TRIGA	85.7	0	2.7	11.6	0.8
PWR	91.8	4.3	0	3.9	3.8
PWR	94.7	N/A	5.2	0	5.1

Chapter 4 MPFD Sensor Fabrication

Simplicity was the primary focus for the modernized MPFD design. Improvements were made across the board, beginning with the insulating substrate that constitutes a majority of the sensor volume, proceeding to the electrodeposition of neutron-sensitive material, to the electrode configuration. The resources of the SMART laboratory and the HTTL at INL were utilized to fabricate and analyze MPFDs throughout the design process. Preliminary studies focused on the optimization of the insulating substrate and the evaporation of the electrode upon which fissile material was to be deposited. Then the electrodeposition process was modified from previous research to develop a reproducible, characterizable method. Preliminary analysis of the effects of high temperature were investigated in an atmospheric environment, but additional studies are necessary to characterize the effects of high temperature in argon. Finally, the electrodeposition process was characterized to enable the deposition of specific amounts of fissile material to fabricate a sensor with a desired neutron sensitivity.

4.1 MPFD Disk Preparation

The first step of the optimization process was to attempt the electrodeposition of uranium onto platinum substrates. In lieu of updated MPFD samples, alumina substrates from prior research were utilized [22]. Four 1-μm thick, 2-mm diameter disks were evaporated onto the 96% alumina strips and broken into separate samples to begin the electrodeposition development process as shown in Fig. 4.1. Upon further inspection however, the platinum electrodes were observed to be discontinuous in nature. The discontinuities of the platinum substrate were observed in prior research, rectified by annealing the samples in an argon furnace [22]. Nevertheless, electrodeposition was attempted using the samples created by this method with no success. Little was known of the source material for these samples. The surface roughness, material purity, and evaporation thickness were all considered important variables for the following process of optimizing the insulating substrate. Shortly after the failures with the old alumina samples, new alumina samples were procured from Valley Design Corp.

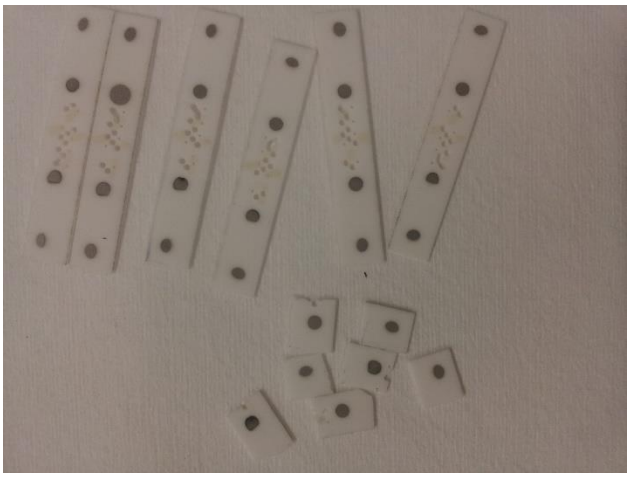

Fig. 4.1 Surplus alumina from previous research was utilized to create samples for preliminary electrodeposition experimentation.

The 8-hole, 98% pure, hard-fired, extruded alumina tubes were cut into 1.5-mm disks for initial evaporation testing. A simple shadow-mask was designed which exposed the entire face of the alumina disks to the material crucible in the electron-beam evaporator. A 1-μm thick platinum layer was evaporated onto several alumina disks. Upon SEM analysis, some of the samples appeared to be uniformly coated, while others exhibited large cracks in the platinum surface, shown in Fig. 4.2. In contrast to the first samples, the large cracks appeared related extrusion of the holes around the periphery of the samples. However, these features were not apparent upon visual inspection of the un-coated alumina. It was determined that sub-surface fractures were present in the alumina which were only exposed during the evaporation process.

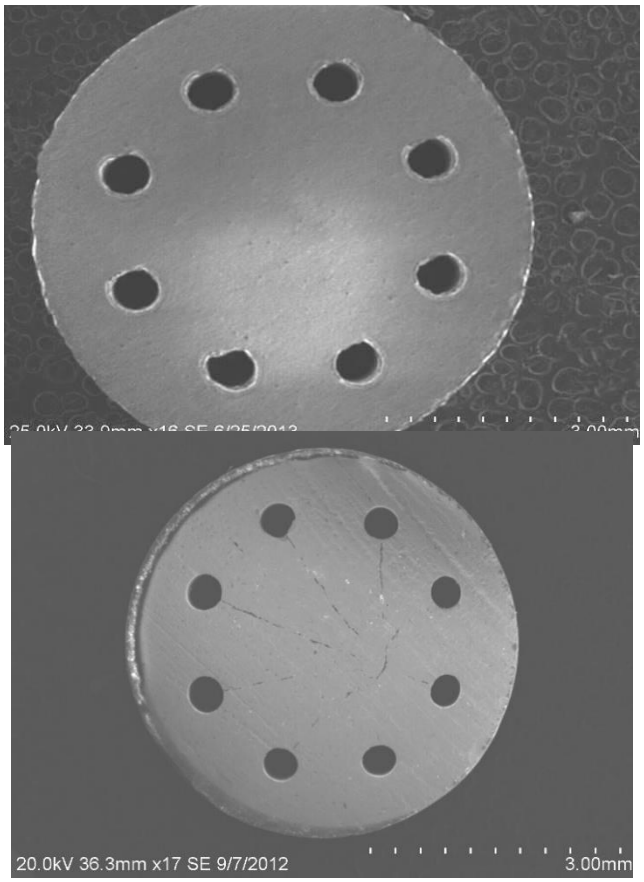

Fig. 4.2 Platinum contacts were evaporated onto the 8-hole extruded 98% alumina yielding mixed results.

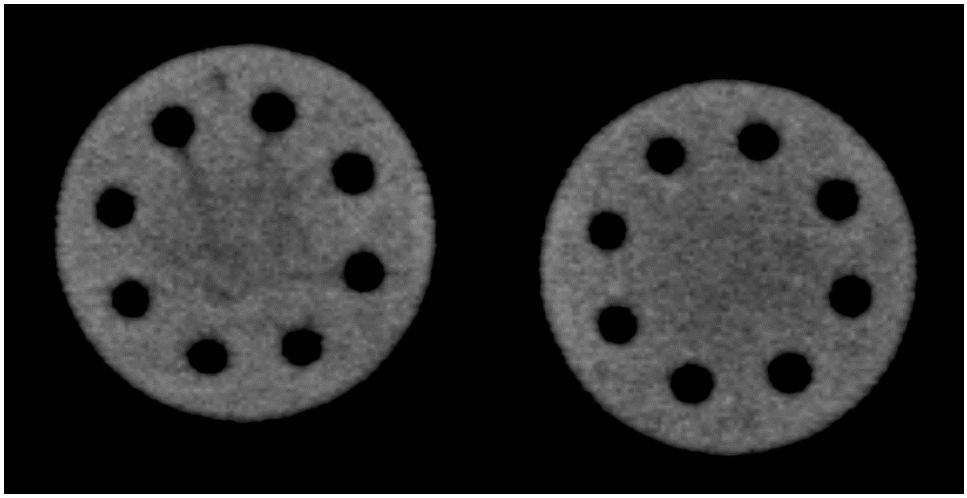

Fig. 4.3 X-Ray images of the 98% extruded alumina revealed some samples had internal fractures that became evident after physical vapor deposition evaporation of platinum.

Numerous samples of the extruded alumina were examined by x-Ray imaging. A majority of the 98% alumina disks exhibited internal fracturing which was clearly visible afer x-Ray imaging, shown in Fig. 4.3. Because of the continued problems, a new source of machined alumina disks was sought. A vendor of highly purified, machined alumina was then identified.

Micro-machining processes were utilized by NucFil® (NFT), a division of NFT, to manufacture 99.9% alumina disks of the same geometry as previous samples. Activation analysis was used to verify the purity of the new samples, exposing an additional advantage of the material. The main impurity of the 98% alumina samples was manganese, which caused minor activation concerns. In contrast, the 99.9% pure alumina possessed sufficiently small amounts of impurities to neglect any activation from the alumina substrate. A new shadow mask was also designed which featured a central evaporated region with a bond-pad over one of the 8 holes in the disk, shown in Fig. 4.4. After preliminary evaporation, the surface roughness of the alumina was of interest. The same 1μm-thick platinum layer was being used, with an added 200Å-thick titanium adhesion layer. The surface-area of the evaporated electrode was of interest for the electrodeposition process. Peeling and dis-continuities in the platinum surface were also observed on some samples. Highly polished samples were acquired from the manufacturer and evaporated with the same 200/10,000Å (Ti/Pt) electrode. The smoother surface was observed visually, shown in Fig. 4.4. The same 'rough' and 'polished' samples were analyzed with a 3-D scanning laser microscope at the HTTL.

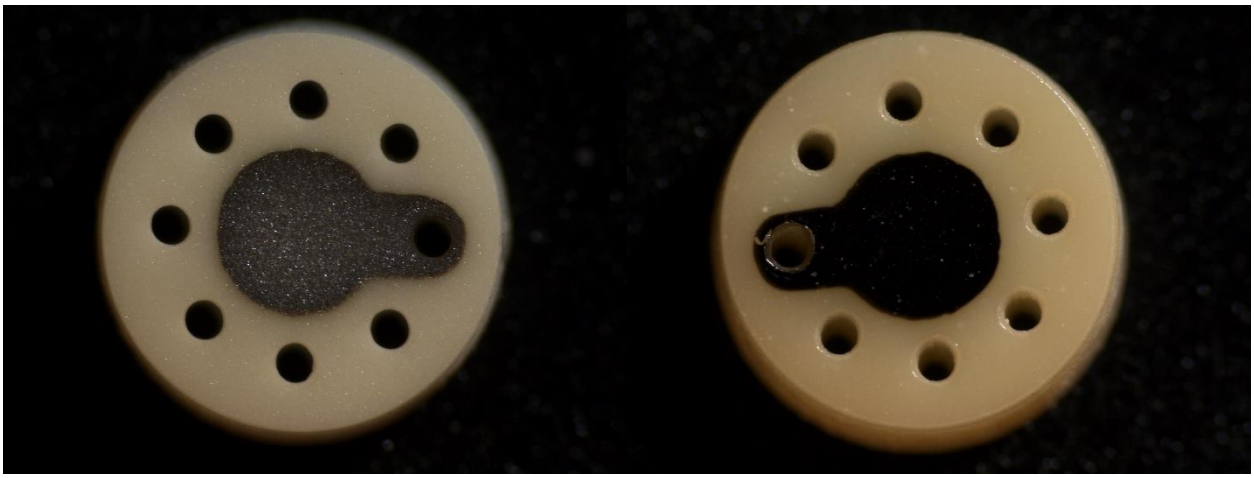

Fig. 4.4 Polishing the 99.9% alumina improved the surface finish of the evaporated contact significantly.

The scanning laser microscope (VK-X260K), capable of 0.5 nm resolution was used to measure the surface roughness value (R_a) for one representative rough and polished sample. The

rough sample yielded R_a = 3.9, where the polished sample yielded R_a = 0.5, with the roughness clearly observed in the cross-sectional scans shown in Fig. 4.5 and Fig. 4.6. Next, attention was turned towards the surface features of the evaporated electrode.

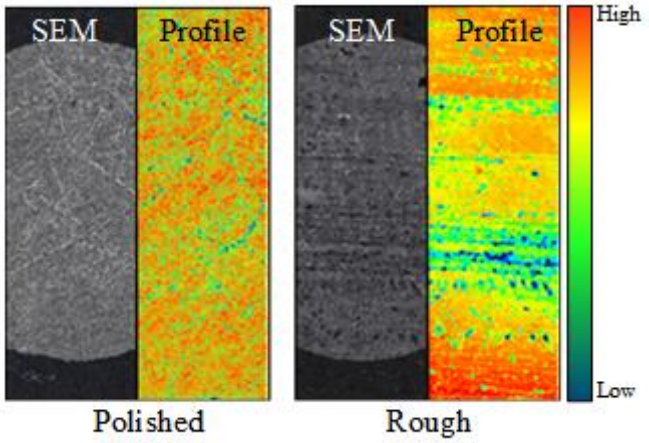

Fig. 4.5 The VK-X260K 3D laser scanning microscope was used to examine the surface features of polished (left) and rough (right) MPFD samples before electrodeposition.

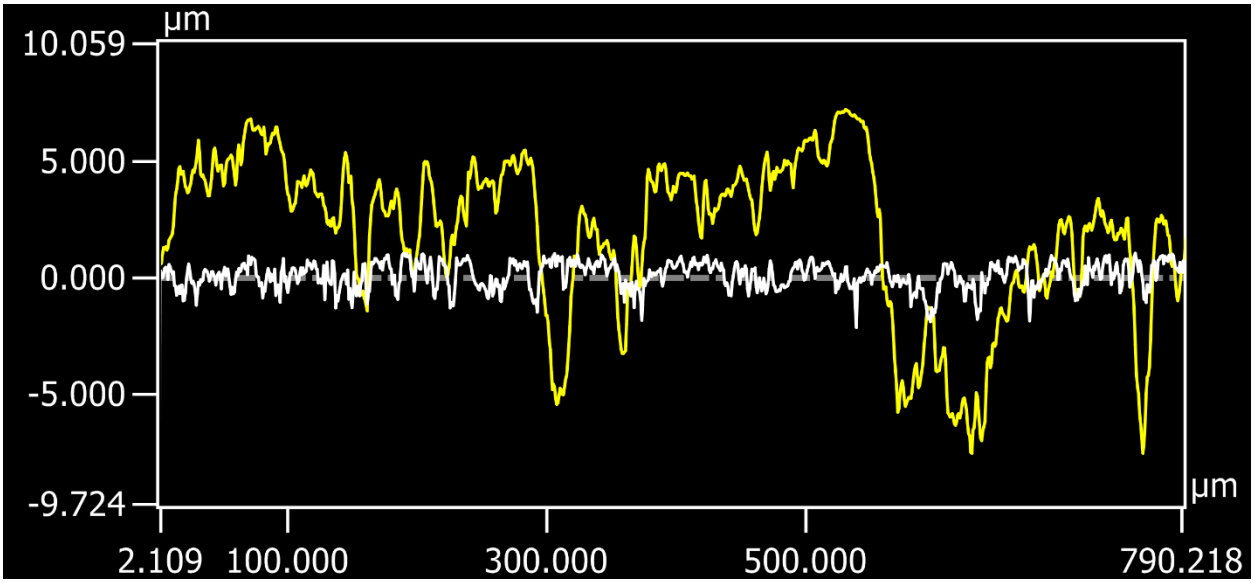

Fig. 4.6 The surface roughness for the polished (white) and un-polished (yellow) 99.9% alumina disks was illustrated with the 3-D scanning microscope at the HTTL.

Even with highly polished alumina samples, cracks in the platinum electrode were observed under SEM analysis, shown in Fig. 4.7. Upon visual inspection, and at low magnification, the cracks were not visible. However under higher magnification the cracks caused concern for the adhesion of the electrodeposited material. At the same time, alternative substrate materials were

being investigated (Ch. 4.2). Thinner adhesion layers and platinum layers were proving successful for the ultra-smooth silicon and quartz samples. Therefore, experimentation with thin evaporations commenced for the highly polished alumina.

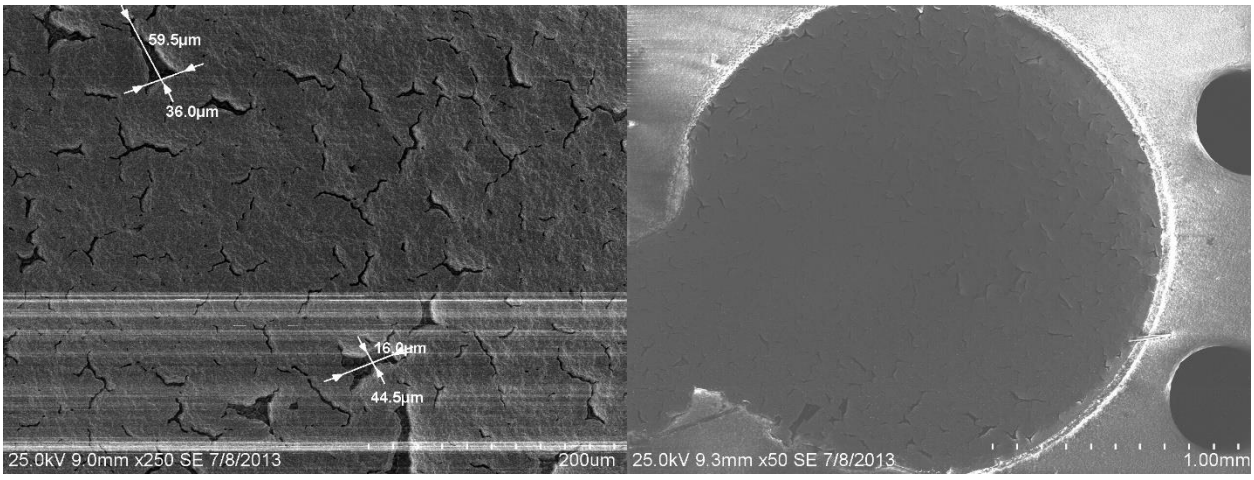

Fig. 4.7 Significant cracking of the platinum surface was observed for thick (1µm) evaporations.

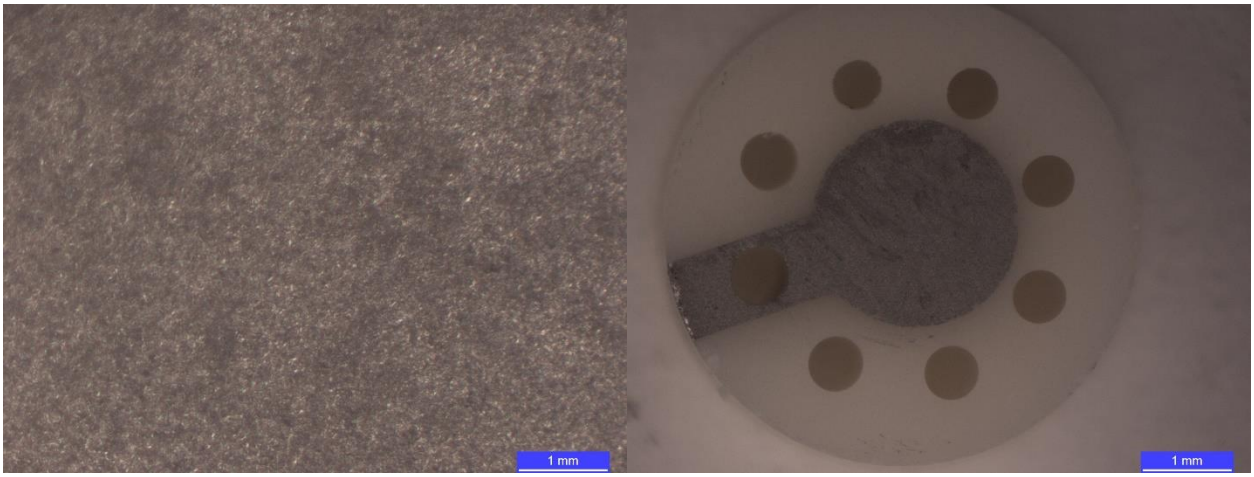

Fig. 4.8 Thin evaporated layers, in conjunction with a thin adhesion layer (Ti/Pt 50Å/500Å respectively) produced uniform coatings on the alumina substrates.

Many adhesion layer and platinum layer combinations were tested. If the adhesion layer was too thin or too thick, the platinum would simply wipe off of the samples after evaporation. Similarly, if the platinum layer was too thick the same cracking was observed as with the 1-µm thick coating. Eventually, a ratio of 50Å titanium with 500Å platinum was successful in uniformly coating the entire alumina surface without cracking or peeling, as shown in Fig. 4.8.

The final substrate design, used for fabrication of current MPFDs utilized a highly-polished, 99.9% alumina substrate upon which a 50Å/500Å Ti/Pt electrode was evaporated, shown in Fig. 4.9. During the process of enhancing the alumina substrate, different materials were also explored. Although these materials were not utilized for the current design, they did aid in the development and may still offer alternative design options in the future.

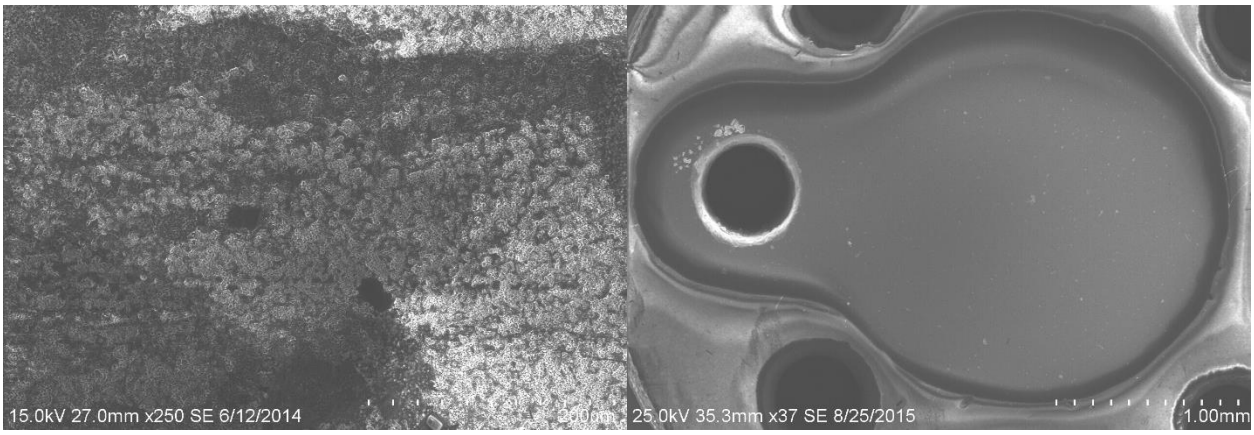

Fig. 4.9 Highly polished, 99.9% alumina with 50Å/500Å Ti/Pt evaporations are utilized for current MPFD assemblies.

4.2 Alternative Material Considerations

During the process of manufacturing numerous alumina samples, concerns were raised about the surface roughness of the material. In conjunction with pursuing polished alumina (previously described), silicon and quartz samples were also considered as MPFD substrates. Silicon and quartz can be purchased with highly-polished surfaces, and can be wet-etched to remove surface defects. Additionally, silicon (also a primary constituent of quartz) has a smaller total neutron absorption cross section than aluminum, as shown in Fig. 4.10.

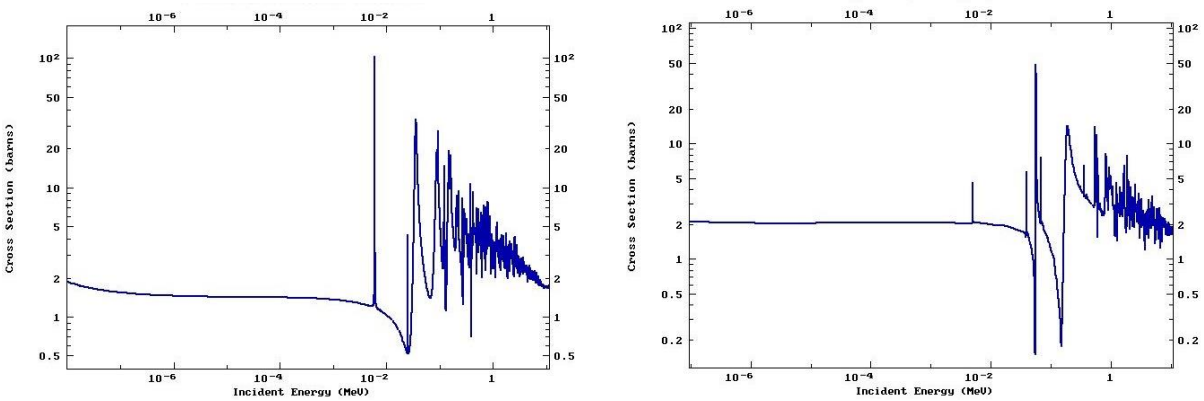

Fig. 4.10 Silicon (left) has a comparable neutron absorption cross section in the thermal region (≈ 2 barns) and a smaller average cross section in the epithermal and fast region than aluminum (right) [11].

Quartz was the first alternative material that was tested as an MPFD substrate. Evaporation techniques were adapted from the methods utilized for the alumina substrates. At the time that quartz was first being investigated, 1-µm thick platinum layers with no adhesion material were being utilized. The first several quartz samples with evaporated Pt contacts suffered poor adhesion, which initiated an investigation into optimal evaporation techniques. A thin titanium layer was found to significantly enhance the adhesion of the evaporated contact onto quartz. Eventually, a 50Å/500Å Ti/Pt evaporation was used. This same evaporation method was shown to adhere well to the polished alumina and subsequently silicon samples. A quartz sample with evaporated contacts and surface features acquired via SEM analysis are shown in Fig. 4.11. Although electrode evaporation was possible onto quartz, the fabrication process to manufacture MPFD disks was not investigated. The evaporation method determined by experimentation with quartz proved sufficient for alumina substrates which were already available in the desired geometry for MPFD fabrication.

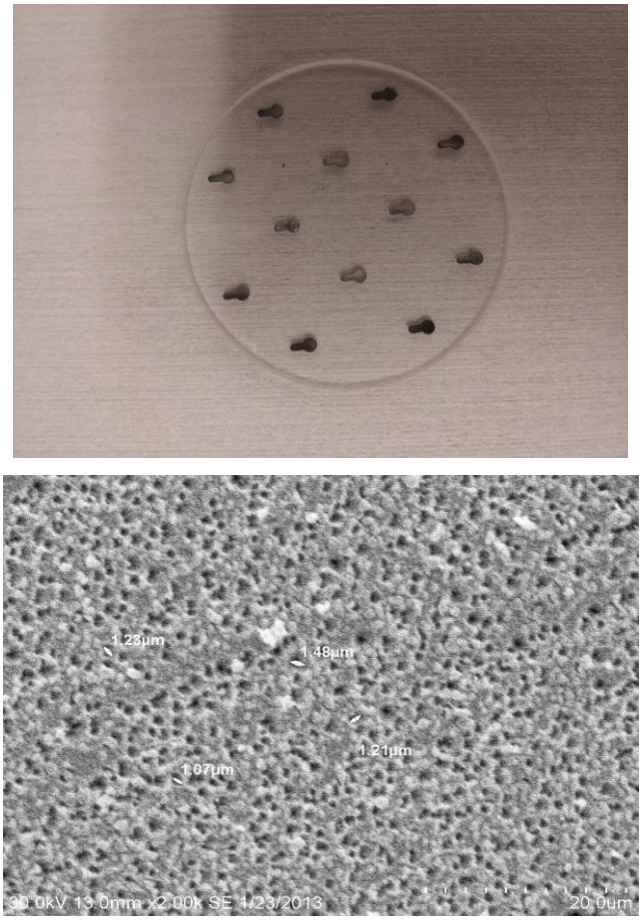

Fig. 4.11 Evaporation of Ti/Pt contacts onto quartz disks was only partially successful, suffering from poor adhesion and surface pitting.

Interest remained in the production of MPFD substrates from silicon. The manufacturing cost of alumina substrates made mass-procurement for purposes of electrodeposition characterization prohibitively expensive. Silicon was an interesting alternative to alumina, taking advantage of manufacturing capabilities at the SMART laboratory. The goal was to produce many samples which could be used to characterize the electrodeposition process before returning to the alumina substrates for MPFD fabrication. The smooth surface of the silicon wafer also had a thin SiO_2 insulating layer upon which the 50Å/500Å Ti/Pt electrode was evaporated. The insulating layer was necessary to counteract the semi-conducting nature of the silicon substrate. A shadow mask was constructed similar to the alumina and quartz designs. Building on experience with quartz and alumina, the evaporation onto silicon required no modification and adhered well to the surface. Electrodeposition testing was then possible with the silicon substrates, an example of which is shown in Fig. 4.12.

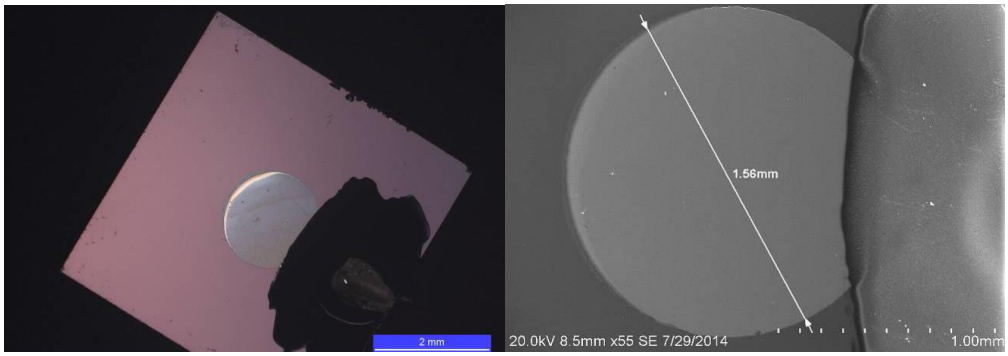

Fig. 4.12 Silicon-dioxide on the surface of a silicon wafer provided an ultra-smooth surface and subsequently a uniform electrode evaporation.

During the development process with silicon, additional interest was generated in the use of wet-etching to fabricate numerous MPFD substrates on a single silicon wafer. The wet-etching process for silicon is well-understood in the SMART laboratory, and should be investigated as a mechanism to greatly reduce the cost of fabrication for MPFDs

4.3 MPFD Electrodes

The design of MPFDs began with two parallel plates, one containing a deposit of fissile material [6]. The basis for the parallel plate design originates in the basic fission chamber design [2]. The implementation of this simple electrode configuration made assembly of prototype sensors simple, avoiding the complication of anode wires which can be troublesome, especially for small devices. The flat electrodes also provided a large, accessible region upon which a fissile coating could be applied. Although some fission chambers are constructed with fissile coatings on the anode or cathode in a co-axial configuration [5], such depositions posed a significant challenge at the beginning stages of development. A parallel plate configuration was so simple in fact that the first proof-of-concept for the MPFD was illustrated using a boron coating that was physically evaporated onto one of the electrodes [6]. Indeed evaporation techniques are preferred for other fissile coatings, however no system currently exists to evaporate radioactive materials (such as uranium and thorium). Prior research did not deviate from the parallel plate design with anode and cathode lead-wires which penetrated the insulating substrate as illustrated in Fig. 4.13.

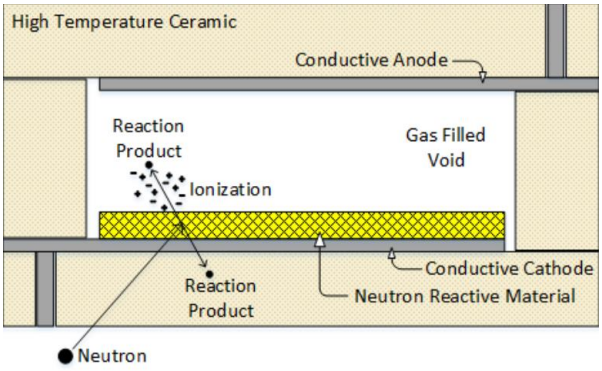

Fig. 4.13 The planar design was adopted from previous research and proof-of-concept experiments [6].

The termination method of the anode and cathode lead wires with the evaporated contact was historically performed by wire-bonding. This fragile method of connecting the lead-wire to the sensitive portion of the sensor caused problems with the detectors malfunctioning during transport into the reactor core, and during operation due to the high-vibration environment of the nuclear reactor from coolant flow. Numerous silver-based epoxies and other conductive adhesives were previously tested with limited success [22]. Previous designs also required that the MPFD chamber be bonded together using ceramic paste or cement, which unfortunately caused additional problems [22]. The first loose-stacked MPFDs were designed with a similar wire-termination in mind, but instead utilized thicker alumina substrates, increasing the surface area for a conductive adhesive bond. A special contact shape was designed which would position the fissile coating in the center of the MPFD and had a bond-pad extending over one of the holes in the alumina as shown in Fig. 4.14. The hole could then be filled with conductive adhesive and a lead-wire could be inserted. This method was also duplicated on flat samples for electrodeposition testing, shown in Fig. 4.15.

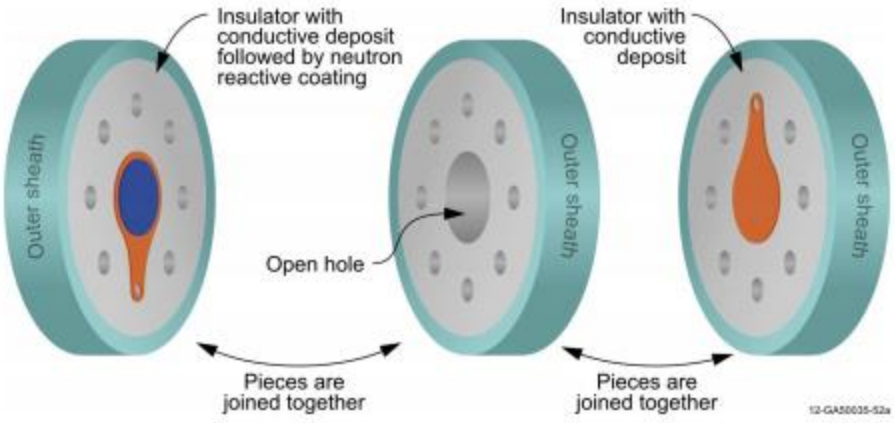

Fig. 4.14 The parallel plate design was adapted into the loose-stack geometry, with a contact pad for electrical leads.

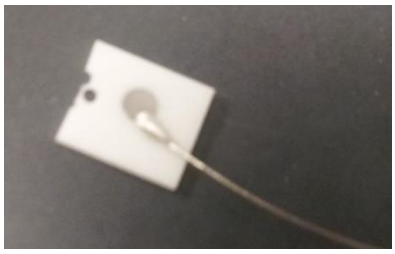

Fig. 4.15 Silver conductive adhesive was used to connect a wire lead to the MPFD electrode for electrodeposition testing.

Fig. 4.16 Specialized evaporation masks were used to index the contact pad with 1 hole in the alumina.

A special shadow mask was constructed, featuring indexing pillars which would align the bond-pad with one of the holes in the alumina. Electron-beam evaporation was used to produce numerous sample substrates with this design for electrodeposition testing and eventually prototype development, shown in Fig. 4.16

Arenco 597-A® Silver Adhesive was tested on MPFD substrates for 1000 hours at 500 °C, shown in Fig. 4.17. Although the conductive adhesive was capable of withstanding many hours at 500°C, the material was only rated for continuous operation up to 1700°F (925°C) and also caused

alignment issues after assembly due to the bulge of the contact, shown in Fig. 4.18. Additionally, the electric-field near the electrode was non-uniform, causing inconsistent electrodeposition. For these reasons, and because the silver in the conductive adhesive also appreciably activated after neutron irradiation, a contactless approach was desired.

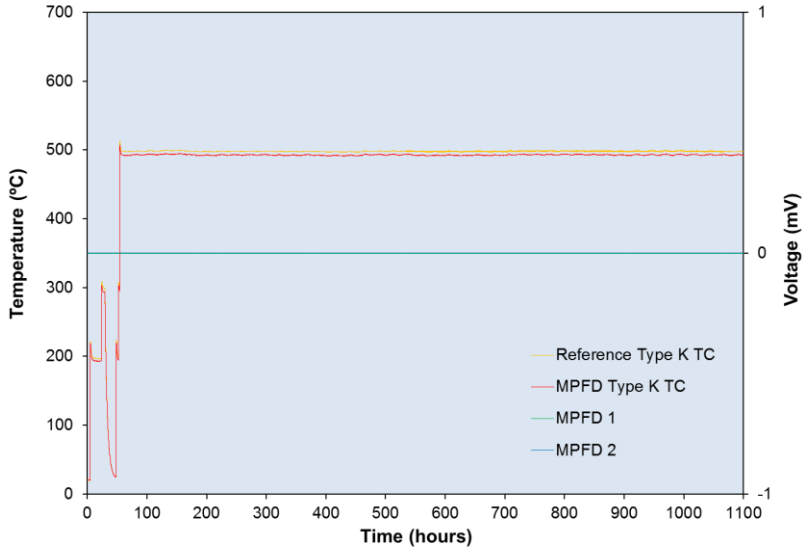

Fig. 4.17 The stability of the silver conductive adhesive was successfully tested at the HTTL at INL.

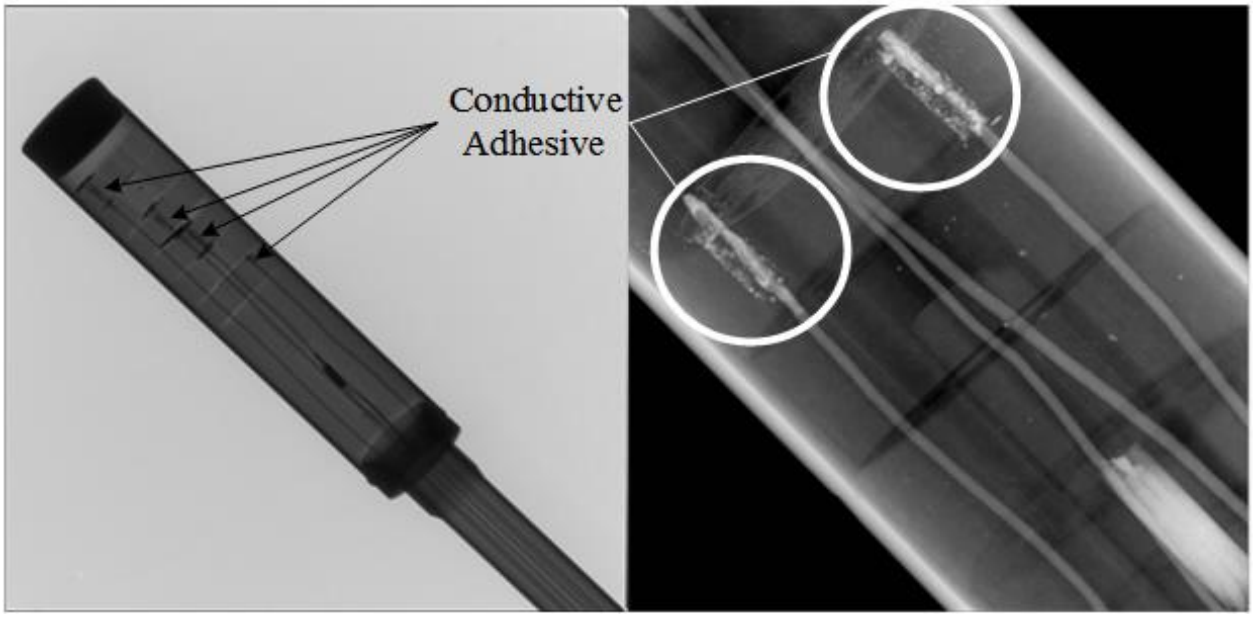

Fig. 4.18 The conductive adhesive previously used is visible by x-ray analysis.

Although the MPFD design discussed thus-far had been developed based on loose-geometric criteria, and with the intention of being encapsulated with irradiation experiments at nuclear test reactors, a new opportunity for MPFD fabrication and testing pushed the limits of the design. Almost all nuclear reactor facilities are equipped with flux ports that are used for iron wire or gold foil irradiation. These small penetrations into the reactor core offer a unique opportunity for MPFDs to be deployed at facilities that otherwise would not be able to facility experimental instrumentation. The small size of the MPFD was utilized to design and construct multi-node arrays that could be inserted into typical flux-wire ports, illustrated in Fig. 4.19. Using a parallel plate design was quickly ruled unfeasible for the small dimensions of the flux-wire port. To this end, a multi-wire design was considered.

Multi-wire gas detectors (also referred to as multi-wire proportional chambers, MWPCs) are commonly used in position-sensitive applications of radiation detection [10]. In contrast to conventional MWPCs, the multi-wire MPFD design does not require charge multiplication and only uses two wires. The anode and cathode in the multi-wire MPFD run parallel to one another, passing through the ionization chamber with fissile material located between the two electrodes as illustrated in Fig. 4.20. The wires in Fig. 4.20 are exaggerated to illustrate the possibility to use wires of different gauges to bias the electric field within the MPFD. Typically, geometry weighting on the anode is preferred to increase the effective pulse contribution from electron motion near the anode, reducing the location dependency of the sensor. However, the small size of MPFD limits the impact of location dependency, and small wires for both the anode and cathode can be used as long as charge multiplication does not take place.

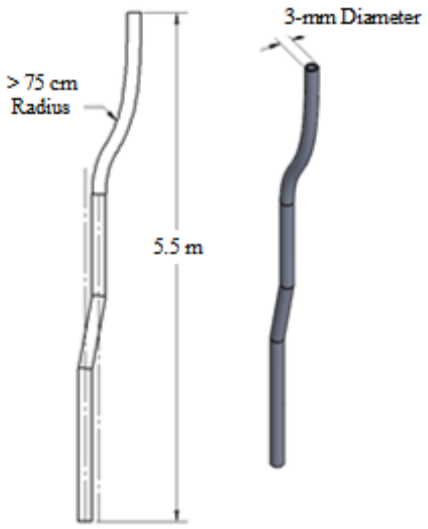

Fig. 4.19 A small tube with several bends is typically used for iron-wire flux ports [12].

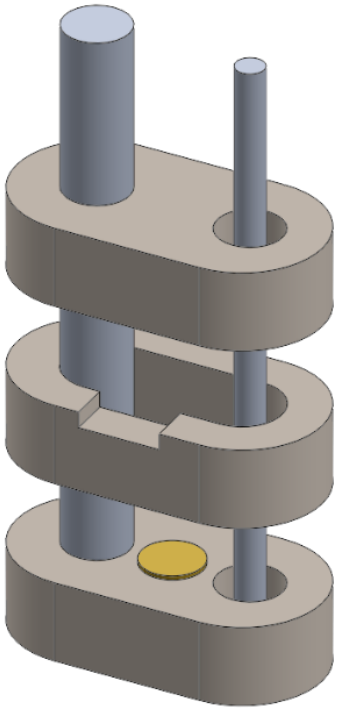

Fig. 4.20 The multi-wire MPFD design no longer required conductive adhesive [12].

Ion-chamber operation is important to MPFD operation. The radiation field within the core of the nuclear reactor is intense and diverse. If MPFDs are operated at high bias, causing charge multiplication, isolation of fission fragments from gamma-ray and beta particle interactions becomes more challenging. The electric field strength for the MPFD modeled in Fig. 4.20 with

+100 V applied bias between the anode and cathode is shown in Fig. 4.21. The smaller anode yields a higher electric field near the anode, but still below the critical electric field strength to induce Townsend avalanching (≈10 kV cm^{-1}). The electric field decreases towards the center of the gas chamber, still exceeding the minimum electric field strength to accelerate electrons and ions to saturation velocity in 1-atm argon (≈150 V cm^{-1}). Due to the cylindrical nature of the cathode, the electric field once again increases near the cathode, however the magnitude is lower near the larger cathode than near the anode. Adjusting the dimensions of the anode and cathode, the spacing between the electrodes and the operating bias all affect the electric field within the sensor. MPFDs have been operated between +50 V and +400 V applied bias for detectors of various geometries; however, the multi-wire design has been typically operated at +100 V.

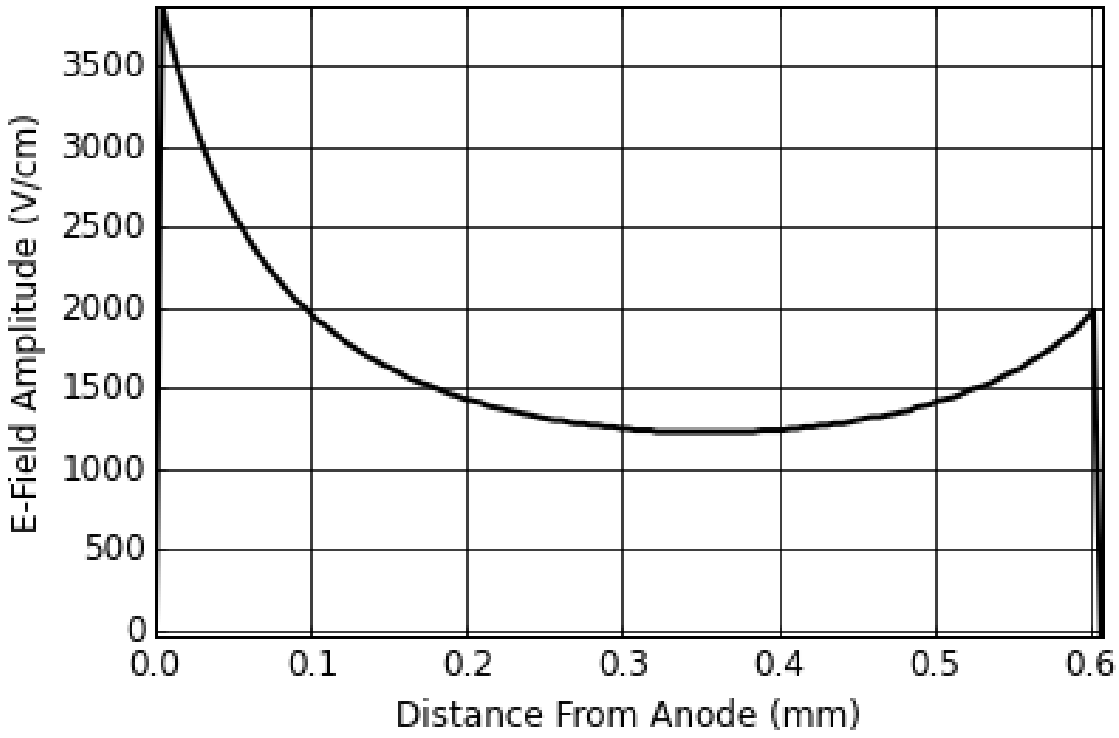

Fig. 4.21 The electric field within the MPFD chamber under a +100 V bias is higher near the anode than the cathode, reaching a minimum between the two electrodes.

The tight geometry constraints of the flux-wire port led to the initial re-design of the MPFD. The project description originally called for 10 MPFD nodes and 4 thermocouples all inside a ≈3-mm inner diameter tube. The plan to use multi-hole alumina insulators for the anode, cathode, and thermocouple wires is illustrated in Fig. 4.22. It did not take long however to discover that this

dense packing made insertion of the array challenging. Initial construction of such an elaborate device was attempted and is documented elsewhere [12]. Eventually, the design was reduced to only 5 MPFD nodes and no thermocouples, making insertion possible with advances in the design and fabrication (Ch. 5.2). The advantages of a common-cathode however were retained, greatly reducing the overall size of the MPFD sensor, and enabling a greater number of detectors to be deployed in an array, as illustrated in Fig. 4.23. The small geometry constraints also lead to the fabrication and testing of the smallest fission chambers ever documented Ch. 6.1 [9]. The multi-wire design also required a new termination method be developed for the anode and cathode wires. The wires in the larger design can be simply cut short and left to terminate within the alumina insulator, depicted in Fig. 4.24. However, the anode and cathode insulation in the flux-wire probe design would simply slide off if no other termination was made. To this end, two termination methods were developed, shown in Fig. 4.25. For the anode wires, a 4-hole alumina insulator was used, threading the anode down one hole and turning around to be thread up into another hole. This method was used to reduce the likelihood that any exposed wire would short to the interior of the flux-wire port. For the cathode, which is grounded, the wire was simply crimped over the end of a single alumina insulator. Contact between the cathode and the flux-wire port wall was un-important in this case because both materials should be at equal potential.

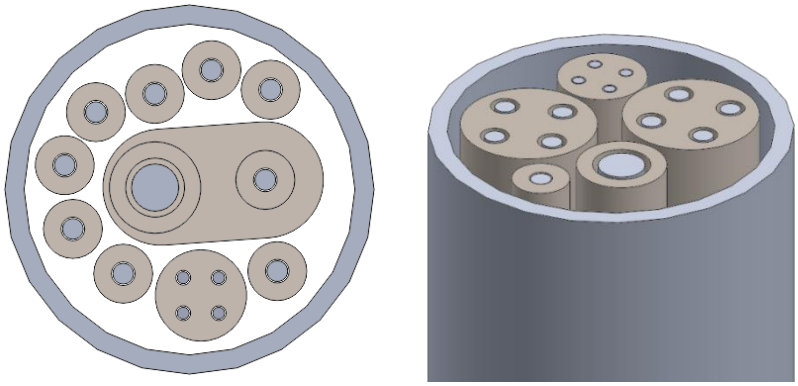

Fig. 4.22 Tight spacing within the flux-wire port limited drove the geometry of MPFD arrays for this application [12].

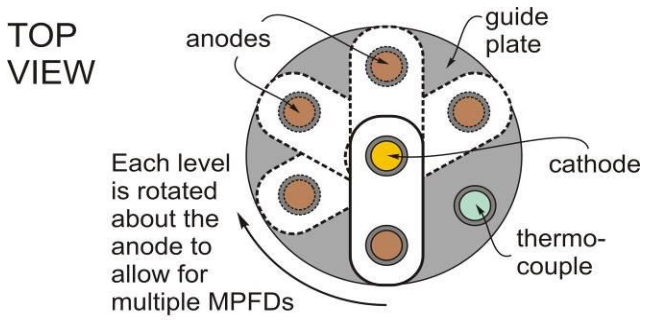

Fig. 4.23 A common cathode design reduced the number of wires required for an MPFD array.

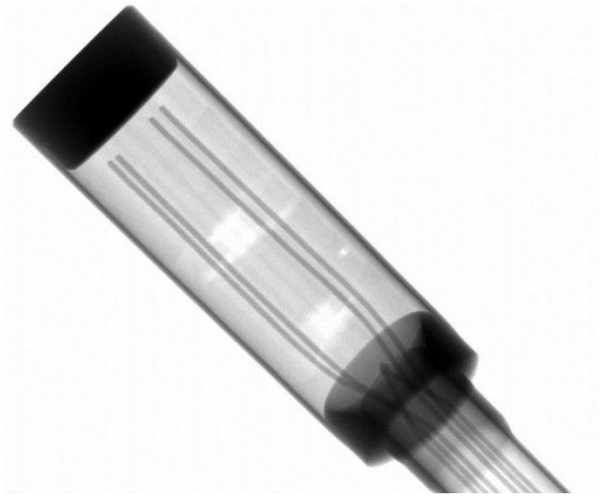

Fig. 4.24 The multi-wire design has also been adapted for the larger MPFD design.

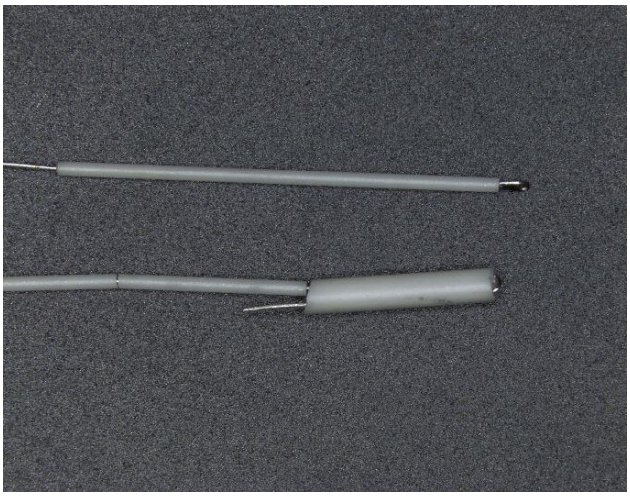

Fig. 4.25 Electrode wires are terminated at the end of the array by looping the wire through a multi-hole section of alumina [12].

4.4 Electrodeposition of Neutron-Sensitive Coatings

The methods developed for electrodeposition of uranium onto MPFD substrates in the past were complex and poorly documented [22]. Based on the information available, the process involved electrolysis using a continuous flow system. The fissile material depositions were not characterized, therefore little is known of the success of the former work. Evaporation of fissile material was the initial desire for the present work, and remains to be of interest. No evaporation chamber for radioactive materials has been identified because of contamination concerns. Therefore, a system to chemically deposit small layers of fissile material onto the small platinum electrodes described in Ch. 4.3 was desired. Capitalizing on the expertise of Dr. Takashi Ito at the Kansas State University department of Chemistry, an electrodeposition method was developed. The equipment to determine the appropriate operating parameters was first made available in Dr. Ito's laboratory, and then purchased specifically for MPFD development. The CH Instruments CHI600E potentiostat was used to perform cyclic potential sweeps between the platinum working electrode on the MPFD surface and the counter electrode suspended in the fissile material electrolytic solution. One early electrodeposition trial is depicted in Fig. 4.26. Preliminary development of an electrolytic solution began with the study of related work [28-40].

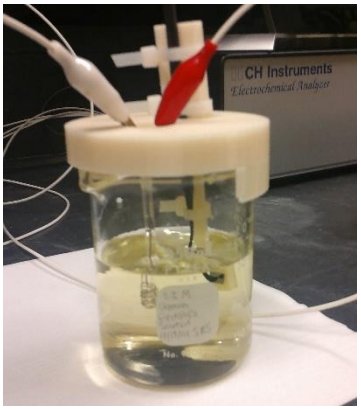

Fig. 4.26 The CH Instruments CHI600E electrochemical analyzer was controlled with a PC to electrodeposit fissile material onto MPFD samples.

After reviewing methods of uranium and thorium electrodeposition and electrolysis methods, a method for the electrodeposition of uranium and thorium onto small MPFD electrodes was developed [8]. Before preparing any electrolytic solution, all glassware was cleaned using dilute HNO_3, acetone, isopropyl alcohol, and de-ionized water. The dilute HNO_3 was found to quickly

dissolve any trace uranium or thorium compounds which may remain from previous solution preparation or electrodeposition. Uranyl nitrate hexahydrate (99.9%) and thorium nitrate hydrate (99.8%) were used as sources of uranium and thorium for each of the electrolytic solutions. Previous research suggested that a solution pH of nearly 10 was desired. Therefore, a 3.6 mol solution NH_4OH was used to increase solution pH. However, the solution pH without the addition of any NH_4OH was < 4 and the addition of NH_4OH quickly caused precipitation to occur. The maximum pH achieved was 7, with a thick cloudy precipitate depicted in Fig. 4.27. It was later determined that pH balancing was not necessary and the use of NH_4OH was abandoned. Even the cloudy solution did yield some preliminary results, however when the solution was mixed with a pH of 3.4 for uranium and 3.0 for thorium solutions, electrodeposition was more successful and reproducible.

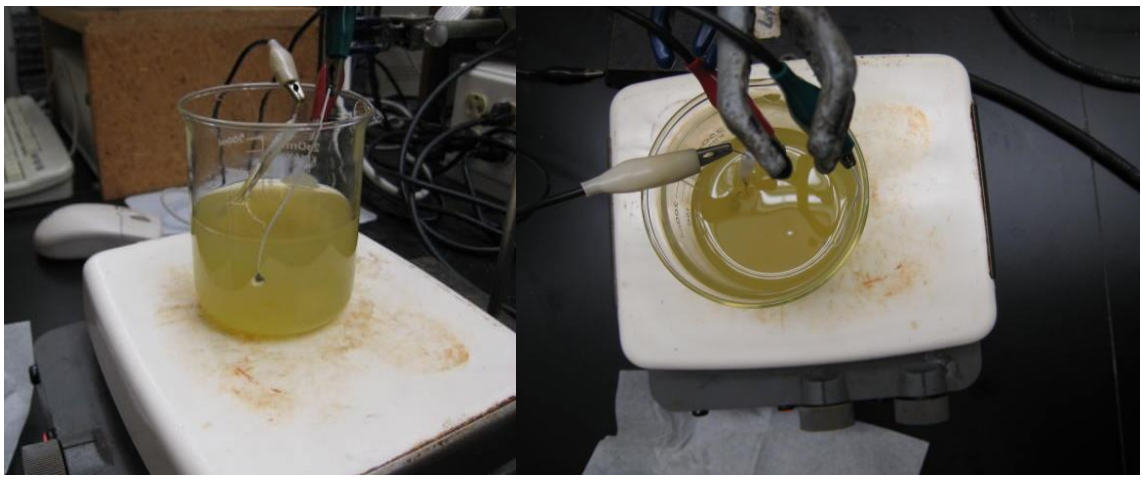

Fig. 4.27 MPFD samples and the counter electrode were both suspended in the electrolytic solution.

Early experimentation with electrodeposition was conducted by suspending the MPFD sample, with lead-wire connected by conductive adhesive, into the electrolytic solution. The vial containing the Ag/AgCl reference electrode submerged in 3.0 M KCl was also suspended in the electrolytic solution. The counter electrode, a 0.33-mm diameter 95% Pt. wire, was wrapped around the reference electrode vial. A best effort was made to maintain approximately 1-cm spacing between the counter electrode and the working electrode. Even this crude method of electrodeposition produced samples with large amounts of uranium deposited on the surface, as shown in Fig. 4.28.

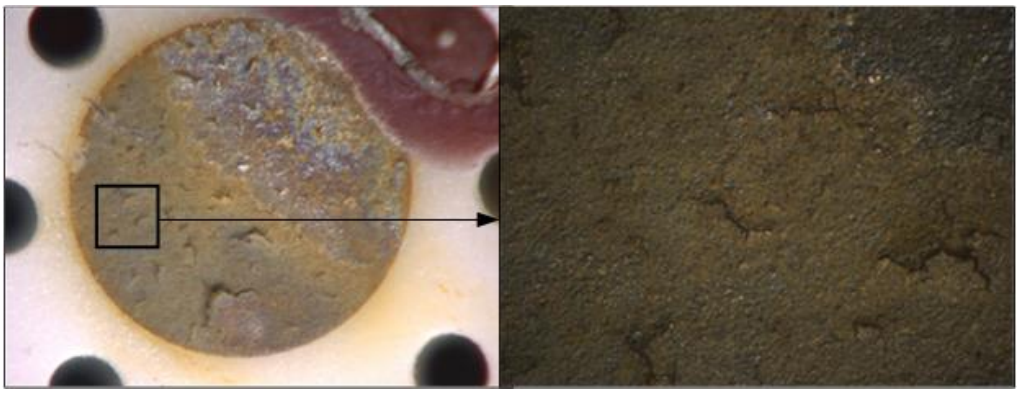

Fig. 4.28 Sample A10.j was the first sample showing successful electrodeposition of uranium onto the small MPFD electrode.

Although the method of hanging the MPFD sample in the electrolytic solution successfully deposited fissile material, the coating was neither uniform nor reproducible. Improvements were made to the electrodeposition process after the preliminary samples provided a proof-of-concept for the method. Removing the NH_4OH improved the clarity of the electrolytic solution as shown in Fig. 4.29. The final electrolytic solution preparation process can be found in Appendix A Improvements were also made to the electrodeposition cell to improve the uniformity of the deposition and reproducibility of the process.

Fig. 4.29 Uranium and thorium solutions were both created for electrodeposition.

The second step in the electrolytic cell optimization attempted to maintain the 1-cm spacing between the working electrode and the counter electrode using a 3-D printed frame on top of a beaker containing the solution as shown in Fig. 4.30. This method did improve sample uniformity, as shown in Fig. 4.31, however made placement of the MPFD sample challenging. The improved potential sweep parameters were also identified with this new electrolytic cell.

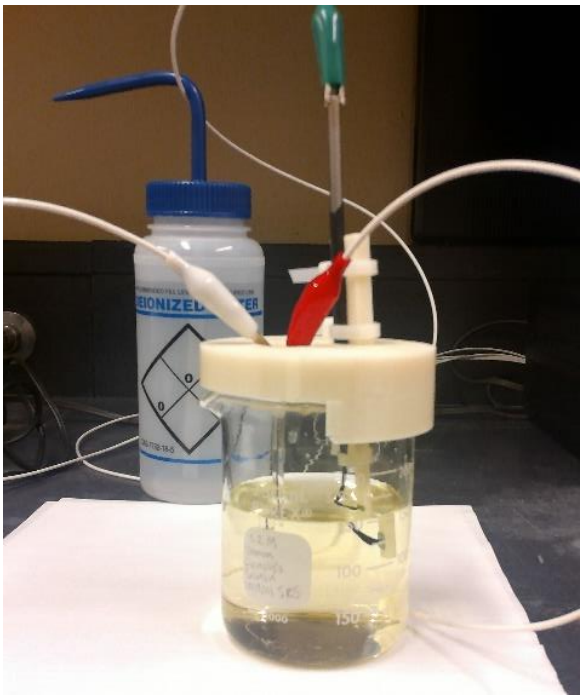

Fig. 4.30 The electrolytic cell improved sample uniformity but was especially challenging to assemble and monitor.

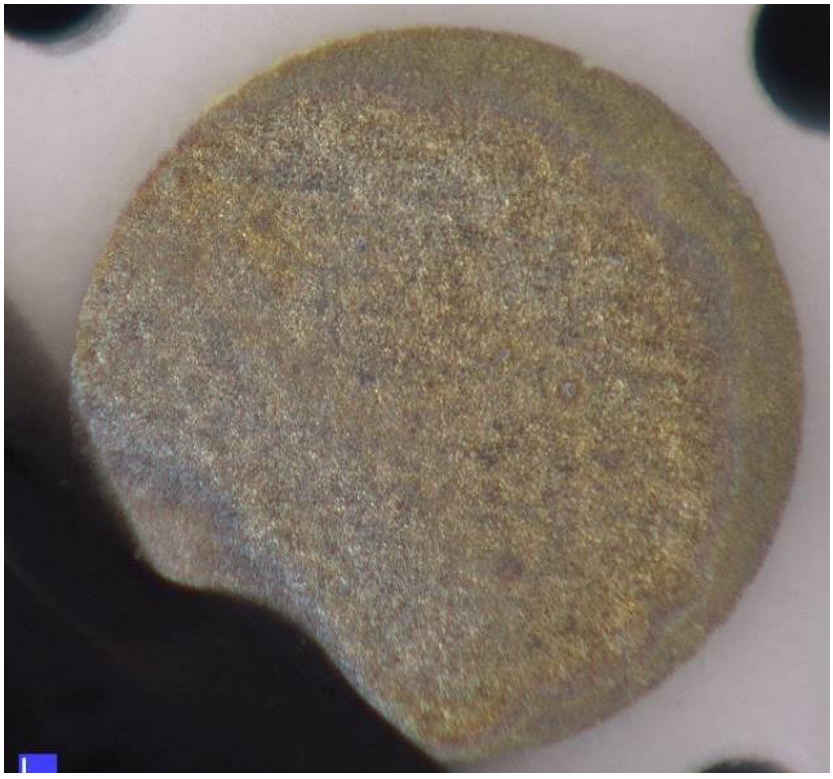

Fig. 4.31 Determining the optimal voltage-sweep interval improved the quality of the electrodeposited layer, shown on sample A12.g.

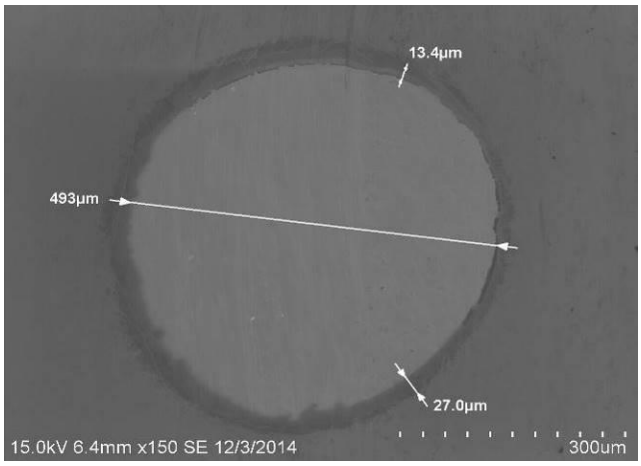

Fig. 4.32 Preliminary characterization of the electrodeposition process was conducted using 0.5-mm diameter electrodes (Ti/Pt 50 Å /500Å) evaporated onto silicone-dioxide.

At the same time that the electrolytic cell was being improved, the surface preparation and evaporation methods were also improving (Ch. 4.1, 4.2). Silicon samples were becoming available for additional testing, shown in Fig. 4.32. In addition to being smoother and more uniformly evaporated than the alumina samples that were previously tested, the metallic contacts on the silicon samples were also smaller to support the flux-wire probe MPFD design. Although several MPFDs were produced using a crystallography microscope to align the probe tip, an improved electrolytic cell and probe configuration was still needed.

The new electrochemical cell was developed to accommodate the smaller electrodes. The cell was designed to support the use of the counter/reference electrode vial and a working electrode probe. The working electrode probe was insulated with Plasti Dip ®, with exception of the tip and a small portion of the handle. The tip was left un-insulated to allow contact with the metallic sample electrode while the handle was left un-insulated to allow connection to the potentiostat lead wire. The counter/reference electrode vial consisted of a Ag/AgCl reference electrode submerged in 3.0 M KCl inside a glass vial. Around the exterior of the glass vial was wrapped a 0.33-mm diameter 99.95% Pt wire which was used as the counter-electrode. The configuration of the electrolytic cell is illustrated in Fig. 4.33. A 3-dimensional translation stage was utilized to maneuver the sample and beaker containing the electrolytic solution. A Leica DMS300 microscope provided a live display of the electrodeposition cell to aid in the positioning of the working electrode probe and enable a preliminary visual inspection of the sample.

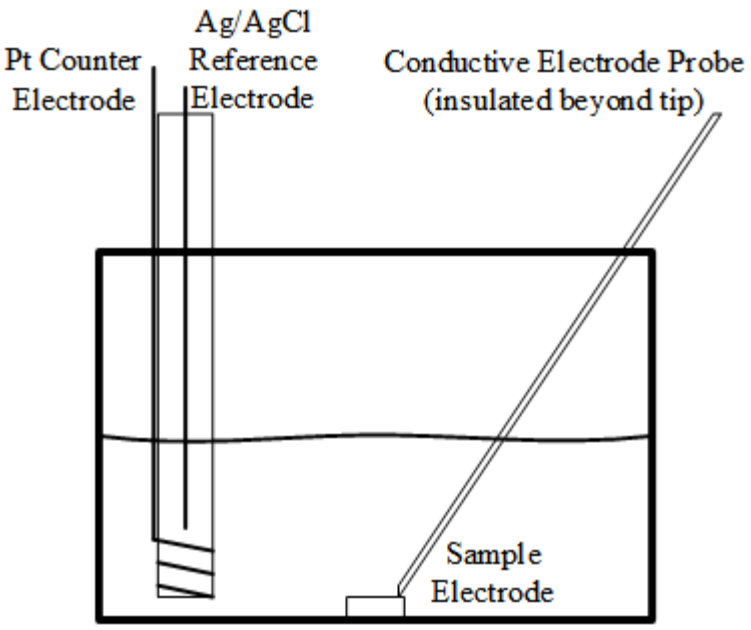

Fig. 4.33 Small electrodes were electrodeposited with uranium and thorium using the improved electrolytic cell with 3-D stage and digital microscope.

After placing the silicon sample with evaporated electrode (sample electrode) into a glass beaker, the 3-D stage was adjusted to make contact between the sample electrode and the conductive electrode probe. Contact was confirmed visually by observing a union of motion between the probe tip and the sample. Then, the pre-mixed electrolytic solution was added to the cell. Cyclic voltammetry was then used to deposit either uranium or thorium, depending on the solution, shown in Fig. 4.34.

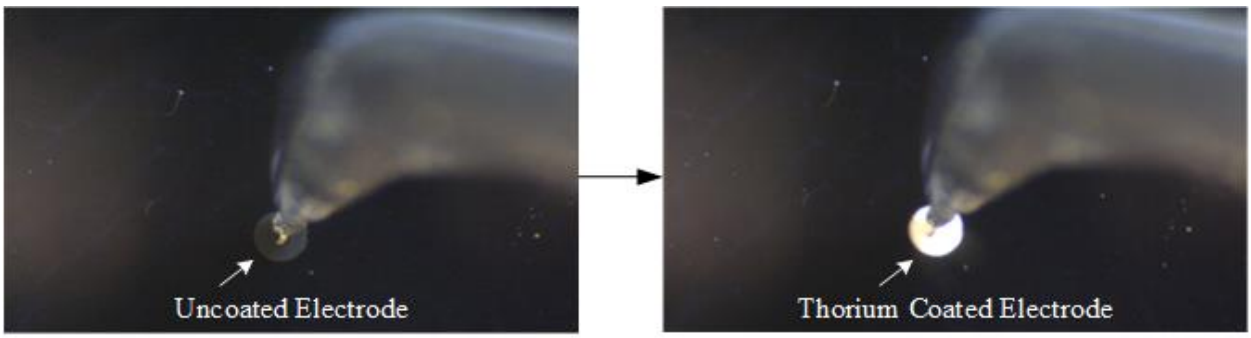

Fig. 4.34 The thorium deposition is visible using an optical microscope during electrodeposition.

An optimal potential sweep interval from -0.62 V to -0.64 V was determined to yield the most consistent surface depositions using a 0.01 Vs^{-1} sweep rate. Beyond -0.64 V, significant bubble generation occurred on the electrode surface, producing unwanted crystalline deposits and non-uniform material deposition [8]. In contrast, no deposition was observed for voltages between 0 V and -0.62 V [8]. The potential sweep method was utilized for electrodeposition of fissile material to control the amount of material deposited. The maximum cathodic current experienced between the working electrode and the counter electrode decreased with each successive sweep for both uranium (A) and thorium (B) electrolytic solutions, shown in the cyclic voltammograms illustrated in Fig. 4.35 [8]. Preliminary analysis of the electrodeposition process examined the effectiveness of a 500 cycle potential sweep process [8].

After electrodeposition, each sample was rinsed with isopropyl alcohol and allowed to dry before being stored in individual containers. Electrodeposition of fissile material was confirmed first by visual inspection, and then by SEM, XRF and alpha spectrometry, shown in Fig. 4.36. Visual confirmation of the uranium deposit was made by observing a yellow deposition, while the thorium yielded a white deposit. Three surface features, A, B, and C, were observed consistently between samples, shown in Fig. 4.36. Region A was smooth, conformally coated, and extended radially outward from the center of the sample [8]. Region B, near the edges of the samples, was composed of thicker cracked layers of fissile material with larger crystalline formations [8]. Finally, some regions of each sample possessed little or no fissile material. Region C varied in size and shape between samples and the lack of material may have been caused by surface contamination, probe contact, or detachment of a larger crystalline formation [8].

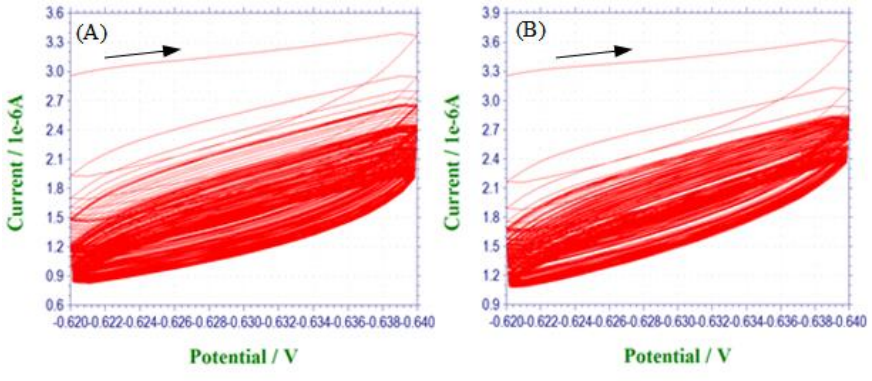

Fig. 4.35 The maximum current flowing through the electrolytic solution decreased with each potential sweep as insulating material was deposited.

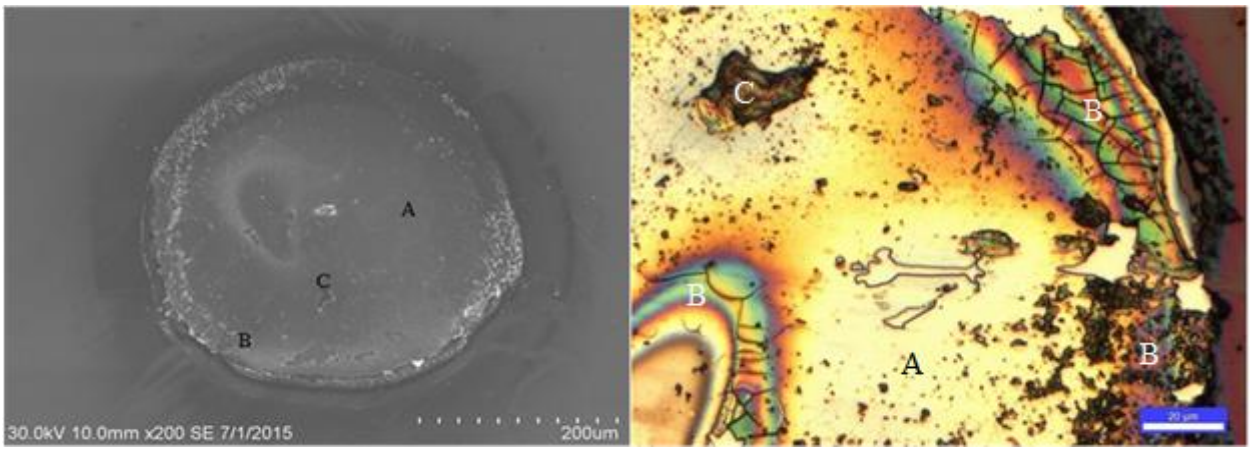

Fig. 4.36 The electric field near the edge of the electrode affects the characteristics of the deposited uranium.

XRF measurements were used to provide a qualitative estimate of the amount of uranium or thorium deposited on each sample. Each region (A, B, & C) was examined for each sample. A trend developed suggesting that the highest concentration of uranium and thorium was in region B and the lowest concentration was in region C. However, the surface features in region A were most desirable for the eventual production of MPFDs. For that reason, the effectiveness of electrodeposition in region A was of the greatest interest. Peaks in the XRF spectra for uranium and thorium respectively were observed, shown in Fig. 4.37. Although the XRF analysis did provide surface composition information, the absolute mass of fissile material could not be determined using this method. A qualitative comparison of samples, summarized in Table 4.1, was used to determine the relative effectiveness of the electrodeposition process, however alpha-particle spectrometry was used to measure the mass of each sample.

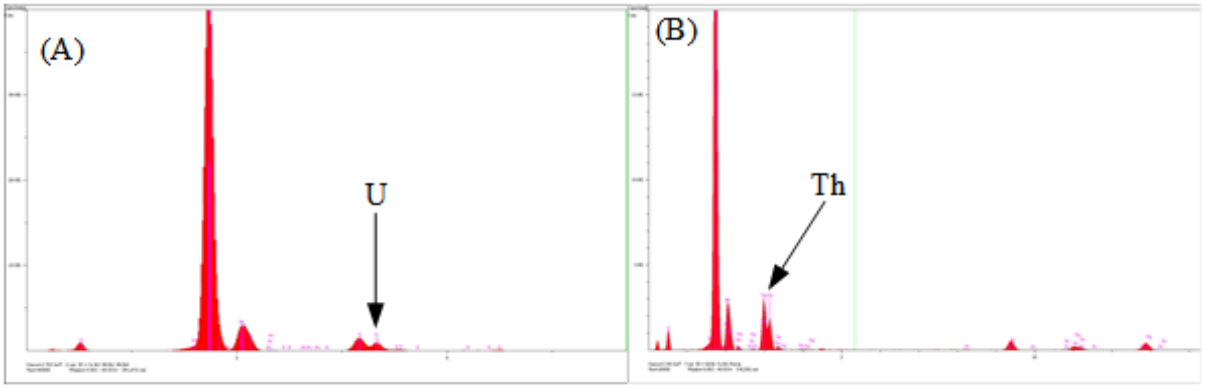

Fig. 4.37 Uranium and thorium peaks were both observed using XRF analysis.

Table 4.1 XRF results representing the relative abundance of four elements on U-deposited and Th- deposited Pt electrodes (≈ 150 µm × 150 µm for each region).

Sample and Region	Si Concentration	Pt Concentration	O Concentration	U / Th Concentration
U Central Region	64 wt. %	6 wt. %	21 wt. %	9 wt. %
U Cracked Region	61wt %	11 wt. %	15 wt. %	13 wt. %
Th Central Region	78 wt. %	10 wt. %	11 wt. %	1 wt. %
Th Cracked Region	53 wt. %	9 wt. %	16 wt. %	22 wt. %

The natural radioactive decay of uranium and thorium was utilized to measure the mass of the deposited fissile material. In secular equilibrium, natural uranium has a specific activity of 2.6×10^{-8} TBq g^{-1}, and thorium has a specific activity of 8.14×10^{-9} TBq g^{-1} [29]. Only the mass of the fissile elements is of interest for the MPFDs. Therefore a measurement of the activity of the entire sample can be divided by the specific activity of the radioactive material to determine the mass of the fissile material. The alpha particles emitted by uranium and thorium range in energy from 4.012 MeV (^{232}Th) to 4.776 MeV (^{234}U) [30], and subsequently have a range of 8.5 to 10.5 µm in UO_2 (calculated using SRIM simulation) [31]. MPFD fissile coatings are expected to be < 1 µm thick. Therefore, attenuation of the alpha particles through the fissile coating was assumed to be insignificant. A low-background ion-implanted silicon alpha-particle detector was used in conjunction with an Ortec Alpha Aria® spectrometer to measure the activity of each electrodeposited MPFD sample. The effects of background, solid-angle, and alpha-particle backscatter were all considered in the mass calculation. Background was found to fluctuate over the course of weeks. As such, a background measurement was repeated every two weeks (or as necessary when longer periods of time elapsed between measurements). Alpha-particle backscatter was determined to be insignificant after simulation in MCNP6 showed a 0.03% contribution of alpha particles in the detector which had scattered off of the platinum electrode or silicon substrate material [7]. The low activity of the MPFD samples required long (typically > 48 hrs.) measurements to achieve < 5% measurement error. Both the surface area of the electrode, and the number of potential sweeps has been shown to affect the total mass of fissile material that was electrodeposited.

4.5 Effects of High Temperature Exposure

Presently, no MPFD deployments involve exposure to high-temperature environments. Deployment environments typically range from slightly above room-temperature (TRIGA reactors) to < 600 °F (test nuclear reactors). Furthermore, current MPFD designs all include a high-purity argon back-fill for the sensor region. However, 10 MPFD samples were used to examine the effects of high-temperature exposure. The A12 series of MPFD test samples were composed of 96% alumina disks which were polished using progressively smaller alumina polishing slurry, down to 0.05 μm slurry. Polishing consisted of 200 passes with each grit with a 2-hr sonication bath in deionized water following the final polishing stage. Then, the alumina was etched with a dilute NH_4OH:H_2O_2:$3H_2O$ solution for 20 hours to yield a smooth surface. The A12 series was evaporated with 35.5 Å/15008 Å Ti/Pt electrode. The samples were then annealed in an atmospheric furnace at 900 °C for 24 hrs. Visual inspection confirmed a smooth coating with small (<2 μm wide) periodic cracks in the surface. Alumel lead-wires were attached using H20E Epo-Tek® silver conductive adhesive which was cured at 150 °C for 2 hrs. Finally three layers of fingernail polish were applied over the silver adhesive to insulate the contact from the electrolytic solution. The uranium electrolytic solution was prepared in a similar manner as described in Appendix A; however, a 1:300 NH_4OH solution was used to increase the electrolytic solution pH to 5.4, where precipitation began. A magnetic stirrer was used to dissolve the precipitate before electrodeposition. The initial scope of the A12 series was to determine the optimal potential sweep parameters for electrodeposition. As such, the sweep rate for electrodeposition and the bounds of the potential sweep were varied and are summarized in Table 4.2. The starting voltage for each electrodeposition was held constant at 0.0 V. The magnetic stirrer was used throughout each of the electrodepositions. Bubbling was observed for samples A12.d, A12.e, A12.f, and A12.i. Significant bubbling was observed for A12.i as the potential exceeded -1.3 V. The XRF analysis of the A12 series showed little (< 6%) uranium present for samples A12.e, A12.f, and A12.i and no uranium present for other samples.

Table 4.2 The rate and bounds of the potential sweep were varied separately to test the effectiveness of electrodeposition.

Sample	A12.a	A12.b	A12.c	A12.d	A12.e	A12.f	A12.g	A12.h	A12.i	A12.j
Minimum Voltage (V)	-0.8	-0.85	-0.9	-0.95	-1.0	-1.1	-1.0	-1.0	-2.0	Control
Sweep Rate (V s^{-1})	0.01	0.01	0.01	0.01	0.01	0.01	0.02	0.04	0.01	Control
Observations	No Change	No Change	No Change	Bubbling	Bubbling	Bubbling	No Change	No Change	Bubbling	Control
Deposition %	0	0	0	0	< 6	< 6	0	0	< 6	Control

A second attempt of electrodeposition was then attempted, with special care taken to avoid precipitation. The solution was mixed in accordance with Appendix A yielding a final solution pH of 3.4. Then, a 1:300 solution of NH_4OH:H_2O was used to increase the solution pH to 4.6. Although no precipitate formed, a second round of electrodeposition yielded no fissile material deposition. The final electrodeposition trial for the A12 series re-used sample A12.g and used the former control sample (which had not previously been electrodeposited), A12.j. The electrolytic solution was prepared in accordance with Appendix A, yielding a final solution pH of 3.4. No magnetic stirrer was used during the electrodeposition. Sample A12.j was electrodeposited with potential sweeps between -0.5 V and -0.64 V at a rate of 0.01 V s^{-1} for 400 cycles. One small bubble was observed near the end of the 400 cycles and the sample changed color from silver to yellow during the process, depicted in Fig. 4.38.

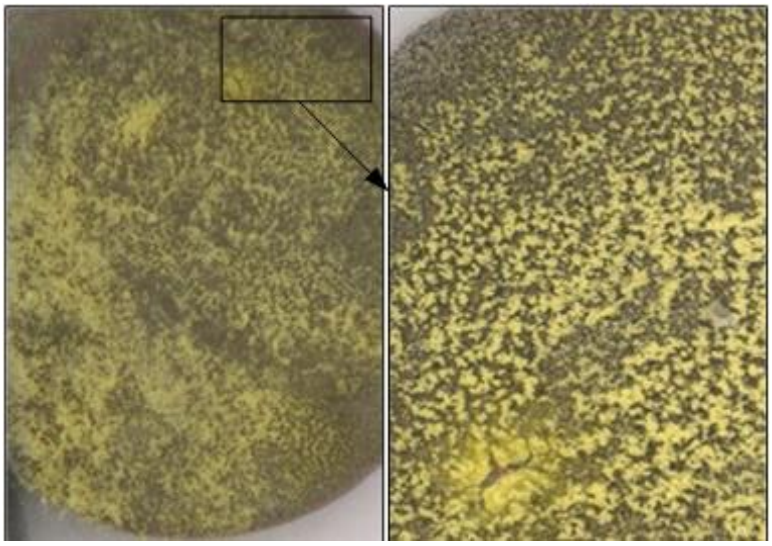

Fig. 4.38 Sample A12.j exhibited micro-spheres of a uranium compound after electrodeposition.

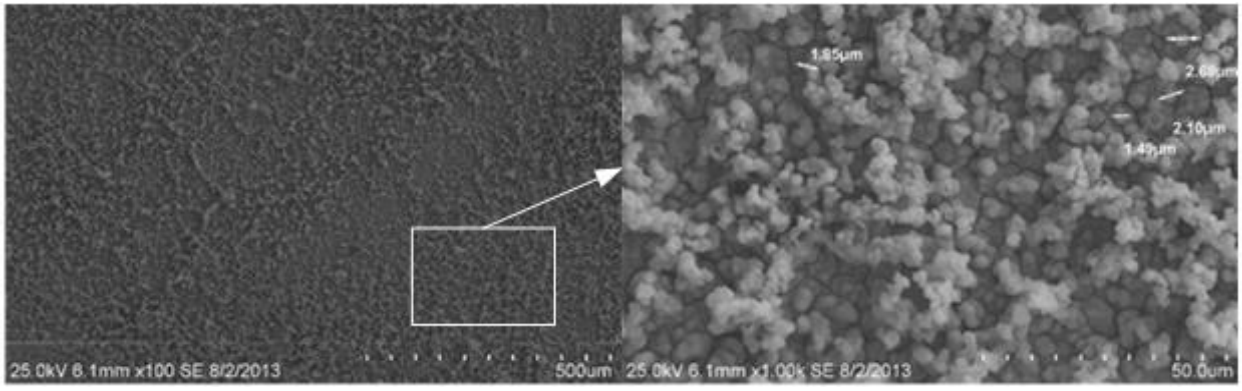

Fig. 4.39 The micro-spheres of uranium compound were relatively uniform in size, between 1 and 3 µm, over the surface of the electrode.

Analysis of sample A12.j showed a high composition of uranium. SEM analysis, depicted in Fig. 4.39, showed that micro-sized balls of a uranium compound formed on the sample surface. XRF analysis of the sample surface reported 67.3% uranium. Sample A12.g was electrodeposited with the same electrolytic solution as A12.j, however the cyclic volumetric parameters were changed. The potential sweep interval for sample A12.g was from -0.62 V to -0.64 V at a rate of 0.01 V s^{-1} for 635 cycles. Only small bubbles were observed during the second electrodeposition of sample A12.g, and the surface of the sample changed color from silver to gold as shown in Fig. 4.40 (left). The surface of sample A12.g was conformally coated with a uranium compound and did not possess any of the balls of material observed on sample A12.j. For this reason, the electrodeposition parameters for sample A12.g were adopted as the standard for MPFD sample

electrodeposition described in Appendix C. XRF analysis of sample A12.g showed a 16% uranium composition on the sample surface.

The results of the electrodeposition of samples A12.g and A12.j were significant in the progress of research on electrodeposition of MPFD substrates. First, sample A12.j proved that even a low pH electrolytic solution could be used to electrodeposit uranium onto the MPFD electrodes. In fact, the low pH solution was far more successful than previous solutions which had been adjusted to higher pH values. This simplified the electrolytic solution preparation process and also made the electrodeposition process more uniform between samples. The removal of the NH_4OH to increase solution pH also allowed for smaller electrolytic solutions to be mixed as the pH meter was not necessary for every solution. The magnetic stirrer used in previous experiments was also shown to be unnecessary. Sample A12.g also yielded important results. The surface features of sample A12.g were more desirable than the large features of A12.j. Although the process to create micro-spheres of uranium compounds described herein may be of interest in future endeavors, a uniform coating of material is preferred for MPFD fabrication.

After all other surface analysis was complete, the samples were prepared for high-temperature testing. The alumel lead-wires which were previously connected with silver conductive adhesive were removed and any remanence of fingernail polish was removed by an acetone bath, followed by isopropyl alcohol and deionized water baths. Three samples were chosen for high-temperature testing, A12.e, which had little detectable fissile deposition, A12.g, which had a uniform coating of fissile material, and A12.j, which had the most fissile material deposited. Having previously cleaned the samples, all three were imaged with a Leica DMS300® digital microscope. Then the three samples were placed in a high-temperature oven under atmospheric conditions. The oven was set to increase in temperature to 900 °C at a rate of 0.3 °C/min. The samples were held at 900 °C for 23 hrs. Then the oven was set to ramp the temperature down to room-temperature at a rate of 0.1 °C/min. After the samples were cooled, visual inspection and digital microscopy were used to analyze the samples.

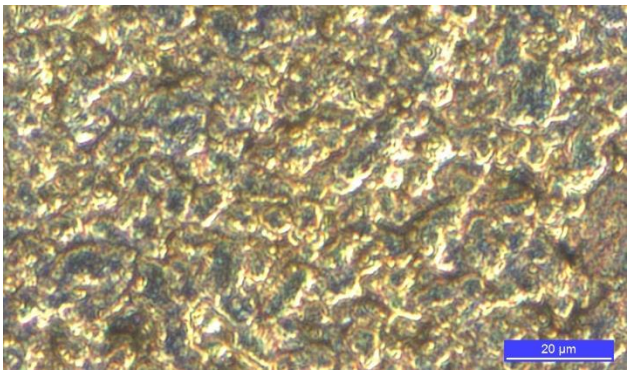

Fig. 4.40 The uranium coating on sample A12.g was conformally applied to the platinum substrate after electrodeposition.

Sample A12.e exhibited discoloration of the alumina and a gradient of peeling. The peeling became more severe further from the contact point of the alumel wire as shown in Fig. 4.41. No changes were observed in the area which was covered with fingernail polish during the electrodeposition, suggesting that some remnant of the electrolytic solution remained in the alumina substrate after electrodeposition. The electrode also exhibited a banded region where the peeling was less severe, but some discoloration was observed.

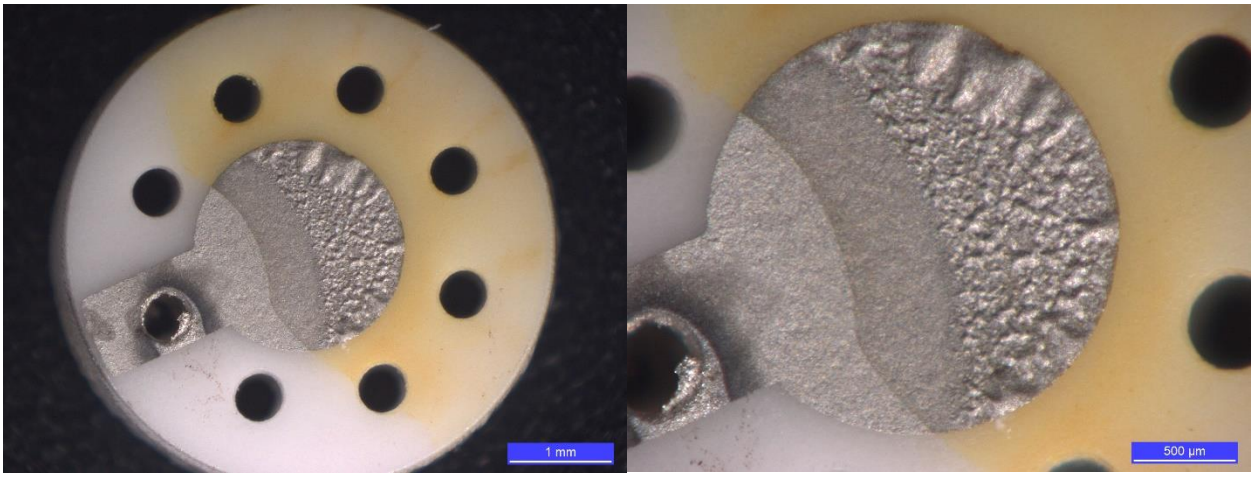

Fig. 4.41 Sample A12.e exhibited discoloration and peeling of the metallic electrode.

Sample A12.g also showed signs of peeling, shown in Fig. 4.42. The alumina substrate was discolored near the electrode. The intensity of peeling increased radially away from the original contact point, in conformance with the observations from sample A12.e. These results suggest that some component of the adhesive epoxy may have enhanced the adhesion of the Ti/Pt electrode, or that the fissile coating, which was thicker further from the contact point, may have contributed to the peeling and discoloration.

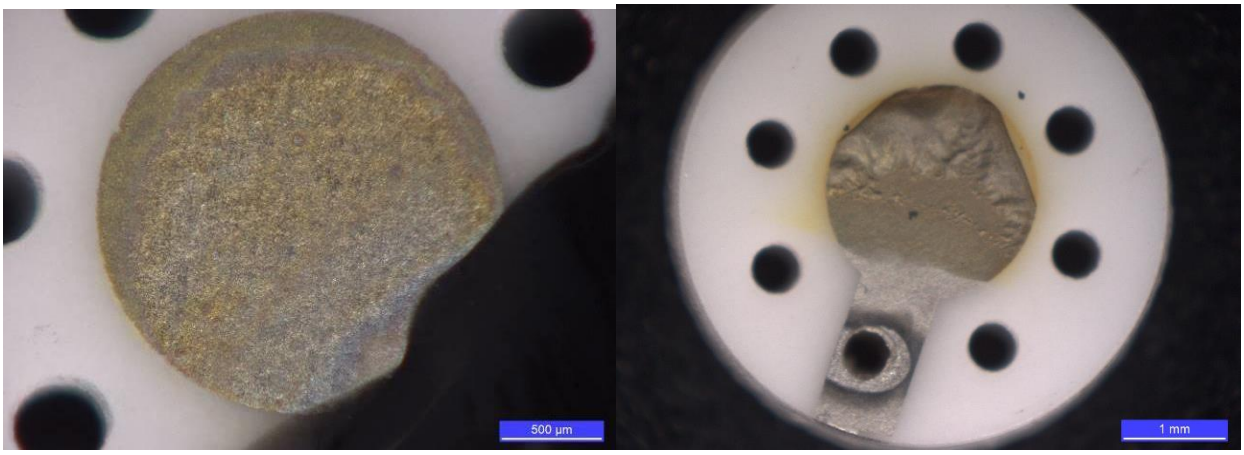

Fig. 4.42 Sample A12.g had a conformal coating of fissile material prior to high-temperature testing (left), but showed discoloration and peeling after (right) heating to 900 °C in an atmospheric environment.

Although sample A12.j showed the greatest change in surface coloration and features after heating, no peeling was observed. Recall the small balls that developed on the surface of sample A12.j following electrodeposition, depicted in Fig. 4.38 and Fig. 4.39. After high-temperature testing in an atmospheric environment, the balls separated from one another and formed a crust-like material on the surface of the sample. More drastically, the material changed in color from bright yellow to burnt orange, as shown in Fig. 4.43.

Based on the results of high-temperature testing in an atmospheric environment, two plausible possibilities were considered. First, two different compounds were deposited in the electrodeposition process. The smooth, conformal coating (golden in color) observed on sample A12.g is tightly adhered to the electrode surface. This material may be a uranium hydroxide compound (possibly $UO_2(OH)_{\#}$), and is deposited at slightly less negative potential sweeps (-0.62 V to -0.64 V). The expansion coefficient for this material is likely different from that of the alumina, causing peeling under high-temperature exposure. Also, any impurities that may have remained on the surface of the alumina before contact evaporation could have exacerbated the peeling. The second, bright yellow material, was deposited at more negative potential sweeps. During the heating process in the presence of oxygen, the uranium peroxide can de-hydrate and change phase to UO_3, a dark orange material.

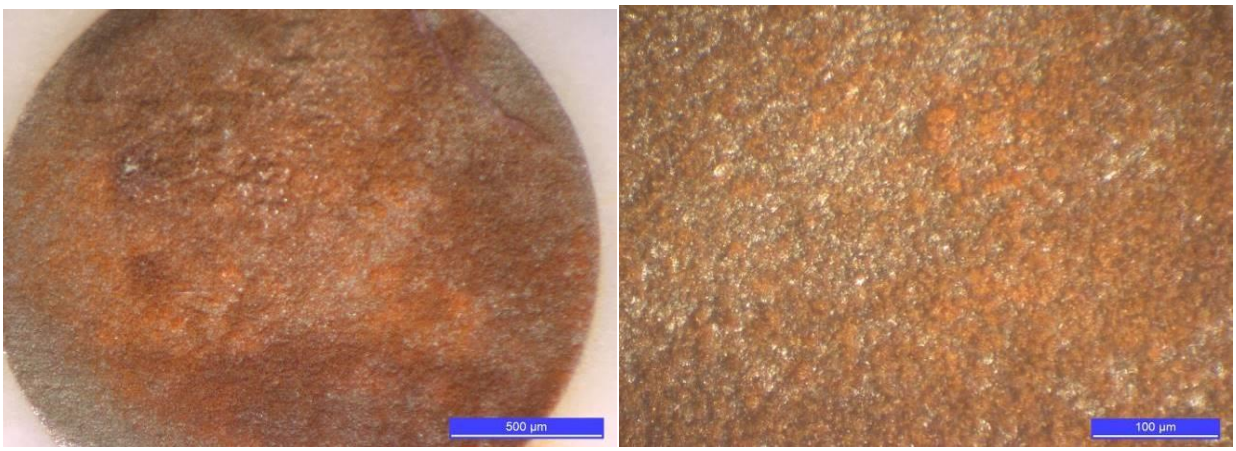

Fig. 4.43 After heating to 900 °C in an air environment the surface of sample A12.j turned from yellow to orange in color and the surface features changed shape.

Chapter 5 MPFD Support Systems

Electronic support components are required for all radiation detection systems. Pulse-processing electronics, testing facilities, and deployment methods are typically required. In addition to support electronics, numerous neutron flux ports were utilized for MPFD testing. The Kansas State University TRIGA Mk. II nuclear reactor contains both in-core and near-core test ports. Flux wire irradiation ports were also used for the design of the smallest fission chambers, and a mockup flux-wire test port was constructed for physical testing of the sensor arrays. Future work will include deployment at the ATR, TREAT, and UWNR facilities. Different variables were considered for each test location. For instance, the KSU reactor has both wet and dry test ports of different dimensions. The location and constituents of the MPFD electronic support system was also affected by the particular flux port of interest.

The design of the MPFD electronic support system has evolved over the course of the present work from a fully integrated board that was designed perviously, to single-node pulse processing, eventually to a multi-nodal support system. The evolution of this design has been motivated by factors that were discovered during the experimental process of MPFD sensor fabrication and testing described herein. Certainly these support systems will continue to evolve with the advancing technology, however, the current status of each support system is summarized in the following sections.

5.1 Kansas State University TRIGA Mk. II Nuclear Reactor and Other Flux Ports

With an operation license approving up to 1.25 MWth power, the TRIGA Mk. II research nuclear reactor is a unique test facility which has supported MPFD development and testing [32]. TRIGA reactors are particularly useful for preliminary neutron sensor testing because of their inherent safety [33]. The insertion of experimental sensors is usually of little concern for the overall safety of the reactor facility, particularly MPFDs which are exceptionally small and induce little additional reactivity. The open-pool design of the TRIGA reactor at KSU also facilitates the testing of MPFDs in and around the reactor core. One challenge of testing neutron sensors at the TRIGA facility, like most reactor complexes, is the substantial shielding present between the reactor core

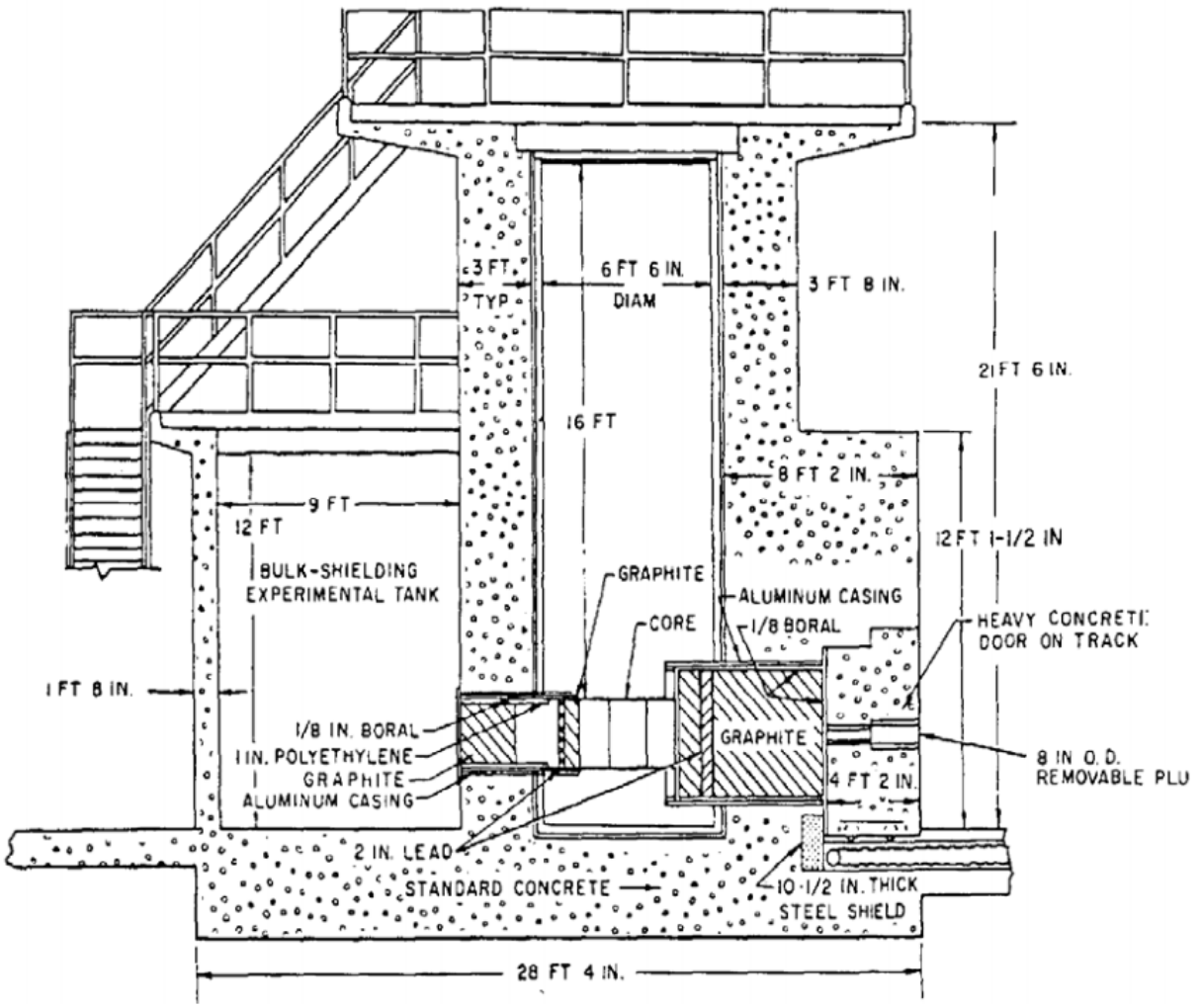

Fig. 5.1 The core of the KSU TRIGA Mk. II Nuclear Research Reactor is located 5 m from the pool surface [33].

and the location of signal processing electronics. For most MPFD operational testing, the support electronics were located on the top level of the reactor containment, while the sensors were located in or around the core, under 16 feet of water, illustrated in Fig. 5.1. Several test ports at the KSU TRIGA facility were utilized for MPFD testing

The central thimble, a water-filled, 1.33-in diameter [33] stainless steel test port extending to the center of the reactor core, has an estimated fast-to-thermal ratio of 1.2 [32]. At 250 kWth, a constant thermal flux of 10^{13} cm^{-2} s^{-1} and fast flux of 1.2×10^{13} cm^{-2} s^{-1} was confirmed by iron-wire activation analysis as part of previous work [12]. Access to the central thimble is located at the pool surface, shown in Fig. 5.2. A special dry-port was constructed from 6.35-mm (0.25-in.) outer-diameter stainless steel tube attached to a gas purge/fill and electronics feedthrough

assembly, shown in Fig. 5.2. The MPFD fabrication and testing procedure for all wet-ports was similar in nature and will be described in greater detail in section 5.2.

The Intra-Reflector Irradiation System (IRIS) was designed to allow easy access to a dry-irradiation port for gamma-irradiation. Neutron flux levels in the IRIS are nearly 100-times lower than in the central thimble; the fast-to-thermal ratio of ≈1:20 was determined experimentally [12]. A thermal flux of 2.2×10^{11} cm^{-2} s^{-1} and fast flux of 1.5×10^{10} cm^{-2} s^{-1} were measured by iron-wire activation analysis [12]. The absence of water made the IRIS a convenient test location for early permutations of the MPFD, however because the IRIS is open, humidity was found to settle at the bottom of the test port. The humidity could be removed by back-filling the port with heavier inert gas, however argon was not allowed due to activation concerns. Preliminary tests measuring a reactor pulse were conducted in the IRIS, taking advantage of the lower amplitude, heavily thermalized neutron flux [9].

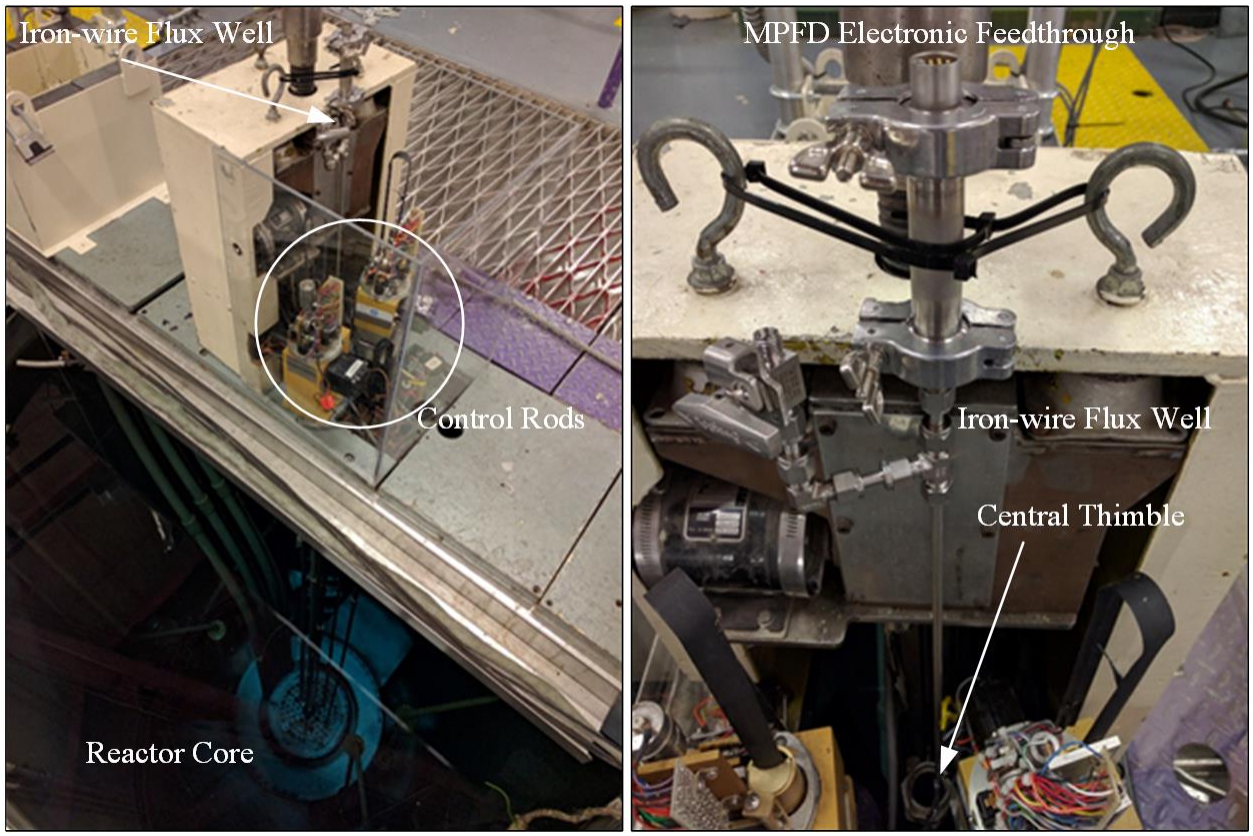

Fig. 5.2 The central thimble offers the highest neutron flux levels at the KSU TRIGA Mk. II Nuclear Research Reactor.

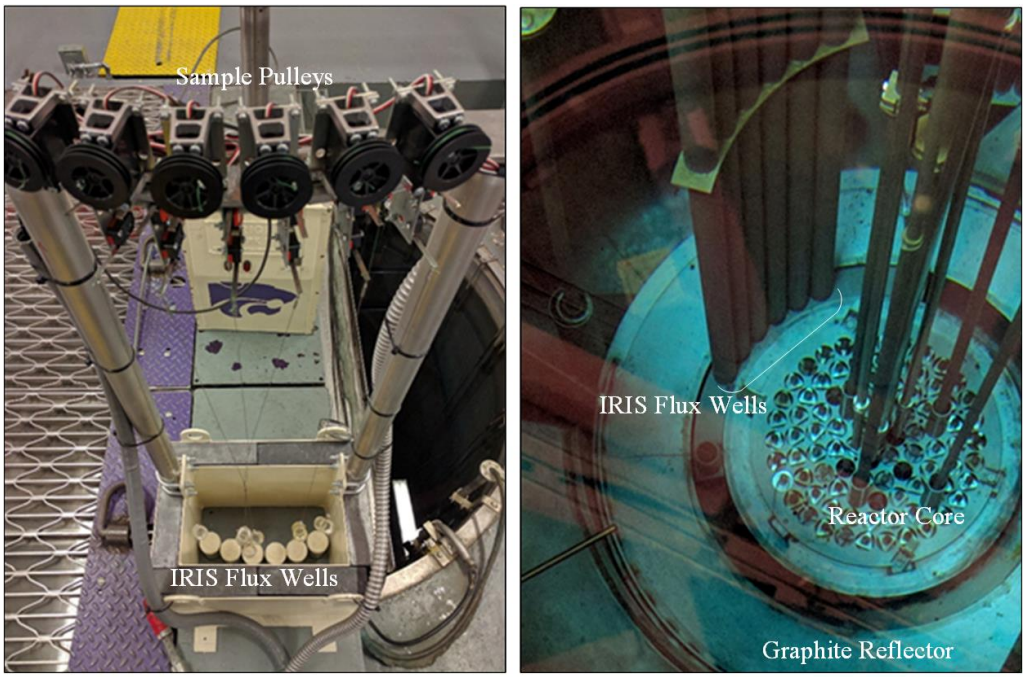

Fig. 5.3 Located within the graphite reflector of the core, the neutron flux in the IRIS test port is more thermal (1:20 fast-to-thermal ratio) than in the central thimble but flux levels are ≈100 times lower.

A second water-filled test port was also available for testing at the KSU facility. The sources-storage port, identified in Fig. 5.4, provided a near-core alternative to test MPFDs. Poor electrical grounding of the central thimble coupled with close proximity to the pulse-rod control drive induced significant RF noise in the MPFD support electronics. This test port used the same 6.35 mm (0.25 in.) stainless steel test assembly used in the central thimble, which could be easily inserted into the reactor pool. The flux levels in the source-storage test port were expected to be similar to the levels present in the IRIS.

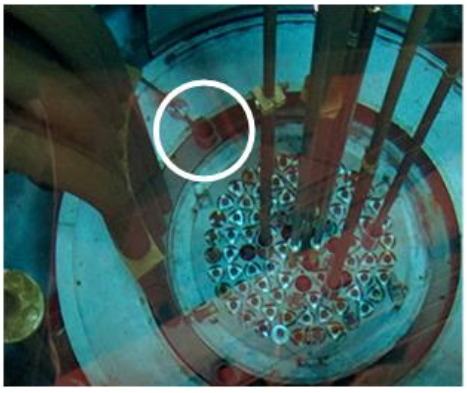

Fig. 5.4 The source-storage port was located next to the reactor core, within the graphite reflector.

The KSU TRIGA Mk. II Nuclear Research Reactor possesses four neutron-beam ports; only the radial beam port was used for MPFD testing. The neutron flux levels in each of the beam ports are much lower than in the reactor core. A maximum thermal neutron flux of $\approx 10^5$ cm^{-2} s^{-1} was expected in the radial beam port. Attempts to test MPFDs constructed with natural uranium in the radial beam port did not yield any positive results due to the extremely low sensitivity of the MPFDs.

Fig. 5.5 The radial beam port was used to test neutron sensors but was not heavily utilized for MPFD testing.

MPFDs were also designed to be deployed into a generic iron-wire flux port. The ease-of-access found at TRIGA reactor facilities is uncommon for nuclear test facilities. In some cases, in particular at high-power facilities, the only available test port to deploy MPFDs were originally installed for iron-wire flux activation. These ports are commonly designed to facilitate the insertion of a high-purity iron wire which can be irradiated and analyzed to determine the total fluence to which it was exposed. A total length of 18 feet (top to bottom) and tube inner-diameter of $\approx$ 3-mm was representative of a typical iron-wire test port, as illustrated in Fig. 5.6. No flux port was deployed into the KSU reactor, however a mock-up test port was constructed to test the feasibility of deploying an MPFD array into such a port [12]. A 6.35-mm (0.25-in.) outer-diameter stainless steel tube with 1.651-mm (0.065-in.) wall-thickness was used in the central thimble to provide a similar test environment but was not bent to the specification in Fig. 5.6. Physical testing of the MPFD arrays in the mock-up port identified many short-comings in the original design which utilized alumina insulation for the anode and cathode wires, discussed in further detail in section 5.2 [12].

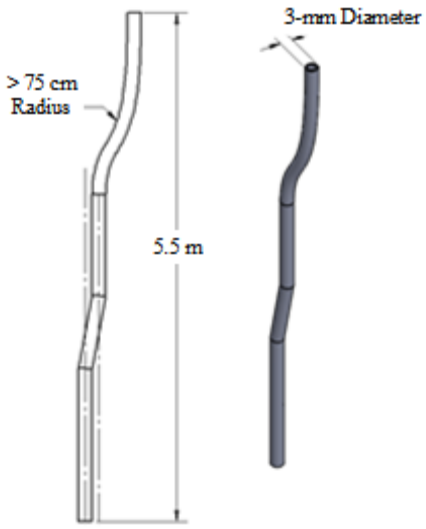

Fig. 5.6 The iron-wire flux port mock-up included two doglegs which the MPFD arrays were required to navigate [12].

5.2 Sensor Deployment Methods

Although several neutron flux wells were utilized for MPFD testing, only two fabrication methods were investigated. The two fabrication methods can be categorized into an encapsulated design and a flux-well design. The encapsulated design, described in greater detail in section 6.2, was designed with larger components than the flux well design. The first encapsulated MPFD tested at KSU was first sent to the Idaho National Laboratory High Temperature Test Laboratory (HTTL) for final assembly and encapsulation before being returned to KSU for testing. The disks and spacers were assembled on the end of a custom-made mineral insulated cable, shown in Fig. 5.7. The array was delivered with spade-style connectors for each of 2 MPFD nodes and coaxial extension cable was constructed which connected the sensor to the signal processing electronics. The encapsulation fabrication method had two distinct advantages. First, the fabrication and analysis techniques developed at the HTTL are unique, yielding a robust sensor. Also, the assembly of the MPFD sensors onto the end of mineral insulated cable produces an instrument that has the extension cable as an integral part of the assembly. Fastening a plug to the end of the extension cable should prove a reliable method of connecting the sensor to readout electronics. Presently however, the fabrication time for the encapsulated MPFD and high capacitance of the mineral insulated cable have produced limited in-core test results [7].

Fig. 5.7 The first encapsulated MPFD utilized a parallel plate geometry with conductive adhesive and was assembled on the end of several feet of custom mineral insulated cable.

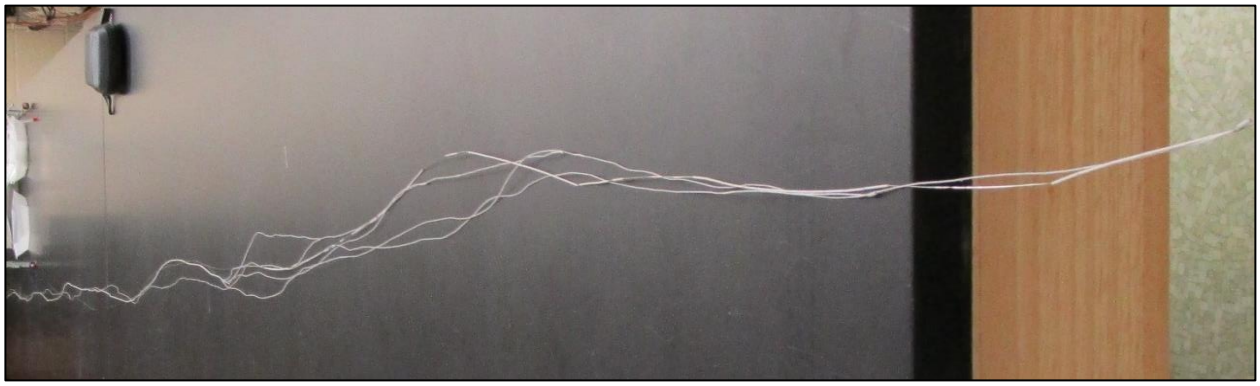

Fig. 5.8 Early MPFD flux well arrays had high capacitance because of the alumina insulation.

Early in the fabrication and testing process, little attention was given to cable selection connecting the MPFD sensor with the preamplifier. Unnecessarily long cables were often chosen, and cable capacitance and impedance were commonly neglected. After the first tests yielded questionable results using older preamplifier technology [7], research was redirected towards the development of the electronic coupling and support system. As different methods of deploying MPFDs into the reactor were explored various wire-insulation and coupling methods were also investigated. Some MPFD arrays were fabricated at the HTTL with extension cable fixed to the sensor. Other arrays were constructed at KSU and required custom insulation of the anode and cathode wires. Various materials were explored during the process of determining how to best construct arrays which could be inserted into iron-wire irradiation flux wells. The original design for a multi-nodal MPFD array which could be deployed into an iron wire flux used alumina insulation for the anode and cathode wires, shown in Fig. 5.8.

Alumina has a hardness similar to diamond and is difficult to form and machine. Cutting the alumina insulation was first attempted the use of a razor blade and tungsten carbide wire shears. Alumina segments cut with the wire cutters and a razor blade were prone to chipping and cracking. For more precise segmentation, a diamond wire saw was used. When threaded onto the anode and cathode wires the alumina would ultimately leave portions of wire uninsulated and exposed. Another issue that resulted from using the alumina as insulating material was the higher probability of pinching and kinking the wire. The alumina was cut into half-inch segments to allow for some flexibility of the assembled array. Over 400 alumina segments were required to insulate a single 2-node MPFD array. Threading the 400 segments was cumbersome and required focus for long periods of time, usually several hours of work. At each joint where two alumina segments met

there was a chance that the wire could get pinched or kinked between the segments. The use of many segments, while helping improve the flexibility of the array, provided multiple points for snagging to occur whenever the array was inserted for testing. A mock-up flux well port was constructed to test the feasibility of inserting multi-nodal MPFD arrays into an iron-wire flux well, depicted in Fig. 5.9.

In addition to mock-up testing, these alumina-insulated arrays were also deployed in the IRIS and central thimble, yielding preliminary neutron measurements (discussed in section 6.1). Connectors were applied to the ends of the anode and cathode wires which supported coaxial RG58 cable with BNC-style connectors, shown in Fig. 5.10. Resistance checks were performed for the sensor arrays to confirm that the anode and cathode did not make contact, but the capacitance of the early test arrays was not characterized. It was not until later in the development cycle, when noise reduction was a primary concern, that the array capacitance and cable impedance were taken into consideration.

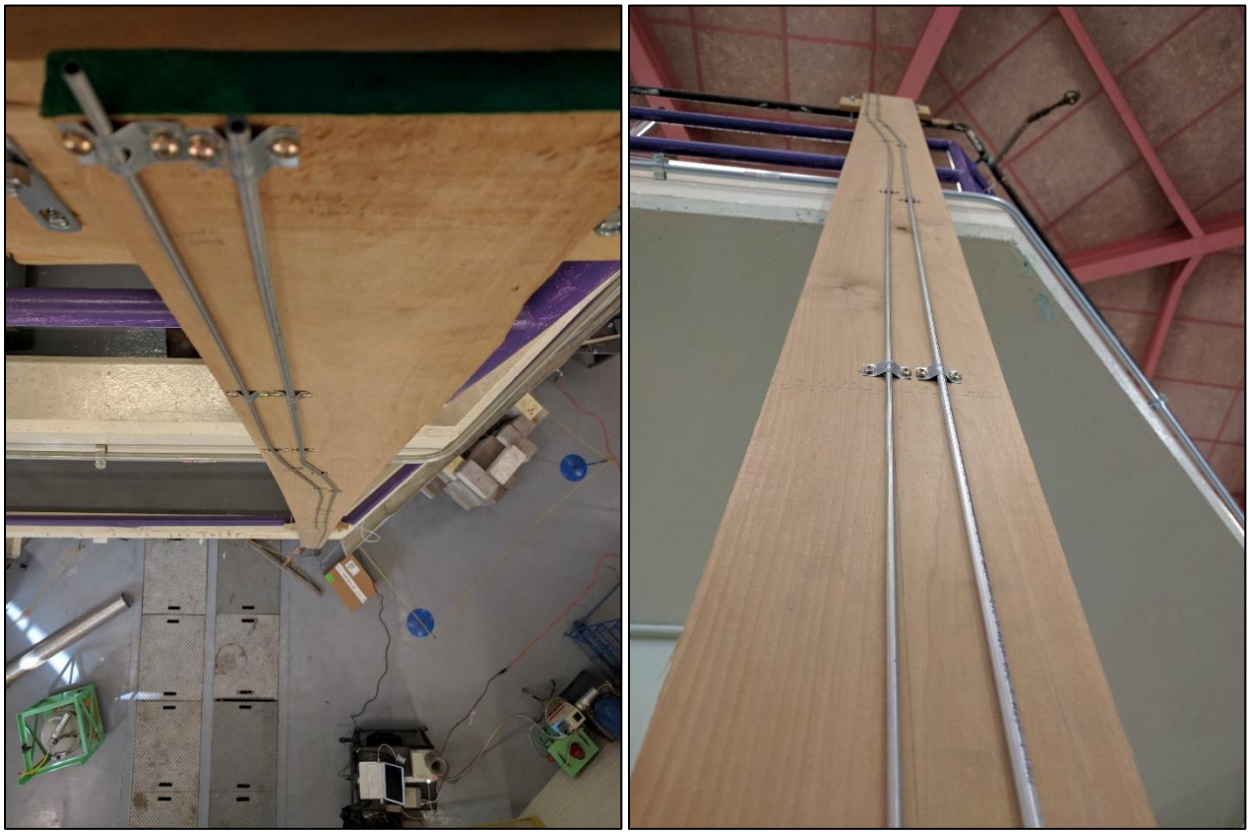

Fig. 5.9 Mock-up test ports were constructed from stainless steel and Inconel, emulating a typical iron-wire flux port.

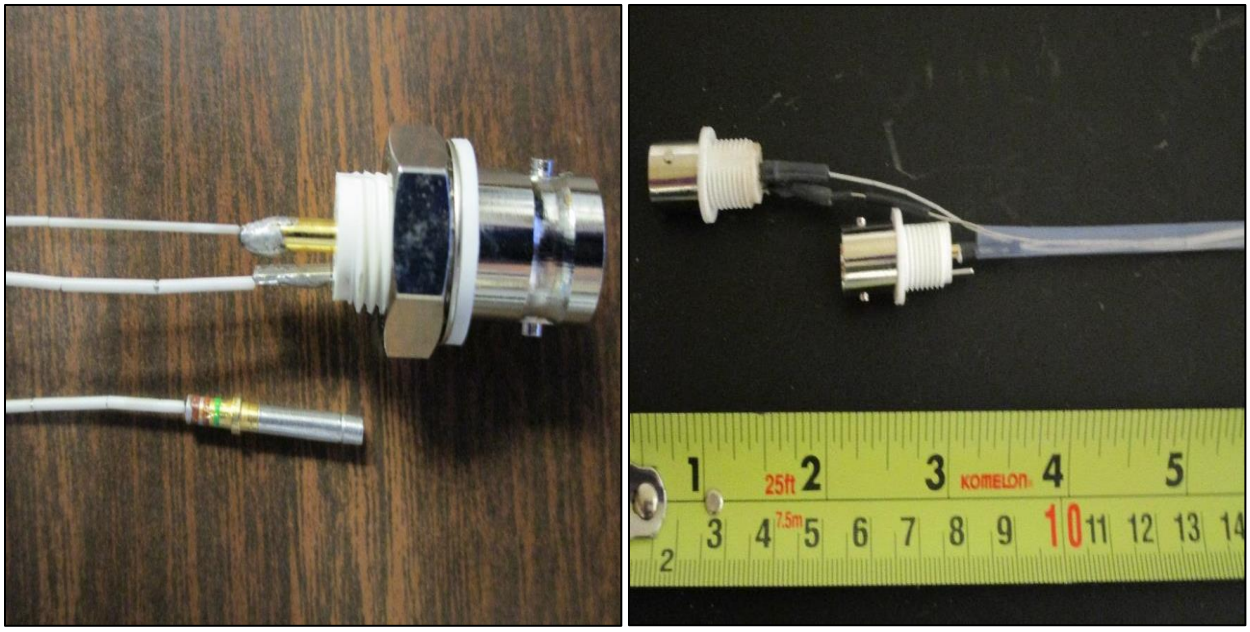

Fig. 5.10 Coaxial BNC plugs were utilized to connect alumina-insulated MPFDs to support electronics.

It was discovered during mockup testing that the alumina generated too much friction during insertion and prevented the array from being fully inserted [12]. The anode and cathode wires of the array would bend sharply and suffer damage during insertion into the mock-up test port, depicted in Fig. 5.11. The friction which developed after only a short section was inserted was the main limitation observed when inserting alumina-insulated MPFDs [12]. The hard alumina rubbed on the inside wall of the mock-up flux well, even producing metal shavings observable in Fig. 5.11. Because of the difficulty inserting MPFD arrays with multiple nodes using alumina insulation, a 2-node design was determined to be the only option which could be insulated with alumina and successfully inserted into the mock-up port [12].

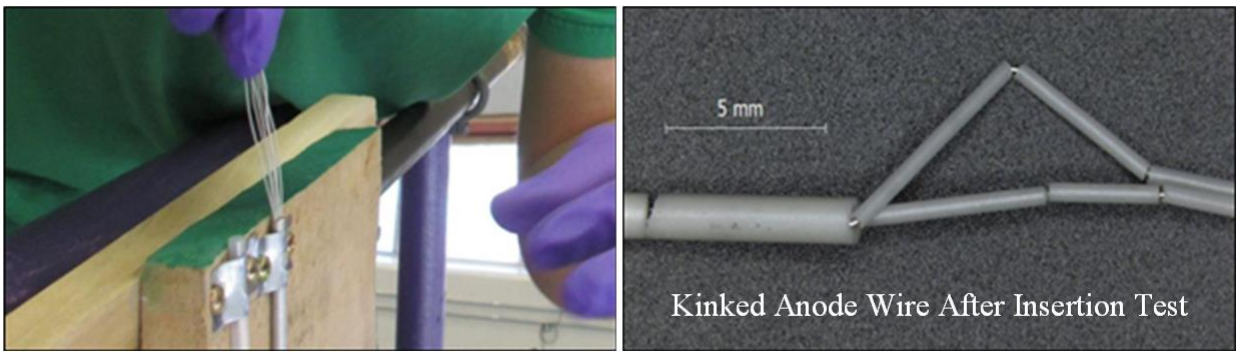

Fig. 5.11 The alumina insulation caused damage to the MPFD array during insertion into the mockup flux well [12].

A PTFE shrink-tube was used to reduce the friction between the alumina and the flux well port, successfully enabling full insertion [12]. However, the PTFE was not allowable for final insertion into the flux well due to breakdown of the material, causing potential for fluorine release which could corrode the flux well. Deficiencies in the alumina anode insulation were observed, depicted in Fig. 5.11, which caused unreliable operation [12]. Then, coated fused silica capillary tubing was identified with appropriately sized dimensions to act as an insulator for the anode wires [12].

Mockup testing showed that the silica with a proprietary coating produced less friction upon insertion [12]. The silica tubing shown in Fig. 5.12 is flexible, lightweight, and relatively neutron transparent. Mock-up MPFD arrays were constructed by hand at first. The use of silica capillary tubing to insulate the MPFD array anode wires is easier and faster than alumina. The silica could be cut with the normal tungsten carbide cutters, or with a specialized capillary tubing cutter that provided high-quality edges and minimal debris accumulation in the tubing, shown in Fig. 5.13. The use of the Shortix™ capillary tube cutter further improved the quality of the MPFD arrays.

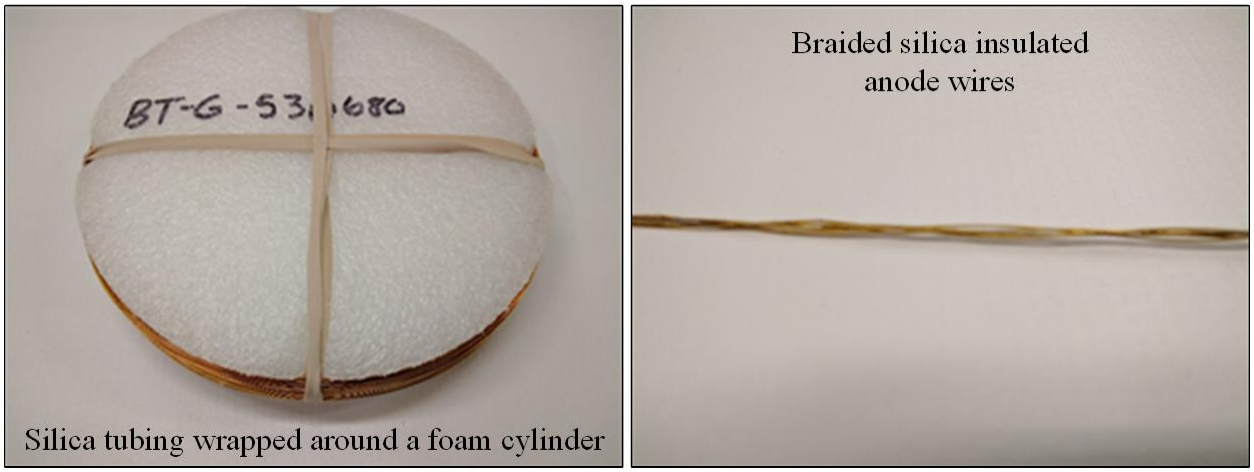

Fig. 5.12 Commercially available, flexible silica capillary tubing was a significant improvement over alumina insulation for multi-nodal MPFDs because it could be braided and produced significantly less friction within the iron-wire flux well tube.

Fig. 5.13 The use of a specialized capillary tube cutter improved the quality of the assembled MPFD array, reducing fracturing and improving wire coverage [34].

Because the silica is flexible, the anode wires could be fully insulated with fewer segments, typically between 3 and 6 segments by hand, and even greater efficiency could be achieved using a mechanical threader designed for the task, depicted in Fig. 5.14. With such a small number of segments, the probability of damaging the wire in the course of threading was reduced. A single anode wire could be insulated in less than an hour, in contrast to the many hours required for each anode using alumina. The reduction in the number of insulation segments, coupled with the inherent smoothness of the silica, reduced the observed damage to MPFD arrays during insertion testing. The silica also generated less friction with the inside wall of the flux well during insertion, decreasing the likelihood of an insertion failure. Another advantage of silica, unexpected at the time, was the lower dielectric constant (≈3) when compared to alumina (≈10). The lower dielectric constant, and thinner walls of the capillary tubing produced MPFD arrays with significantly lower capacitance. The differential capacitance (between anode and cathode) for a typical 6 m MPFD array constructed with alumina insulation was frequently > 1000 pF. In contrast, MPFD arrays constructed with silica capillary tubing typically yield a measured differential capacitance < 300 pF. The lower capacitance significantly reduced the inherent line-noise in the preamplifier, regardless of which preamplifier was tested. The new insulation material did present additional challenges that had not been of concern with the alumina insulation.

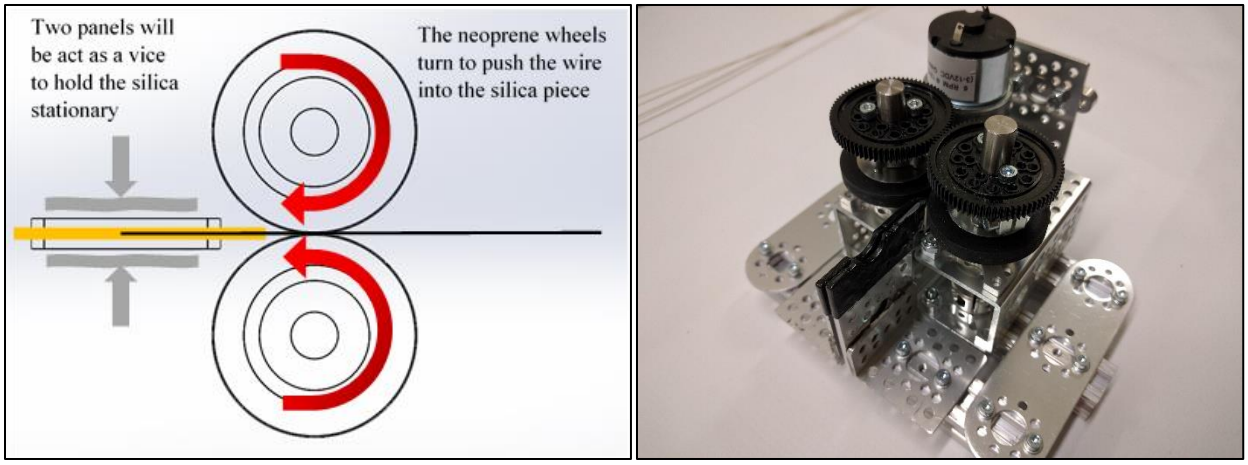

Fig. 5.14 MPFD array fabrication was improved by the development of a mechanical threader for the anode wires.

The new fabrication method did however require additional consideration of the rigidity of the array compared to the alumina-insulated arrays. Loosely assembled, the anode and cathode wires were not able to be inserted effectively into the mockup test port. A braiding procedure was developed which enhanced the rigidity of the array, holding the anode wires together around the cathode wire. The braiding method, referred to as "May-Pole Braiding" was used to create a braid using only the anode wires which wrapped around the straight cathode wire. In this manner, the length of the array was maintained and cross-talk between anodes can be reduced. The hand-braiding process required at least two people for typical 20-foot long arrays.

Although 2-node arrays could be fabricated by hand, the utilization of silica insulation made even the insertion of MPFD arrays with up to 5 nodes possible in the mock-up flux well. Braiding additional anode wires by hand proved to be particularly challenging, however a mechanical braiding system was adapted from a design which was originally designed for crafts [35]. The upgraded mechanical braider, shown in Fig. 5.15(a), was designed and fabricated to allow for braiding of MPFD arrays, depicted in Fig. 5.15(b), with up to 16 anodes (although only 5 anodes have been tested).

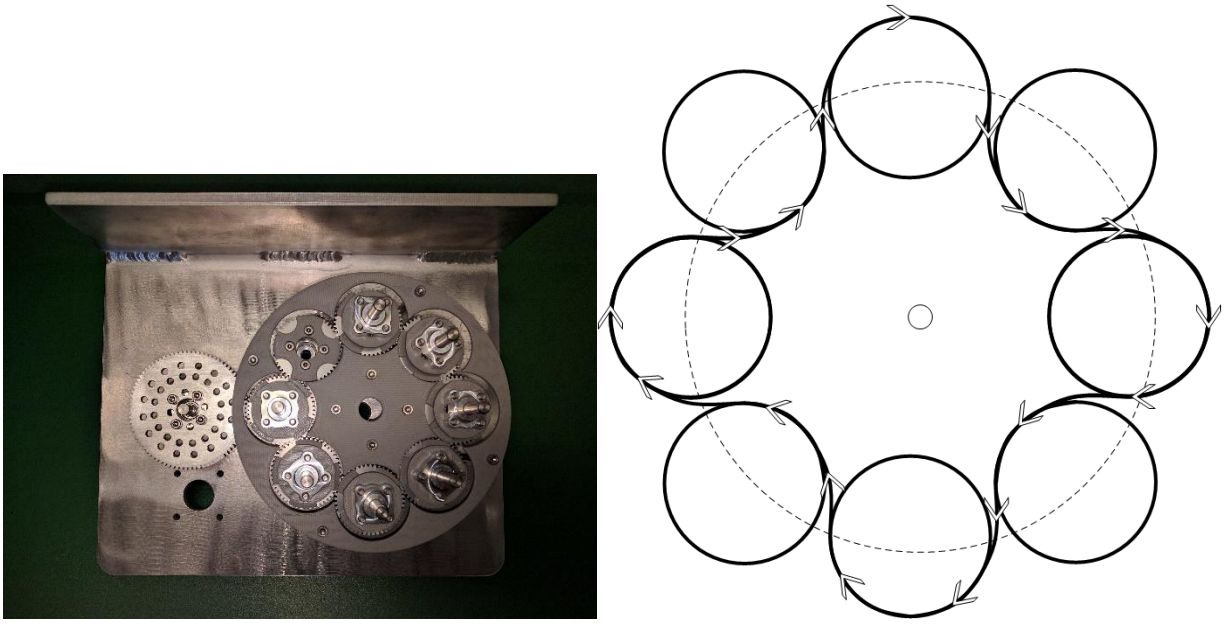

Fig. 5.15 Although braiding by hand was sufficient for 2-node MPFD arrays, expansion to 5-nodes called for a mechanical braider to be developed.

Two other alternatives were explored that could take the place of the silica-insulated, hand braided extension cable. Single-conductor mineral insulated cable was purchased and a single-node MPFD was constructed by stripping the sheath from 2 cables. However, the junction between the mineral insulated cable and the MPFD was not structurally sound, and the array was not tested in-core. Additionally, the magnesium oxide insulation in the mineral insulated cable produced a high capacitance in the cable, not conducive for effective signal propagation. Kapton-insulated K-type thermocouple (chromel-alumel) was also explored. The individually insulated wires were pre-packaged in pairs which were bound by an outer coating of Kapton. Stripping the Kapton insulation proved to be challenging, and the separation between anode and cathode was not sufficient at the junction to prevent discharge under an applied bias. Additionally, the pair of wires did not facilitate a common-cathode design which was a key component of the flux-well MPFD design. For all of the aforementioned flux-well designs, an electronic feedthrough and gas purge/fill system were fixed to the top of the test port, depicted in Fig. 5.16. The gas purge/fill assembly was used to purge all of the gas from the system and fill with high-purity argon before testing the sensors. Argon was used as an inert fill gas which could be used as an ionizing medium within the MPFD sensor. The entire flux-well was filled with argon to allow for natural circulation of the gas to replenish the ionization chamber within each MPFD sensor.

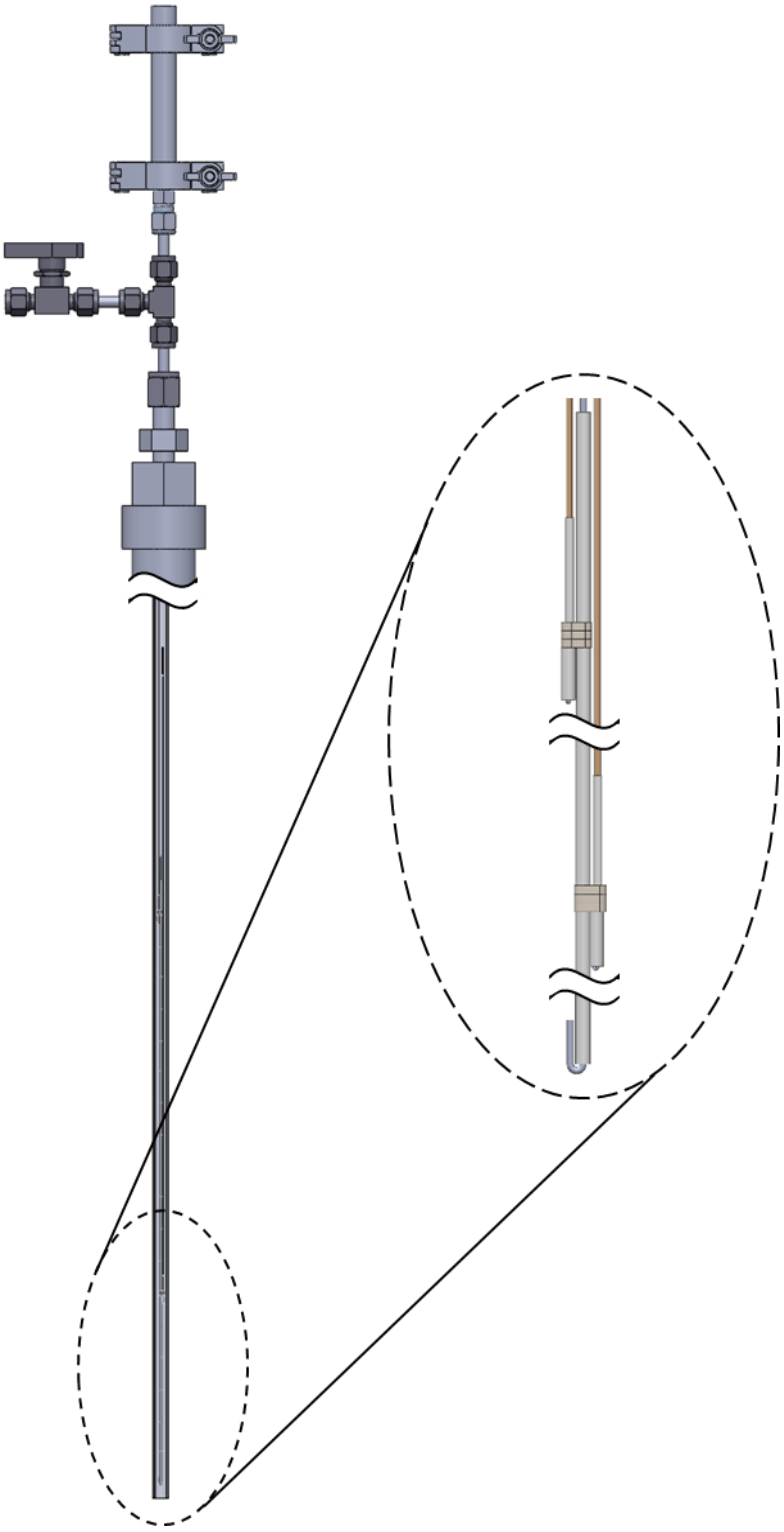

Fig. 5.16 The MPFD array was inserted into the flux well and connected to the electronic feedthrough. The individual MPFD sensors were located near the bottom of the flux well.

Fig. 5.17 An electronic feedthrough (MDC 1039601) and electronic feedthrough plug (MDC 1150101) connected the MPFD array anode and cathode wires with the signal cables.

The electronic feedthrough was connected to the signal processing electronics via the connector shown in Fig. 5.17. Appropriate cabling was connected to the feedthrough to support the various permutations of support electronics explored for MPFD signal processing (described in further detail in section 5.3).

A third MPFD fabrication method has also been developed to support the deployment of large MPFD arrays throughout a research reactor core. A modular MPFD array was designed which would provide 4 equally-spaced MPFD sensors in a linear array. The modular MPFD array used a standard Lemo push-pull-style connector, enabling arrays to be easily swapped out in case of failure or for transfer to a different location. In particular, the modular MPFD design was designed to aid in testing at both the University of Wisconsin's nuclear reactor (UWNR) and the KSU TRIGA Mk. II Nuclear Research Reactor. The MPFD sensors were distributed in a ≈ 2-m (6-ft.) section of 7.94-mm x 0.51-mm (5/16-in. x 0.020-in.) stainless steel tubing with a laser-welded cap on the bottom. The 7.94-mm outer diameter tube was selected to fit in the 8-mm grid-plate holes at the KSU TRIGA facility [13]. A gas purge/fill system and electronic plug were designed to be sufficiently far from the core to reduce activation, illustrated in Fig. 5.18. The MPFD nodes were separated by 10 cm. SiO_2 spacers which were also used to insulate the anode and cathode wires in the top portion of the array.

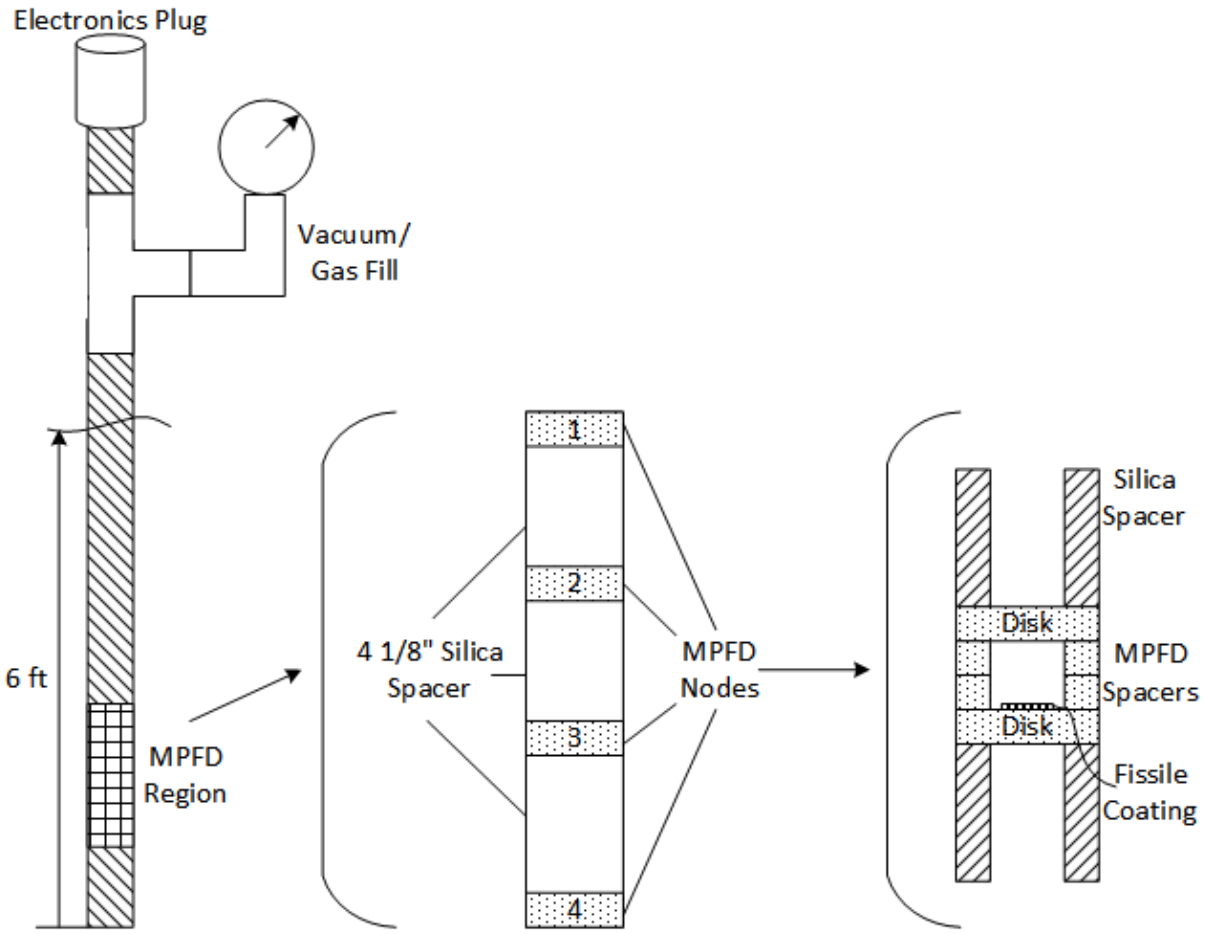

Fig. 5.18 The modular MPFD array was composed of four MPFD sensors separated by SiO_2 spacers encapsulated within the stainless steel tube.

The top of the MPFD array was terminated using a Lemo FG.1K.308.CLAK80 plug designed to fit onto the 7.94-mm (5/16-in.) tube using a collet. A Lemo PHG.1K.308.CLLK75 receptacle was chosen to couple with the plug, secured to a 4-pair shielded cable bundle (Belden 8134E), shown in Fig. 5.19. The linear spacing between MPFD sensors was determined before construction to provide different axial resolution for in-core experiments. The SiO_2 insulators were accurately cut using a diamond wire-saw to provide precise spacing between MPFD nodes. The ability to easily exchange different cables or MPFD arrays with the modular design improved troubleshooting ability, instrument qualification, storage, and transportability. Other MPFD array designs yielded a sensor-wire assembly nearly 20 feet long which is challenging to handle and deploy. Inserting such long assemblies into a reactor vessel at a university research reactor facility posed a risk of damage to the array and produced streaming paths for radiation out of the reactor vessel. The modular design was particularly useful for university research facilities which typically

have easier access to the reactor core. The tubular arrays fit between fuel baskets at the UWNR, which have a 19-mm (0.75-in.) space between each basket. The extension cable can be routed in a manner which eliminates streaming paths and avoids critical reactor control mechanisms. Each modular MPFD array can also be qualified using an electronics system proven to work for other arrays, reducing the variability in the initial testing phase. When the sensor, connector, and cabling selections were maintained constant, greater attention will be given to the optimization of the signal processing system.

Fig. 5.19 The modular MPFD array utilized a Lemo (FG.1K.308.CLAK80, left) plug on the array with a Lemo (PHG.1K.308.CLLK75, right) receptacle on the multi-pair shielded cable.

5.3 MPFD Signal Processing

The design and testing of a signal processing system for MPFD testing was the final major task in the development of MPFDs. Common practice when developing and testing radiation detectors is to use standard Nuclear Instrument Module (NIM) components to conduct preliminary tests and then proceed to customized electronics. Numerous attempts were made to utilize specialized electronics which were designed for other neutron detection systems in an attempt to leverage previous work. All of these attempts failed to produce reliable results. Finally, after returning to

basic signal processing components, the MPFDs were successfully tested. After that time, efforts focused on improving the signal from MPFDs. The high specific energy deposition by fission fragments should produce large pulses, however in early testing the neutron-induced signal was hardly visible above the electronic noise. Noise from reactor control systems and RF background noise deteriorated the signal from the MPFD sensors. Reducing line capacitance, impedance matching, and improved electronics were all important steps in overcoming the noise problems observed in early tests.

5.3.1 MPFD Pulse Calculation

Preamplifier gain for ionization of argon gas can be expressed in units of V per MeV by Eq. 5 [36]. Therefore, the sensitivity of the MPR-16_V100 preamplifier with a 10 nF input capacitor is .006 mV/MeV. Therefore, a large gain must be applied to the preamplifier signal to amplify the pulse to a level that can be transmitted to the shaping amplifier [36].

$$\frac{V_0}{E} = \frac{1.6 \times 10^{-19} \left(\frac{C}{eI}\right)}{C_{pre-amplifier}(F)\ 26.4 \left(\frac{eV}{eI}\right)} \times 10^6 \left(\frac{eV}{MeV}\right), \quad (5)$$

The large gain necessarily applied to the detector signal in a preamplifier also amplifies any noise that is present. Preamplifier noise is most commonly a symptom of RF noise and input capacitance, both a function of the length of cable between the sensor and the preamplifier. Unfortunately, the extension cable for MPFDs must be long enough to extend from the sensor in the reactor core past the reactor containment. A 20-foot extension cable is sufficient to reach the top an open-pool reactor. An additional length of cable is required to connect the flux well feedthrough to the preamplifier typically < 10 feet away. Several preamplifiers and electronics systems were investigated to support MPFD testing. Eventually, a custom designed unit was professionally fabricated and will be available off-the-shelf for future applications.

5.3.2 Preamplifier Selection

Previous development and testing of MPFDs included the design of a custom electronics board [13]. The specific characteristics of this electronics board were unknown at the time of testing but after later investigation it was determined that the board was designed to operate in common anode mode for arrays of multiple MPFDs. Radio frequency filters with unknown cutoff frequencies were also observed in the circuit which was designed to produce a differential output signal. There were

several characteristics of this first electronics test board, depicted in Fig. 5.20, that have proven illustrative of the eventual design, but that were not appreciated at the time of testing.

First, the use of a differential-mode preamplifier output greatly reduces the common-mode noise observed in a radiation detection system. This common approach to noise reduction was not applied until late in the present work and could have improved the signal-to-noise ratio and subsequently the quality of test results early on in the research. Radio frequency (RF) filtering was a second method to reduce electronic noise from external sources. Band-pass-filters (BPFs) can be designed to target a specific signal frequency, attenuating other frequencies. Although a BPF does shape the pre-amplified pulse, RF filtering can be used to effectively eliminate electronic noise that is both lower and higher frequency than the expected signal. RF filtering was also used as part of the present work to reduce electronic noise in the KSU TRIGA reactor facility during preliminary testing. Although MPFDs were tested with this custom electronics board, the results were inconclusive. Electronic pulses were observed that were presumed at the time to be from incident neutrons. However, the high cable capacitance during the test and unknown configuration of the electronics board produced a tail-pulse with a rise-time longer than expected for the MPFDs, shown in Fig. 5.21. The MPFD system which was first tested as part of the present work was unreliable and eventually failed to produce any signal. At the time, a leak was determined to be the cause of sensor failure, however it was later discovered that the instrument passed helium leak checks at the HTTL before being shipped to KSU. It now seems more reasonable that improper electronics coupling was to blame for the poor operation of the instrument.

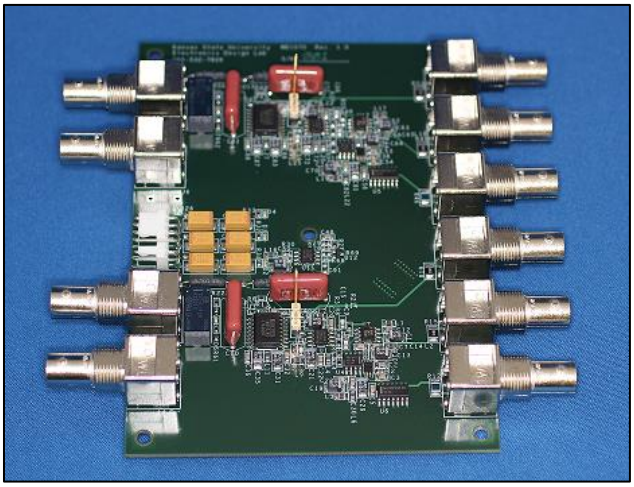

Fig. 5.20 A custom MPFD electronics board was used for preliminary testing at the beginning of the MPFD research [13].

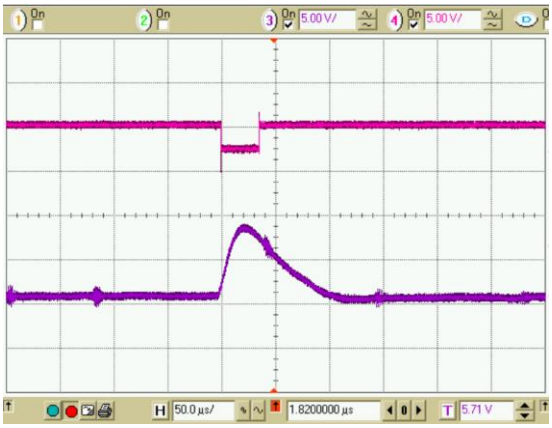

Fig. 5.21 A custom electronics board was used to test early MPFDs in the KSU TRIGA Mk. II Nuclear Research Reactor central thimble, producing a tail-pulse (purple) and digital (pink) discriminator pulse indicating neutron interactions [7].

The second all-inclusive electronics system that was tested with MPFDs was originally developed to support Li-Foil neutron detectors shown in Fig. 5.22 [37]. The energy deposition anticipated from an MPFD is generally on the order of a few MeV [22]. Similarly, the energy deposited by the reaction products from the fission of lithium in a Li-Foil neutron detector deposit a maximum of 4.78 MeV (the total Q-value of the reaction) and typically between 0.5 and 3.0 MeV [37]. The concept of using the specially designed Li-Foil neutron detector electronics came at a time when the original electronics were being abandoned. The all-inclusive unit provided a potentially simple test-bed for MPFDs if it could be adapted to suit the sensor. The main difference between the Li-Foil neutron detector system and the MPFDs being tested was the amplitude of the bias required. The Li-Foil neutron detectors were typically operated at ≈ +900 V applied bias. However, MPFDs required < +200 V applied bias. The potentiostat used to control the applied bias was extremely sensitive at low biases and difficult to set. In addition, the only output on the Li-Foil neutron detector electronics was a digital output from the internally set discriminator. The discriminator had been previously set for Li-Foil neutron detector testing. Adjusting the discriminator required the replacement of resistors in the electronic circuit, a task that complicated the process of setting the LLD for the detector. Finally, the input capacitance from the MPFD arrays which were being tested at the time (alumina insulated flux-well probes) was higher than the capacitance for which the electronics were designed. No neutron interactions were ever observed using the Li-Foil neutron detector electronics package. After having exhausted two possible electronics packages, the decision was made to return to the ‘best-practice’ of radiation detector fabrication by using stand-alone NIM-compatible electronics.

Fig. 5.22 Lithium-foil neutron detectors used a custom-built electronics system which included high-voltage supply, preamplifier, shaping amplifier, and a preset discriminator [37].

Previous research had successfully tested other versions of MPFDs using standalone electronics [22]. An Ortec 142IH preamplifier had been used to test an MPFD^3-T prototype deployed with 900 pF of line capacitance [22]. By this point in time the impact of capacitance on the signal had been clearly identified, and an Ortec 142PC preamplifier supporting input capacitance up to 1000 pF was chosen. The first clearly identifiable neutron-induced signals were captured using the 142PC for the flux-wire probe MPFDs, depicted in Fig. 5.23.

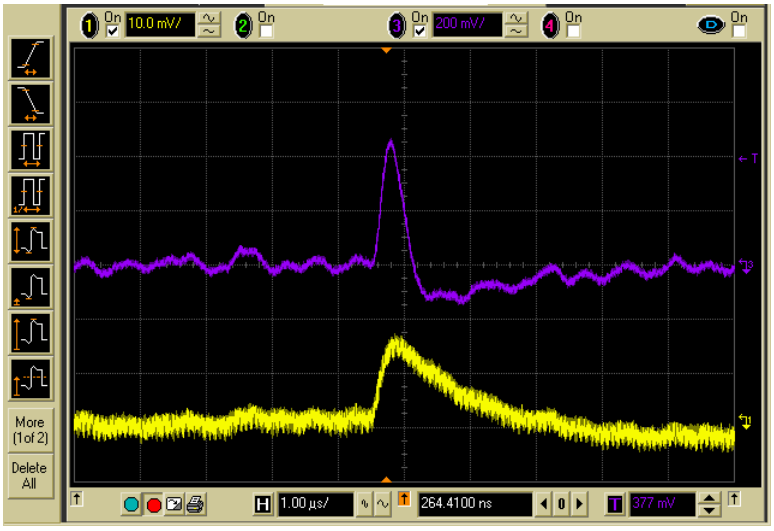

Fig. 5.23 Adjusting the input capacitance setting on the Ortec 142PC reduced line noise and exposed the neutron-induced signal (yellow) which was shaped using a Canberra 2022 amplifier (purple) [38].

Testing continued with the Ortec 142PC preamplifier, however RF interference and line noise continued to degrade the signal from the MPFD. The Ortec 142PC preamplifier was not well-shielded, nor was it stable. MPFD testing was unreliable using the Ortec 142PC preamplifiers that were available and new preamplifiers were costly, with long lead-times. Another charge-sensitive preamplifier was identified which could be ordered in a specification that would yield a superior signal-to-noise ratio for the MPFD sensors, could be customized by the manufacturer, had a short lead-time, and was delivered in a well-shielded casing. The Mesytec MPR-1_V100 preamplifier, depicted in Fig. 5.24, was the next improvement to the MPFD signal processing system.

The MPR-1_V100 preamplifier was more stable than the 142PC. A typical pre-amplified signal rise-time of ≈ 300 ns was observed for neutron-induced pulses, depicted in Fig. 5.25. A selectable gain setting allowed for the gain to be increased by 5 times, however the signal-to-noise ratio was still lower than desired. Both the 142PC and MPR-1_V100 preamplifiers produced a unipolar amplified signal. The unipolar signal amplification uniformly amplifies both the signal from the detector and the common-mode noise. One way to reduce the observed noise on the detector signal cable was to implement RF filters to attenuate high- and low-frequency signals outside of the approximate neutron-induced pulse frequency.

Fig. 5.24 The MPR-1_V100 charge sensitive preamplifier further reduced line noise, especially when coupled with RF filtering [39].

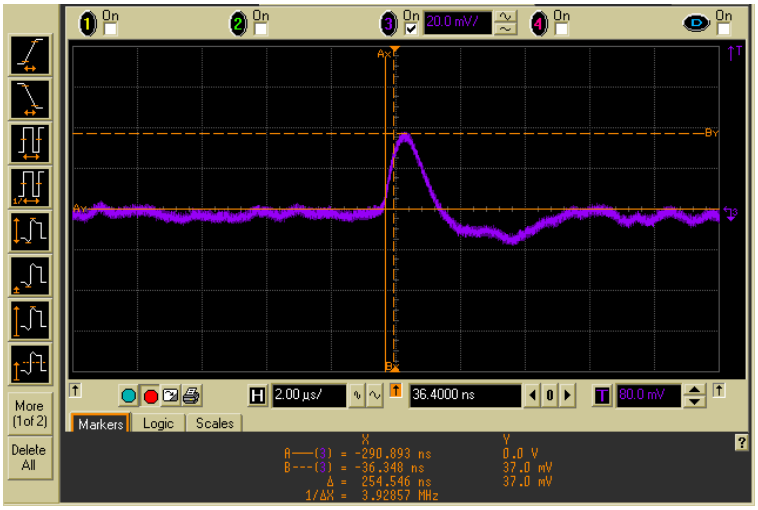

Fig. 5.25 The MPFD signal frequency was determined to be approximately 1.75 MHz.

The frequency of the neutron-induced pulses can be approximated by dividing *ln(2)* by the signal rise-time. The rise-time of the pre-amplified pulse varied between preamplifiers and even between pulses, as fast as 200 ns and as slow as 600 ns. A characteristic signal frequency of ≈ 1.75 MHz was determined based on these variations. Using basic low-pass and high-pass filters, a band-pass filter was designed and constructed with cutoff frequencies of 1.75 MHz and 0.5 MHz in order to reduce noise that was observed in the 10 MHz and 300 kHz region by 84% and 99% respectively, illustrated in Fig. 5.26. However, the use of a band-pass filter also attenuated the MPFD signal by 50%, and a superior alternative was desired.

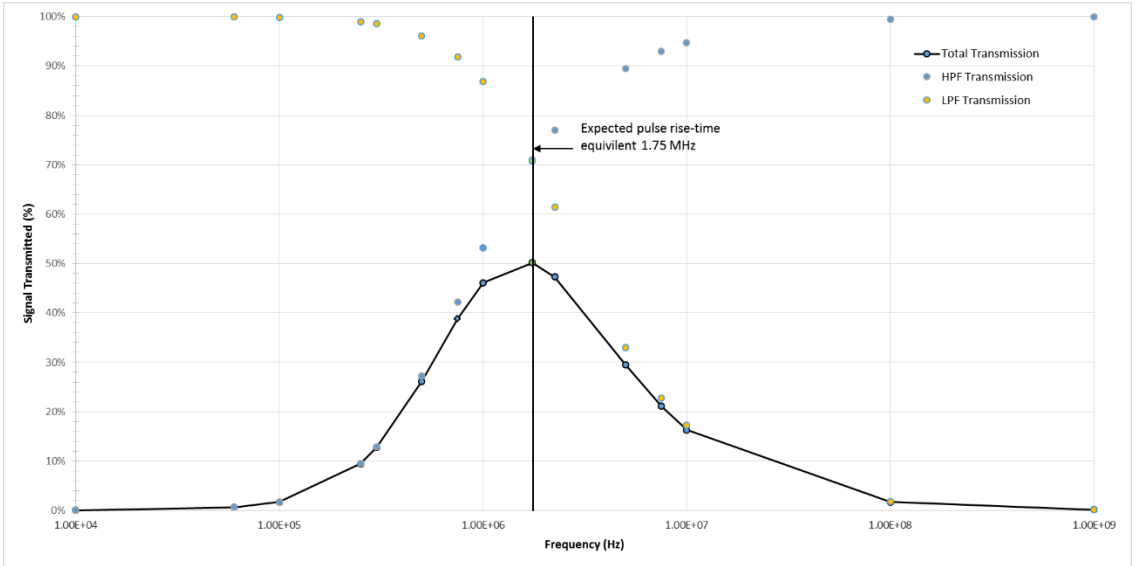

Fig. 5.26 RF filtering attenuated low- and high-frequency noise but also attenuated the MPFD signal.

The 16-channel MPR-16_V100 preamplifier, depicted in Fig. 5.27, was the first off-the-shelf differential-mode preamplifier to be explored for MPFD support electronics. The only trouble switching to the MPR-16 was the design of the unit to support 16 channels of operation having a 25-pin SubD input connector. The additional challenge building cables to support the 25-pin connector was quickly overcome however and a Belden 8134E multi-pair shielded cable was used to fabricate MPFD support cables which have the 25-pin connector on one end and the MDC 9924082 electronic feedthrough connector on the other end to support in-core testing at the KSU TRIGA Mk. II Nuclear Research Reactor facility.

Preliminary testing of the differential mode MPR-16_V100 preamplifier was conducted in conjunction with an MSCF-16 shaping amplifier which was designed to couple with the differential input of the MPR-16. The shaped signal from the MSCF-16 had a superior signal-to-noise ratio than any other support electronics tested up until that time, depicted in Fig. 5.28. A detector array was fabricated and deployed into the reactor core before any electronics tests. After an array was deployed, the electronics were set-up in the reactor bay and tested. However, testing the electronics for neutron-induced signals was difficult and required reactor operations. Frequently the tests concluded with no results due to excessive RF noise or reactor malfunction. A method to test electronics on the laboratory bench was desired.

Fig. 5.27 The MPR-16_V100 preamplifier supports 16 channels of operation with a differential output signal which couples to a differential-mode MSCF-16 [40].

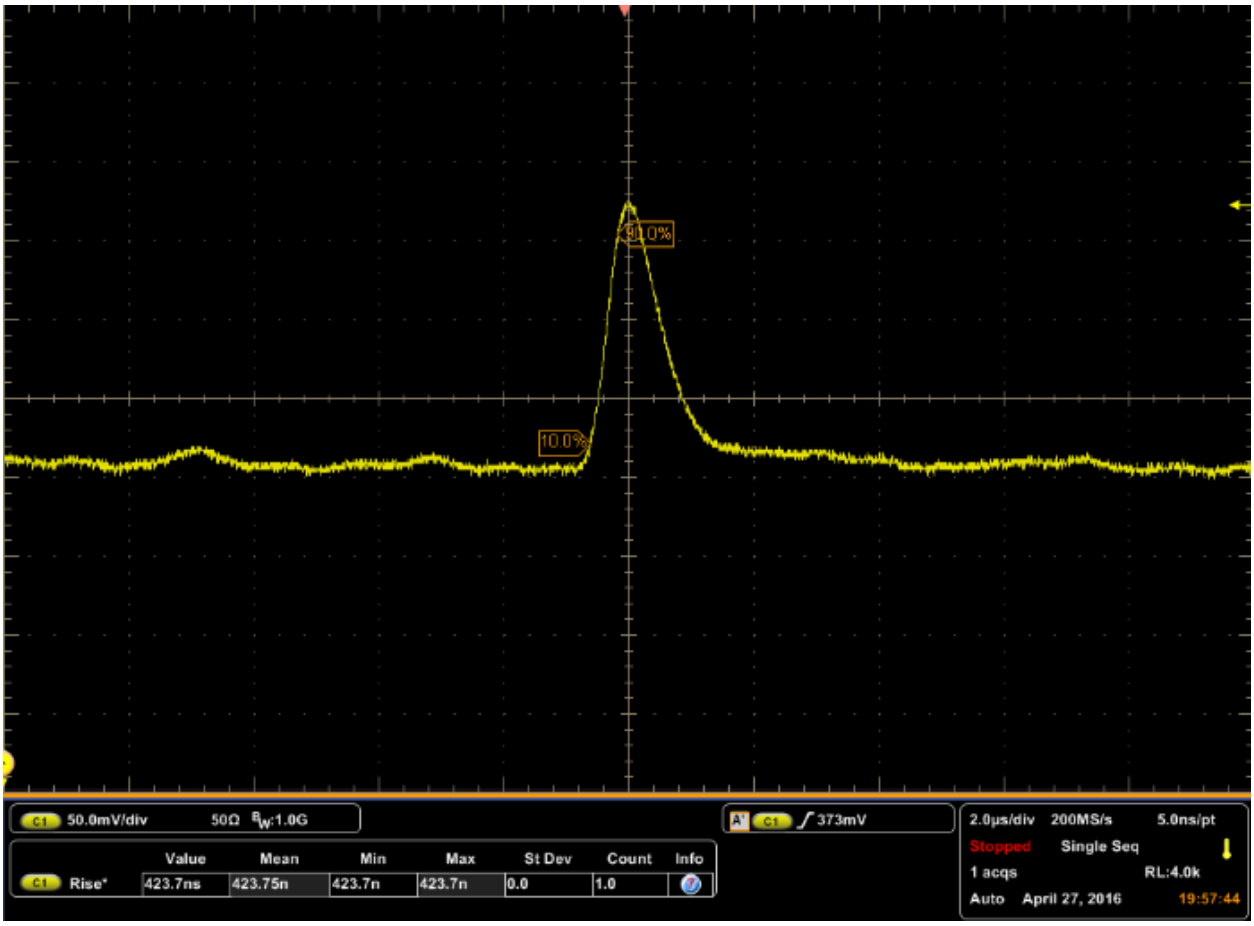

Fig. 5.28 Utilization of a differential preamplifier (MPR-16) and differential shaping amplifier (MSCF-16) improved the signal-to-noise ratio for neutron induced signals from MPFDs.

5.3.3 Emulated MPFD

The charge generated within the ionization chamber of an MPFD can be simply calculated by dividing the total energy deposited (typically ≈ 3 MeV) by the average ionization potential for the ionization gas (26.4 eV per electron/ion pair in Ar [2]) and multiplying by the charge of an electron, -1.6×10^{-19} coulombs/electron. For a typical MPFD, the total charge deposited in the ionization chamber is ≈ 20 fC. An electronic circuit was designed to inject a test pulse into the preamplifier by using a small capacitor, emulating the ionization within an MPFD. A precise unipolar test pulse generator was developed which was capable of injecting single-ended charge into a preamplifier to simulate a neutron interaction [41]. A 0.1 pF capacitor was used to generate an 18 fC charge injection, emulating a smaller-than-average neutron-induced signal. Using the MPFD emulator, depicted in Fig. 5.29, electronic configurations could be tested on the bench-top at KSU.

Fig. 5.29 The MPFD emulator box was be used in place of a full-scale MPFD array for bench-top electronics testing and optimization.

The MPFD emulator was tested using the same electronic configuration that was used to capture the first differential MPFD signals. Initially, the emulator was designed to include approximately the same capacitance measured on a recent MPFD assembly. The maximum total line capacitance expected for MPFD testing (sensor, extension to feedthrough, and cable to preamplifier) was ≈ 600 pF. The capacitance measurement included capacitance between the signal and return lines at the preamplifier connector as well as between the signal and shield at the preamplifier. The specific noise for the MPR-16 preamplifier is 5 keV + 0.04 keV/pF. An RMS noise level of 29 keV (≈ 8 mV) was expected for an input capacitance of 645 pF. In fact, the RMS noise was 5 mV for the 645 pF case. Proper grounding was observed to reduce the peaked noise, and the emulator was used generate input pulses for electronics testing. The emulator was connected to the preamplifier. The high-voltage and test inputs of the preamplifier were terminated with 50 ohms [40]. The preamplifier was then connected to the MSCF-16 with a 0.25 μs shaping time and minimum gain of 2 (1/15 of 30 max). The pulse from the 18 fC charge injected by the emulator was visible above the noise, depicted in Fig. 5.30. The rise-time of the emulated pulse is faster than the observed neutron pulse however the pulse amplitude is comparable. The difference in rise-time can be attributed to the 0.5 μs shaping time used for in-core testing [41]. A longer shaping time also decreases pulse amplitude. The pulses from MPFDs can vary in magnitude based on the trajectory of the fission fragments in the ionization chamber [22]. The emulator, therefore, is a conservative diagnostic tool, generating a signal which is representative of neutron interactions within the MPFD.

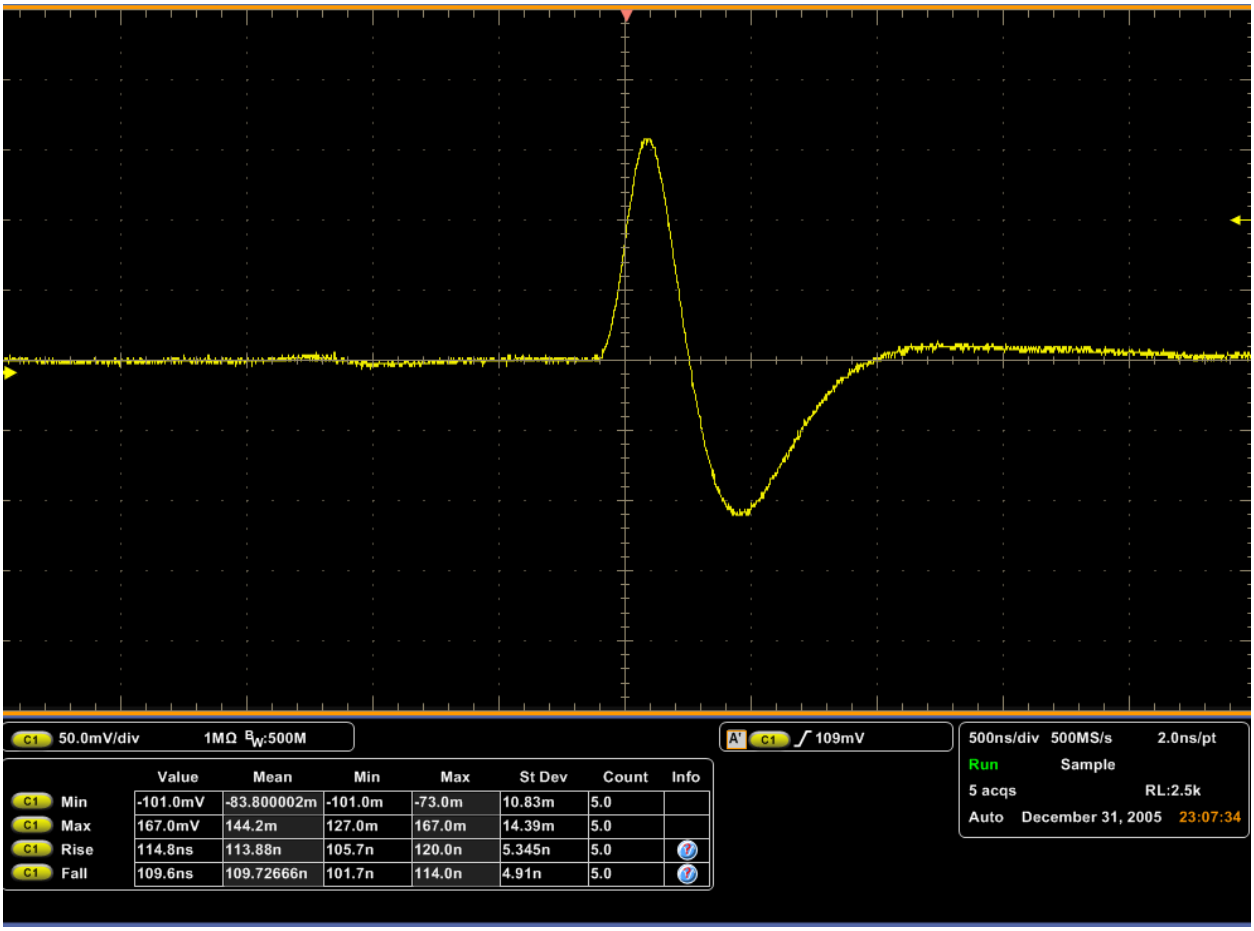

Fig. 5.30 The MPFD emulator was used for benchtop testing of electronics with artificial line capacitance of 645 pF.

5.3.4 Addition Electronics

For the preliminary MPFD testing two all-inclusive electronics boards were tested which did not produce reliable results (described previously in section 5.3.2). From that point forward, separate units were used for high-voltage power supply (HVPS), pre-amplification, shaping amplification, discrimination, and counting. A stable HVPS is necessary for MPFDs which operate on the multi-wire design. It was observed that variations in the applied bias change the electric field strength in the ionization chamber and can cause several micro-amperes of current to flow through the system. A Mesytec MHV-4, 4-channel HVPS was used for many MPFD test campaigns and has been a stable alternative to older HVPSs that were tested. Two different shaping amplifiers have been used. The Canberra 2022 amplifier is a common option which includes a wide range of amplifications and shaping times between 0.5 µs and 12 µs. MPFDs have been tested with the Canberra 2022 using shaping times of 0.5, 1.0, 2.0, and 4.0 µs. Faster shaping times are

generally preferred to increase the bandwidth of operation for the sensors however longer shaping times were utilized to integrate out high-frequency noise before RF filtering and differential electronics were implemented. The Canberra 2022 shaping amplifier was always accompanied by a Canberra 2031 single channel analyzer. The Canberra 2031 was used to discriminate neutron-induced signals from the background using a lower-level discriminator. The Mesytec MSCF-16 was utilized as a unipolar shaping amplifier with a constant fraction discriminator and later as a differential shaping amplifier with leading edge discrimination. During the preliminary testing of MPFDs using the unipolar preamplifiers, the signal-to-noise ratio of the neutron-induced signal was poor. The use of a constant fraction discriminator was attempted in order to provide a faster discrimination between the pulses, which had a characteristic rise-time between 200 ns and 600 ns, and the RF noise. This method did not prove to be optimal, because each channel required a separate preamplifier and independent high voltage supply.

A full electronic support system was required for completion of a funded research milestone. The flux-well deployable MPFDs were delivered with a signal processing box which utilized the MPR-1_V100 preamplifiers, RF filtering, and an MSCF-16 shaping amplifier illustrated in Fig. 5.31. The signal was generated at each of the two MPFD nodes located within the flux well. Traveling up the flux well through the electronic feedthrough, the signal transitioned to the signal processing box. The pre-amplified signal traveled through the RF filter, then to the shaping amplifier. If the signal exceeded the discriminator threshold, the ECL output from the MSCF was converted to TTL and output from the signal processing box. The TTL pulse then traveled out of containment, to the customer-supplied counting station. The high- and low-voltage was also supplied at the customer-supplied counting station and connected to the signal processing box.

Each of the components of the signal processing box were located within a custom-built stainless steel container, illustrated in Fig. 5.31. The signal processing box was assembled and tested successfully. Then a NIM-mounted 16-channel system was designed which could provide additional functionality.

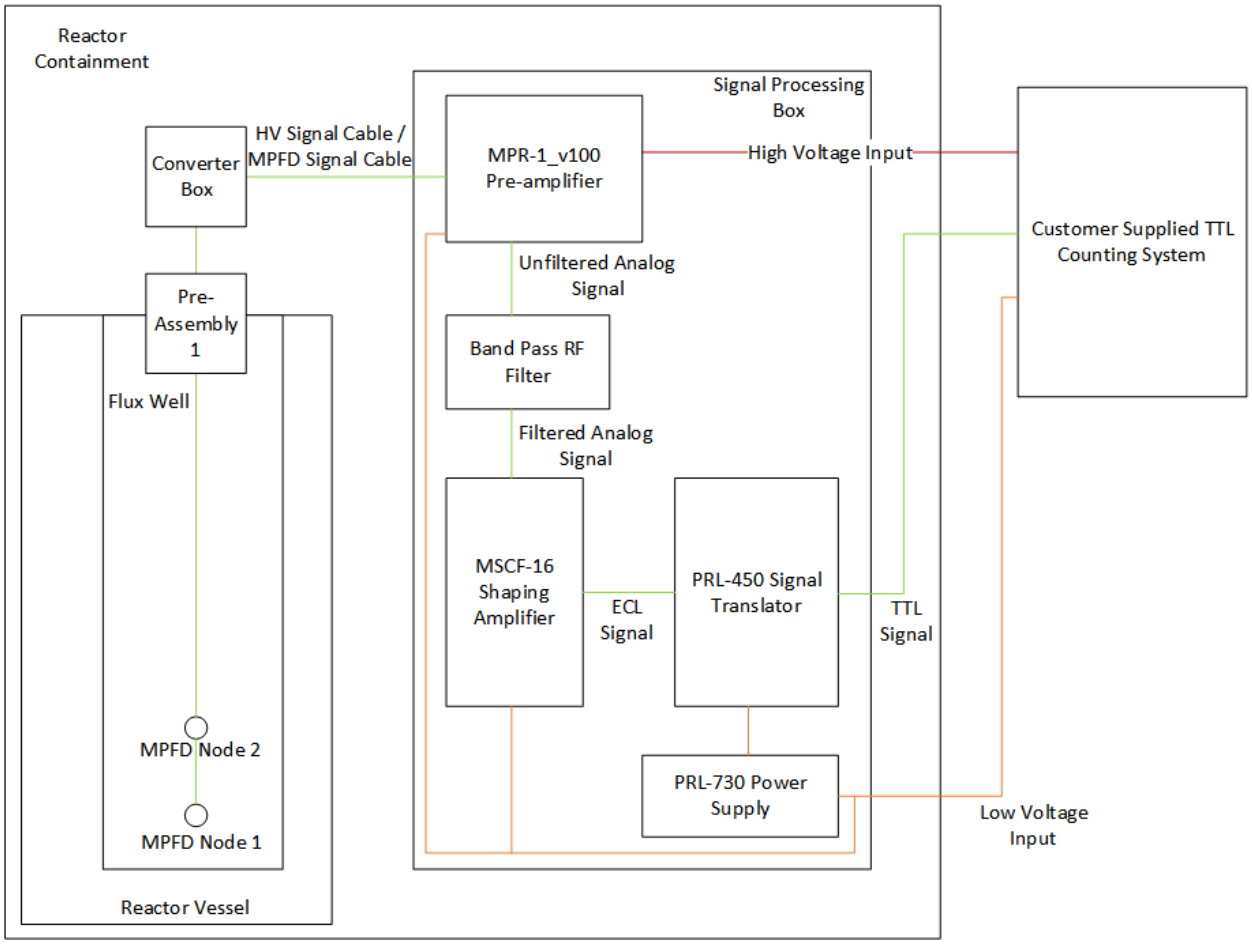

Fig. 5.31 The signals generated at the MPFD sensor nodes traveled through the signal processing box and then to a counting station.

Later, when a differential preamplifier was tested, a differential-mode MSCF-16 was procured which was designed to couple with the MPR-16 differential preamplifier. Both the MPR-16 and MSCF-16 support 16 channels of differential-mode signals. The built-in leading-edge discriminator in the MSCF-16 allows a lower level discriminator to be set. Additionally, both the MPR-16 and MSCF-16 could be controlled remotely using Mesytec-supplied software. The MSCF-16 used a leading edge discriminator to determine if the shaped signal exceeded a threshold value. If the threshold value (which was set by the user) was exceeded, a digital ECL pulse was generated on the MSCF-16 output. An ECL signal is particularly useful as a digital signal because it can be transmitted long distances with little attenuation due to its differential nature. However, all of the counting electronics that are currently employed by KSU and at other facilities which wish to use MPFDs require a TTL signal. For that reason, a Philips Scientific 726 Logic Level Translator was used. The Philips 726 converted an ECL signal on 34-pin ribbon cable (the same

output as the MSCF-16) into individual TTL and NIM signals, output on lemo-00 terminals. Then the TTL and NIM signals were counted using a counter. A dual-channel counter-timer was used to count up to 2 channels, however a Wiener NIMBox was also utilized as a PC interface allowing the counting of up to 20 channels via LabView software (using custom firmware available from the manufacturer) described in Appendix F. A mock-up of a 16-channel support system without cables (and omitting the preamplifier) is depicted in Fig. 5.32. All of the necessary components for the 16-channel system can fit into a portable NIM bin, or could be placed into a full-sized NIM bin to allow extra room for air-cooling and accessory components.

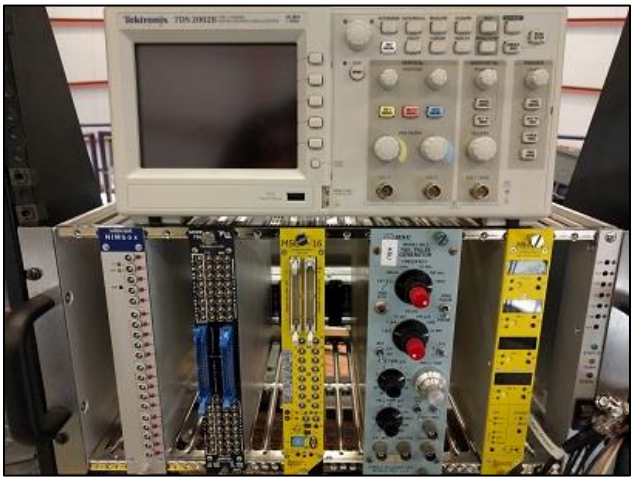

Fig. 5.32 The 16-node support system fit into a single full-sized NIM Bin with extra room for air-cooling and supplementary equipment.

MPFDs must be able to respond to a wide range of neutron flux levels to provide useful measurements in-core. In the past, signals from MPFDs were severely degraded by dead-time [22]. The MPR-16 preamplifier is capable of operating up to 1 MHz before pulse pile-up occurs. With the exception of Geiger-Müller detectors, most dead-time in a radiation detection system is typically induced by the processing electronics (namely the pulse shaping) [42]. Therefore, the dead-time of the MPFD signal processing system can be found using a tail-pulse generator. The count rate of the detector system, n_1, n_2, and n_{12}, where the input frequency for n_{12} is the sum of the input frequencies from the tail-pulse generator for n_1 and n_2, the detector dead-time, τ, can be found by Eq. 6 [42]. Although there are some disadvantages of the dual-pulser method of dead-time determination, source methods are not possible for the MPFD system due to the low sensitivity of the sensors.

$$\tau = \frac{n_1+n_2-n_{12}}{2n_1n_2}, \quad (6)$$

A tail-pulse generator was set to generate pulses with a similar rise-time and amplitude to those observed during operational demonstration of the MPFDs. A 1-μs shaping time and gain of 10 were set on the MSCF-16 to generate a 200 mV shaped pulse. Then the shaping time was increased to 2 μs. Tail-pulse generator frequencies of 50 kHz, 100 kHz and 150 kHz were used to determine a dead-time of 0.11 ns. Then, the shaping time was decreased to 0.25 μs. Again, tail-pulse generator frequencies of 50 kHz, 100 kHz and 150 kHz were used to determine a dead-time of 0.09 ns using Eq. 6. The dead-time of the detector system is directly related to the shaping time of the MSCF-16. Therefore, the utilization of the shortest possible shaping time is preferred to extend the operational range of the detector system. Using a minimum shaping time, the MPFD array should be capable of measuring interaction rates up to 250 kHz. The MPFD electronics were not tested up to 250 kHz due to limitations of the tail-pulse generator used for the measurement. In the past, longer shaping times were necessary to integrate out common-mode noise. Noise reduction has made possible the use of faster shaping times at the KSU test facility.

5.3.5 Mesytec Integrated MPFD Electronics Support System

The full 16-channel support system is a sufficient design for deployment of large MPFD arrays. However, more common has been the need for support of a single array. The large investment in all of the electronics that comprise the 16-channel support system is then unnecessary. Need for a humidity-resistant preamplifier unit has also been expressed as many nuclear reactor research facilities operate in areas of elevated humidity. Design of a custom electronic support system that can facilitate the deployment of 4 MPFDs in a single array has commenced. The system will include two distinct units, a preamplifier box and a processing module. The preamplifier box will be based on similar electronics as the MPR-16_V100, but will have only 4-channel support. The HVPS and low-voltage power will be supplied to the preamplifier box via a Cat5 cable from the processing module. The processing module will fit into a single-wide NIM slot and will be connected to the preamplifier output via an additional Cat5 cable. Shaping-time, amplification, and leading-edge discriminator thresholds will all be set by a USB interface which can also transfer counter results from the built-in FPGA to an external computer. Optional analog and digital outputs will also be available for troubleshooting purposes. This all-inclusive unit will be provided by

Mesytec after development for a significantly reduced cost compared to the full 16-channel support system and signal processing box which were previously described. The unified design will also provide a stable foundation upon which to test future permutations of the MPFD design.

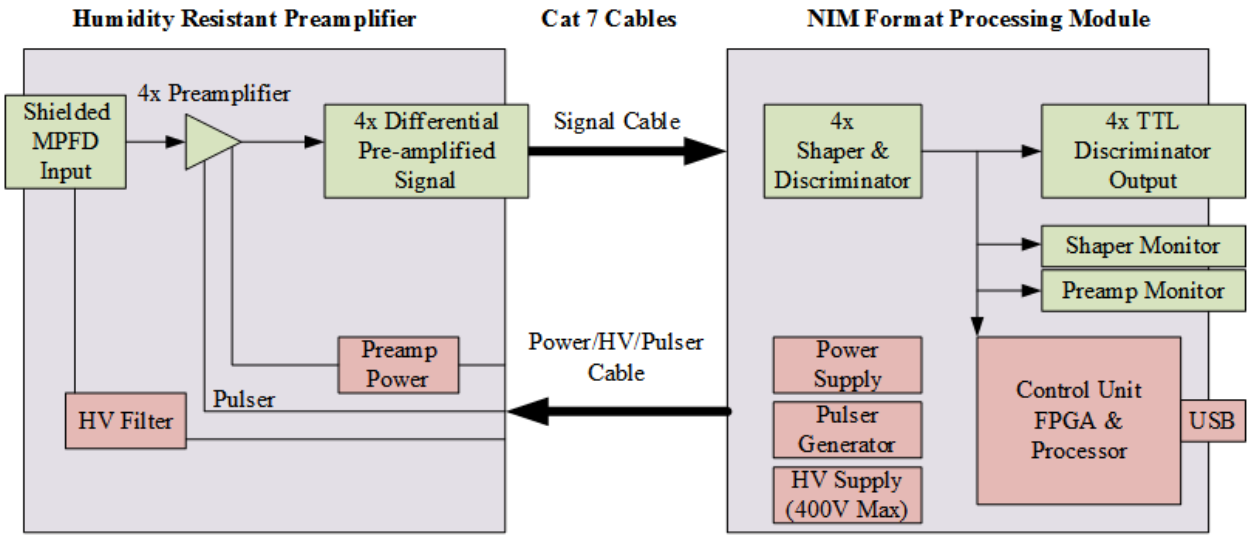

Fig. 5.33 The specially designed MPFD support system includes 2 units, a preamplifier box and signal processing module.

Chapter 6 In-Core MPFD Testing

The incremental improvements discussed in the previous sections led to the fabrication of numerous MPFDs. Not all of the detectors were successfully tested, some were used to identify and resolve problems such as electronic noise and insertion into flux-wire ports as discussed in Chapter 5. The first tests from an encapsulated MPFD yielded uncertain results [7]. A flux-wire port MPFD assembly was the first in-core MPFD to respond linearly to reactor power up to 750 kWth at the KSU TRIGA Mk. II facility [9]. The same MPFD was also used to follow transient reactor power during positive and negative reactivity insertions [9]. An encapsulated 4-node MPFD array was later constructed and tested in steady-state and transient reactor conditions. Finally, a single 5-node flux-wire probe MPFD array was fabricated and tested in-core. All testing was conducted with cooling pumps disabled to reduce electronic noise. The fabrication and testing process for the first successful flux-wire probe MPFD, the 4-node encapsulated MPFD array, and 5-node flux-wire probe are described in the following sections.

6.1 Preliminary Neutron Flux Measurements Using a Single-Node Flux Wire Port MPFD Probe

Flux wire port MPFDs were first constructed with alumina-insulated anode and cathode wires, described in Ch. 5.2. Although deployment and electrical problems prevented the successful testing of most of the early sensors, one MPFD was constructed that provided positive test results. The anode wire of the MPFD array was insulated with alumina sleeves while the cathode was left bare. Then the entire length of the array above the MPFD node was encapsulated in polytetrafluoroethylene (PTFE) shrink-tubing to prevent shorting between the anode and the flux well wall and to increase the rigidity of the array. The MPFD disk was prepared as previously described (Ch. 4.4) with 0.106 ± 0.006 μg of natural uranium electrodeposited onto one 0.33-mm diameter platinum electrode, shown in Fig. 6.1. The MPFD array was inserted into a 6.35-mm (0.25-in.) outer diameter stainless steel flux port which had been inserted into the central thimble of the KSU TRIGA Mk. II research nuclear reactor and back-filled with ultra-high-purity argon (UHPAr) gas.

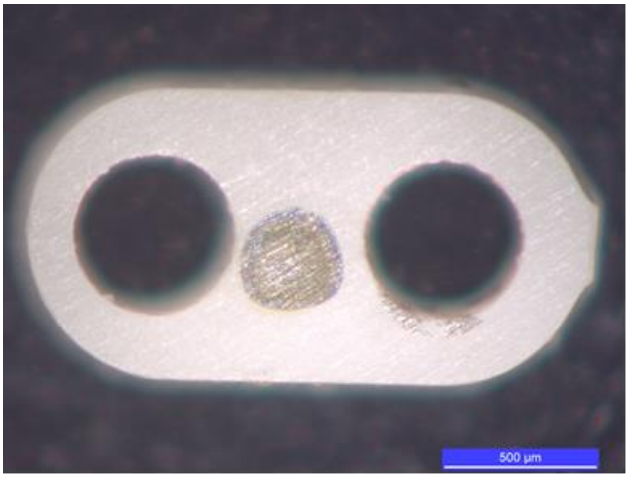

Fig. 6.1 Natural uranium was electrodeposited onto the platinum electrode located in the center of the surface of the machined alumina MPFD substrate.

The total array length was nearly 5 meters, including the extension cables which ran from the top of the flux well port to the 142PC preamplifier. High-frequency and low-frequency noise were observed during preliminary testing of the assembly using a Canberra 2022 shaping amplifier. Efforts were made to reduce noise by grounding the flux well, adding tinned-copper overbraid to all signal cables between the flux well and the preamplifier, and shielding the preamplifier from electronic noise. Furthermore, the previously described band-pass filter was placed in-line with the preamplifier to isolate the neutron-induced signal (Ch. 5.3.2). Gain, 4-µs shaping time, and the lower level discriminator were set while operating the detector with the reactor was powered off. The reactor was then operated at 100 kWth. Neutron-induced pulses from the 142PC preamplifier, 2022 shaping amplifier, and 2031 single channel analyzer were observed, as shown in Fig. 6.2.

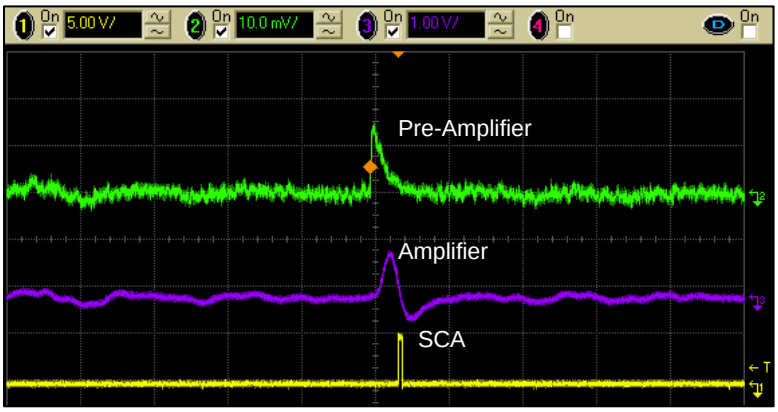

Fig. 6.2 An Ortec-142 PC preamplifier (green), Canberra 2022 shaping amplifier (purple) and Canberra 2031 SCA pulses were produced in sequence from a neutron interaction.

Following the successful construction and preliminary testing of the flux wire MPFD assembly, the following sensor calibration procedure was conducted to determine the response rate of the sensor with respect to different reactor power levels. A linear detector response with power was observed, data shown in Fig. 6.3.

1) While the reactor was in the shutdown condition, the discriminator threshold on the single channel analyzer was set such that zero counts were registered from the electronic noise. This was performed by powering on the electronic support system and supplying the high-voltage to the MPFD array while the reactor was shut down.
2) The reactor was brought to 100 kWth power and allowed to stabilize, yielding an average count-rate of 392 ± 3 cps.
3) With the reactor held stable at 100 kWth, 1-minute long measurements were made. Only measurements that did not contain spikes in counts from noise were retained. In total, 5 1-minute long measurements were used to calculate the average count-rate for 100 kWth. Subsequently, 392 cps at 100 kWth was set as the first point on the calibration curve for the detector.
4) The reactor power was then increased to 500 kWth yielding an average count-rate of 1,754 ± 7 cps.
5) While maintaining stable power, 5 1-minute long measurements were taken. The 5 measurements were used to calculate the average count-rate for 500 kWth. Subsequently, 1,754 cps at 500 kWth was set as the second point on the calibration curve for the detector.
6) Steps two and three were repeated for reactor powers of 10 kWth, 300 kWth, 400 kWth, 600 kWth, and 700 kWth, producing additional calibration points. The linear response of the MPFD depicted in Fig. 6.3 was observed and is summarized in Table 6.1.

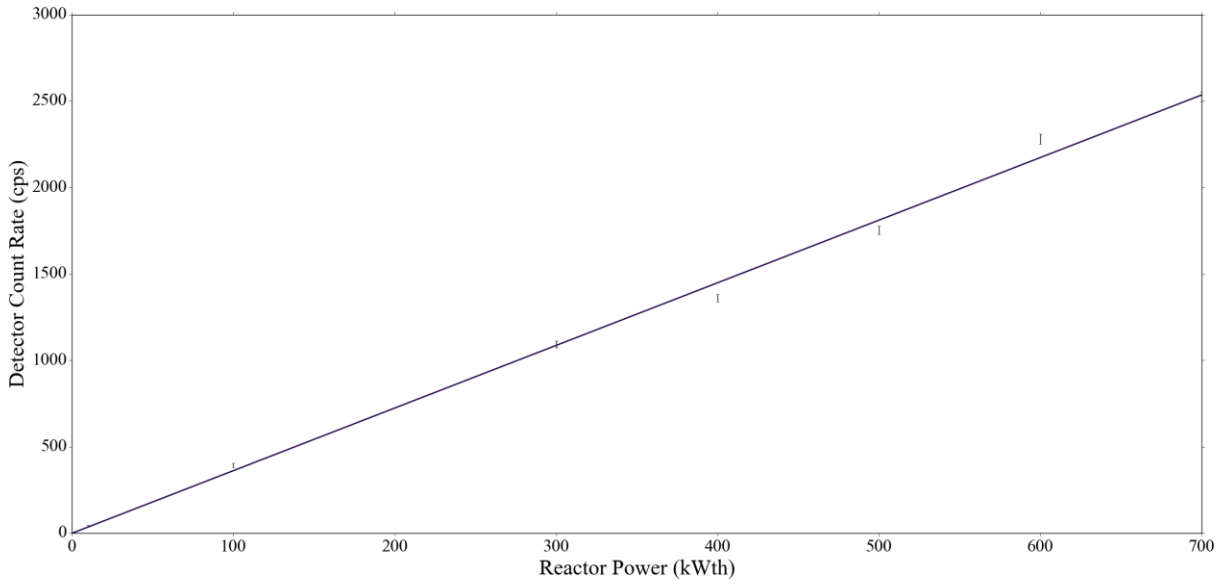

Fig. 6.3 MPFD sensor calibration for a single flux-port probe in the central thimble of the KSU TRIGA Mk. II Nuclear Research Reactor produced a linear response to reactor power levels from 10 kWth to 700 kWth.

Table 6.1 Five 1-minute measurements were summed at each power level to determine the average count-rate and standard deviation of the MPFD response.

Reactor Power (kWth)	Total Counts (5 minutes)	Counting Error	cps	Standard Deviation (cps)	Standard Deviation (%)
10	12,207	110.49	41	2.80	6.8
100	117,658	343.01	392	3.32	0.8
300	327,879	572.61	1093	27.8	2.5
400	408,205	638.91	1361	27.1	2.0
500	526,212	725.40	1754	7.05	1.0
600	684,170	827.15	2281	53.4	2.3
700	757,362	870.27	2525	65.4	2.6

The response rate of the MPFD in the central thimble was sufficient to measure reactor power at steady-state. Testing continued with positive reactivity insertions to observe the response of the MPFD in real-time. A count integration time of 1 second was used. The reactor operator was asked to establish criticality at 1 kWth and then perform positive reactivity insertions which yielded positive power periods of 40, 20, and 10 seconds and asked to maintain power after each insertion

before reducing power back to 1 kWth. Power excursions for each of the three reactivity insertions, along with overshoot and temperature feedback are depicted in Fig. 6.4. Error bars were removed from Fig. 6.4 for clarity, but it should be noted that the counting error for each 1-second measurement interval was > 10% for most data points due to low interaction rates. Each positive period produced power overshoot that was inversely proportional to the period. Power overshoot is common, particularly when increasing power at a fast rate (low period). When the operator stops increasing power, the increased temperature of the fuel then causes a reduction in power because of the negative temperature coefficient for TRIGA fuel.

Negative reactivity insertions were also monitored with the MPFD from within the central thimble. After establishing criticality at 700 kWth, negative reactivity insertions of -$0.10, -$0.20, -$0.40, -$0.80, and a SCRAM were all executed by the reactor operator. The reactor power was increased to 700 kWth after each negative reactivity insertion, with exception of the -$0.20 insertion which was a combination of two sequential -$0.10 insertions. Following the -$0.80 reactivity insertion, all control rods were removed from the core, bringing the reactor to full power and a SCRAM was executed. The MPFD response during each of the negative reactivity insertions was recorded in real-time and is shown in Fig. 6.5.

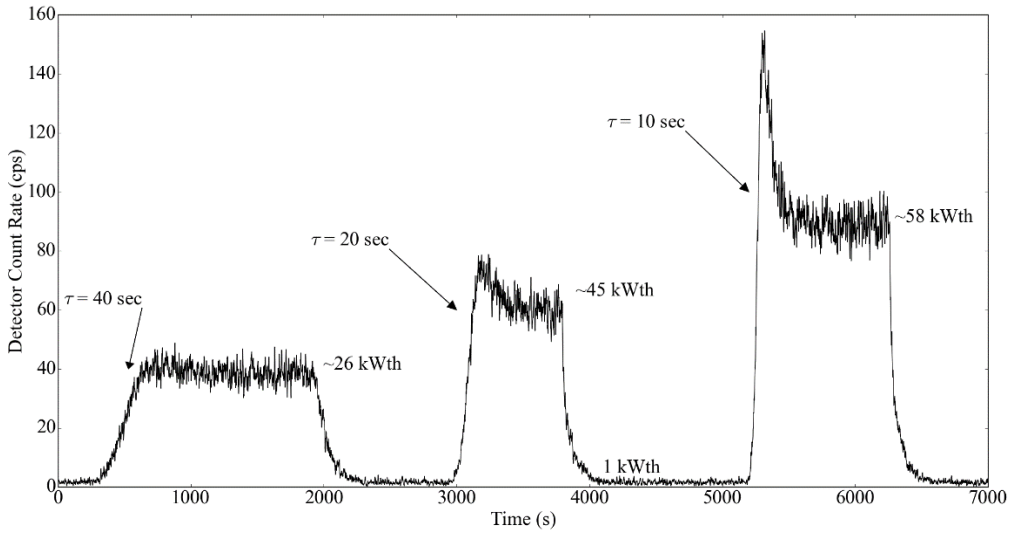

Fig. 6.4 Positive reactivity insertions yielding reactor power periods of 40, 20, and 10 seconds were all tracked with the MPFD located in the central thimble.

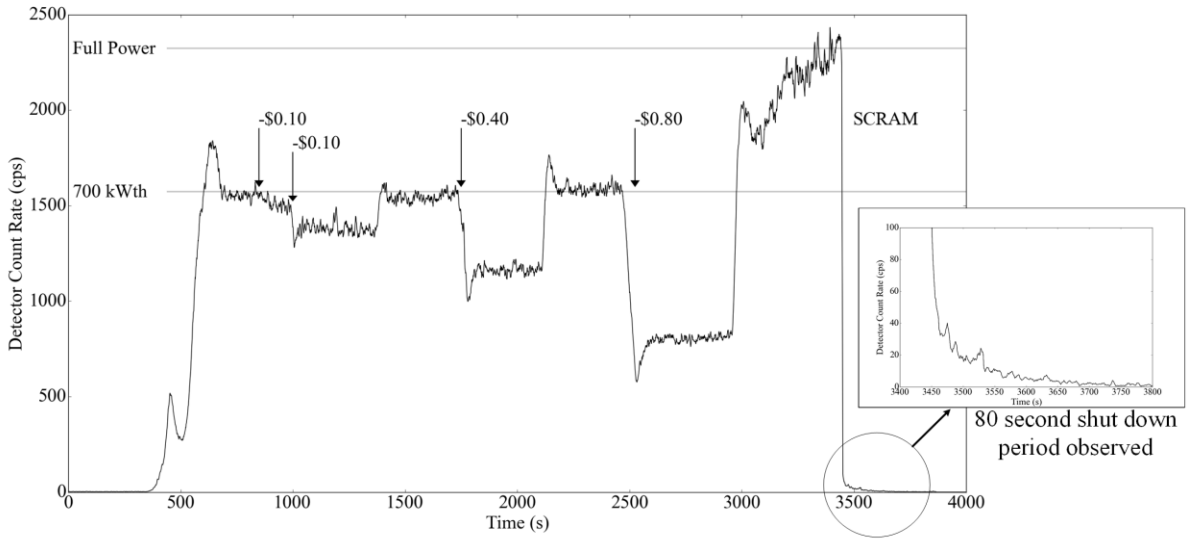

Fig. 6.5 Negative reactivity insertions of -$0.10, -$0.40, and -$0.80 followed by a reactor SCRAM were successfully tracked by the MPFD in the central thimble.

One unique feature of TRIGA reactors is the ability to pulse, a procedure wherein a pneumatically-operated control rod (pulse rod) is ejected from the reactor core. The core, being critical at low power prior to the pulse rod ejection, becomes prompt supercritical with the additional of > $1.00 of reactivity. The supercritical excursion causes reactor power to increase from 10 Wth to over 1 GWth in approximately 10 ms. The negative temperature coefficient for TRIGA reactor fuel then compensates for the added reactivity in the following 10 ms, decreasing reactor power. During the supercritical excursion the neutron flux level in the central thimble can approach 10^{17} cm^{-2} s^{-1}. Test results for a reactor pulse in the central thimble were recorded and reported to have saturated the detector system using a 4-μs shaping time [12]. However, neutron flux levels in the IRIS have been reported to be approximately 100 times lower than in the central thimble [12]. Therefore, neutron flux in the IRIS during a reactor pulse should only approach 10^{15} cm^{-2} s^{-1}. The MPFD array was deployed into the IRIS and used to monitor neutron flux during a $1.50 reactor pulse. A 1-ms count-time was used for the pulse testing in order to provide sufficient time-resolution to follow the pulse power transient. The full-width at half maximum (FWHM) for the reactor pulse measured by the MPFD and shown in Fig. 6.6 was 12 ms. The KSU TRIGA facility uses an external compensated fission chamber to monitor and report power levels and FWHM for reactor pulses.

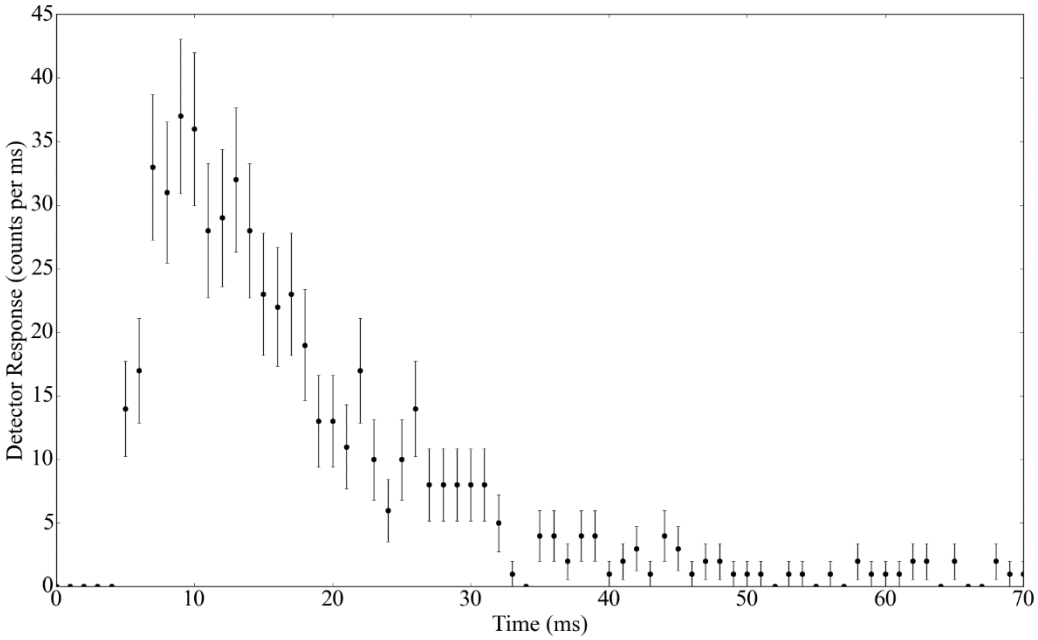

Fig. 6.6 A $1.50 reactor pulse with a 12 ms FWHM was tracked with the MPFD deployed in the IRIS flux well.

The smallest MPFDs to be constructed were tested using materials and electronics that were sub-optimal. However, the testing of this MPFD showed the feasibility of using MPFDs to monitor neutron fluxes in a nuclear reactor in real time. The MPFD was operated in steady-state up to 700 kWth, corresponding to a total neutron flux of $> 6 \times 10^{13}$ cm^{-2} s^{-1}. Additionally, the MPFD was able to monitor the fast transient power excursion of a reactor pulse using 1 ms time bins in a neutron flux exceeding 10^{15} cm^{-2} s^{-1}, measuring a FWHM of a $1.50 reactor pulse comparable with the standard monitoring equipment at the facility. Improvements to the MPFD manufacturing processes, materials, and electronics system have enhanced the capabilities of the sensors which have culminated in the fabrication and testing of two additional MPFD designs.

6.2 Four-Node Encapsulated MPFD Probe Fabrication and In-Core Testing

Continued deployment of MPFD arrays into research reactors benefits from the development of a standard instrument package with modular components. Previous designs required the fabrication of the sensor array in conjunction with an extension cable and the acquisition of single-channel electronics. A new MPFD fabrication and deployment method was developed to support

research projects wishing to deploy arrays of MPFD sensors into nuclear reactor cores. The data from such 3-dimensional MPFD arrays will be used to enhance reactor material experimentation and certification and to benchmark nuclear reactor simulations. First, a modular MPFD array was designed consisting of 4 MPFD sensors separated by insulating silica spacers. The array was encapsulated in a straight 6-foot long stainless-steel tube. The individual MPFD sensors were distributed within the tube to cover the fuel region of a TRIGA fuel rod. The entire tube was filled with ionization gas which can circulate into and out of each MPFD sensor, reducing the potential for fission fragment saturation in the gas chambers. A vacuum and gas fill assembly was fabricated at the top of the MPFD array to facilitate the purge of the tube and back-fill with high-purity ionization gas. An electrical plug at the top of the array connected the anode and cathode wires of each sensor to a commercially available extension cable. A commercially available electronics package was also used for pulse-processing. This modular design has improved the robustness of the MPFD instrument assembly by reducing the failure modes of the assembly. Failure of the electronics and extension cable are unlikely, having been procured from reliable commercial sources. A shorter (6 feet vs 20 feet) MPFD array also reduced the likelihood of failure in the array during fabrication and transportation to the test facility. Each step of the fabrication and testing process for the first modular MPFD array is described in the following sections. The first of several modular arrays was constructed and tested in-core, yielding a stable response to reactor power and successfully tracking reactor transients. Future arrays will be improved based on the findings of these preliminary tests and subsequently constructed in support of MPFD deployments described in Chapter 7.

6.2.1 MPFD Array Fabrication

The modular MPFD array utilized the same sensor geometry as the encapsulated design discussed previously (Ch. 5.2). The disks and spacers were each produced by slicing sections of hard-fired, extruded alumina into 1-mm thick units using a diamond wire saw. The individual samples were then processed by NucFil Inc. The faces of the disks were polished while the spacers were machined to have a 1-mm wide, 0.5-mm deep trench connecting two holes across from one another, shown in Fig. 6.7. The trench connecting electrode holes was utilized to provide a path for ionization to travel within the ionization chamber of the MPFD as previously described.

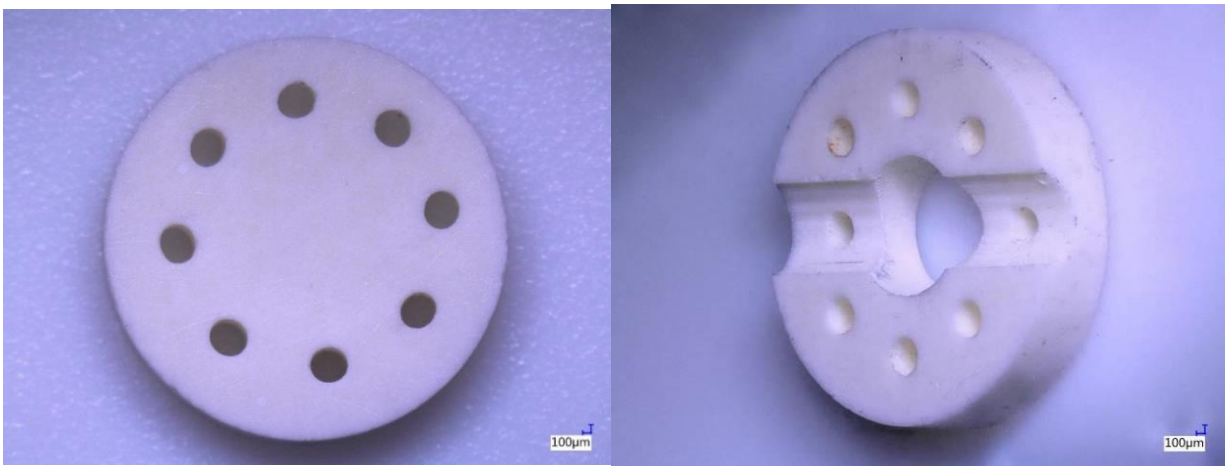

Fig. 6.7 Each MPFD node was composed of two disks (left) and 2 spacers (right) creating the ionization chamber with a channel exposing the appropriate anode and cathode wires.

Next, 1.5-mm diameter electrodes were evaporated onto each of the polished disks. A 50 Å titanium adhesion layer and 500 Å platinum electrode were deposited by electron-beam evaporation. Electrodeposition of natural uranium followed, using a solution which was prepared according to Appendix A, and deposited in conformance to Appendix C., The sample appeared grey prior to electrodeposition and rapidly changed to yellow during the electrodeposition process shown in Fig. 6.8. The deposition of insulating material was eluded to by the cyclic voltammetry plot shown in Fig. 6.9. As with previous experimentation, the maximum current decreased with each successive potential sweep, suggesting that additional resistive material had been deposited.

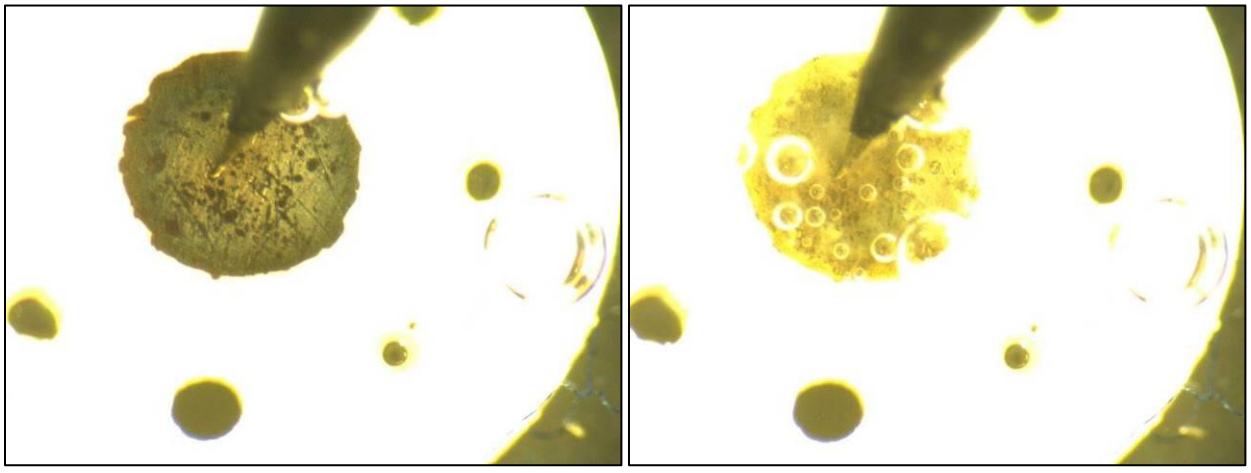

Fig. 6.8 The uranium was clearly visible on the surface of each substrate during the electrodeposition process. The uncoated sample appeared grey (left) while the coated sample appeared yellow (right) from the presence of the uranium compound.

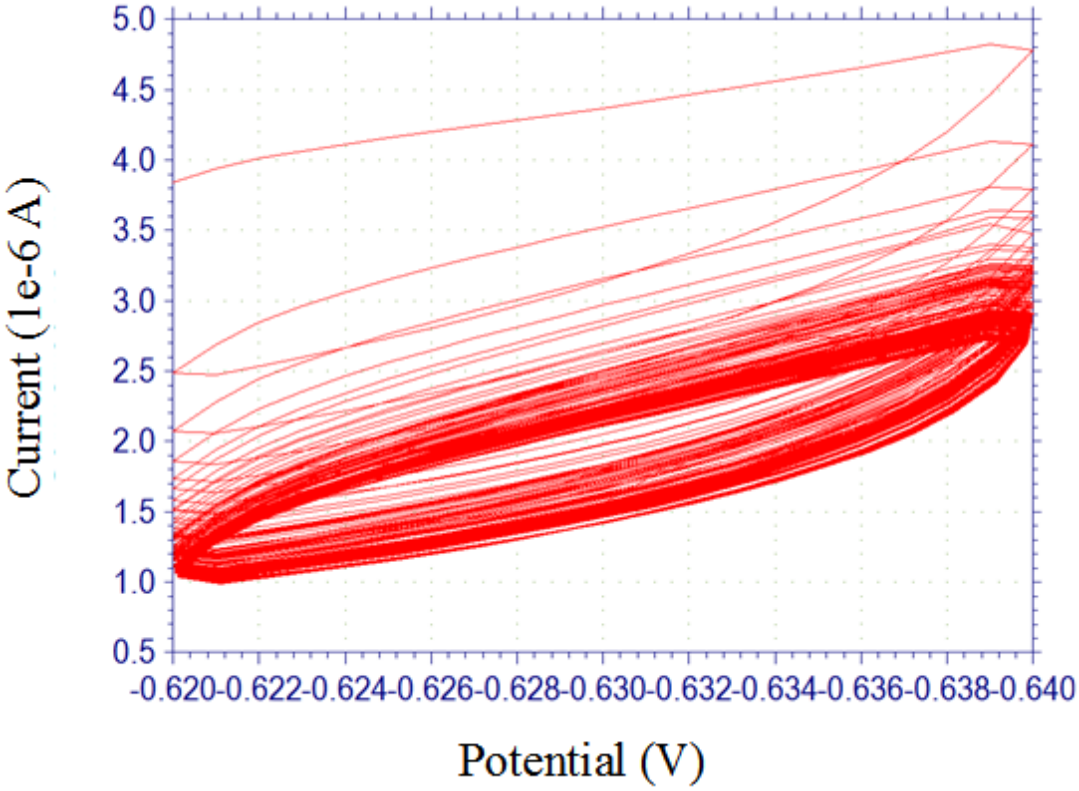

Fig. 6.9 The electrodeposition of uranium onto the MPFD substrates produced a cyclic-voltometric curve with typical features based on previous trials (4.4).

X-ray fluorescence confirmed the presence of uranium on each sample which was then measured using alpha spectrometry. The mass of each of four disks is summarized in Table 6.2. The variation in sample mass is most likely due to variations in the evaporated surface area of each sample. It was observed that the edges of the shadow mask used for electron-beam evaporation melted slightly during the evaporation process. The high-temperature plastic (RGD525) used for the 3-D printed shadow masks has a heat deflection temperature of only 65ºC [43]. The effects of heat deflection are particularly noticeable for very thin features, such as the edge of the shadow mask. The heat deflection temperature can be increased to 80ºC by thermal treatment [43]. The deflection of the shadow mask edge created small features on the edges of each sample which either increased or decreased the total surface area of the electrode slightly. Metallic shadow masks or heat treated plastic shadow masks with thicker features are recommended for future applications.

Table 6.2 Alpha spectrometry was used to measure the activity, and subsequently the mass of uranium deposited onto each sample.

Node	Uranium Mass (µg)	Mass Error (± µg)
1 (top of array)	0.533	0.023
2	0.630	0.026
3	0.548	0.025
4 (bottom of array)	0.619	0.014

After four MPFD disks were deposited with uranium and analyzed, fabrication of the array began. The design of the array and sensor region are illustrated in Fig. 6.10. A single 5/16 x 0.020 x 72 inch 316 stainless steel tube was used to house the MPFD assembly. A 5/16-inch outer diameter tube was selected to fit within the 8-mm diameter penetrations in the upper grid plate of the KSU TRIGA Mk. II research nuclear reactor [13]. A 316 stainless steel plug was welded onto the end of the tube, capping the end which penetrated the top grid-plate and rested on the bottom grid-plate of the KSU TRIGA Mk. II reactor. Each MPFD node was composed of two disks and 2 spacers, however only 1 disk contained fissile material. The two spacers were aligned such that the trenches formed a single 1-mm deep x 1-mm wide channel connecting 1 pair of opposing anode and cathode wires, illustrated in Fig. 6.10. Each MPFD sensor was indexed in order to dedicate a single anode/cathode pair for each sensor.

The MPFDs were each separated by a single 4 1/8-inch silica spacers as depicted in Fig. 6.10 and shown in Fig. 6.11. The total distance between each MPFD was therefore 4 3/8 inches, including the thickness of the MPFD. Additional silica insulation was added beneath the MPFD region to separate the bottom MPFD (node 4) 7 inches from the bottom of the exterior of the encapsulation tube, illustrated in Fig. 6.12. In this manner, the four MPFD sensors were equally distributed within the fuel region of a typical TRIGA fuel rod at distances 18.26-cm (7 3/16-in.), 29.37-cm (11 9/16-in.), 40.48-cm (15 15/16-in.), and 51.44-cm (20 1/4-in.) from the bottom of the array.

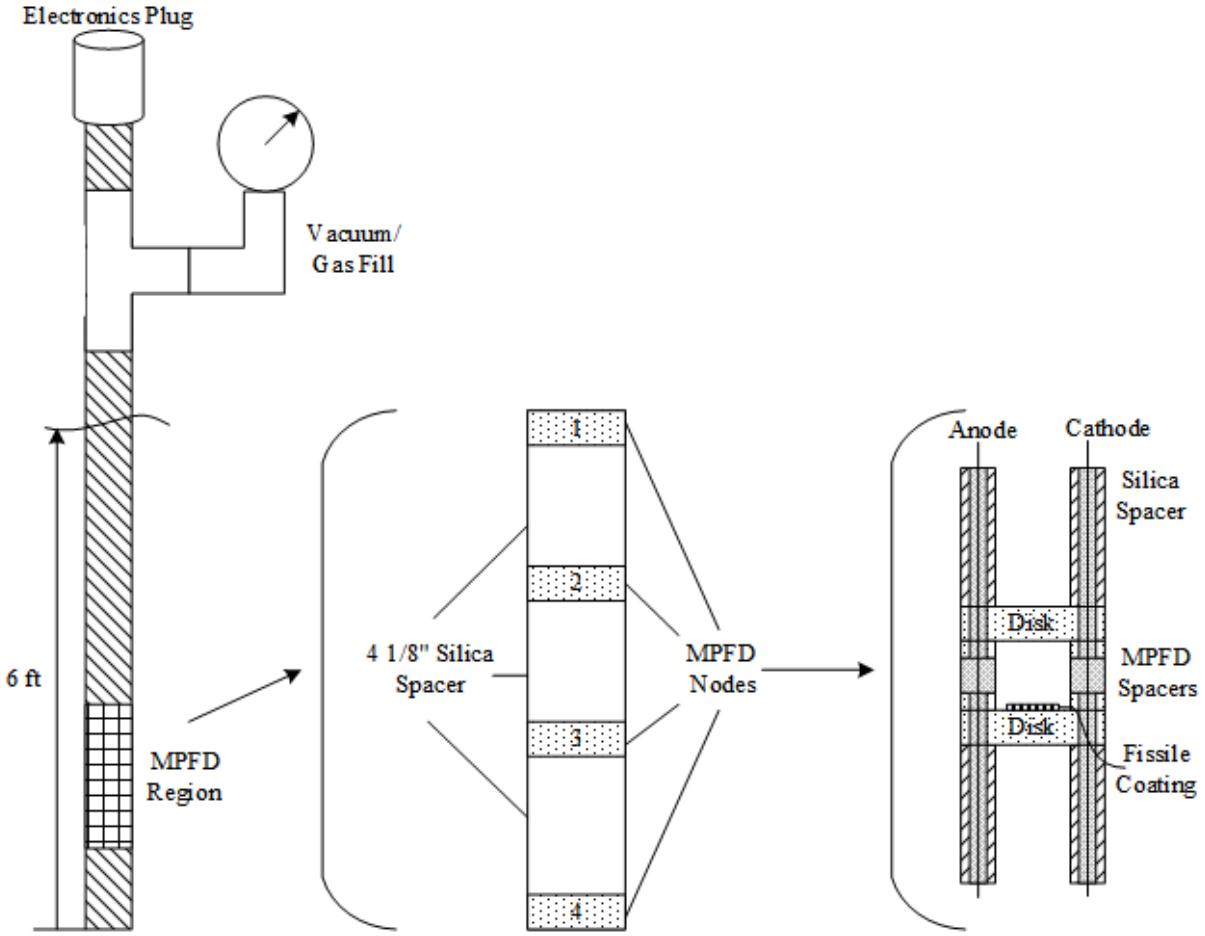

Fig. 6.10 The modular MPFD wand included four MPFD nodes at the distributed near the bottom of a 6-foot long stainless steel tube which was purged and back-filled with ionization gas (UHPAr).

Fig. 6.11 Four MPFD nodes were constructed with 10.48-cm (4 1/8-in.) silica spacers between each node. The total distance between the node center points was 11.11-cm (4 3/8-in.) due to the length of each MPFD node.

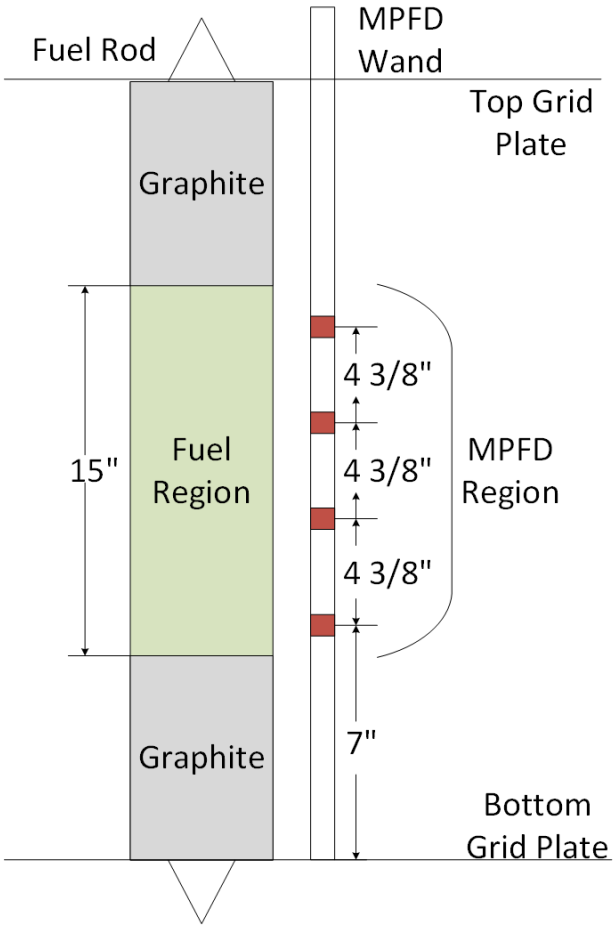

Fig. 6.12 The MPFD nodes were distributed evenly throughout the fuel region of the core.

Following the assembly of the MPFD region, additional silica insulation was added to the array, isolating each anode and cathode wire and providing structural support for the wires within the encapsulation tube. The 30 AWG alumel anode and cathode wires were kept straight and separated during the assembly process to prevent damage to the wires as shown in Fig. 6.13. The crushable silica insulation was designed with a central hole, resembling the cross-section of the spacer depicted in Fig. 6.7. This particular geometry was chosen to increase the volume of gas within the encapsulation tube and decrease the total capacitance of the array. It was determined that high sensor capacitance was contributing to electronic problems during previous experiments (Ch. 5.3.2). Silica was chosen because of its low relative permittivity (between 3 and 4) compared to other mineral insulation (approximately 10).

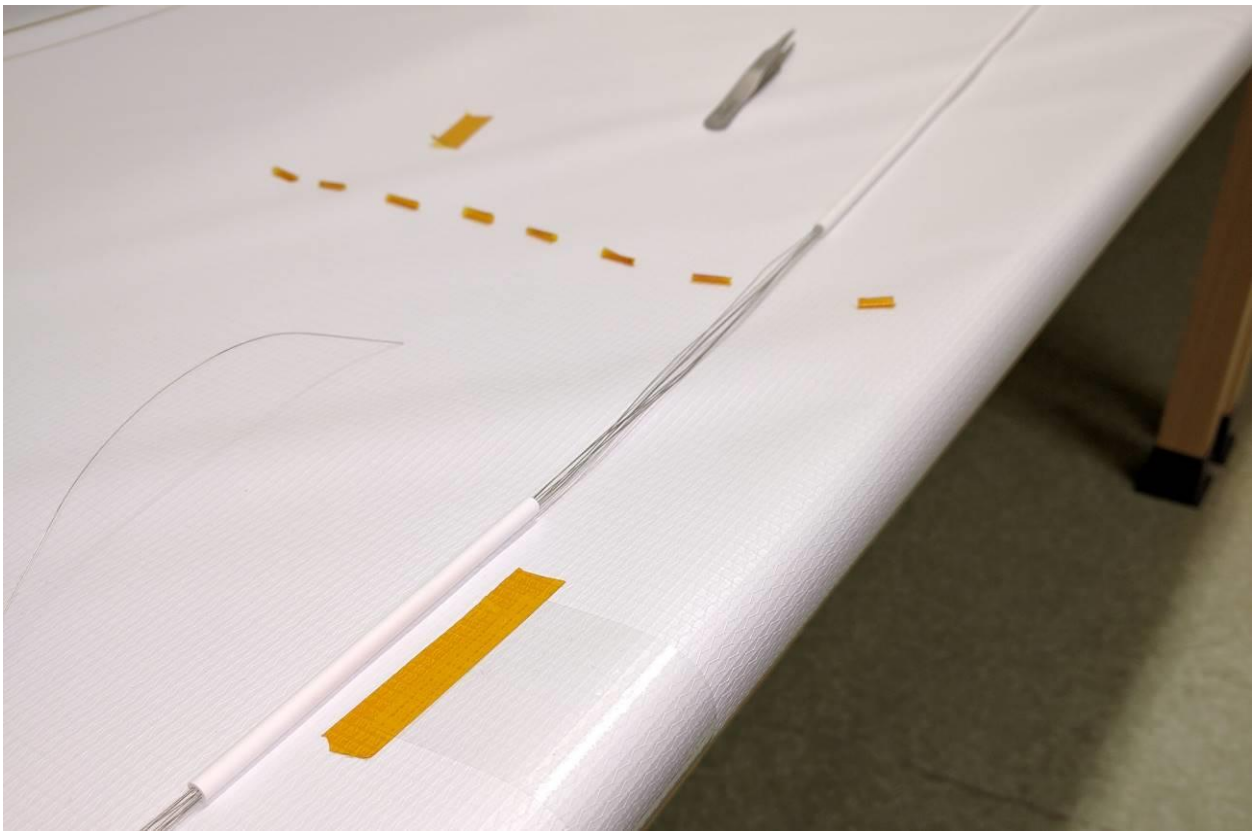

Fig. 6.13 Anode and cathode wires (30 AWG alumel) were threaded through crushable silica spacers to insulate the wires between the electrical plug and the MPFD sensors.

The silica insulation extended the entire length of the stainless steel encapsulation tube, depicted in Fig. 6.14. Beyond that point, fiberglass insulation was used to insulate each electrode. Flexible fiberglass insulation was necessary to allow for the assembly of the gas purge/fill system and electrical feedthrough plug shown in Fig. 6.15

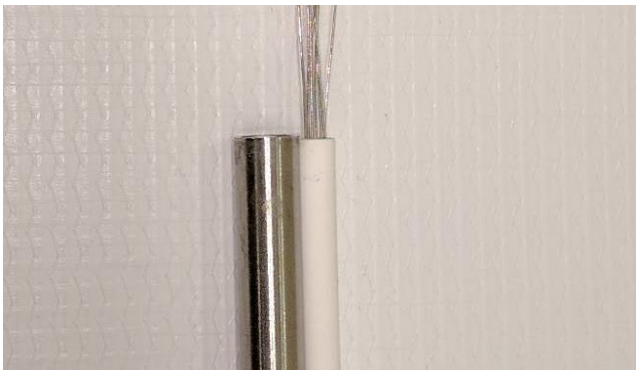

Fig. 6.14 The silica insulation was used throughout the length of the stainless-steel encapsulation tube. Fiberglass insulation (not pictured) was used to insulate the remaining 4 inches of wire which was connected to the electrical plug.

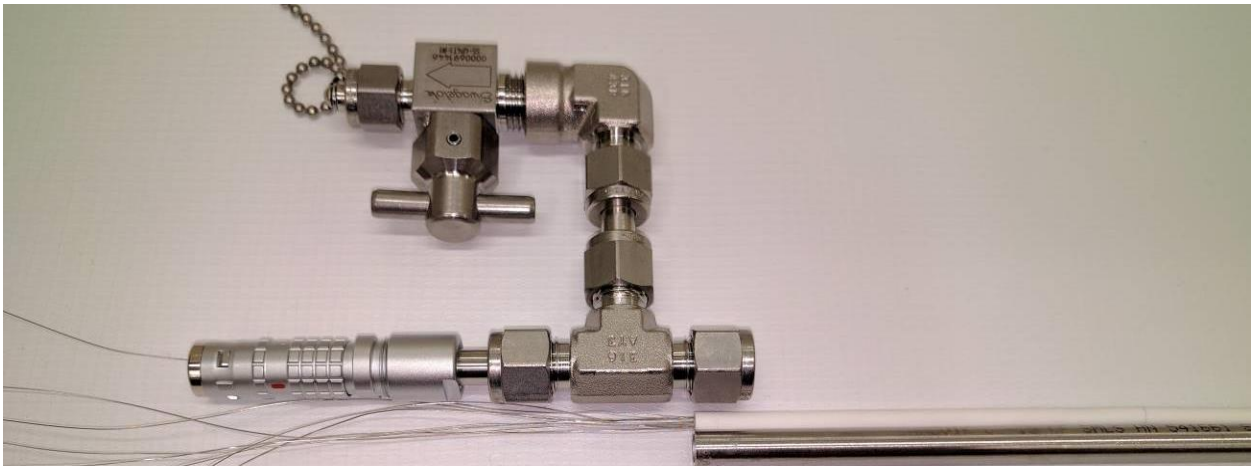

Fig. 6.15 The vacuum/fill assembly was mounted next to the electronic plug to allow the anode and cathode wires to pass out of the encapsulation tube through the electronics plug.

Prior to final assembly, each anode and cathode was soldered to the appropriate pin of the FGG.1K.308.CLAK80 Lemo ® plug [44], shown in Fig. 6.16. Each anode and cathode was confirmed to correspond to the correct MPFD node prior to final assembly according to Fig. 6.16. The respective PHG.1K.308.CLLK75 Lemo ® receptacle [45] was connected to the Belden 8134E extension cable [46], providing a connection between the modular MPFD array and the electronics.

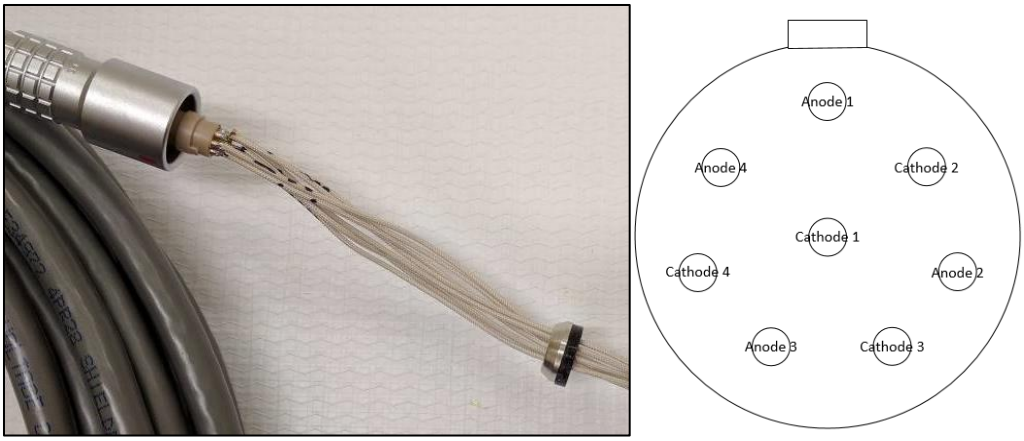

Fig. 6.16 The anode and cathode wires were connected to their corresponding solder terminals on the back of the electronic plug before the final assembly.

The fully assembled array, shown in Fig. 6.17, measured over 6 feet long due to the gas purge/fill assembly and electronic feedthrough. The materials at the top of the array were located sufficiently far from the top of the reactor core to minimize the effect of neutron irradiation (both activation and material degradation).

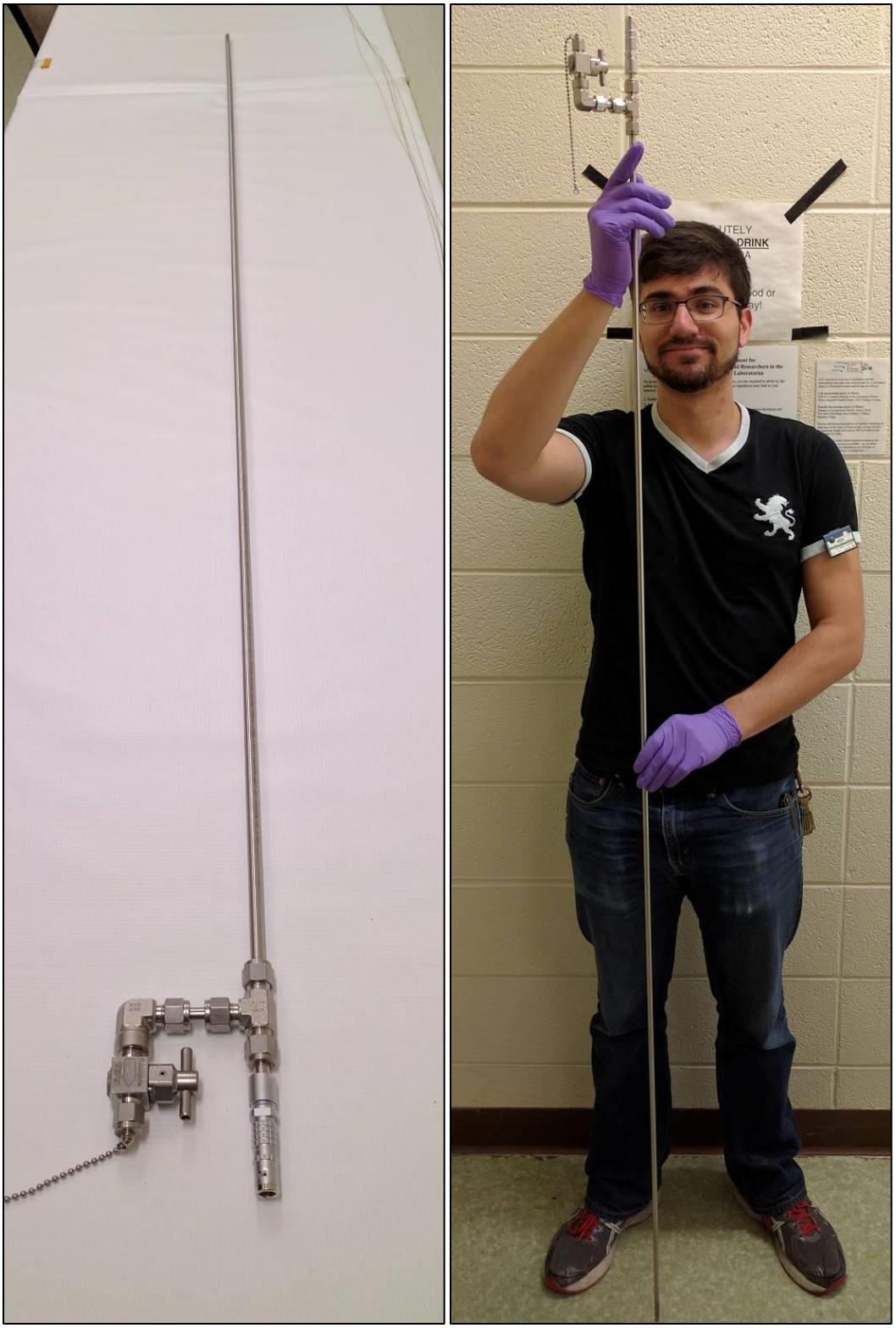

Fig. 6.17 The full array measured over 6 feet in length but was easily handled by a single individual.

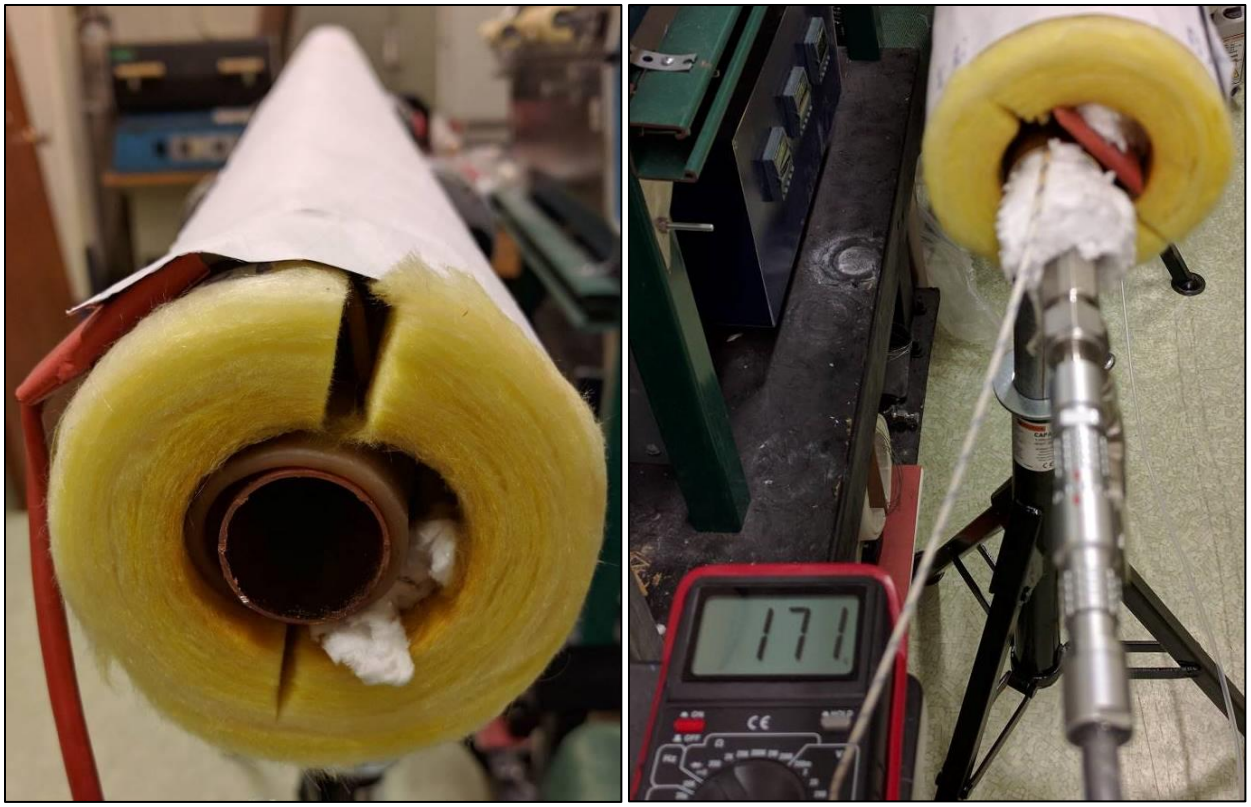

Fig. 6.18 A low-temperature bake-out furnace was constructed to heat the entire array during the purge process, removing any residual humidity from the silica and alumina components.

Ceramic materials can absorb humidity when exposed to air, changing the electrical properties of the material. A rudimentary tube oven was constructed to bake humidity out of the MPFD array. A 20-foot long silicone heating tape was wrapped around a 1-inch diameter copper pipe and insulated by 1.5-inch thick fiberglass insulation. The heat-tape is capable of temperatures up to 450ºC; however, it was used on its lowest setting to achieve approximately 175ºC in the center of the pipe, shown in Fig. 6.18. A rough vacuum pump was connected to the purge system and allowed to pull a vacuum while at an elevated temperature for 24 hours in order to remove humidity from within the array.

After the heated vacuum purge was completed, the tube was filled to 30 psig with UHPAr. The purge and gas fill process were repeated 2 additional times. After the array was filled a third time, final assembly was complete and the array was ready to deploy in the KSU TRIGA Mk. II research nuclear reactor. The capacitance of each node was measured between 350 pF and 400 pF, including a 25-foot long extension cable (11 pF/ft) [46].

Prior research necessitated the modification of the KSU TRIGA Mk. II research nuclear reactor to include 15 8-mm diameter penetrations in the upper fuel grid-plate with locations illustrated in Fig. 6.19 [13]. The location situated between two instrumented fuel rods was chosen for preliminary testing of the 4-node encapsulated MPFD array to provide real-time fuel temperature data alongside the MPFD test results. The neutron flux near the center of the core is also greater than the neutron flux extending radially outward. Therefore, MPFD response should be greatest in the center of the core, enhancing the data acquisition ability for preliminary testing.

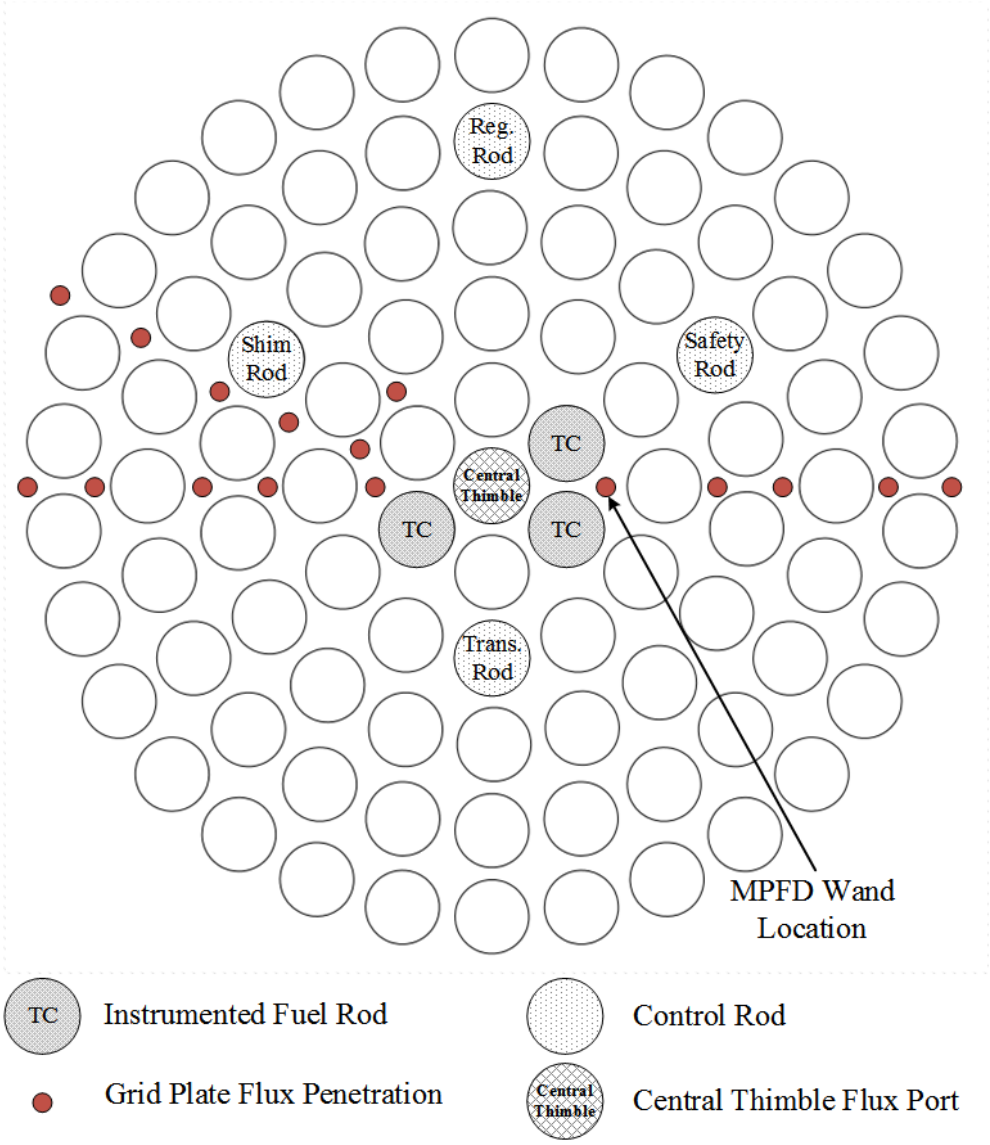

Fig. 6.19 The flux penetration between two instrumented fuel assemblies was chosen for close proximity to the center of the core and access to fuel temperature data.

The electronic support system for the MPFD array included an MPR-16 preamplifier, MSCF-16 shaping amplifier with leading edge discrimination, a Philips scientific 726 signal translator, NIMBox digital I/O unit, and custom LabView interface described in Appendix F. The MPR-16 was set to 20 MeV mode for preliminary testing, and the entire support system was tested with the MPFD emulator. Emulated pulses were observed with a pulse amplitude of approximately 500 mV using an MSCF-16 shaping time of 0.25 μs and a gain of 10. Then, the MPFD array was connected to the MPR-16 (still located outside of the reactor pool) with the cable shield connected to the input ground. High voltages of 10V, 100V, 200V, and 400V were applied to the array, checking for HVPS current draw and increased noise on the oscilloscope. No additional noise was observed during out-of- core testing, and the HVPS current draw remained relatively constant < 0.005 μA. The electronics were then powered off and the array was inserted manually into the flux port, shown in Fig. 6.20. The electronics were re-enabled and a +200V bias was applied to the array. HVPS current and noise were monitored to ensure that no current flowed between anode and cathode wires. The reactor was then brought to 10 kWth with cooling off.

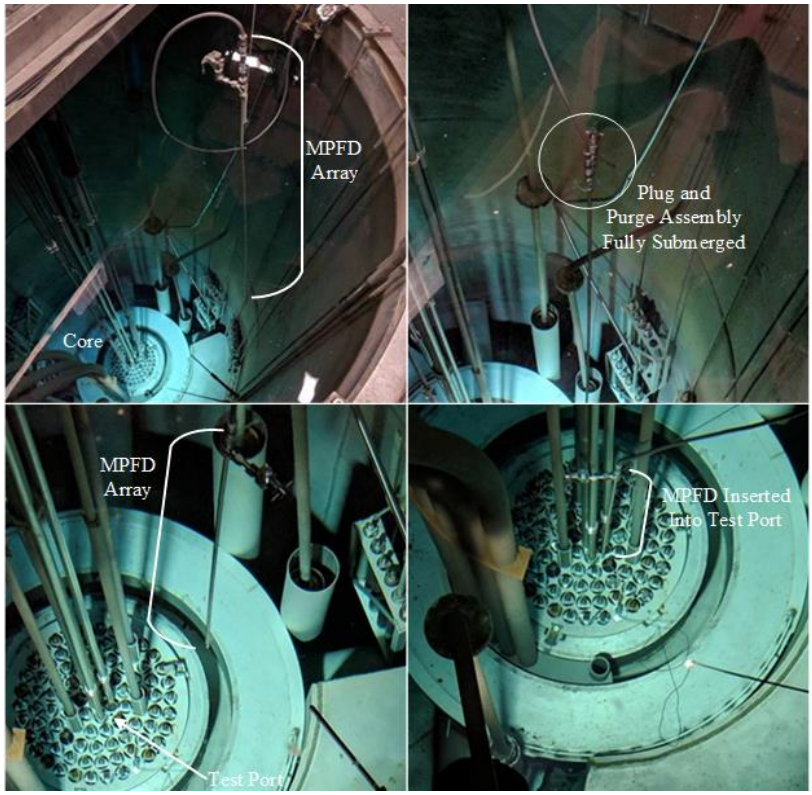

Fig. 6.20 A string was used to lower the array into the reactor pool, reducing stress on the wire connection. Carefully, the MPFD array was inserted into the 8-mm diameter grid plate penetration, into the reactor core.

6.2.2 Detector Pulses

While the reactor was increasing in power, neutron-induced pulses were observed. After establishing criticality at 10 kWth, stability testing and neutron-induced pulse observation commenced. Using the MPR-16 in 20 MeV sensitivity mode with an MSCF-16 shaping time of 0.25 μs and gain of 10, high-frequency noise was observed. The shaping time was increased to 0.5 μs to eliminate the high-frequency noise. A representative neutron-induced pulse, depicted in Fig. 6.21, triggered the discrimination threshold of 15 on the MSCF-16, producing a > 500 mV pulse. The pulse amplitude varied slightly between pulses. The noise was under 100 mV and the average pulse amplitude was higher than the noise value.

After observing large pulse amplitudes in 20 MeV mode, the MPR-16 sensitivity was reduced to 100 MeV mode. The neutron-induced pulses decreased in amplitude by approximately a factor of 5, to approximately 100 mV, shown in Fig. 6.22. The signal-to-noise ratio did not change significantly between 20 MeV and 100 MeV mode, however the pulse amplitude decreased. Further operation continued in 20 MeV mode.

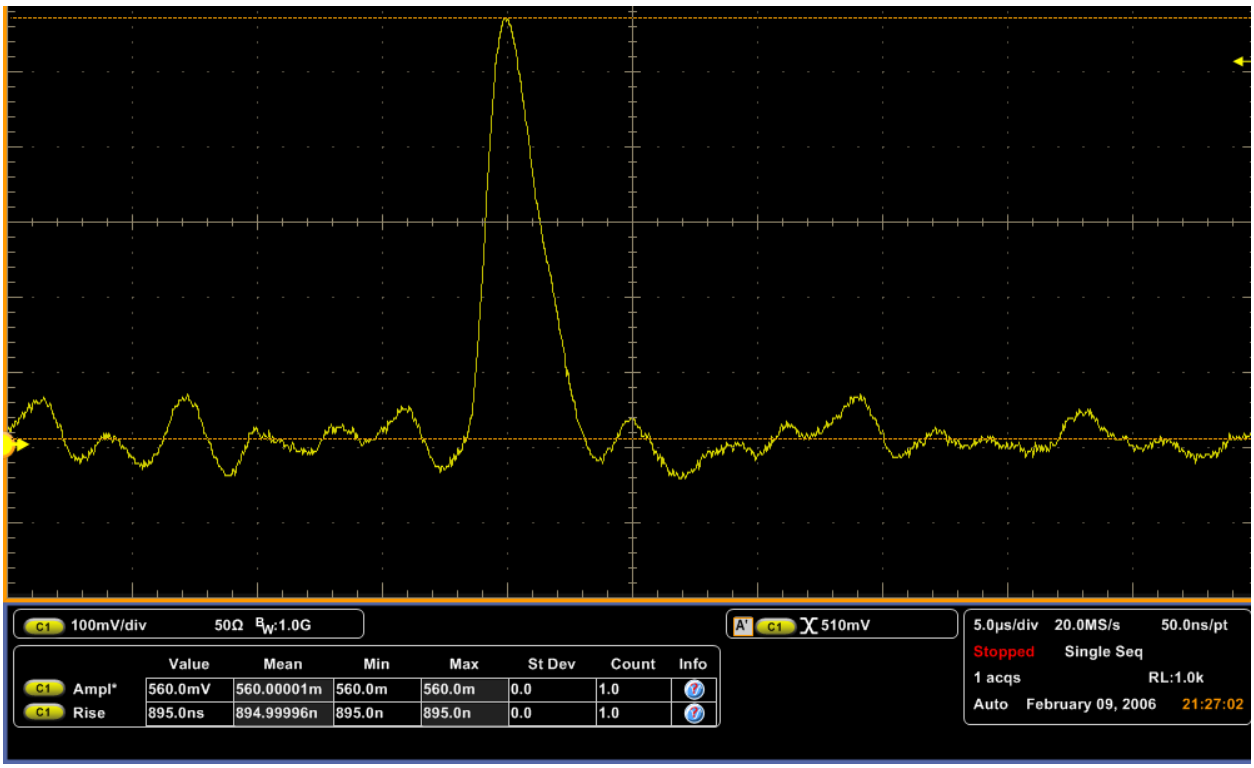

Fig. 6.21 Neutron pulses were first observed using the MPR-16 preamplifier in 20 MeV mode and with the MSCF-16 gain of 10 and shaping time of 0.5 μs.

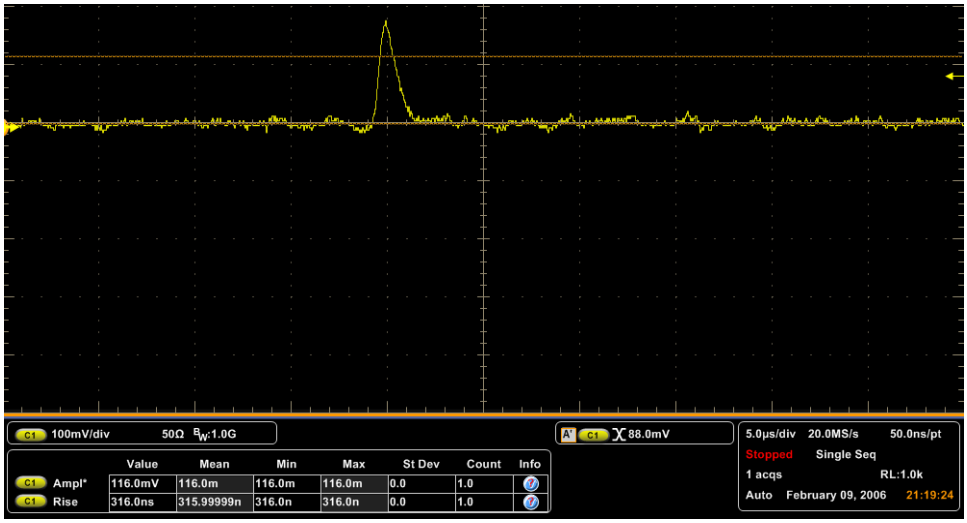

Fig. 6.22 Reducing the MPR-16 sensitivity to 100 MeV mode reduced pulse amplitude but also reduced noise amplitude. The signal-to-noise appeared to remain relatively constant between 100 MeV and 20 MeV mode (approximately 9).

The potential for cross-talk was a concern for multi-sensor MPFD arrays [13]. Each channel of the modular MPFD array was used to trigger the oscilloscope while all four channels were monitored. Cross-talk could then be identified if coincident pulses were observed on multiple channels. No correlated pulses were observed. Multiple pulses are shown in Fig. 6.23 on different channels without perturbing the signal on other channels.

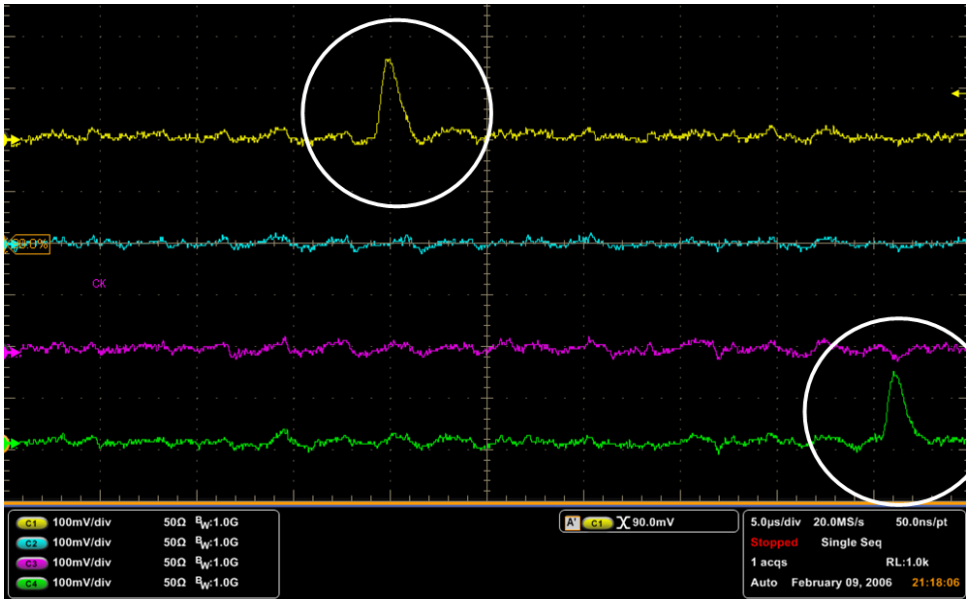

Fig. 6.23 Cross-talk was not observed between MPFD channels. Independent interactions could be observed on multiple channels at different times.

The stability of the detector array was also of great concern. Previous experiments had produced unstable or unreliable response rates after extended testing. The modular MPFD array was tested at 10 kWth for 20 minutes with stable response depicted in Fig. 6.24. The average response rate for each MPFD sensor is summarized in Table 6.3. The mass-normalized response-rate for nodes 1 and 4 should be relatively close because of the nodal spacing in the fuel region of the reactor. Channels 1 and 4 are indeed within 2σ of one another. Similarly, nodes 2 and 3 should have similar mass-normalized response-rates. The low discrimination threshold (15 of 255), likely did not discriminate all of the electronic noise in channel, 3 which responded at a much higher rate than channels 1, 2, and 4. Additional testing was required to confirm proper discriminator setting, however testing was halted due to excessive current flow which was observed when the plug connecting the MPFD array to the extension cable began to leak water. The water leak into the plug was identified by a sharp increase in detector response rate and an increase in HVPS current draw from < 0.005 μA to > 10 μA. The noise signal on the oscilloscope masked neutron-induced signals.

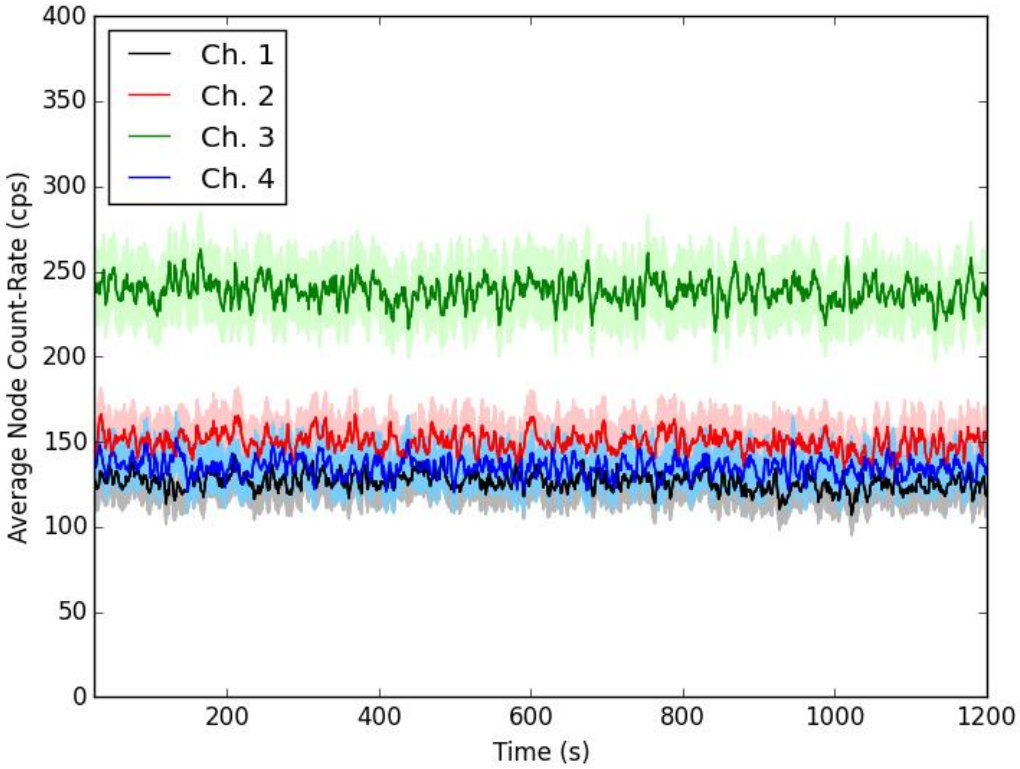

Fig. 6.24 The MPFD array was tested at 10 kWth for 20 minutes with stable responses on every channel.

Table 6.3 The stable detector response over 20 minutes for each channel was used to determine an average count-rate at 10 kWth for the experiment with a threshold setting of 15 for all channels.

Channel	1 (top)	2	3	4 (bottom)
10 kWth response (cps)	125.9	149.4	237.8	134.0
Error (cps)	0.3	0.3	0.4	0.3
Mass normalized response (cps/μg U)	236	237	434	216
Mass normalized response error (cps/μg U)	10.2	9.8	19.8	4.9

The array was removed from the reactor core and the plug was disassembled. The entire array was re-inserted into the heating tube and re-purged. No condensation was observed in the vacuum tube, confirming that water had only leaked into the plug. Water was observed within the mating portion of the plug as shown in Fig. 6.25. The plugs were dried and additional silicone sealing was applied to the mating surfaces of the plug. Additional shrink-tubing was used to seal the plug from water. A new plug will be procured for future array deployments, however the enhanced plug assembly was used to conduct further testing. The purge/fill procedure was executed three times with UHPAr and the array was re-deployed into the same test location between instrumented fuel rods at the KSU TRIGA Mk. II research nuclear reactor depicted in Fig. 6.19.

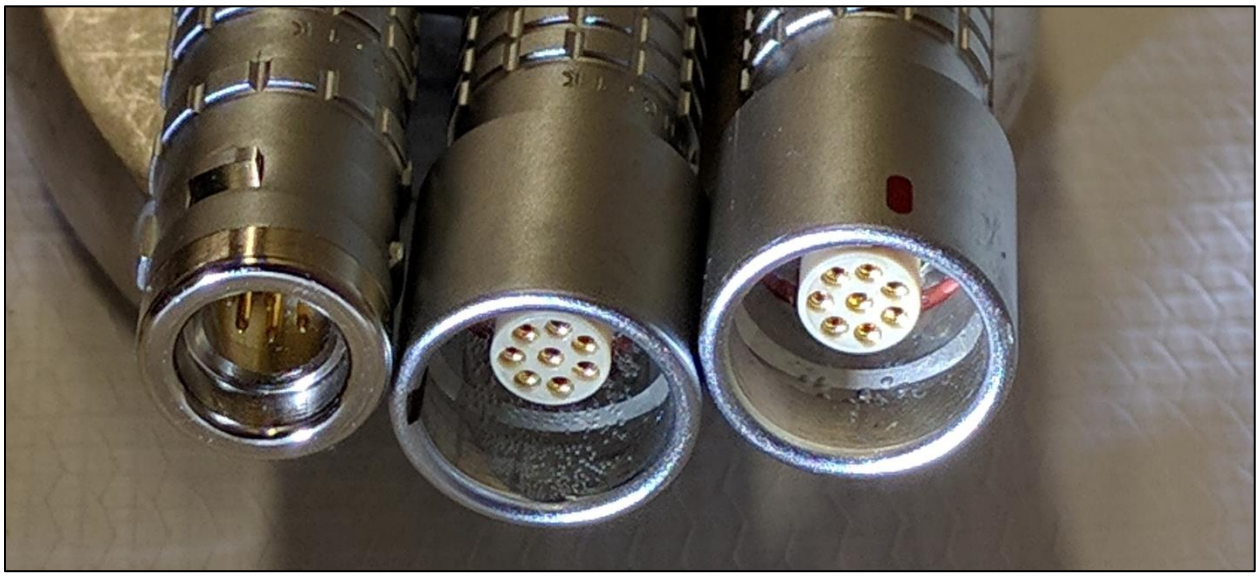

Fig. 6.25 The Lemo FGG/PHG.1K.308 assembly was not entirely water-tight. The penetration of water into the electrical plug produced sufficient conductivity to contaminate the MPFD signal.

6.2.3 Detector Response to Reactor Power

After repairing the water leak in the plug assembly, array testing resumed. The 4-node detector array was deployed into the flux port shown in Fig. 6.19. The detector array was operated under a +200 V applied bias with the MPR-16 in 20 MeV mode, MSCF-16 gain of 5 and shaping time of 1 μs. Neutron-induced pulses triggered the digital counting system using a discriminator setting of 5 on the MSCF-16. First, the sensor response was observed for reactor powers of 10, 200, 400, 600, and 700 kWth. Counts were summed over 5-minutes for each power level (2-minutes at 700 kWth), shown in Fig. 6.27

The detector count rate was stable for power levels of 400 kWth and below. However at power levels above 400 kWth the response of each node increased slightly with time. Overall, the response of each MPFD node in the array increased as the reactor power increased. The rate of increase in detector response was linear between 10 kWth and 400 kWth for all four nodes, but increased at a higher rate for powers above 400 kWth, as depicted in Fig. 6.26.

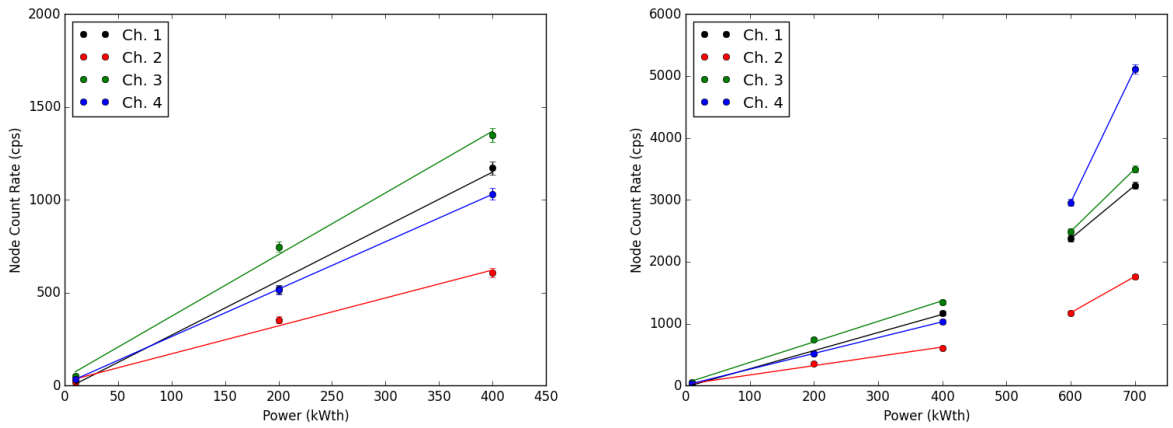

Fig. 6.26 The MPFD response rate was linear with power for all channels below 400 kWth but followed a different trend above 400 kWth.

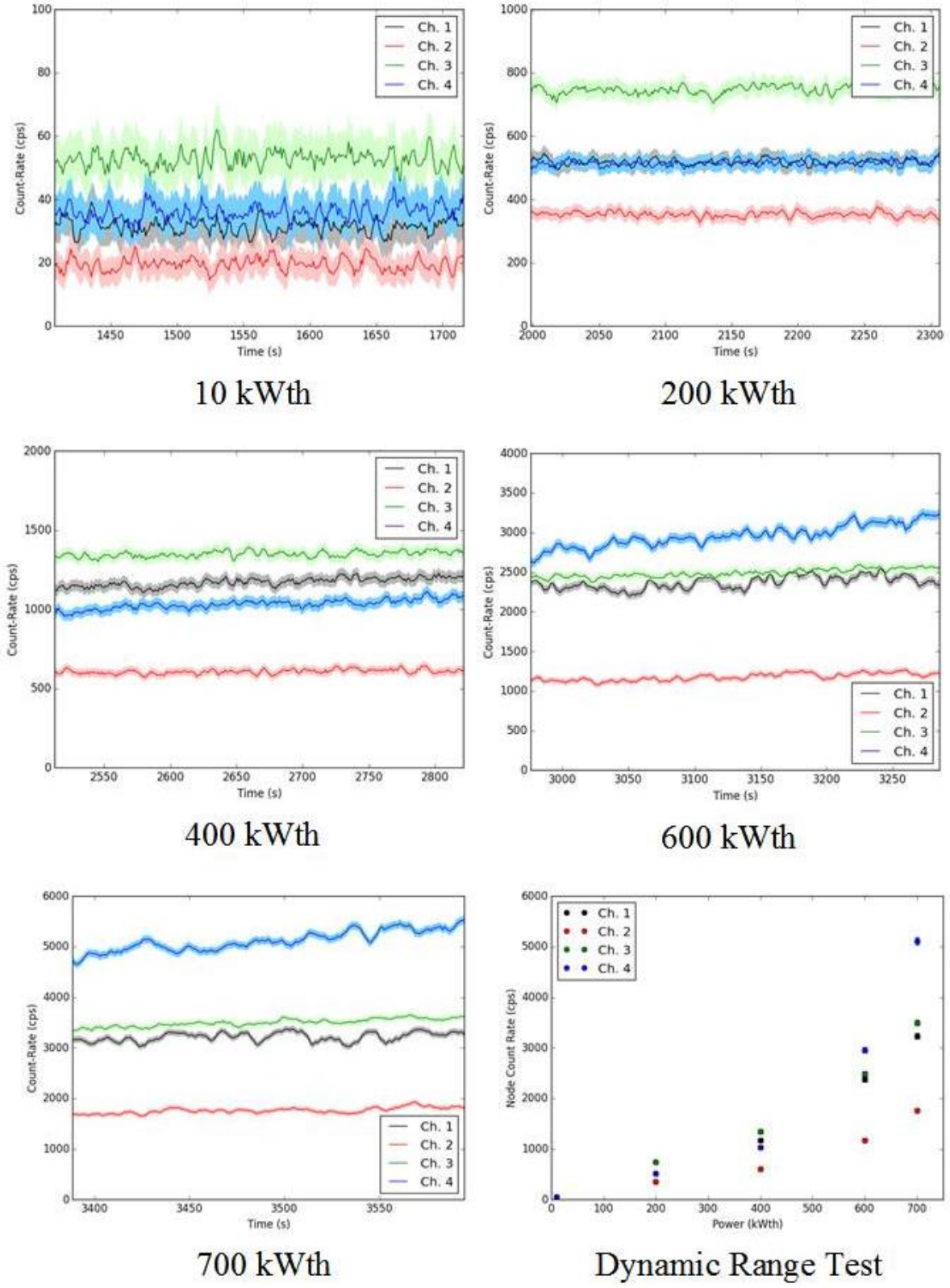

Fig. 6.27 All four channels of the MPFD array were tested at 10, 200, 400, 600, and 700 kWth reactor power.

6.2.4 Tracking Reactor Transients

While the 4-node encapsulated MPFD array was deployed in the reactor core, three different transient experiments were conducted to observe the capability of the MPFD array to respond to real-time changes in reactor power. First, positive reactivity insertions were observed. The rate of increase in reactor power is commonly characterized by the reactor period (the amount of time in which the reactor increased in power by a factor of *e*). The reactor was brought to criticality at 10 kWth using the regulating rod while the shim rod remained fully inserted. Then the reactor operator executed three positive reactivity insertions yielding reactor periods of approximately 30, 15, and 5 seconds by extracting the shim control rod. The reactor was returned to 10 kWth critical state with the shim rod fully inserted between each transient. Maintaining a constant period requires manual extraction of the control rods and was therefore only approximate. The resulting real-time MPFD response rate for three consecutive positive reactivity insertions is depicted in Fig. 6.28. A 1-second measurement interval was used to track real-time MPFD response on the digital counting system. All four detector nodes measured increasing neutron-flux as the shim control rod was removed. Strong effects of temperature feedback were observed, embodied by the peak in detector response followed by a sharp decline and leveling of the detector response. Temperature feedback is an expected feature in a TRIGA nuclear reactor because of the negative temperature coefficient of reactivity for the reactor fuel, and was observed in earlier MPFD transient tests at lower powers [9].

Next, the measurement interval was decreased to 100 mS and manual power oscillation was measured using the MPFD array. Reactor criticality was established at 600 kWth with the safety, shim, and pulse rods fully removed. The regulating rod remained fully inserted. The regulating rod was then removed at a constant rate yielding positive reactor period of approximately 30 seconds until a reactor power of 900 kWth was reached. In order to prevent a linear power SCRAM (triggered at 1 MWth) the reactor operator then fully inserted the regulating rod to reduce the reactor power to the original 600 kWth level. The oscillating reactivity insertion was repeated a total of 5 times. The real-time response of all four MPFD nodes tracked the oscillation of reactor power in the core as shown in Fig. 6.29.

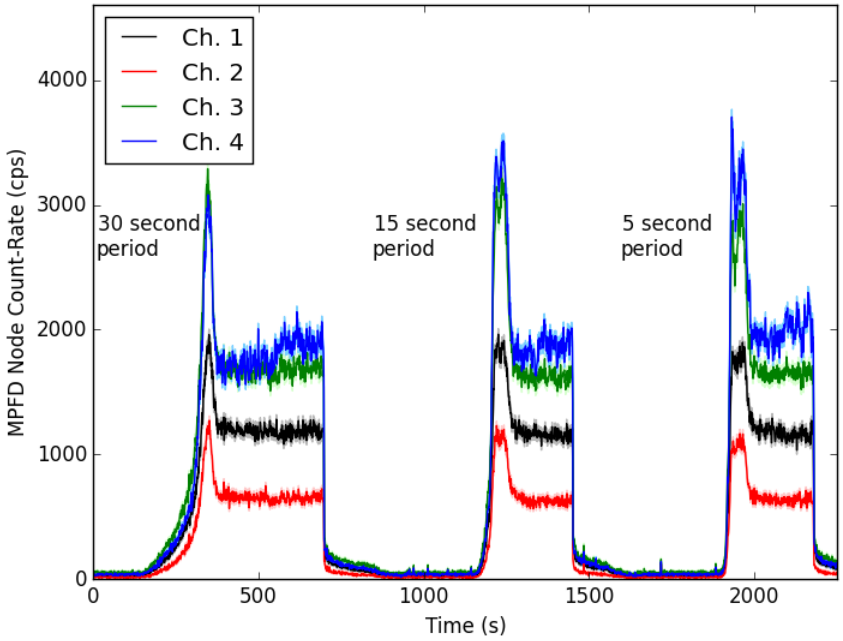

Fig. 6.28 Positive reactivity insertions with power periods of 30, 15, and 5 seconds were tracked using a 1-second counting interval.

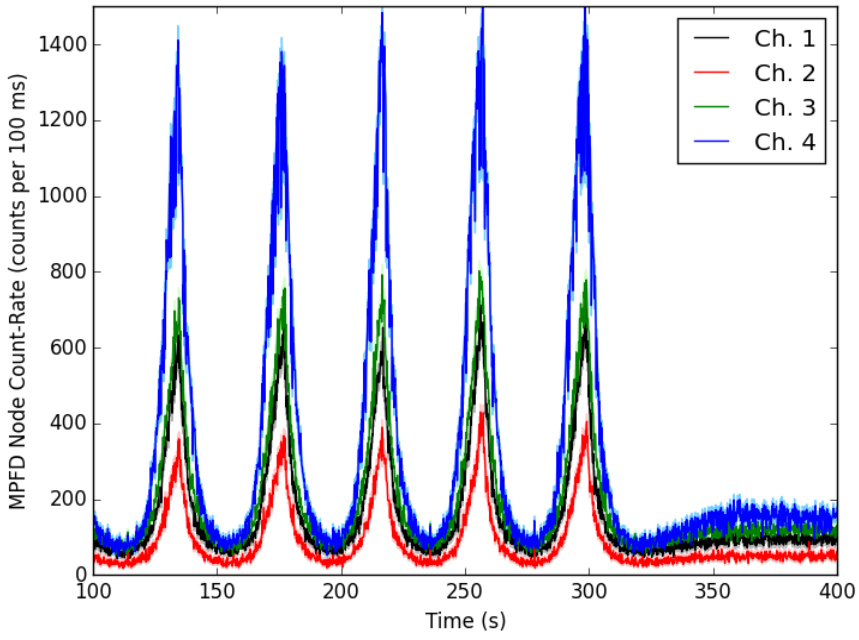

Fig. 6.29 Increasing and decreasing power transients were tracked using a 100-ms counting interval.

Finally, the measurement interval was decreased to 1-ms, providing maximum data acquisition rate for the MPFD array (limited by the digital counting system) to measure the effects of a reactor SCRAM in real-time. Reactor criticality was established at 750 kWth with all control rods out (full power). The counting system was enabled and allowed to collect data at full power for 5 seconds before a SCRAM was executed, immediately driving in all control rods. The neutron response decreased rapidly as the rods were dropped into the reactor core, shown in Fig. 6.30. Although data was collected for four channels, the data for channel-4 appeared to be corrupted during acquisition. The data shown in Fig. 6.30 represents a 5-ms average of each channel for clarity.

The fabrication and testing of a modular 4-node MPFD array at the KSU TRIGA Mk. II research nuclear reactor clearly indicate the capability of such devices to be used for real-time, in-core monitoring of neutron flux. However, several improvements remain for the design, fabrication, and application of MPFDs. First, better materials should be selected that eliminate the possibility of water leaking into the electrical connections of the sensor. Also, the operating parameters must be investigated in greater detail to determine optimal operating bias, gain (for both the preamplifier and shaping amplifier), shaping time, and discriminator setting.

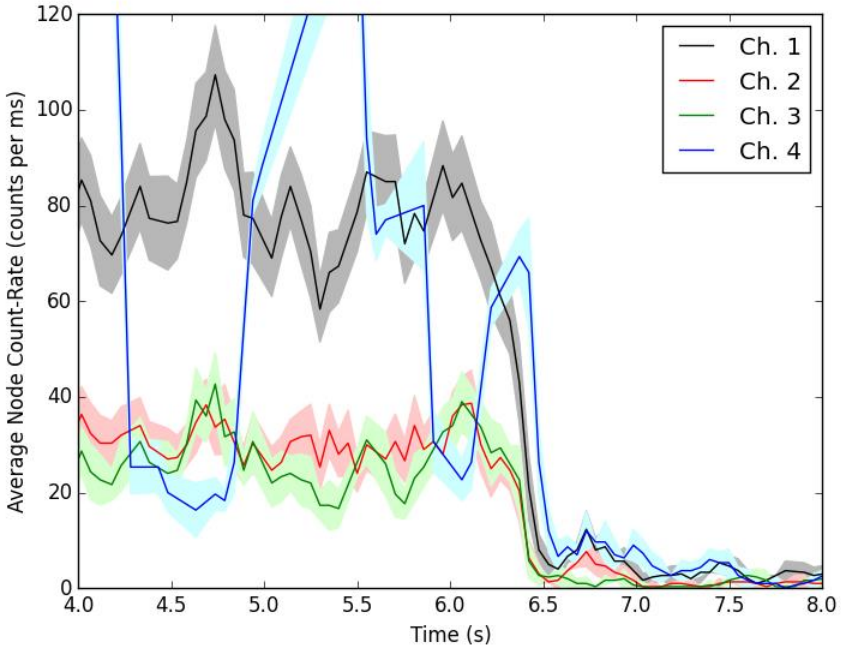

Fig. 6.30 The rate of power reduction from a full-power reactor SCRAM was tracked using 1-ms counting intervals.

6.3 Five-Node Flux Wire Port MPFD Probe Fabrication and In-Core Testing

Multi-nodal MPFD arrays are also of interest for deployment into iron-wire flux ports. In the past, only single-node sensors were constructed and tested [9]. After the advances discussed in Ch. 5.2, a 5-node MPFD array was fabricated and tested in the central thimble of the KSU TRIGA Mk. II research nuclear reactor. Increasing the number of nodes complicated the fabrication process, particularly the braiding procedure. However, the rigidity of the array was improved by the addition of more anode wires into the braid. The silica insulation process was also improved through practice by fabricating additional mockup test arrays. Numerous mockup arrays were tested in the mockup test port described in Ch. 5.2. The arrays were inserted into and removed successfully from the mockup port without damage. Resistance and capacitance of each anode with respect to the common-cathode was verified after insertion and after removal to confirm that each anode was electrically isolated and no damage to the insulation had occurred. The flux wire MPFD probe utilized the same pulse processing electronics as the previously described modular MPFD array. Neutron induced pulses were observed on all five MPFD channels. Stability testing suggested that the sensor response was sensitive to changes in operating bias. Dynamic range testing was conducted to determine if the array responded linearly to reactor power. During dynamic range testing, linearity was only observed for power levels < 100 kWth, in contrast to previous detectors which operated linearly up to 750 kWth [9]. After the array was removed from the reactor, post-irradiation examination suggested that array had been constructed with disks that caused the non-linear response to reactor power. The electrode upon which the fissile coating was deposited appeared to have been placed too close to the anode wire hole and allowing excess current to flow through the chamber at elevated power levels.

6.3.1 MPFD Array Fabrication

Similar to other MPFD designs, the individual sensors which constitute each of the five nodes for the flux wire array were constructed from two disks and 1 spacer. Each of the machined alumina disks measured 2-mm long x 1-mm wide and was fabricated with a polished face by NucFil Inc. The two holes in the disks were 0.5-mm diameter, large enough for the 26 AWG nickel common cathode wire. Individual 32 AWG anode wires were used for each node, providing a read-out electrode corresponding to that node. A 0.5-mm wide platinum electrode was deposited by

electron-beam evaporation onto one disk for each MPFD node, shown in Fig. 6.31. A 0.5-mm thick alumina spacer was used to separate the MPFD disks from one another and to provide an ionization chamber. The electrode was evaporated using the same process described for the modular MPFD array, utilizing a 50 Å titanium adhesion layer followed by a 500 Å platinum layer.

Each of five MPFD disks were electrodeposited using the electrolytic solution procedure described in Appendix A. The cyclic voltometric electrodeposition procedure was followed as described in Appendix C with a total of 250 potential sweeps. Alpha particle spectrometry was used to measure the mass of uranium deposited on each sample, summarized in Table 6.4. The variation in surface area for each electrode caused the variations in the amount of deposited material between samples.

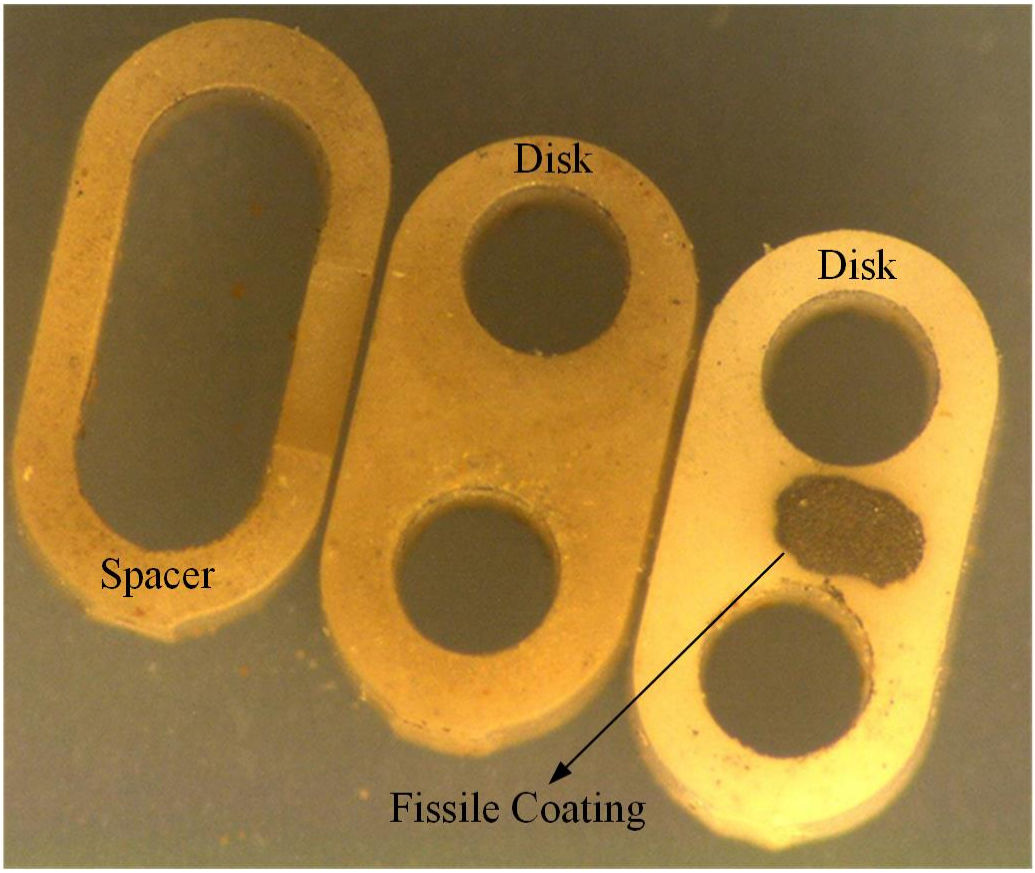

Fig. 6.31 Each MPFD node was composed of two disks (right) and one spacer (left). Natural uranium was electrodeposited onto one of the disks.

Table 6.4 Alpha spectrometry was used to measure the activity of each sample which and subsiquently to calculate the mass of natural uranium deposited on each sample.

Node	Uranium Mass (µg)	Mass Error (± µg)
1 (bottom of array)	0.09	0.01
2	0.05	0.01
3	0.07	0.01
4	0.12	0.01
5 (top of array)	0.09	0.01

The array fabrication began by straightening and cleaning each of the five anode wires with acetone, isopropyl alcohol, and deionized water. Then, silica insulation was threaded onto each anode wire. The cathode wire was then straightened and cleaned in a similar manner and secured at one end to the 20-foot long assembly table. Afterwards, 1-inch sections of alumina insulation were threaded onto the end of the cathode wire to provide spacing at the bottom of the array, securing the location of the first MPFD node 1-inch above the bottom of the array. The first MPFD was assembled onto the cathode as shown in Fig. 6.32. The anode wire was terminated using a 4-hole alumina spacer by threading the excess portion of anode wire past the MPFD, into one hole of the 4-hole spacer and back through a second hole in the 4-hole spacer. Excess anode wire was removed from the end of the 4-hole spacer to reduce the likelihood of shorting with the flux well wall.

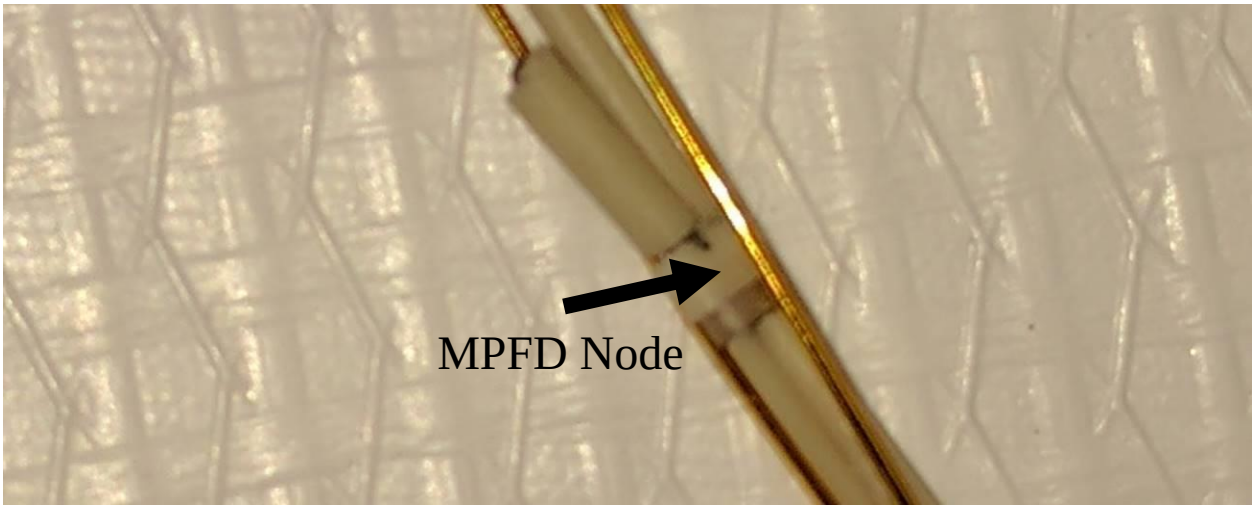

Fig. 6.32 Each MPFD node was fabricated in-line with a common cathode design.

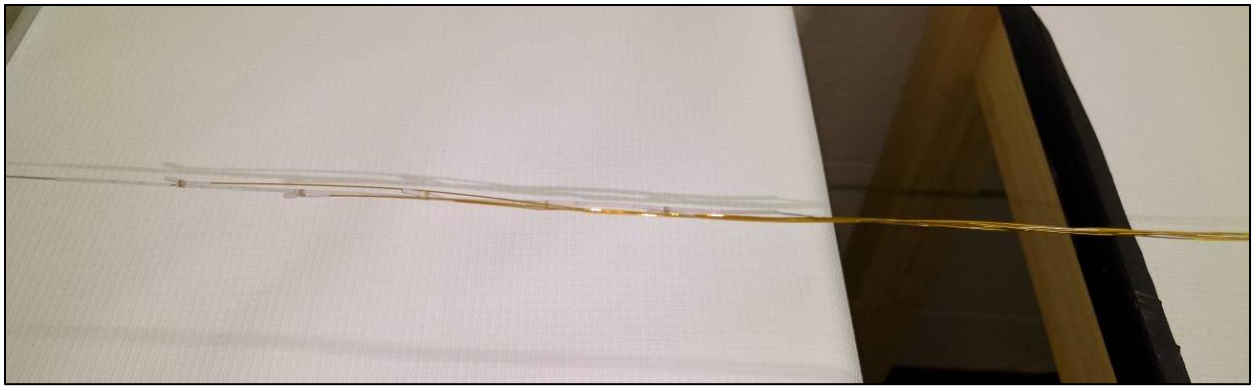

Fig. 6.33 Five MPFD nodes were constructed in a linear array at the end of the assembly.

Four additional MPFD nodes were added in a similar fashion, separated by 1 inch of alumina insulation on the common cathode wire. An additional ½ inch of cap material was positioned between the bottom of the central thimble and the bottom of the interior of the flux well. Accounting for the additional cap material, the MPFD nodes were located at positions 1.5 inches, 2.5 inches, 3.5 inches, 4.5 inches, 5.5 inches, and 6.5 inches above core center. The linear array of MPFD sensors, shown in Fig. 6.33, was distributed within the top half of the reactor core after insertion because the central thimble terminates at the center of the 15-inch tall reactor core.

The anode and cathode wires were left unbraided during the MPFD fabrication process. After all five nodes had been assembled, the remainder of the array was braided to improve the rigidness of the array and reduce the likelihood of kinking or bending in the individual anode wires during insertion. The braiding process described in Ch.5.2 was used to hand-braid the 5-node MPFD array, shown in Fig. 6.34. The ‘may-pole’ braiding method helps to reduce the inductive coupling between the anode wires and the cathode wire while also relying on the thicker cathode wire for structural integrity. After braiding with a frequency of 0.5 braids per inch, shown in Fig. 6.35, the array was inspected for quality. During the quality inspection, gaps and fractures in the silica insulation, as well as kinks in the wire were identified and repaired. No such imperfections were identified for the 5-node MPFD array shown in Fig. 6.36. However, as an additional precaution to prevent shorting between the terminated anode wires and the flux well wall, a thin quartz tube was added around the MPFD sensor region of the array, shown in Fig. 6.37. Sufficient space remained at the top and bottom of the quartz tube to allow for gas to flow into and out of the MPFD sensors while creating an additional insulating layer between any protruding anode wires.

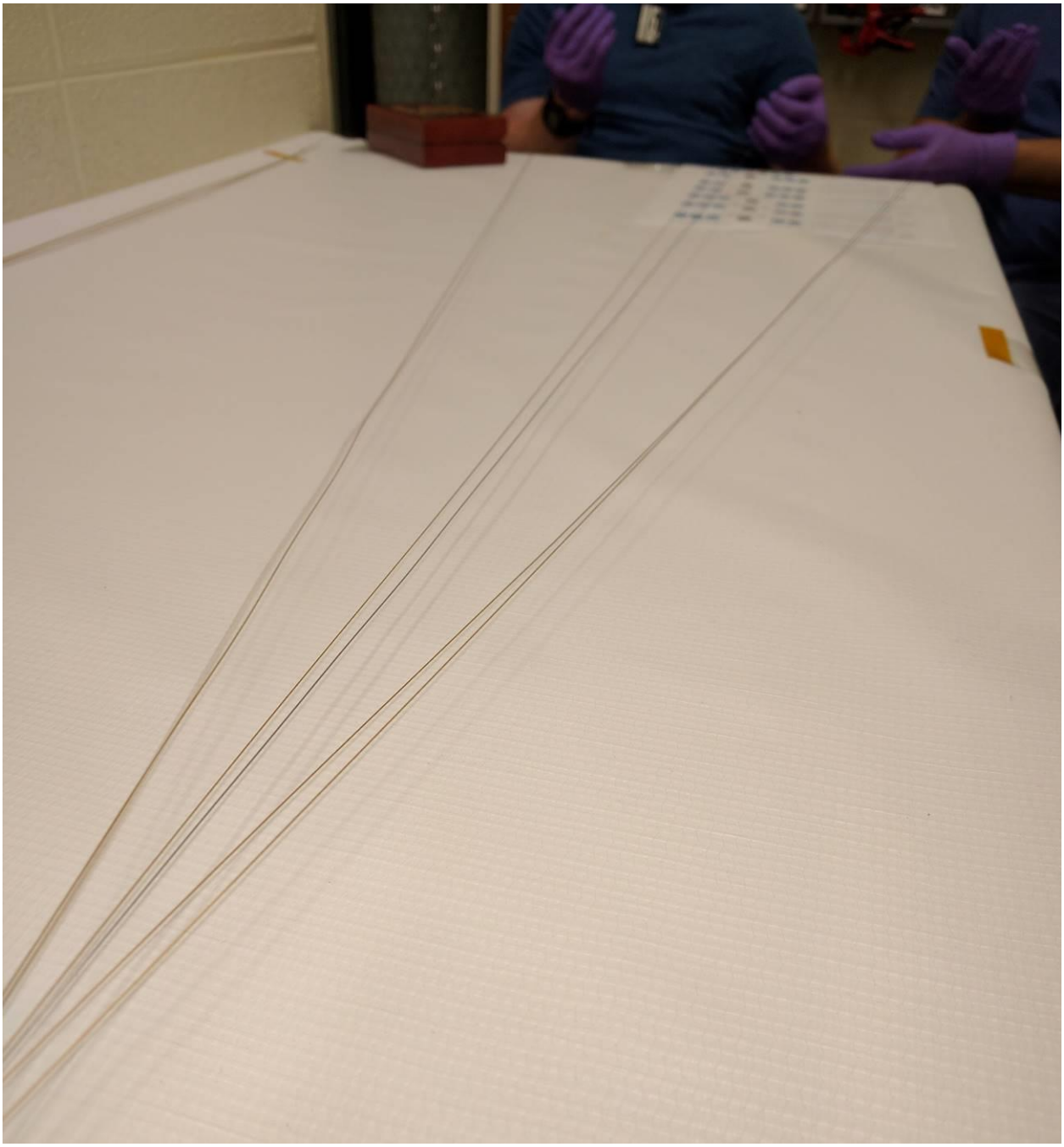

Fig. 6.34 The anode wires were braided around the cathode wire following the standard braiding procedure described in Ch. 5.2

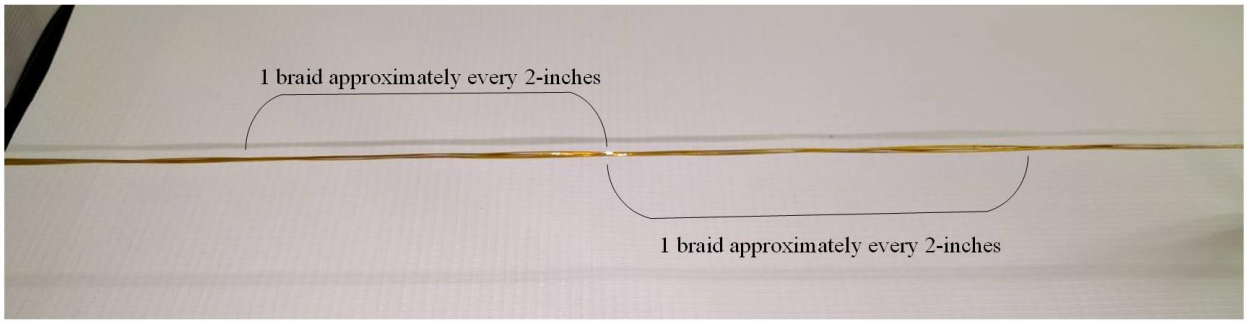

Fig. 6.35 A braid frequency of one braid per two inches was used to reduce the stress on the silica capillary tube insulation.

Fig. 6.36 Braiding the anodes around the cathode wire adds regidity to the array while still allowing the array to bend as necessary.

Fig. 6.37 A small quartz tube was added to the MPFD region of the array to reduce the liklihood of shorting between the anode terminations and the flux port wall.

The vacuum purge/gas fill assembly was then added to the array and the electrical feedthrough was assembled and connected to a 10-foot long extension cable, shown in Fig. 6.38. The same Belden 8134E cable was used for the 5-node MPFD array as for the modular MPFD array, however only 6 of the 10 wires were used. Additional tinned-copper overbraid was added to the assembly, covering the electronic feedthrough to reduce RF interference. The flux well was grounded to the preamplifier input ground through the cable shield which was connected to the gas purge/fill system.

A three-way valve was used to connect a rough vacuum pump and UHPAr tank to the vacuum purge/gas fill system. Prior to array insertion, the flux well located within the central thimble of the KSU TRIGA Mk. II research nuclear reactor was purged using a rough vacuum pump and back-filled with UHPAr. Then the array was inserted into the flux well as shown in Fig. 6.39. One-hour long vacuum purge and back-fill with UHPAr was repeated three times after insertion.

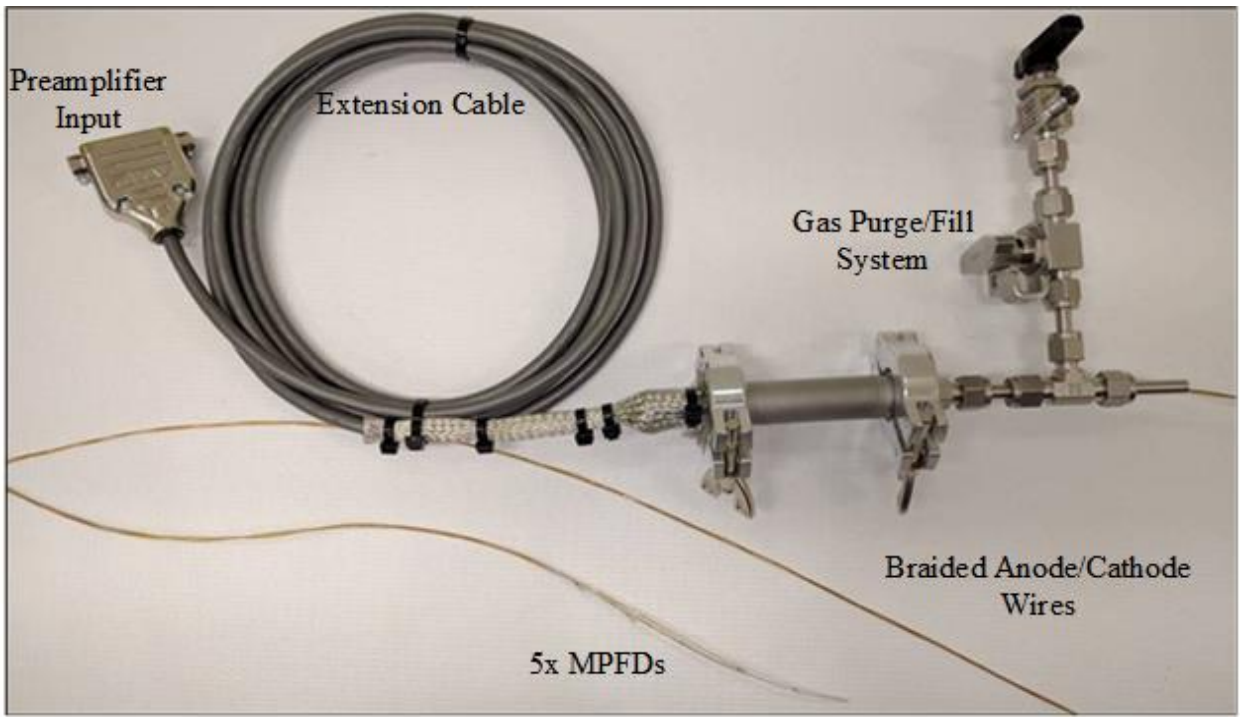

Fig. 6.38 The electronic feedthrough and gas purge/fill system were added to the array along with a 10-ft extension cable before deployment.

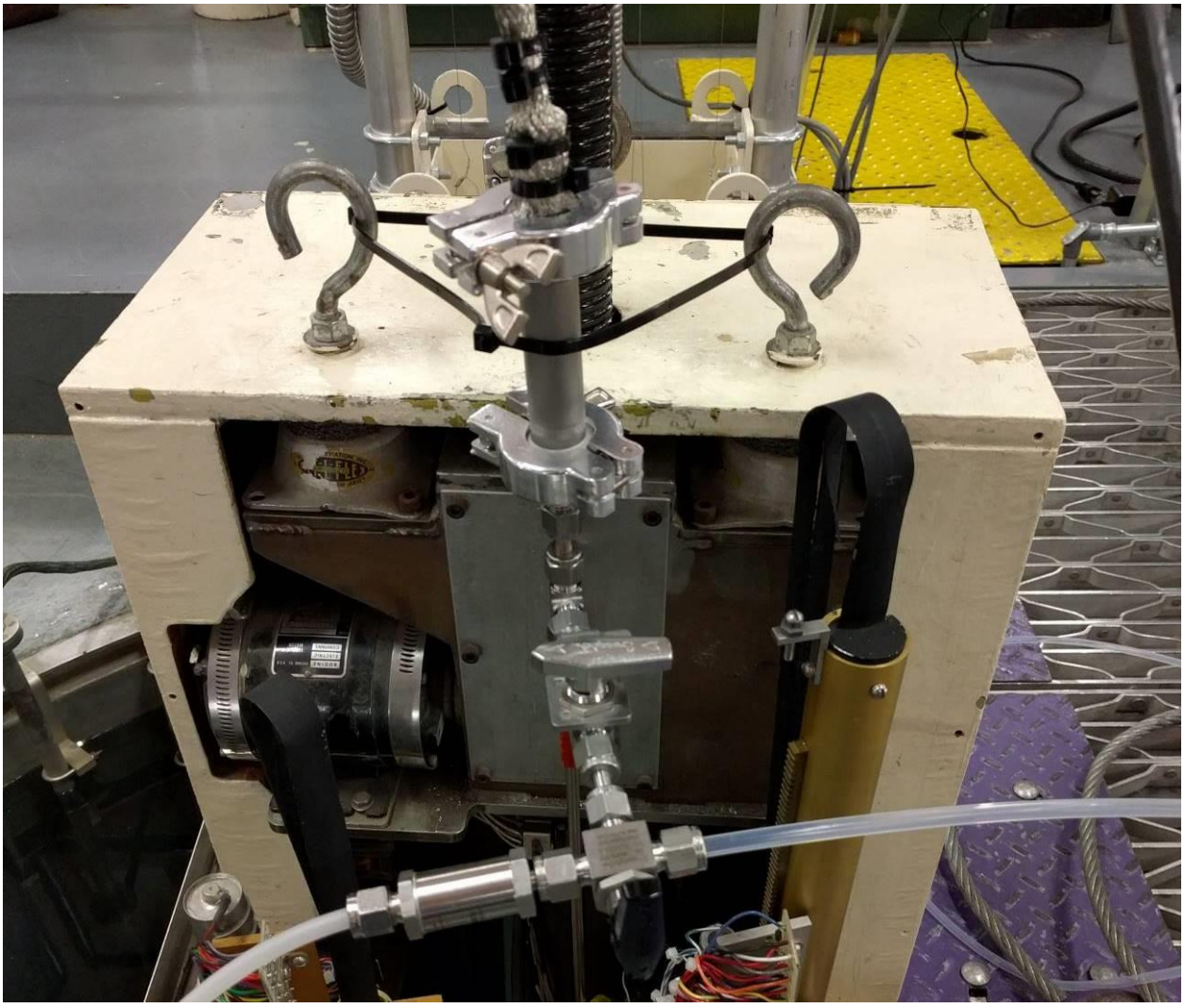

Fig. 6.39 The MPFD array was deployed into the central thimble of the KSU TRIGA Mk. II research nuclear reactor and a three-way valve was used to control the vacuum and back-fill of UHPAr.

6.3.2 Electronics Configuration and Detector Pulses

The MPFD emulator (described in Ch. 5.3.3) was used to set MSCF-16 parameters before connecting the MPFD array. The MSCF-16 gain was set to 14, shaping time set to 0.25 μs, and discriminator threshold set to 40, producing an emulated test pulse amplitude of 500 mV. The MPFD array deployed into the central thimble flux well The MPR-16 preamplifier was set to 20 MeV mode and connected to the MPFD array. The shield of the cable connecting the MPFD array to the preamplifier was connected to the input ground terminal on the MPR-16. The MPR-16 output was connected to the MSCF-16 shaping amplifier via 34-pin ribbon cable. Four channels of operation were observed on an oscilloscope using the analog output from the MSCF-16. The

MSCF-16 ECL output was connected to the Philips Scientific 726 signal translator. The NIM output from the signal translator was connected to the NIMbox. Custom LabView software, described in Appendix F, was used to count digital pulses received by the NIMbox. An MHV-4 high-voltage power supply was connected to the MPR-16, providing a +200 V operating bias to each MPFD node.

The reactor power was increased to 10 kWth and neutron induced pulses were observed, shown in Fig. 6.41. The signal-to-noise ratio of 8 was recorded for the test configuration. The amplitude of neutron-induced pulses varied but was typically between 100 mV and 200 mV with pulse rise times of approximately 200 ns. In contrast to the encapsulated and modular MPFD designs, more electronic noise from control rod motion was observed between steady-state operation conditions. It is likely that the close proximity of the central thimble to the control rod drive motors enhances the effects of electromagnetic noise in the detector cabling.

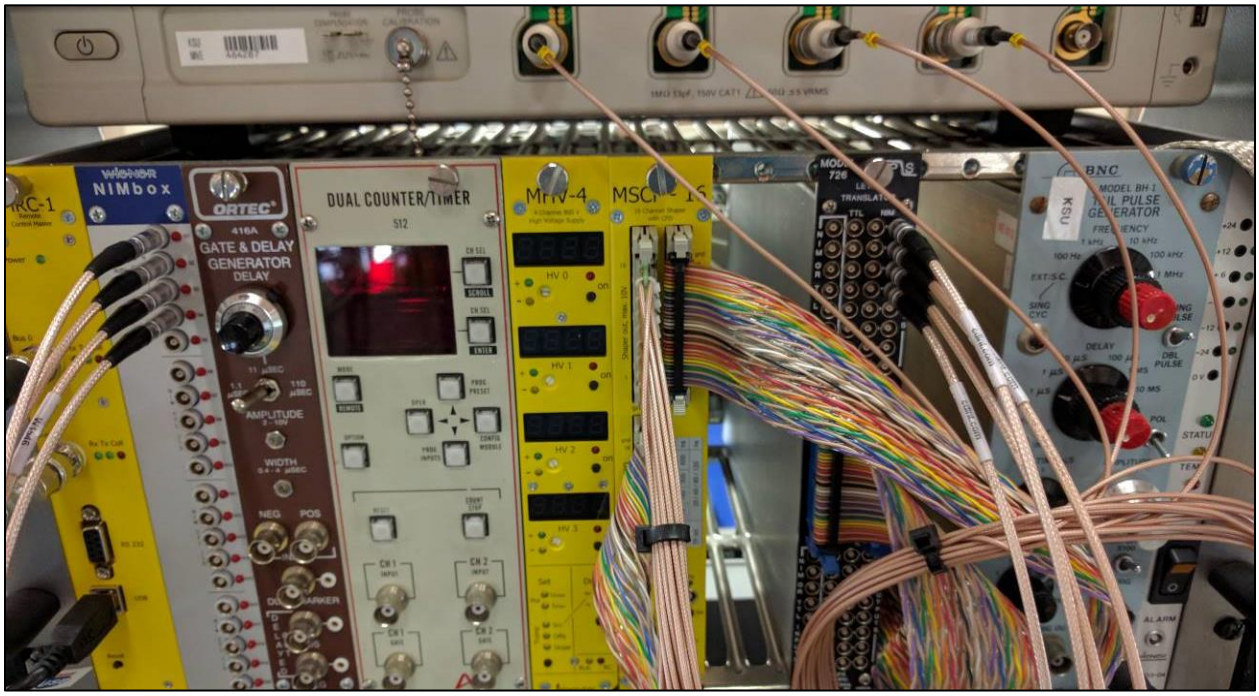

Fig. 6.40 High voltage power supply, shaping amplifier, signal translator, and digital I/O were used to measure the MPFD responses after being deployed.

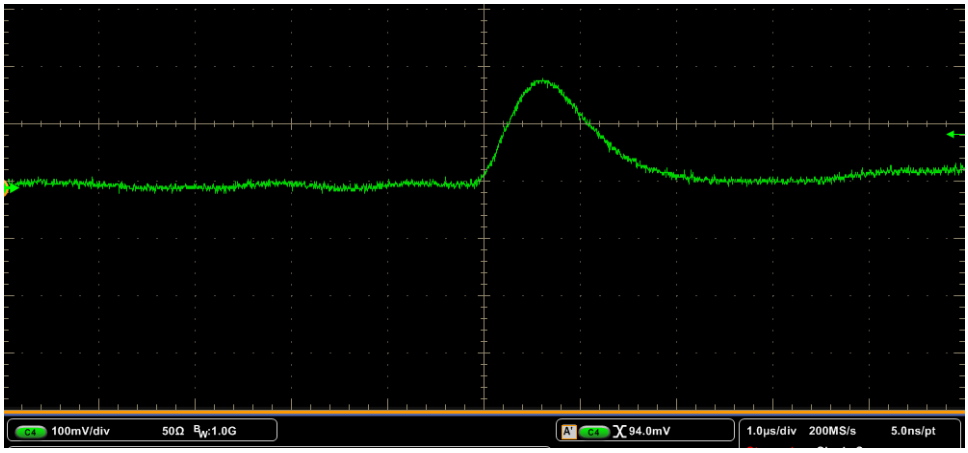

Fig. 6.41 Neutron-induced pulses were observed above the electronic noise.

The analog output of the MSCF-16 was used to monitor four MPFD channels simultaneously on the oscilloscope. Cross-talk between channels can occur if the signal on one anode wire induces a pulse on subsequent channels. After triggering the oscilloscope on a neutron-induced signal on one channel, all other channels should be clear of any pulses in the immediate time vicinity of the triggered pulse as shown in Fig. 6.42. Cross-talk testing was conducted at 10 kWth reducing the possibility for coincident interactions in multiple chambers that usually increases at higher reactor powers. No cross-talk was observed.

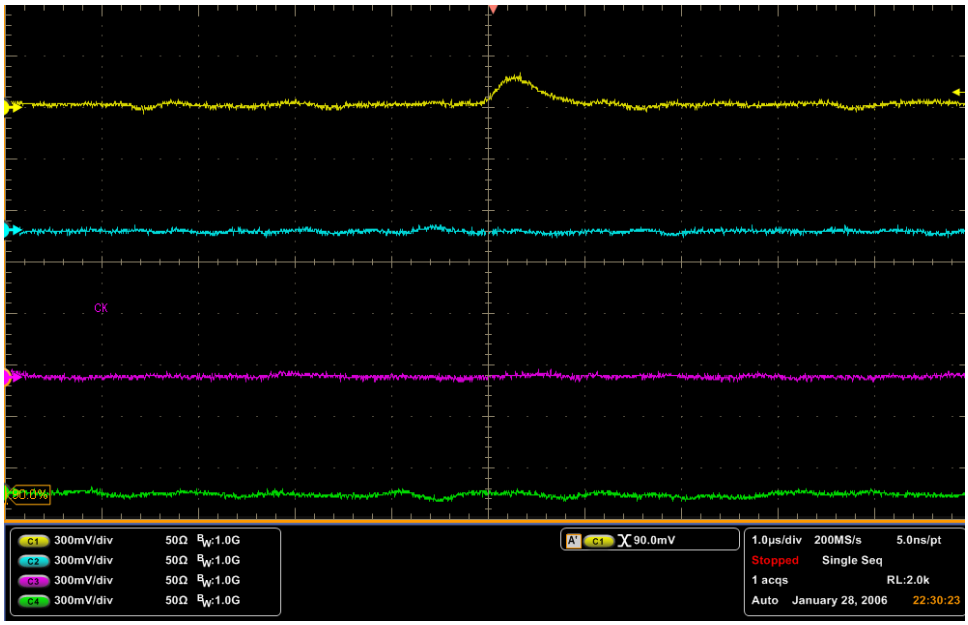

Fig. 6.42 No cross-talk was observed between MPFD channels.

After conducting preliminary observation of neutron-induced pulses and checking for cross-talk at 10 kWth, reactor power was increased to measure the change in detector response. Criticality was established at 500 kWth and excessive current flow through the HVPS was observed. Typically HVPS current < 1 μA was observed for all reactor power levels. Current flows from the HVPS as the operating bias is maintained in the sensor due to the motion of ionization in the detector chamber. Excessive current flow induces significant electronic noise in the system along the channel through which the current is flowing, shown in Fig. 6.43. Both channels 1 (yellow) and 2 (cyan) in Fig. 6.43 exhibited noise from current flow. The amplitude of the noise in both channels was sufficient to exceed the discriminator setting, exaggerating the detector response. The current was most problematic when operating at applied biases > 100 V, and increased in magnitude as reactor power increased.

Subsequent analysis of the disks used to fabricate the 5-node array suggests that the platinum electrodeposition substrate (Fig. 6.31) was located close enough to the anode and cathode wires to provide a path for current to flow in the presence of high amounts of ionization that occur at elevated reactor power levels. However, further testing was still possible by operating the detectors at a lower applied bias, neglecting the noisiest of the detector channels, and at reactor power levels at or below 100 kWth.

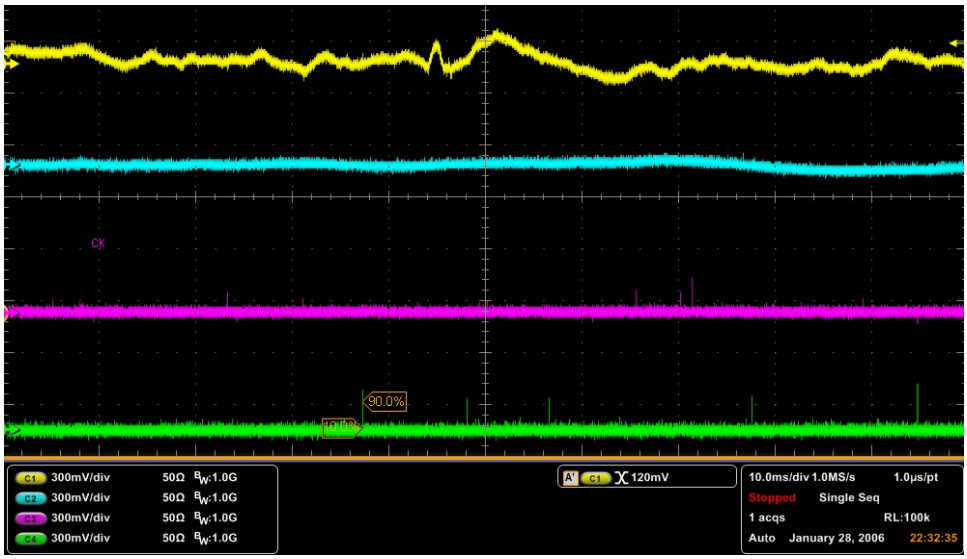

Fig. 6.43 Two detector channels exhibited more noise than the other channels. In the oscilloscope trace depicted, channel 1 (yellow) and channel 2 (cyan) exhibited noise from current flow in the sensor.

6.3.3 Detector Response to Reactor Power

First, the MPFD array was tested at a constant reactor power of 100 kWth with applied biases of +50, +100, and +200 V. When a +50 V applied bias was used, the detector response was unstable, increasing on three channels, and decreasing on one channel over a 30-minute measurement time, shown in Fig. 6.44.

Next, the operating bias was increased to +200 V. With a constant reactor power of 100 kWth, the detector response was not stable. All channels increased response rate over a 30-minute measurement period. Channel 4 exhibited a discontinuity in the detector response during the measurement while channels 1 – 3 increased linearly throughout the measurement as shown in Fig. 6.45.

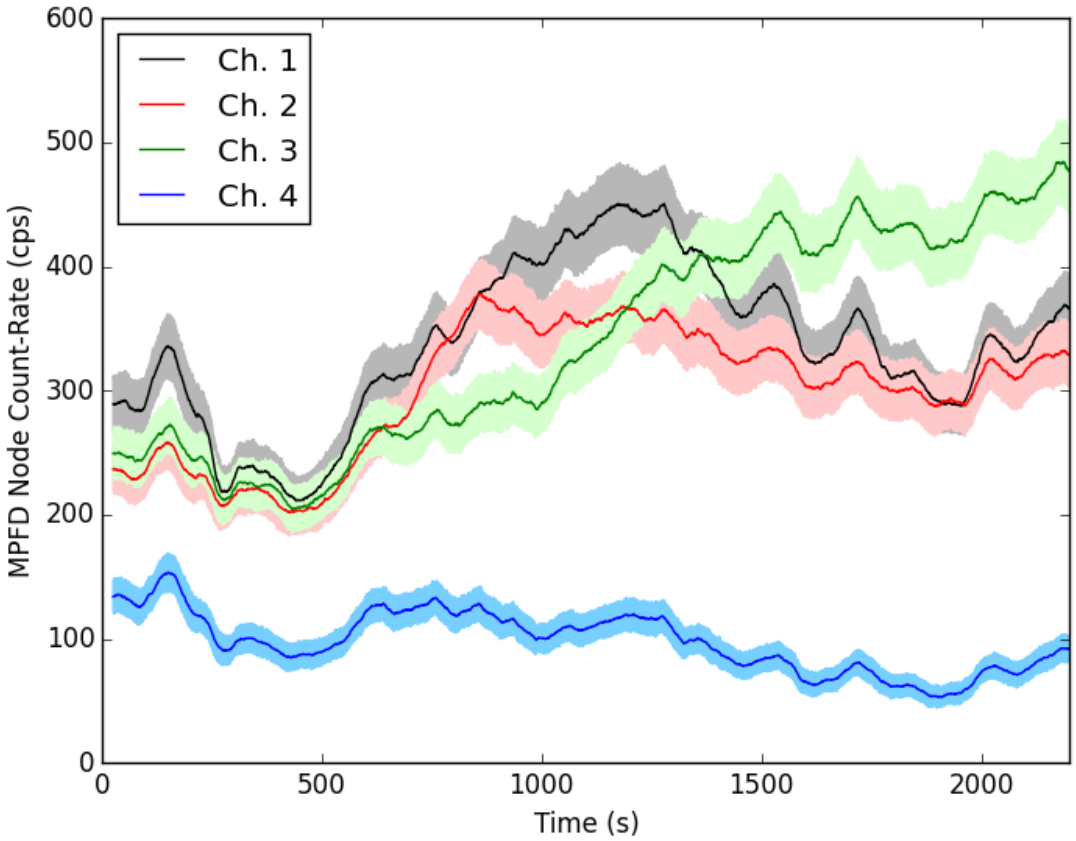

Fig. 6.44 Detector response was not stable with only +50V applied bias.

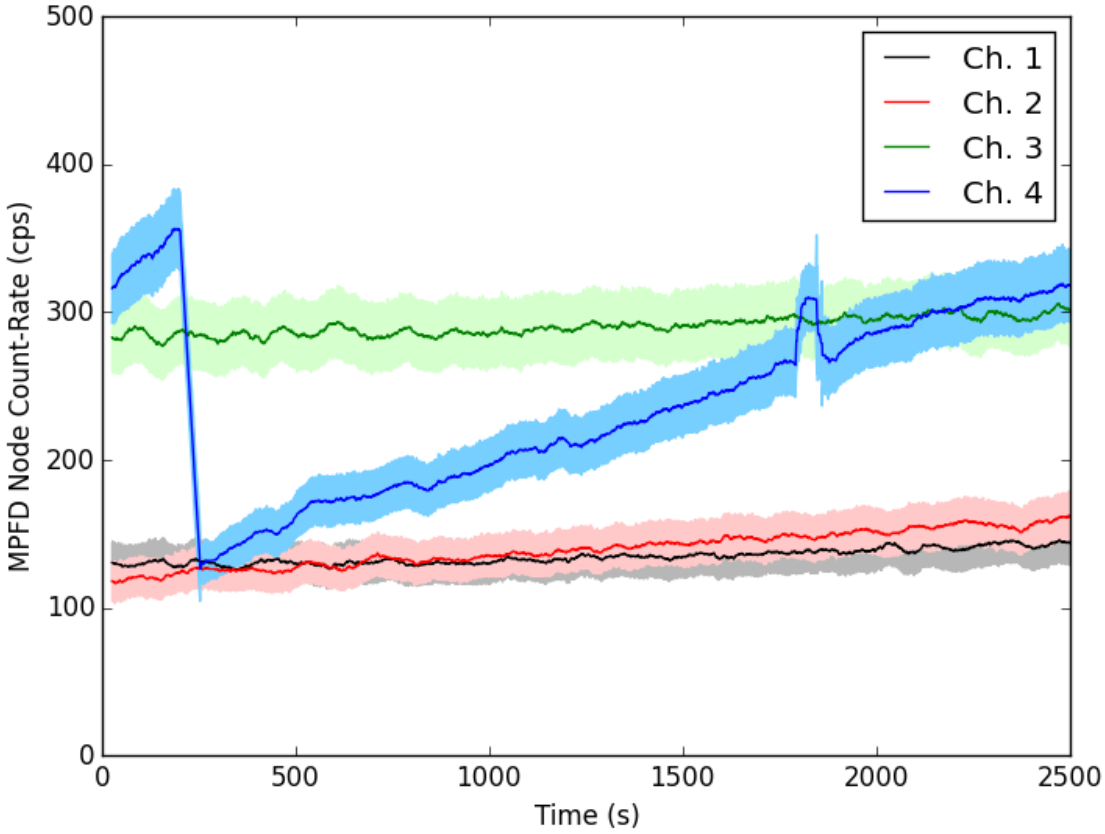

Fig. 6.45 Using +200V applied bias caused a linear increase in detector response with time on channels 1-3 and caused instability in channel 4.

Finally, a +100 V applied bias yielded a stable response on all 4 channels shown in Fig. 6.46. Maintaining a +100 V applied bias, the measurements were taken with reactor powers of 10, 25, 50, and 100 kWth in sequence. Reactor power was maintained for 5 minutes at each power level. Real-time MPFD response for the entire experiment including all four reactor power levels show power tracking between steady-state conditions, depicted in Fig. 6.47. The counts from each five-minute measurement were summed to determine the average detector response rate for each detector channel at each power level. A linear detector response to reactor power between 10 kWth and 100 kWth was observed, shown in Fig. 6.48.

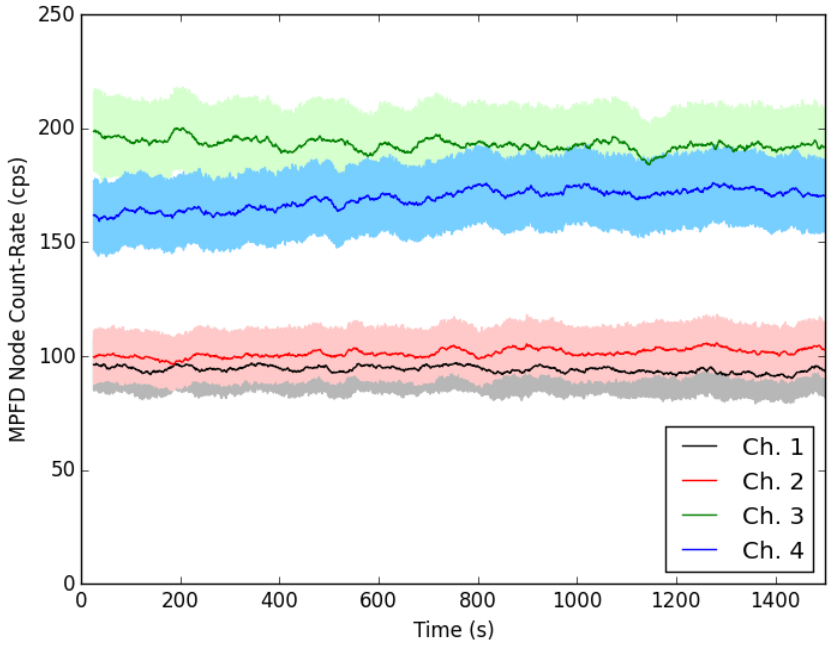

Fig. 6.46 A stable response at constant power was observed with +100V applied bias over 25 minutes at 100 kWth reactor power.

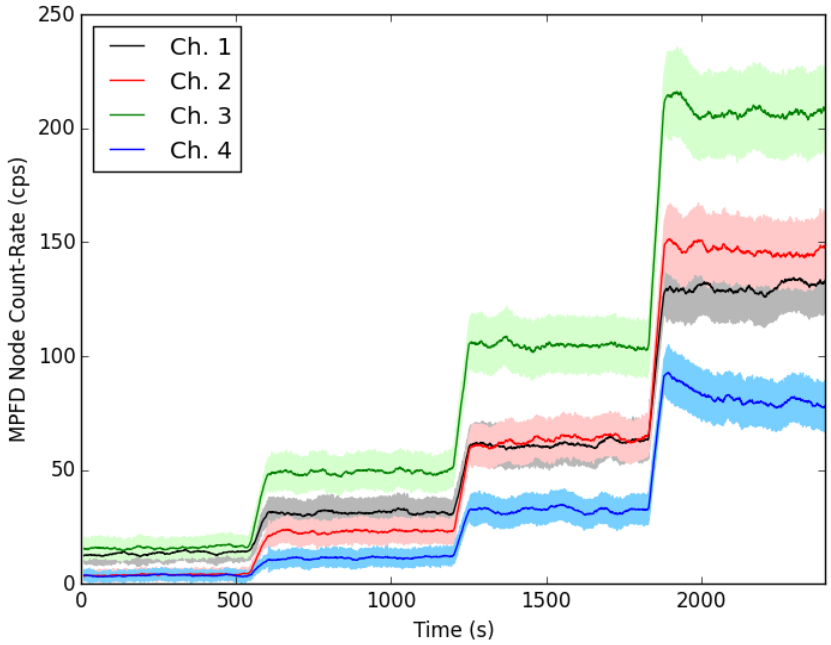

Fig. 6.47 Increasing power transients were observed at reactor powers of 10, 25, 50, 100 kWth.

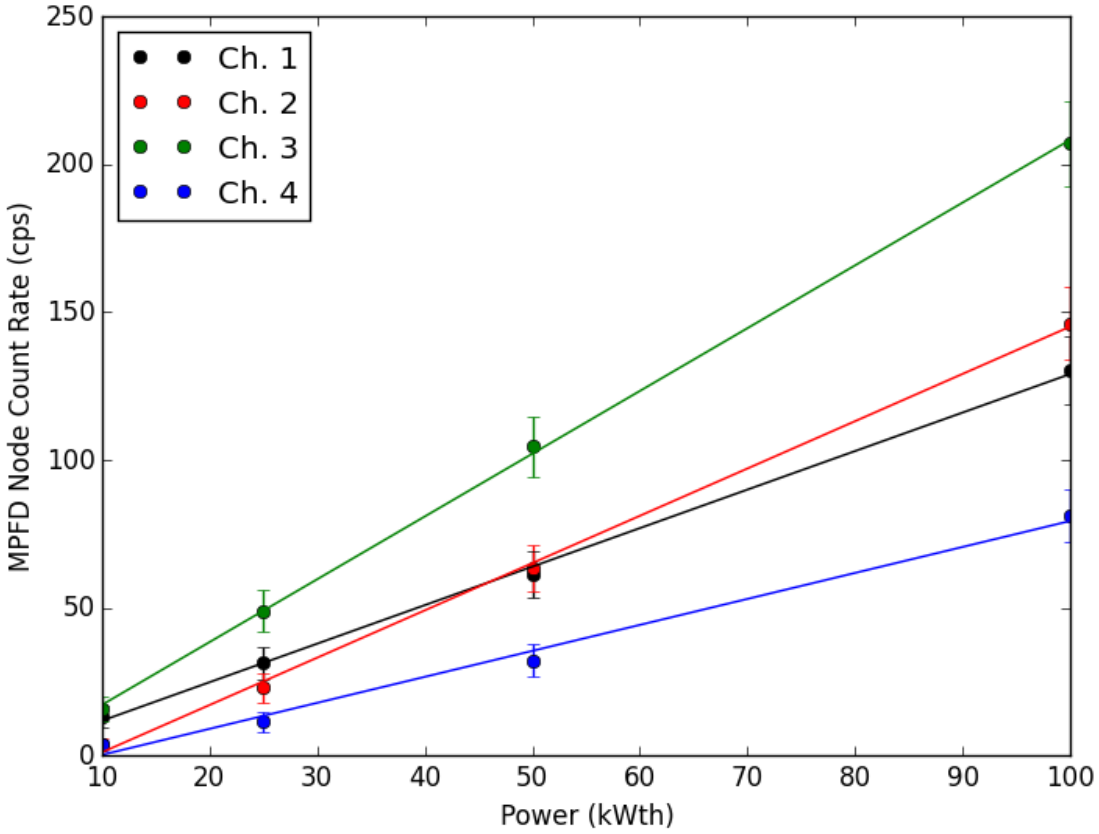

Fig. 6.48 Four of the five MPFD nodes exhibited linear response rates with reactor power, however the slope of the nodes differed.

Chapter 7 Conclusions

The results of MPFD research and development have already contributed to the field of nuclear science, and will continue to create further impact as MPFDs are deployed at several key research facilities. The design, fabrication, and testing of MPFDs, the world's smallest fission chamber, has laid groundwork to continue refining the technology and to eventually utilize MPFDs for advanced nuclear research.

7.1 Contributions to the Science

Few options presently exist for in-core neutron flux measurement. Although compact, robust sensors are available for in-core neutron measurements (SPNDs & miniature fission chambers), the extensive calibration measures and limited capabilities of these sensors has driven research further from active flux monitoring, towards post-irradiation examination (PIE). The financial and time burdens of PIE, coupled with the limited data which can be extracted from PIE inhibit the pace at which nuclear research is conducted. Therefore, progress developing advanced fuels and materials for nuclear technology has been slow. Micro-Pocket Fission Detectors offer an innovative alternative to PIE and other in-core flux monitoring devices. Many engineering challenges have been overcome to realize the successful testing of MPFDs at the KSU TRIGA Mk. II Nuclear Research Reactor facility. The transition from a parallel-plate-style ionization chamber, to a multi-wire chamber design has improved the ruggedness of MPFDs, enhanced the internal electric field of the sensor, and greatly simplified the fabrication process of MPFD arrays which can now benefit from a common-cathode. Successful fabrication and testing of a multi-node MPFD array required refinement of the fabrication process for each MPFD component as well as development of entirely new fabrication methods to facilitate the common-cathode design which fits inside an iron-wire flux well. Flux-well deployable MPFD arrays were tested at the KSU TRIGA Mk. II Nuclear Research Reactor. The MPFDs responded linearly to reactor power under steady-state conditions, and were able to track positive and negative power transients with greater spatial resolution than the external reactor power monitors. Testing of the MPFD sensors was only possible after development of a signal processing system was complete.

The configuration and testing of the electronic support system for MPFDs has also significantly improved the performance of sensors in single-channel and multi-channel configurations. In the past, only highly custom, one-of-a-kind electronics have been used to operate MPFDs, with limited success. Custom off-the-shelf electronics are being fabricated and tested which will serve as a reliable processing system to support the numerous ongoing efforts to deploy and utilized MPFDs for nuclear research. Access to electronics from a trusted electronics manufacturer will aid in the extensive preparatory work which is required for most irradiation testing at nuclear test facilities.

Finally, three distinct deployment methods are being developed for MPFDs. First, a fully-encapsulated MPFD can be fixed to the end of custom-made or commercially available mineral insulated extension cable. This method, being investigated in collaboration with the Idaho National Laboratory, will prove particularly useful for irradiation experiments at the ATR and TREAT facilities where a neutron flux measurement near an experimental specimen is desired. Next, a modular MPFD assembly has been designed and tested which is composed of four MPFD nodes spaced within the confines of a stainless steel tube. The standardization of the electronic connections and use of a straight tube simplified manufacturability and allowed the arrays to be calibrated at KSU and then delivered to other locations for deployment. An array of modular MPFDs will be deployed at the UWNR in the summer of 2017 where transient testing will be conducted in order to validate transient reactor simulation and modeling efforts. Finally, an active flux-wire, composed of numerous MPFD sensors has been developed which can be used in place of an iron-wire for real-time neutron flux measurements. At the present time, each of these projects is at a different level of ongoing work which will continue to be supported in the coming years.

7.2 Ongoing MPFD Instrumentation Efforts

The promise of MPFD development presented in this work has instigated several parallel deployment projects which will take advantage of MPFDs to validate nuclear reactor flux modeling, to monitor neutron flux for Accident Tolerant Fuels experiments at the TREAT and ATR facilities, and to serve as an active flux-wire at other nuclear test facilities. The recent developments of support electronics have taken into consideration the various requirements of each deployment in an attempt to equip each project with a support system that suits the unique requirements of each facility. The following summaries provide a brief description of the ongoing

deployment plans for MPFDs at nuclear test facilities. The variations in each project illustrate the wide impact that advanced MPFDs with reliable electronic support will have on the future of nuclear research capabilities.

7.2.1 INL HTMPFD Development

In collaboration with Idaho National Laboratory and the French Atomic Energy Agency, KSU is continuing MPFD development through the Nuclear Energy Enabling Technologies (NEET) Advanced Sensors and Instrumentation (ASI) program. The High Temperature Micro-Pocket Fission Detector (HTMPFD) is a variant of the MPFD which is specifically designed for high-temperature applications to measure fast neutron flux, thermal neutron flux, and temperature simultaneously [47]. This advanced MPFD technology is intended to support irradiation of reactor fuel and reactor materials in material test reactors. The development of a temperature resistant MPFD with incorporated thermocouple has inspired additional interest at the Idaho National Laboratory to deploy MPFDs as part of experimental sensor evaluation irradiation tests.

7.2.2 ATR Reactor Deployment

A suite of advanced real-time in-core sensors are being evaluated at the Advanced Test Reactor (ATR) as part of the AGR 5/6/7 irradiation program [47]. An MPFD and associated data acquisition system is being integrated into the sensor test train depicted in Fig. 7.1. In particular, the MPFD array developed as part of the NEET ASI HTMPFD program will be deployed and tested. Self-powered neutron detectors and ionization chambers will also be tested. The AGR 5/6/7 experiment will expose these novel sensors to total fluences well above the levels ever previously tested and will showcase the capability of MPFDs to measure neutron flux during long-duration experiments. One significant challenge of deploying an experimental technology such as MPFDs is the installation of an electronic support system. Originally, all MPFD support electronics were requested to be placed almost 200 feet from the reactor containment. As previously discussed in Ch. 5.3, close proximity of the preamplifier is critical to proper MPFD operation. As such, adjustments were made to the installation plan to facilitate a preamplifier unit placed closer to the reactor vessel. Continued improvement of the electronic support system will also take into consideration the requirements of the test facilities where MPFDs will continue to be deployed for testing.

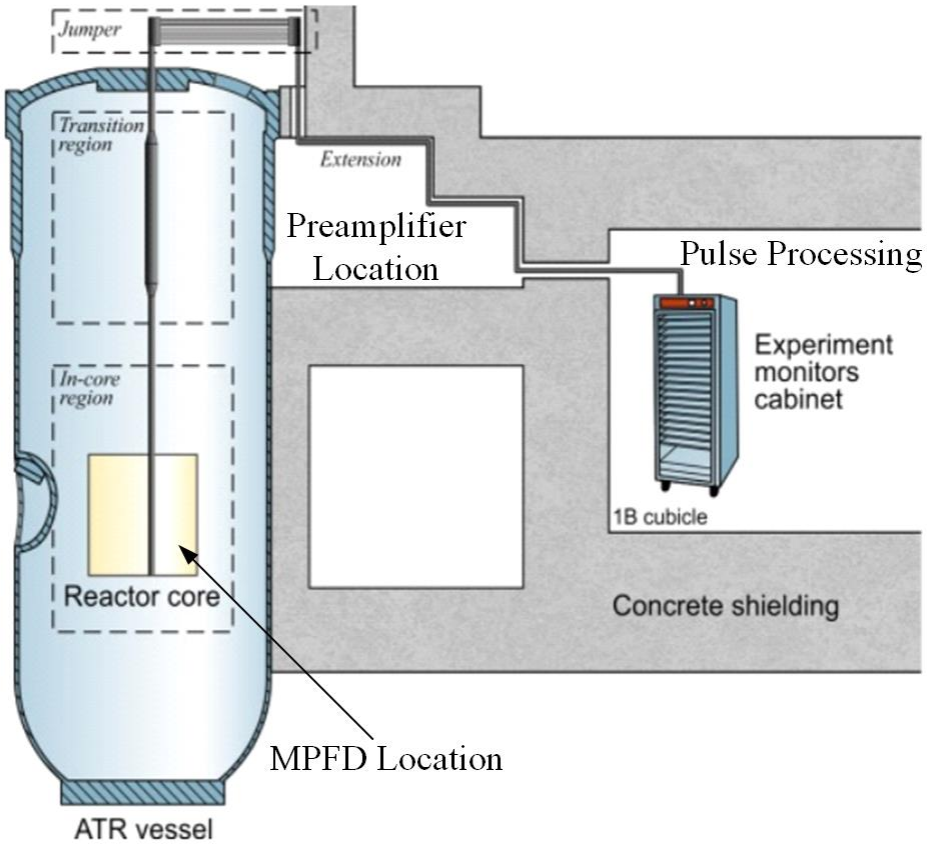

Fig. 7.1 A single MPFD array will be assembled and deployed at the ATR facility with a preamplifier box located near the reactor vessel with other support electronics located far from the reactor [48].

7.2.3 TREAT Reactor Deployments

Multiple research programs are investigating the deployment of MPFDs at the Transient REActor Test (TREAT) facility. The Accident Tolerant Fuels (ATF) program will test MPFDs as a means to measure the local neutron flux in the vicinity of experimental fuel rodlets [47]. A specialized version of the MPFD will be installed as part of the multi Static Environment Rodlet Transient Test Apparatus (multi-SERTTA), depicted in Fig. 7.2. The MPFD will be used to monitor transients in TREAT. Numerous DOE-NE programs, including TREAT, are interested in the continued development, testing, and deployment of MPFDs for transient research. Although specific consideration for the high flux present during a TREAT transient is not addressed in the current deployment, valuable information will be gathered by the MPFD testing which will assist in the future development of transient-specific MPFD designs.

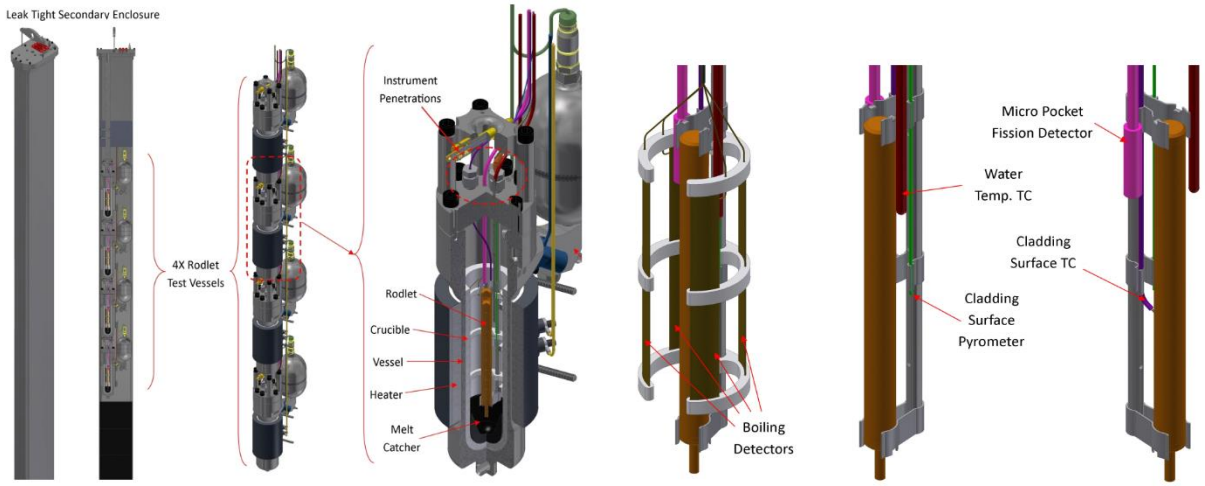

Fig. 7.2 An MPFD is included as part of a suite of sensors in the multi-SERTTA test vehicle which will be tested as part of the ATF-3 experiment program [48].

7.2.4 University Of Wisconsin Nuclear Reactor Deployment

Encapsulated MPFDs are being fabricated for deployment at the University of Wisconsin Nuclear Reactor (UWNR). The MPFDs will be deployed in tubes with 4 sensors each. The open pool and fuel basket configuration of the UWNR provides access to numerous sensor deployment locations within the core, depicted in Fig. 2.3. At least 25 MPFDs will be used to measure the neutron flux throughout the reactor core during steady-state and transient experiments including step reactivity insertions, SCRAMS, and reactor pulses. The data acquired from the MPFD array will be compared to simulation results from the NEAMS toolkit and other tools. Future benchmarking efforts will be able to refer to the experience and results of these experiments to improve simulation validation efforts.

7.3 Applications of MPFDs

The successful development of MPFDs has significant implications for the future development and safe operation of nuclear reactors. Accurate, real-time flux measurements will drastically improve the effectiveness and safety of research involving high performance reactors, transient test reactors and critical mock-ups. The use of MPFDs in transient power reactors will allow dense instrumentation of the reactor core because of the small size and low sensitivity of MPFDs. Also, real-time flux maps can be generated without significantly perturbing the neutron flux by strategically placing an array of MPFDs throughout the reactor core.

7.3.1 Research reactors

Advancements in fuel and cladding materials may enable new reprocessing and reactor technologies. New fuels, non-nuclear materials, and reprocessing technologies will benefit from advanced instrumentation that is currently unavailable. MPFD deployment will enhance real-time measurement capabilities used to evaluate non-nuclear materials and new fuel designs. One objective of current research is to develop and test a robust MPFD to enhance the flux detection capabilities for irradiation tests in Material Test Reactors (MTRs). The realization of the most recent design of MPFD is intended to advance fuel and cladding irradiation testing by providing a small, multi-purpose sensor that is robust enough to survive the harsh conditions in a US MTR. In addition to non-fuel materials testing, MPFDs could enhance new fuel testing. Currently, evaluation of new fuels can be difficult because accurate, real-time, high fidelity, irradiation measurements are not always available and post-irradiation testing must be performed at a later date. For example, radiochemical analysis of fuel is one process used to determine the isotopic compositions and concentrations of key isotopes in many types of experimental nuclear fuels. Isotopic composition of spent fuel provides a basis upon which to determine the integral irradiation of the fuel. Typically, a fuel sample of 1g to 25g is used for the radiochemical analysis. Acquiring and handling a sample of highly radioactive material requires specialized facilities and presents safety and engineering challenges. The real-time data provided by MPFDs could reduce the reliance on post-irradiation examination of test samples. MPFDs could also be constructed using the same fissile material being tested during new fuel experiments. Post-irradiation examination of the MPFD could be performed, reducing the mass of the sample that is required.

7.3.2 Commercial reactors

MPFDs are also envisioned to aid out-of-core fuel management. The once-through fuel cycle policy in the U.S.A. requires spent fuel to be stored after use. While many other countries worldwide reprocess spent fuel, accurate analysis and monitoring of spent fuel is important whether reprocessed or stored. Burnup calculations of commercial fuel are typically based on estimates from specialized computer codes. While these burnup estimates are sufficient for spent fuel storage, more accurate real-time data would aid in validating the various computer codes used for transport, storage, and reprocessing of spent fuel, as well as fissile material safeguards and evaluating the performance of new nuclear fuels in MTRs. MPFDs could be integrated into a fuel

assembly and used to calculate the integral and time-dependent radiation exposure of the fuel in that region. The radiation measurement from a MPFD in commercial power reactors could also provide more accurate input for burnup simulations of spent fuel increasing plant efficiency.

Chapter 8 References

[1] J. Duderstadt and L. Hamilton, Nuclear Reactor Analysis, Wiley, 1967.

[2] G. Knoll, Radiation Detection and Measurement, 4th ed., Wiley, 2010.

[3] T. Unruh, J. Rempe, D. McGregor, P. Ugorowski and M. Reichenberger, "NEET Micro-Pocket Fission Detector - FY 2013 Status Report," Idaho national Laboratory, Idaho Falls, ID, 2013.

[4] G. Imel, "Performance of Hafnium and Gadolinium Self Powered Neutron Detectors in the TREAT Reactor," *Nucl. Instrum. and Meth.,* no. B111, pp. 325-336, 1996.

[5] C. Blandin, S. Breaud, L. Vermeeren and M. Webber, "Development of New Sub-Miniature Fission Chambers: modelling and Experimental Tests," *Progress in Nuclear Energy*, vol. 43, pp. 349-355, 2003.

[6] D. McGregor, M. Ohmes, R. Ortiz, A. Ahmed and J. Shultis, "Micro-Pocket Fission Detectors (MPFDs) for In-Core Neutron Flux Monitoring," *Nuclear Instruments and Methods in Physics research A,* no. 554, pp. 494-499, 2005.

[7] M. Reichenberger, T. Unruh, P. Ugorowski, T. Ito, J. Roberts, S. Stevenson, D. Nichols and D. McGregor, "Micro-Pocket Fission Detectors (MPFDs) for In-Core Neutron Detection," *Annals of Nuclear Energy,* vol. 87, no. Technical Note, pp. 318-323, 2016.

[8] M. Reichenberger, T. Ito, P. B. Ugorowski, B. W. Montag, S. R. Stevenson, D. M. Nichols and D. S. McGregor, "Electrodeposition of Uranium and Thorium onto Small Platinum Electrodes," *Nucl. Instrum. and Meth.,* no. A812, pp. 12-16, 2016.

[9] M. Reichenberger, T. George, R. Fronk, P. Ugorowski, J. Geuther, J. Roberts, T. Ito, H. Vo-Le, S. Stevenson, D. Nichols and D. McGregor, "Advances in the Development and Testing of Micro-Pocket Fission Detectors (MPFDs)," in *IAEA International Conference on Research Reactors: Safe Management and Effective utilization*, Vienna, Austria, 2015.

[10] N. Tsoulfanidis, Measurement and Detection of Radiation, 2nd Ed., Washington DC: Taylor & Francis, 1995.

[11] M. Chadwick, M. Herman, P. Obložinský, M. Dunn, Y. Danon, A. Kahler, D. Smith, B. Pritychenko, G. Arbanas, R. Arcilla, R. Brewer, D. Brown, R. Capote, A. Carlson, Y. Cho, H. Derrien, K. Guber, G. Hale, S. Hoblit, S. Holloway and T. Johnson,

"ENDF/B-VII.1: Nuclear Data for Science and Technology: Cross Sections, Covariances, Fission Product Yields and Decay Data," Nucl. Data Sheets, 2011.

[12] T. D. F. George, "Design and Testing of long-Lifetime Active Sensor Arrays for In-Core Multi-Dimensional Flux Measurements," Kansas State University, Manhattan, KS, 2015.

[13] M. F. Ohmes, "Deployment of a Three-Dimensional Array of Micro-Pocket Fission Detector Triads for Real-Time, In-Core Neutron Flux Measurements in the Kansas State University TRIGA Mark-II Nuclear Reactor," Kansas State University, Mnahattan, KS, 2012.

[14] C. J. Staum, "Characterization of Gamma Radiation Fields at the University of Wisconsin Nuclear Reactor," University of Wisconsin, Madison, WI, 2006.

[15] J. Campell, "Transient Reactor Test Facility Fact Sheet," [Online]. Available: http://www4vip.inl.gov/research/transient-reactor-test-facility/d/transient-reactor-test-facility.pdf. [Accessed 6 June 2016].

[16] C. Schultz, "Advanced Test Reactor," [Online]. Available: http://www4vip.inl.gov/research/advanced-test-reactor/d/advanced-test-reactor.pdf. [Accessed 16 June 2016].

[17] M. Agu and H. Petitcolas, "Gamma-Compensated Self-Powered Detectors for Reactor Instrumentation and Control," *Measurement Science Technology*, no. 1, pp. 1047-1051, 1990.

[18] H. Warren and N. Shah, "Neutron and Gamma-Ray Effects on Self-Powered In-Core Radiation Detectors," *Nucl. Sci. Eng.*, no. 54, pp. 395-415, 1974.

[19] J. K. Shultis, "Measurement of Thermal and Fast Neutron Fluxes by Gold Foil Activation," Unpublished, 2002.

[20] G. Klotzkin, R. W. Swanson, P. Hart and L. J. Harrison, "Time Dependence of Test Fuel Power Coupling During Transient Reactor Test Facility Irradiation Experiments," *Nuclear Science and Engineering*, no. 86, pp. 206-218, 1984.

[21] M. F. Ohmes, A. S. M. S. Ahmed, R. E. Ortiz, J. K. Shultis and D. S. McGregor, "Micro-Pocket Fission Detector (MPFD) Performance Characteristics," in *IEEE Nuclear Science Symposium*, San Diego, CA, USA, 2006.

[22] M. F. Ohmes, "Micro-Pocket Fission Detector (MPFD) Development for the Kansas State University TRIGA Mark-II Nuclear Reactor," Kansas State University, Manhattan, KS, 2006.

[23] V. K. Patel, M. A. Reichenberger, J. A. Roberts, T. C. Unruh and D. S. McGregor, "Simulated Performance of Micro-Pocket Fisison Detectors (MPFDs) in the Transient REAactor Test (TREAT) Facility using MCNP6," Annals of Nuclear Energy, submitted.

[24] S. Kahn, R. Harman and N. Forgue, "Energy Distributions of Fission Fragments from Uranium Dioxide Films," *Nuclear Science and Engineering,* vol. 23, pp. 8-20, 1965.

[25] G. R. Imel, W. P. Poenitz and A. M. Snyder, "Measurement of Fission Fragment Induced Fluorescence in Xenon," *Nucl. Instrum. and Meth.,* no. B103, pp. 1-14, 1995.

[26] H. Bock and E. Balcar, "Long-Time Behaviour of Regenerating In-Core Neutron Detectors with U-238 - Pu-239 Electrodes During Power Cycling," *Nucl. Instrum. and Meth.,* no. A124, pp. 563-571, 1974.

[27] M. A. Reichenberger, P. B. Ugorowski, J. A. Roberts and D. S. McGregor, "First-Order Numerical Optimization of Fission-Chamber Coatings Using Natural Uranium and Thorium," in *IEEE Nucl. Sci. Symp.*, Seatle, WA, 2014.

[28] O. R. N. Laboratory, "SCALE: A Modular Code System for Performing Standardized Computer Analyses for Liscensing Evaluations," ORNL/TM-205/39, Version 6, 2009.

[29] Department of Transportation Report, "49 CFR 173.434 Activity-Mass Relationships for Uranium and Natural Thorium," 2011.

[30] Knolls Atomic Power Laboratory, "Nuclides and Isotopes: Chart of the Nuclides," Lockheed Martin Distribution Services, 2002.

[31] J. F. Ziegler, M. D. Ziegler and J. P. Biersack, "The Stoping and Range of Ions in Matter (SRIM)," SRIM.com, Annapolis, MD, 2012.

[32] Kansas State University, "Triga Mark II Nuclear Reactor Facility," Kansas State University, 26/ 8/ 2016. [Online]. Available: http://www.mne.k-state.edu/research/reactor/. [Accessed 12 9 2016].

[33] Kansas State University, "TRIGA Mk. II Nuclear Reactor Facility Training Manual," 2002.

[34] PostNova Analytics GmbH, "Shortix Tubing Cutter for Fused Silica Capillary," [Online]. Available: http://www.postnova.com/fused-silica-capillaries.html?file=tl_files/postnova/content/products/supplies/downloads/Fused%20Silica%20Capillaries/Postnova_FusedSilicaCutter_2014_04.pdf. [Accessed 12/ 9/ 2016].

[35] Mixed Media Engineering, "Rope-O'Matic," Mixed Media Engineering, 2016. [Online]. Available: https://www.kickstarter.com/projects/1640002012/rope-omatic. [Accessed 12/ 9/ 2016].

[36] "Preamplifier-Introduction," 27/ 08/ 2009. [Online]. Available: www.ortec-online.com/download/Preamplifier-Introduction.pdf. [Accessed 15/ 09/ 2016].

[37] K. A. Nelson, M. R. Kusner, B. W. Montag, M. R. Mayhugh, A. J. Schmidt, C. D. Wayant, J. K. Shultis, P. B. Ugorowski and D. S. McGregor, "Characterization of a Mid-Sized Li Foil Multi-Wire Proportional Counter Neutron Detector," *Nucl. Instrum. and Meth.,* no. A762, pp. 119-124, 2014.

[38] AMETEK, Inc., "Model 142PC Preamplifier Operating and Service Manual," 2002. [Online]. Available: www.ortec-online.com/download/142PC.pdf. [Accessed 12/ 9/ 2016].

[39] Mesytec GmbH & Co. KG, "MPR-1 Datasheet," 2016. [Online]. Available: http://www.mesytec.com/products/datasheets/MPR-1.pdf. [Accessed 12/ 9/ 2016].

[40] Mesytec GmbH & Co. KG, "MPR-16 Datasheet," 2016. [Online]. Available: http://www.mesytec.com/products/datasheets/MPR-16.pdf. [Accessed 12/ 9/ 2016].

[41] M. A. Reichenberger, T. C. Unruh, J. A. Geuther, D. M. Nichols, T. J. Sobering, J. A. Roberts, P. B. Ugorowski and D. S. McGregor, "Electronic Support System Enchnacements for Micro-Pocket Fission Detectors (MPFDs)," in *Conf. Proc. IEEE Nucl. Sci. Symp.*, Strassbourg, FR, 2016.

[42] National Council on Radiation Protection and Measurements, "A Handbook of Radioactivity Measurement Procedures," NCRP, Washington, D.C., 1978.

[43] Stratasys, "High-Temperature RGD525 Model Material," Stratasys, Eden Prairie, MN, 2014.

[44] LEMO, "FGG.1K.308.CLAK80 Specification," 2016.

[45] Lemo, "PHG.1K.308.CLLK75," 2016.

[46] Belden, "8134 Multi-Conductor, Low-Capacitance Computer Cable for EIA RS-232/485," 2016.

[47] T. Unruh, D. McGregor, P. Ugorowski, M. Reichenberger and T. Ito, "NEET Enhanced Micro-Pocket Fission Detecotr for High Temperature Reactors - FY15 Status Report," Idaho National Laboratory, Idaho Falls, ID, 2015.

[48] T. Unruh, M. Reichenberger, S. Stevenson, K. Tsai and D. McGregor, "NEET Enhanced Micro-Pocket Fission Detector for High Temperature Reactors - FY16 Status Report," Idaho National Laboratory, Idaho Falls, ID, 2016.

[49] L. C. Hao, C. V. Tao, N. V. Dong, H. N. Nghi, P. T. Dung and L. V. Thong, "Rapid Prearation of Uranium and Thorium Alpha Sources by Electroplating Technique," *Kerntechnik,* vol. 75, no. 6, pp. 381-385, 2010.

[50] D. Luna-Zaragoza and J. S. G., "Preparation of Uranium Targets by Electroplating," *Applied Radiation and Isotopes,* no. 51, pp. 499-503, 1999.

[51] J. W. Dini and H. R. Johnson, "Plating on Some Difficult-to-Plate Metals and Alloys," Sandia Laboratories, Alburquerque, NM, 1980.

[52] A. M. Adamska, E. L. Bright, J. Sutcliffe, W. Liu, O. D. Payton, L. Picco and T. B. Scott, "Characterisation of Electrodeposited Polycrystalline Uranium Dioxide Thin Films on Nickel Foil for Industrial Applications," *Thin Solid Films,* no. 597, pp. 5-64, 2015.

[53] S. R. Qiu, C. Amrhein, M. L. Hunt, R. Pfeffer, B. Yakshinskiy, L. Zhang, T. E. Madey and J. A. Yarmoff, "Characterization of Uranium Oxide Thin Films Grown from SOlution onto Fe Surfaces," *Applied Surface Science,* no. 181, pp. 211-224, 2001.

[54] C. J. Rao, K. A. Venkatesan, K. Nagarajan, T. G. Srinivasan and P. R. V. Rao, "Electrodeposition of Metallic Uranium at Near Ambient Conditions from Room Temperature Ionic Liquid," *Journal of Nuclear Materials,* no. 408, pp. 25-29, 2011.

[55] O. A. Dumitru, R. S. Begy, D. C. Nita, L. D. Bobo and C. Cosma, "Uranium Electrodeposition for Alpha Spectrometric Source Preparation," *Journal Radioanal Nuclear Chemistry,* no. 298, pp. 1335-1339, 2013.

[56] R. G. Robins, "Uranium Dioxide Single Crystals by Electrodeposition," *Journal of Nuclear Materials,* vol. 3, no. 3, pp. 294-301, 1961.

[57] T. Sato, "Preparation of Uranium Peroxide Hydrates," *Journal of Applied Chemistry,* vol. 13, no. 8, pp. 361-365, 1963.

[58] H. Jia-heng, C. Qi-ping, Z. Wen-bin, D. Yu-feng, L. Xing-liang, W. Jing and L. Guo-ping, "Preparation fo Uranium Targets by Electro-Deposition Method," *Yuanzineng Kexue Jishu,* vol. 44, no. 10, pp. 1161-1167, 2010.

[59] A. Ljubicic, M. Krcmar, S. Kaucic and B. A. Logan, "Experimental Determination of Uranium and Thorium in Allchar Ore," *Nucl. Instrum. and Meth.,* no. A271, pp. 262-263, 1988.

[60] R. A. Henderson, J. M. Gostic, J. T. Burke, S. E. Fisher and C. Y. Wu, "Electrodeposition of U and Pu on Thin C and Ti Substrates," *Nucl. Instrum. and Meth.*, no. A655, pp. 66-71, 2011.

[61] Y. V. Lobanov, G. V. Buklanov, F. S. Abdullin, A. N. Polyakov, I. V. Shirokovsky, Y. S. Tsyganov and V. K. Utyonkov, "Targets of Uranium, Plutonium, and Curium for Heavy-Element Research," *Nucl. Instrum. and Meth.*, no. A397, pp. 26-29, 1997.

Appendix A Uranyl Nitrate Solution Preparation Procedure

**NOTE: pH meter must be calibrated within 2 months for accurate measurement. Use Appendix B to perform this calibration if necessary.

1. Label a clean 250 mL beaker with:
    a. The solution name
    b. The current date
    c. Your initials

2. Turn on scale and observe the power symbol:

    a. If flashing press the hit the home button and select leveling assistant
        i. Follow directions to level device

        ii. Once done, press home button to get to the main screen
    b. If not flashing, proceed to step 3
3. Adjust target weight by selecting the weight located in the top center of the main screen

    **NOTE: Our target weight of ammonium nitrate is 14,410 mg **

    **NOTE: Since we expect about 25 mg of residue to be left on weigh boat, the target weight is set to 14,435 mg **

4. Place a large weigh boat on scale and zero:
5. Before opening the ammonium nitrate bottle, shake well to ensure any large grains are broken up

6. Use a clean, large powder scoop to add the intended weigh of ammonium nitrate to large weigh boat
7. Scrape ammonium nitrate into the labeled 250 mL beaker from step 1, reweighing the weigh boat to determine and record how much ammonium nitrate was left in the weigh boat.

    NOTE: Throw weigh boat into trash bin once finished

8. Weigh 420 mg of uranyl nitrate and add to the 250 ml beaker from step 1)

    NOTE: Re-weigh the boat after adding the uranyl nitrate to the mixture and record the mass that was added

    NOTE: Dispose of the weigh boat in radioactive waste trash bin once finished
9. Add enough DI until the beaker is approximately 100 mL filled
10. Grab a small clean 50 mL beaker and measure out approximately 10 mL of ethanol
11. Use the 50 mL beaker to pour 5.78 mL of ethanol into a small graduated cylinder
12. Pour contents of the graduated cylinder into a clean 100 mL beaker
13. Add DI into graduated cylinder to try to get all the ethanol out
14. Add DI to the 100 mL beaker to achieve a level of approximately 50 mL
15. Add contents of 100 mL beaker to the solution beaker and top off to a level of 150 mL
16. Add a magnetic stir rod to the beaker

    NOTE: Try using another magnetic stir rod on the outside of the beaker to slowly ease the rod into the solution
17. Set beaker onto stir plate and increase the revolutions to about 5 revolutions per second

    NOTE: Keep track of the time during which the solution is being stirred

18. Prepare the pH meter by rinsing both probe heads with DI water
19. Secure both probes in a grip attached to a ring stand, and ensure both probe tips are vertical and probe tips are at an equal level
20. Place solution beaker under probes, and lower probes into solution so that both probe heads are fully submerged
21. Turn on pH meter and wait until pH stabilizes, (expected: 3.4 pH)
22. Record the solution pH
23. Turn off pH meter, and raise probes out of solution
24. Place weigh boat under probes to catch any drips and then move beaker to new location and place parafilm wax over the top of the beaker
25. Place beaker onto stir plate and start at 5 rotations per second

    NOTE: Keep track of the time during which the solution is being stirred
26. Rinse the pH meter probes with DI over the weigh boat to decontaminate
27. Dispose of weigh boats as contaminated waste
28. Replace pH meter probes in storage beaker
29. Rinse out any beakers that had ethanol with Isopropanol alcohol three times and then rinse with DI three times

Appendix B pH Meter Calibration

1. Remove temperature probe and pH probe from storage breaker, and put protective cap on probe

   NOTE: Be careful to not touch the pH bulb

2. Rinse both temperature and pH probe with DI into a rinse waste beaker
3. Unplug blue plug on side of pH meter probe and add 2.0 Mol KCl until just below hole for the blue plug
4. Plug blue plug back into pH meter probe
5. Prepare pH 10, pH 7, pH 4 buffer solution packets and the electrode rinse solution
6. Open all packets and set to the side
7. Power on Thermo pH meter with power button:

8. Unplug blue plug for calibration
9. To begin calibration, press the calibration button:

10. Start the calibration by rinsing the probe head in the electrode rinse solution

    NOTE: Try to not move the probe during the rinse, in order for the pH to stabilize

    NOTE: Ensure probe does not touch sides of solution bags as it will pick up charge

11. Next use pH 10 buffer to calibrate first point
12. Hold probe fully submerged in solution until the arrow left of the number starts blinking:

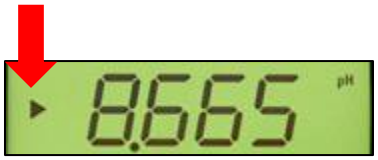

13. To set the calibration point press the digit editor button:

    a. Edit each digit to the solution pH by using the up and down arrows:

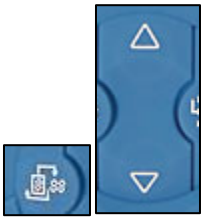

14. Repeat steps 10-13 for pH 4 buffer and pH 7 buffer

15. Once calibration is completed, press the measure button and use one of the pH buffer bags to verify the calibration was successful

    **Close the blue plug after measurement is completed (for storage only) **

16. Hold power button to turn off, take off protective cap and plunge into storage beaker

    **When putting pH meter probe in storage beaker, avoid touching probe head to any surface **

Appendix C Electrodeposition Procedure

1. Turn on Lecia microscope using the on/off switch located on the top of the microscope
2. Open the Lecia microscope software and ensure it is in the acquire tab
3. Press the power on button on the CH Instruments Electrochemical Analyzer
4. Open up the CH Instruments program
5. Click setup→parameters
6. Add in parameters listed below:
    a. Init E (V): -0.62
    b. High E (V): -0.62
    c. Low E (V): -0.64
    d. Final E (V): -0.62
    e. Initial Scan Polarity: Negative
    f. Scan Rate (V/s): 0.01
    g. Sweep Segments: 250 **NOTE: This will vary depending on the desired cycles**
    h. Sample Interval (V): 0.001
    i. Quiet Time (s): 2
    j. Sensitivity (A/V): 1e-005
7. Once parameters are set click OK
8. With all leads detached from the probes and electrode, click setup→Hardware Test
9. Unwrap the parafilm that is around the reference and counter electrode (reference electrode)
10. Rinse the reference electrode into a rinse beaker using DI
11. Set a clean short/wide beaker on 3D stage
12. If the microscope does not already, change the microscope lens to the small lens
13. Suspend the reference electrode in beaker
14. Put parafilm over the storage vial used for the reference electrode and set aside

15. Position plasti-dipped probe (working electrode) over the short/wide beaker and under the microscope lens
16. Attach green lead to the end of the working electrode
17. Adjust the microscope so that working electrode probe tip is in focus and centered under lens
18. Clip the red lead to the platinum wire (counter electrode) and the white lead to the silver wire (reference electrode)
19. Reposition the reference electrode to be approximately 1 cm away from working electrode tip
20. Add enough uranium solution into short wide beaker to cover up the coiled platinum wire counter electrode
21. Before adding samples into uranium solution, wash samples with isopropanol alcohol and DI
22. Use tweezers to transfer sample into solution

    NOTE: Try shaking sample before letting go to ensure no bubbles have clung to the sample
23. Position sample under working electrode with the electrode tip in the center of the platinum region

    NOTE: To ensure contact, manipulate the stage until the video of the sample shows both the sample and working electrode tip moving in unison when the stage is raised
24. Before starting the electrodeposition program, take a picture of the setup using the Lecia software

25. To begin electrodeposition program, click Run
26. Take a short video using the Lecia program at the beginning of the electrodeposition process

    NOTE: Bubbling may occur on the surface of the platinum during electrodepositon, this is normal

    NOTE: While deposition is in progress, it is important to avoid bumping the table, this will interfere with the deposition process
27. After all cyclic voltammetry cycles have completed, lower the stage in order to disconnect the contact between the platinum and the working electrode
28. Remove sample from solution and rinse with isopropanol alcohol and set out to dry
29. Save the cyclic voltometric plot for the deposition process by copying and pasting the image into Microsoft paint, and saving it as a JPEG file
30. Repeat steps 22-29 for any subsequent samples

Appendix D MPFD Sensor Schematics

Encapsulated MPFD Design

Disk:

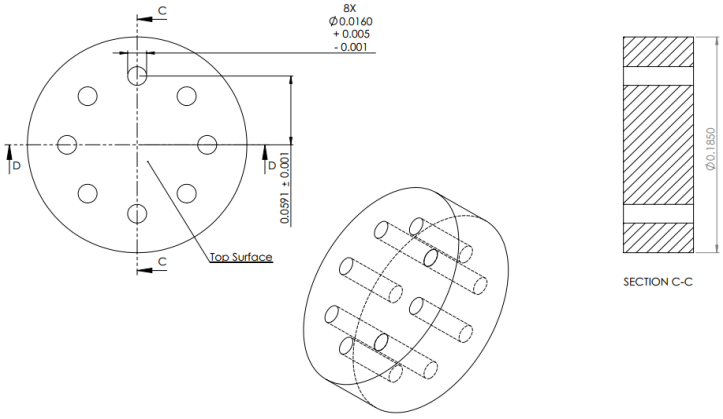

Spacer:

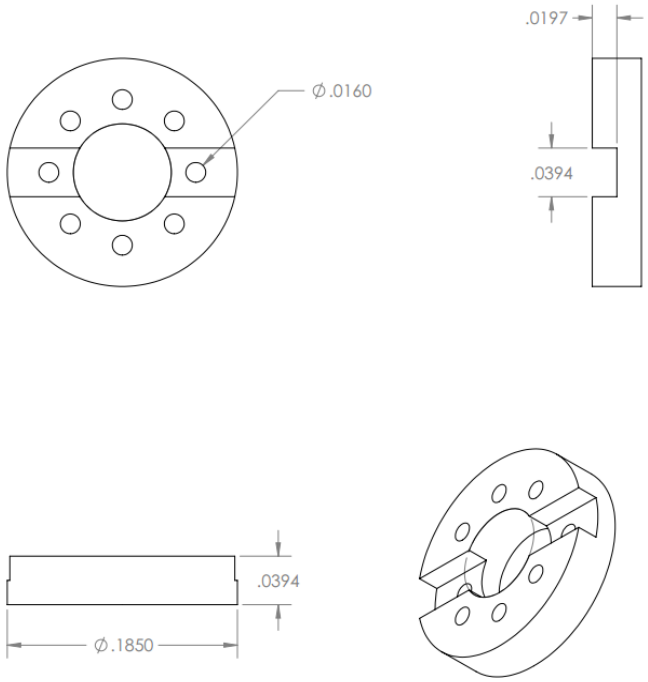

Flux-Well Port Design:

Disk:

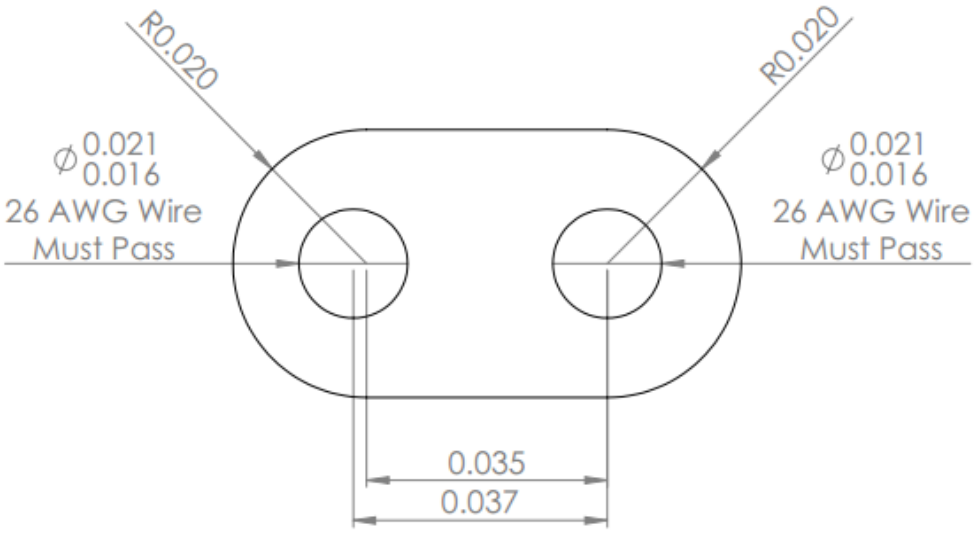

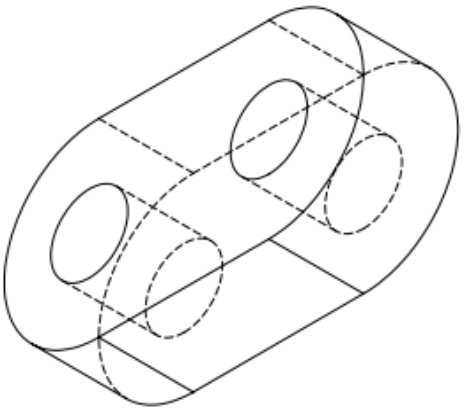

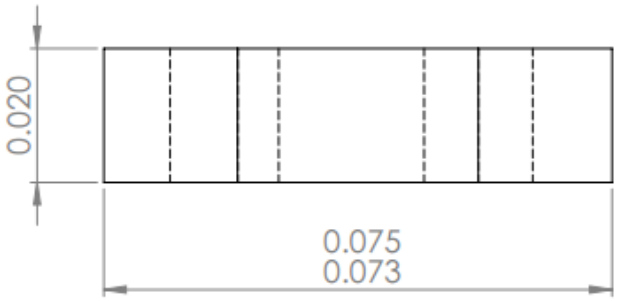

Spacer:

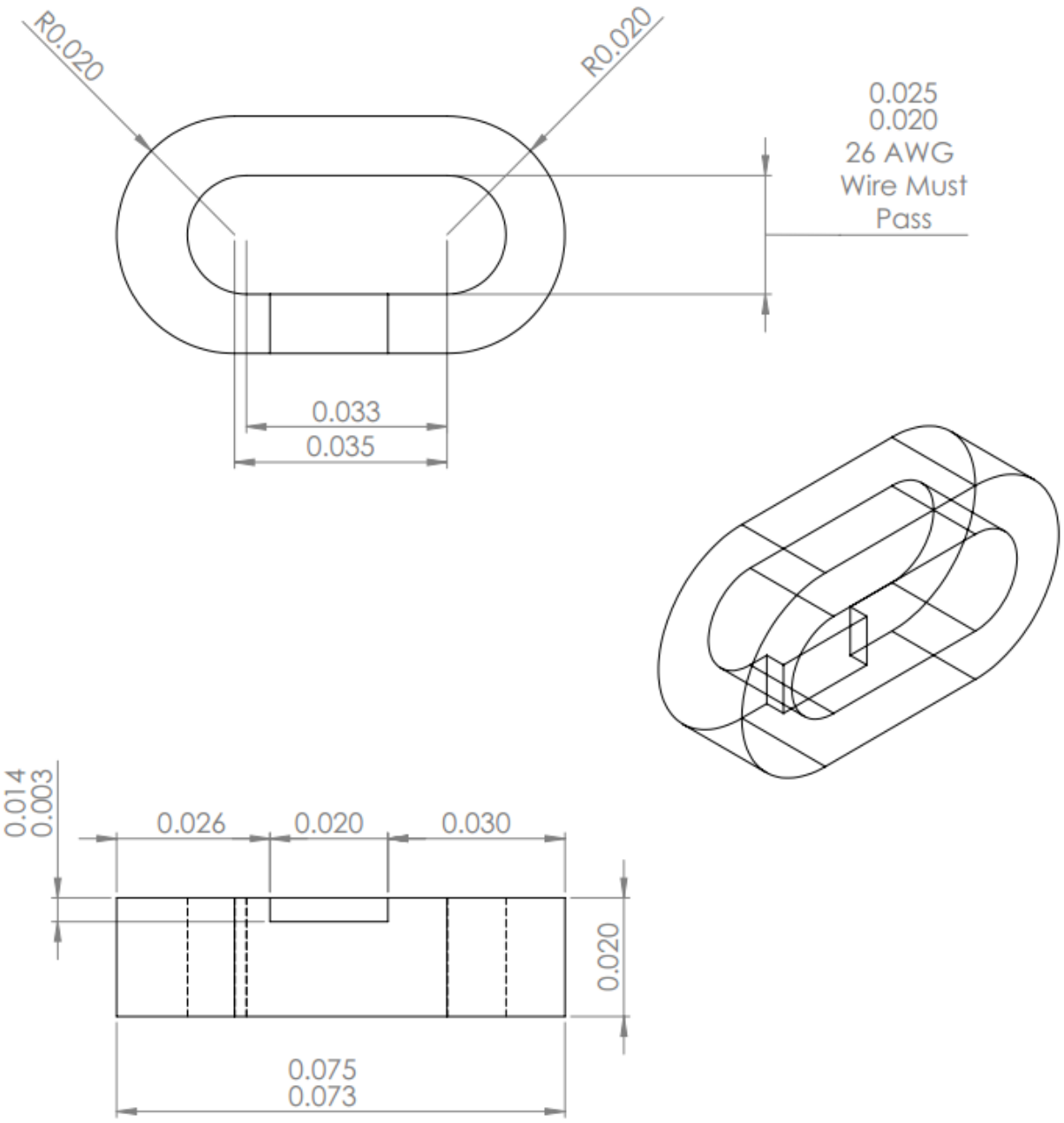
R0.020
R0.020
0.025
0.020
26 AWG
Wire Must
Pass
0.033
0.035
0.014
0.003
0.026
0.020
0.030
0.020
0.075
0.073

Appendix E MPFD Support Electronics

A signal processing unit for a 4 channel micro ionization chamber. It includes charge sensitive preamplifiers in a separate box, a HV bias supply for the IO-chamber, a filter stage and discriminators. Al adjustments can be controlled and data can be transmitted via USB interface. It outputs the 4 discriminator signals for an external counter.

Features:

Preamplifier Box:

- Humidity resistant preamplifier box
- Detector input: D Sub-9 (4x detector with HV, 3x signal ground, 2x shield ground)
- Maximum detector capacity (with cable) 1nF.
- 4 channel preamplifier, high capacity low noise, high rate
- Pulser coupling to preamp inputs for full test of the electronics.
- Common and individual HV filtering for the independent channels.
- Maximum distance from preamp to NIM interface module: 70m via 2 Ethernet Cat5 cables.

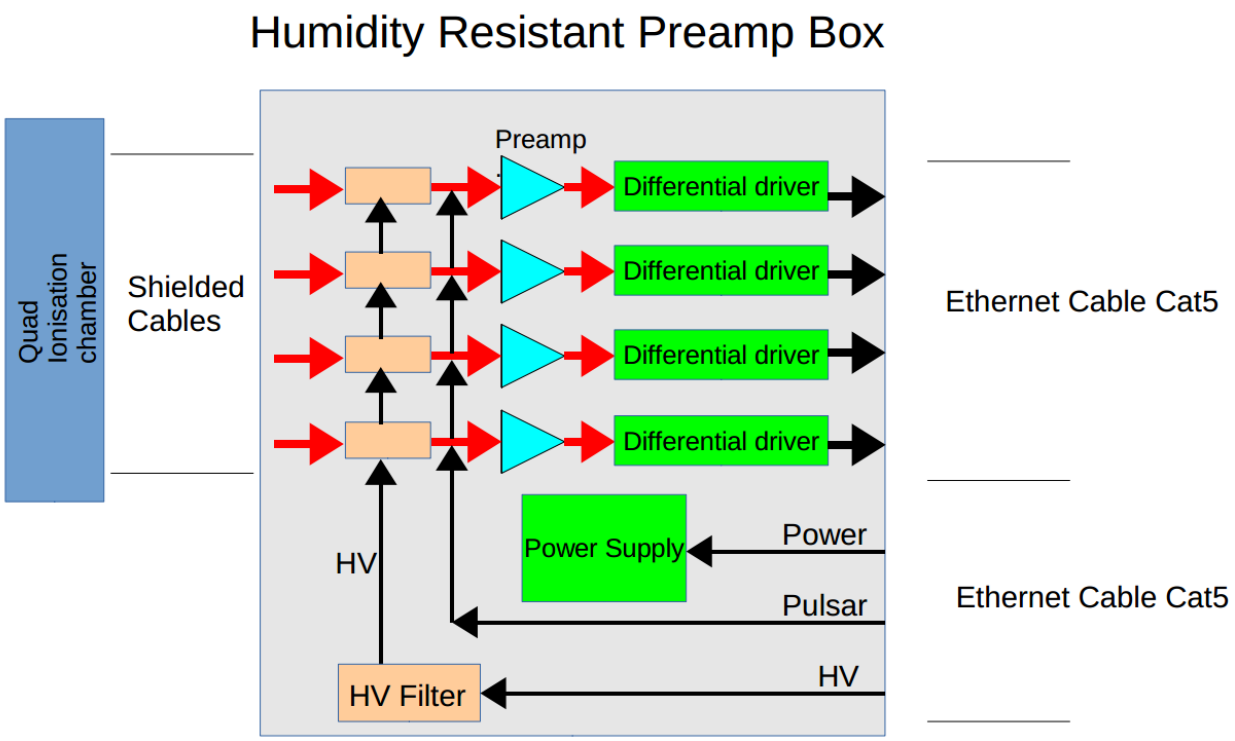

Processing Module (Single-wide NIM unit):

- Detector bias common for all 4 channels
  - Adjustable by RC
  - Stable at +25V to +400 V (Ethernet connector has to be completely dry)
  - Max 50uA per channel
- Shaping filter
  - 250ns, 500ns, 1us, 2us
  - Adjustable by RC
- Discriminator
  - Leading edge
  - 4 independent thresholds
  - Adjustable by RC
- FPGA for digital data handling
  - 4x Discriminator output
  - TTL4x Shaper output
  - 0 to + 4V
- USB interface for data transmission and Parameter setting
  - 4x Discriminator outputs (TTL)
  - 4x Shaper outputs

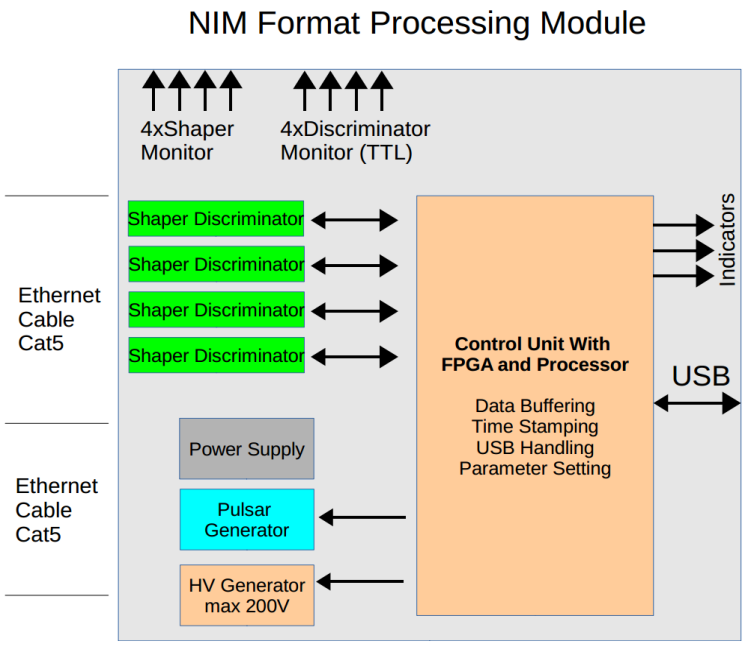

Appendix F LabView Data Acquisition System for 4-node MPFD arrays

Front Panel Display

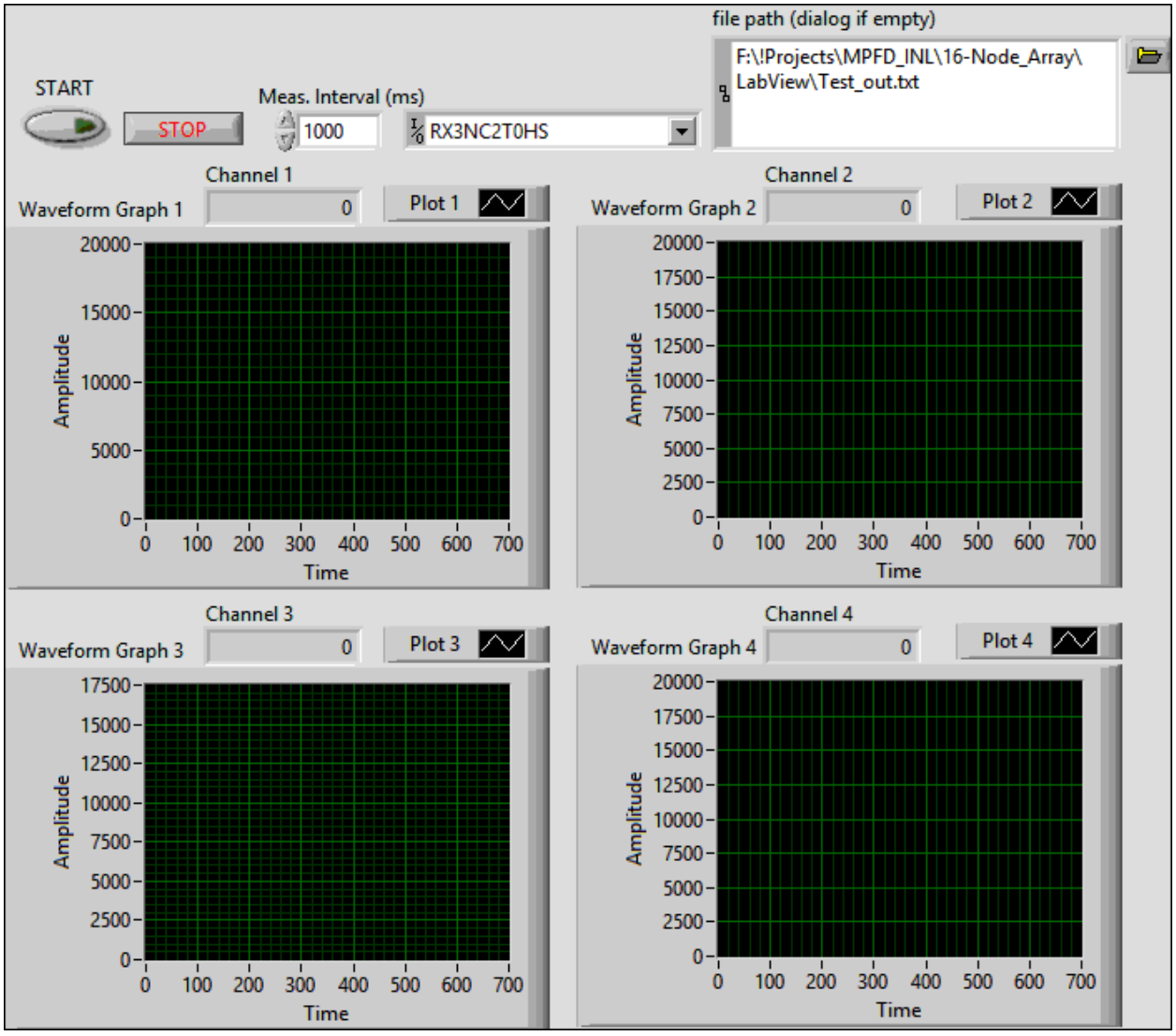

LabView Block Diagram: